

SILICONE-BASED HYDROGELS FOR USE IN BIOMEDICAL APPLICATIONS

GEORGINA DUROWOJU

Doctor of Philosophy

Aston University

December 2022

© Georgina Durowoju, 2022

Georgina Durowoju asserts their moral right to be identified as the author of this thesis

This copy of the thesis has been supplied on condition that anyone who consults it is understood to recognise that its copyright belongs to its author and that no quotation from the thesis and no information derived from it may be published without appropriate permission or acknowledgement.

Silicone-based Hydrogels for use in Biomedical Applications
Georgina Durowoju | Submitted for the degree of Doctor of Philosophy | 2022

Hydrogels can be explained in a variety of descriptions, but they are overarchingly defined as three-dimensional polymer structures with the ability to absorb and retain large amounts of water. This project aimed to synthesise variations of silicone-based hydrogels with formulations that were inspired by commercially available contact lenses, with *N*-vinyl-pyrrolidone (NVP), *N,N*-dimethylacrylamide (DMA) and tris(trimethylsiloxy)-3-methylacryloxypropyl silane (TRIS) as monomers, and determine whether changes in reaction conditions (the use of a diluent and/or post-cure) could trigger changes in their fundamental characteristics including water content, permeation, partitioning and morphology. These characteristics are important when determining the suitability of a hydrogel in biomedical applications, particularly those that rely on the ability of a hydrogel membrane to absorb and release substances.

The equilibrium water content (EWC) of the hydrogels was determined and differential scanning calorimetry (DSC) was utilised to determine the freezing water content (FWC), ice-like water content (ILWC) and polymer-associated water content (PAWC) whilst non-freezing water content was extrapolated. Permeation studies were conducted on a single-salt and multiple-salt basis, making use of calcium, sodium, potassium and magnesium chloride salts within a hydrated ion radius of 0.31 to 0.39 nm. Tests were carried out to determine partition coefficients, using the same salts as those used in permeation studies. Comparative elemental analysis studies of the hydrogels were conducted using energy-dispersive X-ray spectroscopy (EDX) and X-ray photoelectron spectroscopy (XPS) whilst environmental scanning electron microscopy (ESEM) captured images of the hydrogels to determine the occurrence of phase separation.

The different water types within the hydrogels were identified and their quantities varied depending on their formulation. Permeability wise, the hydrogels showed an ability to elute salts within a mixture on the basis of size/charge, which was not explicitly seen on a single-salt basis – the order of salt permeation did not follow their size/charge trends. Relationships between the established parameters were considered and discussed where applicable. Opportunities for further study were identified and suggestions for the suitability of the hydrogels in biomedical applications were considered.

Keywords: hydrogels, ion permeability, characterisation, silicone-based

To all the kids out there who dream the impossible

Acknowledgments

It is impossible for a task like this to be completed on one's own, so I would like to show gratitude to the people who helped me along the way:

Thank you to my supervisor, Dr Anisa Mahomed, and my associate supervisor, Prof. Brian Tighe, for their advice and guidance throughout the course of the PhD project.

To all the specialists who assisted with analytical experiments: Dr Yang Bai who facilitated the EDX & ESEM experiments; Dr Jakob Sacharczuk for his help with EDX analysis, Dr Jinesh Manayil who assisted with the ICP-OES, Jem for everything DSC-related – thank you for all your help & answering all my emails!

I acknowledge the Research England funded TALENT: Technician Led Equipment Fund for enabling the XPS measurements, carried out by Dr Marc Walker (Warwick University).

All of the members of the Biomaterials Research Unit, thank you for your kindness. Dr Val Franklin, my fairy godmother, thank you for your support and reassurance (and Terry's Chocolate Orange coffees!). To all the students in MB182A, our little haven, thanks for your compassion and all the snacks you gave me along the way.

To my chosen family - Ladi, Jas, Uroosha, SET (the list is endless) for always reminding me I could do it, for looking after me, for loving me and keeping me sane.

Finally, to my parents and my brother, for all their love, their encouragement and for being my much-needed constant.

List of Contents

Thesis Summary	2
Acknowledgments.....	4
List of Abbreviations.....	8
List of Tables, Figures & Images.....	9
List of Equations	13
1 Introduction	14
1.1 Literature Review	16
1.1.1 Hydrogels	16
1.1.2 Biomedical Applications: Extracorporeal Devices	20
1.1.3 Characteristics Background: water content, partition coefficient, permeability, morphology.....	24
1.1.4 Scope of Study	27
2 Materials & Methodology.....	28
2.1 Chemicals	28
2.2 Hydrogel Synthesis	30
2.3 Permeation assays.....	31
2.3.1 Single-salt permeation assays	31
2.3.2 Multiple-salt permeation assays	34
2.4 Water Content.....	34
2.4.1 Equilibrium Water Content.....	34
2.4.2 Differential Scanning Calorimetry	35
2.5 Partition Coefficient	36
2.6 Membrane Characteristics.....	36
2.6.1 Environmental Scanning Electron Microscopy & Energy-dispersive X-ray Spectroscopy 36	
2.6.2 X-ray Photoelectron Spectroscopy	37
2.7 Calibration Curve Development.....	38
2.7.1 Single-salt calibration curve.....	38
2.8 ICP-OES Method Development	38
2.9 Statistical Analysis	39
3 Water Content.....	41

3.1	Introduction	41
3.2	Results	43
3.2.1	Equilibrium Water Content Results: E & F Series	43
3.2.2	DSC Results: E & F Series	46
3.3	Discussion	53
3.3.1	Relationship between water content & formulation	53
3.3.2	Peak Splitting & Water Structuring	60
3.3.2	Relationship between water content & synthesis conditions	64
3.4	Conclusion	65
4	<i>Partitioning</i>	67
4.1	Introduction	67
4.2	Results	69
4.3	Discussion	72
4.3.1	Relationship between water content & partition coefficient	73
4.3.1.1	The relationship between partitioning & equilibrium water content	74
4.3.1.2	The relationship between partitioning & freezing/non-freezing water content	78
4.3.1.3	The relationship between partitioning and ice-like/polymer-associated water content	81
4.3.2	Relationship between formulation & partition coefficient	86
4.4	Conclusion	92
5	<i>Single-salt Permeation</i>	94
5.1	Introduction	94
5.2	Results	97
5.2.1	Permeation Coefficient	97
5.2.2	Diffusion Coefficient	99
5.3	Discussion	103
5.3.1	Effects of formulation & reaction conditions on permeation	104
5.3.2	Differences in permeation between chloride salts	109
5.3.3	The relationship between water content & permeation	115
5.3.3.1	Equilibrium Water Content	116
5.3.3.2	Freezing Water Content	119
5.3.3.3	Non-Freezing Water Content	122
5.3.3.4	Ice-like Water	124
5.3.3.5	Polymer-associated Water	127
5.3.4	The relationship between partitioning, diffusion & permeation	129
5.3.4.1	Permeation & Partitioning	130

5.4.3.2	Diffusion vs Permeation	132
5.5	Conclusion.....	133
6	<i>Multiple-salt Permeation.....</i>	134
6.1	Introduction	134
6.2	Results	136
6.2	Discussion	139
6.2.1	Permeation profiles.....	139
6.2.2	Factors influencing multiple-ion permeation	143
6.3	Conclusion.....	148
7	<i>Membrane Characteristics.....</i>	149
7.1	Introduction	149
7.2	Results	152
7.2.1	EDX.....	152
7.2.2	XPS	154
7.2.3	ESEM Imaging.....	155
7.3	Discussion	162
7.3.1	ESEM Image Interpretation & Phase Separation.....	162
7.3.2	The relationship between optical clarity & morphology	170
7.3.3	Elemental compositions: EDX.....	172
7.3.3	Elemental compositions: XPS.....	174
7.3.4	The influence of reactivity ratios on monomer incorporation.....	176
7.4	Conclusion.....	178
8	<i>Summary & Future Works.....</i>	179
8.1	Summary.....	179
8.2	Future Works.....	181
	<i>References.....</i>	183

List of Abbreviations

°C/min – degrees Celsius per minute	ml - millilitre
AIBN - 2,2'-azobis(2-methylpropionitrile)	mM – milli-molar
CaCl ₂ – calcium chloride	mm – millimetre
cm – centimetre	mS – milli Siemens
DMA – <i>N,N</i> -dimethylacrylamide	NaCl – sodium chloride
DSC – differential scanning calorimetry	NFWC – non-freezing water content
EDX – energy-dispersive X-ray spectroscopy	nm – nanometre
EGDMA – ethylene glycol dimethacrylate	NVP – <i>N</i> -vinyl-2-pyrrolidone
ESEM – environmental scanning electron microscopy	Pa – pascal
eV – electron volt	PAN – polyacrylonitrile
EWC – Equilibrium Water Content	PAWC – polymer-associated water content
FWC – Freezing Water Content	PEG – polyethylene glycol
g - grams	PTFE – polytetrafluoroethylene
(p-)HEMA – (poly-)hydroxyethyl methacrylate	Tetra-PEG – tetra-maleimide-terminated poly-ethylene glycol hydrogels
ILWC – ice-like water content	TEGDMA – Tetraethylene glycol dimethacrylate
J/g – joules per gram	TRIS – tris(trimethylsiloxy)-3-methylacryloxypropyl silane
KCl – potassium chloride	XPS – X-ray photoelectron spectroscopy
kV – kilo volt	µS – micro-Siemens
MgCl ₂ – magnesium chloride	

List of Tables, Figures & Images

Figure 1.1 Structure of silicone polymer (Image source: Polymer Database)	14
Figure 1.2 Vinyl functional group (Image source: UCLA Chemistry & Biochemistry)	18
Figure 1.3 The Human Liver (Image Source: American Liver Foundation, 2022)	21
Figure 1.4 Haemodialysis vs hemofiltration (Image source: Forni & Hilton, 1997)	22
Figure 1.5 example DSC trace, thermogram representing freezing water in green (Image source: author's own)	25
Figure 1.6 schematic of the apparatus used to measure water permeability (Image source: Fujiyabi et al, 2017)	26
Table 2.1 Specifications of reagents & salts used	28
Table 2.2 Structures of chemicals	29
Table 2.3 Synthesis conditions for each hydrogel set	30
Table 2.4 Formulations of E & F hydrogels: set 1-3	30
Figure 2.1 Schematic of mould used during hydrogel synthesis (Image source: author's own)	31
Figure 2.2 Permeation rig set-up, labelled (image source: author's own)	32
Figure 2.3 Schematic representation of permeability cell (Image source: Hamilton et al, 1988)	33
Table 3.1 Formulations of E & F Hydrogels	43
Table 3.2 EWC values for hydrogels E1 to E7 of sets 1-3 (n=4) (brackets indicate standard deviation)	44
Table 3.3 EWC values for hydrogels F1-F3 of sets 1-3 (n=4) (brackets indicate standard deviation) ..	44
Figure 3.1 hydrogel F3 EWC from set 1-3	45
Figure 3.2 hydrogel F1 EWC from set 1-3	45
Figure 3.3 hydrogel F2 EWC from set 1-3	46
Table 3.4 Freezing water contents of E hydrogels in sets 1-3 (n=9) (brackets indicate standard deviation)	48
Table 3.5 Non-freezing contents of E hydrogels in sets 1-3 (n=9) (brackets indicate standard deviation)	48
Figure 3.5 Freezing and non-freezing water contents of set 1 E hydrogels	49
Figure 3.6 Freezing and non-freezing water contents of set 2 E hydrogels	49
Figure 3.7 Freezing and non-freezing water contents of set 3 E hydrogels	50
Table 3.6 Freezing water contents for the F hydrogels sets 1-3 (n=9) (brackets indicate standard deviation)	50
Table 3.7 Non-freezing water contents for the F hydrogels set 1-3 (n=9) (brackets indicate standard deviation)	50
Figure 3.8 FWC & NFWC of F hydrogels: set 1	51
Figure 3.9 FWC & NFWC of F Hydrogels: set 2	51
Figure 3.10 FWC & NFWC of set 3 hydrogels	52
Figure 3.11 DMA content (%) vs EWC (%) – E hydrogels of set 1	53
Figure 3.12 NVP content (%) vs EWC (%) – E hydrogels of set 1	54
Figure 3.13 DMA content (%) vs EWC (%) – E hydrogels of set 2	55
Figure 3.14 NVP content (%) vs EWC (%) – E hydrogels of set 2	55
Figure 3.15 DMA content (%) vs DMA content (%) – E hydrogels of set 3	56
Figure 3.16 NVP content (%) vs EWC (%) – E hydrogels of set 3	56

Figure 3.17 DMA content (%) vs FWC (%) – E hydrogels of set 1	57
Figure 3.18 DMA content (%) vs FWC (%) – E hydrogels of set 2	57
Figure 3.19 DMA Content (%) vs FWC (%) – E hydrogels of set 3	58
Figure 3.20 NVP Content (%) vs NFWC (%) – E hydrogels of set 3	59
Figure 3.21 DMA Content (%) vs NFWC (%) – E hydrogels of set 3.....	59
Figure 3.22 Water molecule & its electron pairs (source: Narichika Honda, Spring 8).....	61
Figure 3.23 DSC thermogram of hydrogel E3 (set 2). Thermogram shown, black line separating peaks.	61
Figure 3.24: Set 1 Hydrogels: Water Structuring	62
Figure 3.25: Set 2 Hydrogels: Water Structuring	63
Figure 3.26: Set 3 Hydrogels: Water Structuring	63
Image 4.1 schematic representing hydrogel polymer matrix and how an aqueous solute could interact with the network (Image source: Liu et al, 2015).....	68
Table 4.1 Partition Coefficients for E Hydrogels of Set 1 (brackets indicate standard deviation).....	69
Table 4.2 Partition Coefficients for F Hydrogels of Set 1 (brackets indicate standard deviation).....	69
Table 4.3 Partition Coefficients for E Hydrogels of Set 2 (brackets indicate standard deviation).....	69
Table 4.4 Partition Coefficients for F Hydrogels of Set 2 (brackets indicate standard deviation).....	70
Table 4.5 Partition Coefficients for E Hydrogels of Set 3 (brackets indicate standard deviation).....	70
Table 4.6 Partition Coefficients for F Hydrogels of Set 3 (brackets indicate standard deviation).....	70
Image 4.2: Variations in hydrodynamic radii of ions (Image source: Railsback, 2006)	73
Figure 4.1 Set 1 - CaCl ₂ Partition Coefficient vs EWC (expanded view).....	75
Figure 4.2 Set 1 - KCl Partition Coefficient vs EWC (expanded view).....	75
Figure 4.3 Set 1 - NaCl Partition Coefficient vs EWC (expanded view)	76
Figure 4.4 Set 1 - MgCl ₂ Partition Coefficient vs EWC (expanded view)	76
Figure 4.5 Set 2 – CaCl ₂ Partition Coefficient vs FWC (%)	79
Figure 4.6 Set 2 E Hydrogels – CaCl ₂ Partition Coefficient vs NFWC (%).....	80
Figure 4.7 Set 1 E Hydrogels – KCl Partition Coefficient vs ILWC (%)	82
Figure 4.8 Set 2 E Hydrogels – CaCl ₂ Partition Coefficient vs ILWC (%).....	83
Figure 4.9 Set 3 E Hydrogels – MgCl ₂ Partition Coefficient vs ILWC (%)	84
Figure 4.10 Set 1 E Hydrogels – MgCl ₂ Partition Coefficient vs PAWC (%).....	85
Figure 4.11 Set 2 E Hydrogels – KCl Partition Coefficient vs PAWC (%).....	85
Figure 4.12 Set 1 E Hydrogels – NaCl Partition Coefficient vs DMA Content (%).....	87
Figure 4.13 Set 1 E Hydrogels – KCl Partition Coefficient vs DMA Content (%).....	87
Figure 4.14 Set 1 E Hydrogels – MgCl ₂ Partition Coefficient vs DMA Content (%).....	88
Figure 4.15 Set 2 E Hydrogels – CaCl ₂ Partition Coefficient vs DMA Content (%).....	89
Figure 4.16 Set 3 E Hydrogels – CaCl ₂ Partition Coefficient vs DMA Content (%).....	90
Figure 4.17 Set 3 E Hydrogels – KCl Partition Coefficient vs DMA Content (%).....	90
Figure 4.18 KCl Partition Coefficient: Hydrogel F1 – all sets.....	91
Image 5.1 Schematic of Franz Cell (image source: PermeGear, Inc., 2015)	95
Image 5.2 Schematic of Side-Bi-Side Cell (image source: PermeGear, Inc., 2019)	95
Table 5.1 Permeation Coefficients for E hydrogels of Set 1 (brackets indicate standard deviation)....	97
Table 5.2 Permeation Coefficients for F hydrogels of Set 1 (brackets indicate standard deviation)	97
Table 5.3 Permeation Coefficients for E hydrogels of Set 2 (brackets indicate standard deviation)....	98

Table 5.4 Permeation Coefficients for F hydrogels of Set 2 (brackets indicate standard deviation)	98
Table 5.5 Permeation Coefficients for E Hydrogels of Set 3 (brackets indicate standard deviation) ...	98
Table 5.6 Permeation Coefficients for F hydrogels of Set 3 (brackets indicate standard deviation)	99
Table 5.7 Diffusion Coefficients for E Hydrogels of Set 1 (brackets indicate standard deviation)	99
Table 5.8 Diffusion Coefficients for F Hydrogels of Set 1 (brackets indicate standard deviation)	100
Table 5.9 Diffusion Coefficients for E Hydrogels of Set 2 (brackets indicate standard deviation)	100
Table 5.10 Diffusion Coefficients for F Hydrogels of Set 2 (brackets indicate standard deviation)	100
Table 5.11 Diffusion Coefficients for E Hydrogels of Set 3 (brackets indicate standard deviation)....	101
Table 5.12 Diffusion Coefficients for F Hydrogels of Set 3 (brackets indicate standard deviation)	101
Table 5.13 Reaction conditions between sets	104
Figure 5.1 Set 1 E Hydrogels – KCl Permeation vs NVP Content (%)	105
Figure 5.2 Set 2 E Hydrogels – CaCl ₂ Permeation vs NVP Content	106
Figure 5.3 Set 2 E Hydrogels – NaCl Permeation vs NVP Content (%)	107
Figure 5.4 Set 3 E Hydrogels – CaCl ₂ Permeation vs NVP Content (%)	107
Table 5.14 Formulations of the F hydrogels	108
Figure 5.5 Hydrogel F2 Permeation Coefficients (set 1-3): CaCl ₂	108
Figure 5.6 Permeation profile of hydrogel E5 – set 1	110
Figure 5.7 Permeation profile of hydrogel E4 – set 2	111
Figure 5.8 Permeation profile of hydrogel E7 – set 2	111
Figure 5.9 Permeation profile of hydrogel E3 – set 3	112
Figure 5.10 Permeation profile of hydrogel E1 – set 3	112
Figure 5.11 Permeation profile of hydrogel F1 – set 2.....	113
Figure 5.12 Permeation profile of hydrogel E2 – set 1	114
Figure 5.13 Permeation profile of hydrogel E2 – set 2	114
Figure 5.14 Permeation profile of hydrogel E2 – set 3	115
Table 5.15 Reaction conditions of set 1, 2 & 3	115
Figure 5.15 Set 1 E hydrogels – CaCl ₂ Permeation vs EWC (%).....	117
Figure 5.16 Set 2 E hydrogels – NaCl Permeation vs EWC (%)	118
Figure 5.17 Set 1 E hydrogels – MgCl ₂ Permeation vs EWC (%)	119
Figure 5.18 Set 1 E hydrogels – KCl Permeation vs FWC (%).....	120
Figure 5.19 Set 2 E hydrogels – MgCl ₂ Permeation vs FWC (%)	121
Figure 5.20 Set 3 E hydrogels – KCl Permeation vs FWC (%).....	122
Figure 5.21 Set 2 E hydrogels – NaCl Permeation vs NFWC (%).....	124
Figure 5.22 Set 1 E hydrogels – MgCl ₂ Permeation vs ILWC (%).....	125
Figure 5.23 Set 2 E hydrogels – NaCl Permeation vs ILWC (%).....	126
Figure 5.24 Set 3 E hydrogels – KCl Permeation vs ILWC (%).....	127
Figure 5.25 Set 1 E hydrogels – NaCl Permeation vs PAWC (%).....	128
Figure 5.26 Set 2 E hydrogels – CaCl ₂ Permeation vs PAWC (%)	129
Figure 5.27 Set 1 E hydrogels – NaCl Permeation vs Partitioning	130
Figure 5.28 Set 3 E hydrogels – MgCl ₂ Permeation vs Partitioning	131
Image 6.1 Visible emission spectrum of calcium (image source: Thermo-Scientific).....	134
Table 6.1 Permeated Concentrations (ppm) of hydrogel E1 of set 2.....	136
Table 6.2 Permeated Concentrations (ppm) of hydrogel E1 of set 3.....	136

Table 6.3 Permeated Concentrations (ppm) of hydrogel E2 of set 2.....	136
Table 6.4 Permeated Concentrations (ppm) of hydrogel E2 of set 3.....	137
Table 6.5 Permeated Concentrations (ppm) of hydrogel E4 of set 3.....	137
Table 6.6 Permeated Concentrations (ppm) of hydrogel E6 of set 2.....	137
Table 6.7 Permeated Concentrations (ppm) of hydrogel F1 of set 1.....	137
Table 6.8 Permeated Concentrations (ppm) of hydrogel F3 of set 1.....	138
Table 6.9 Permeated Concentrations (ppm) of hydrogel F3 of set 2.....	138
Table 6.10 Permeated Concentrations (ppm) of hydrogel F3 of set 3.....	138
Figure 6.1 Hydrogel E4 Set 3: Multiple-ion permeation profile	139
Figure 6.2 Hydrogel F3 Set 3: Multiple-ion permeation profile	140
Figure 6.3 Hydrogel E6 Set 2: Multiple-ion permeation profile	141
Figure 6.4 Hydrogel E6 Set 2: Conductivity (μS) vs. time	142
Figure 6.5 Hydrogel F1 Set 1: Multiple-ion permeation profile	143
Figure 6.6 K^+ (intensity: 760.490) permeation profile	147
Figure 6.7 Mg^{2+} (intensity: 279.553) permeation profile	147
Image 7.1 schematic representation of environmental scanning electron microscope (Image source: Zimmermann et al, 2007).....	150
Image 7.2 schematic representation of X-ray photoelectron spectroscopy (image source: Yale University).....	151
Table 7.1 EDX data for hydrogels tested (surface).....	153
Table 7.2 EDX data for hydrogels tested (cross-section)	153
Table 7.3 XPS data for hydrogel E1 of set 1-3	154
Table 7.4 XPS data for hydrogel E4 of set 1-3	154
Table 7.5 XPS data for hydrogel E7 of set 1-3	154
Table 7.6 XPS data for hydrogel F1 of set 1-3	154
Table 7.7 Hydrogel E1 Set 1.....	156
Table 7.8 Hydrogel E1 from Set 2	157
Table 7.9 Hydrogel E4 from Set 3	158
Table 7.10 Hydrogel E6 from Set 3	159
Table 7.11 Hydrogel F1 from Set 1.....	160
Table 7.12 Hydrogel F1 from Set 2.....	161
Figure 7.3 various morphologies a phased hydrogel could express (source: Nicolson & Vogt, 2001).....	162
Image 7.4 hydrogel E4 of set 3, surface corner (image source: author's own)	164
Image 7.5 hydrogel E4 of set 3, surface view at $50\mu\text{m}$ (image source: author's own)	164
Image 7.6 hydrogel E4 of set 3, surface view at $10\mu\text{m}$ (image source: author's own)	165
Images 7.7 & 7.8 (L-R): hydrogel E4 of set 3, surface view at $2\mu\text{m}$ & 500nm (image source: author's own).....	165
Image 7.9 hydrogel E1 of set 2, surface corner at $100\mu\text{m}$ (image source: author's own)	166
Image 7.10 hydrogel E1 of set 2, surface view at $50\mu\text{m}$ (image source: author's own)	166
Images 7.11 & 7.12 (L-R): hydrogel E1 of set 2, surface view at $5\mu\text{m}$ & $1\mu\text{m}$ (image source: author's own).....	167
Image 7.13 hydrogel F1 of set 2, surface view at $100\mu\text{m}$ (image source: author's own)	168
Image 7.14 hydrogel F1 of set 2, surface view at $50\mu\text{m}$ (image source: author's own)	168

Images 7.15 & 7.16 (L-R) surface view of hydrogel F1 set 2 + magnified view of same surface at 20 & 10µm respectively (image source: author's own)	169
Table 7.13 descriptions of the physical appearance of each hydrogel.....	171
Image 7.17 schematic detailing the valence shells for different elements and the energy transfer that occurs during ionisation (image source: Microscopy Australia, 2014).....	172
Table 7.14 theoretical compositions of hydrogels E1, E4, E6, E7 & F1 in a dehydrated state.....	173
Figure 7.1 Hydrogel F1 (sets 1-3) surface elemental composition via XPS analysis	174
Figure 7.2 Hydrogel E1 (sets 1-3) surface elemental composition via XPS analysis	175
Figure 7.3 Hydrogel E4 (set 1-3) surface elemental composition via XPS analysis.....	175
Figure 7.4 Hydrogel E7 (set 1-3) surface elemental composition via XPS analysis.....	176
Figure 7.5 schematic representing different types of co-polymers influenced by reactivity ratios	177
Table 8.1 Synthesis conditions for each hydrogel set	179
Figure 8.1 Conventional techniques to mechanically characterize hydrogels: (a) strip extensometry; (b) ring extensometry; (c) compression test; (d) bulge test; (e) indentation (F = force, P = pressure) (Image source: Ahearne et al, 2008)	182

List of Equations

Equation 2.1 Equilibrium Water Content.....	35
Equation 3.1 Freezing Water Content.....	46
Equation 3.2 Normalised area of endotherm.....	47
Equation 3.3 Non-freezing Water Content.....	47
Equation 4.1 Partition Coefficient.....	67
Equation 5.1 Diffusion Coefficient.....	99
Equation 5.2 Permeation Coefficient.....	103
Equation 7.1 Reactivity Ratio.....	176

1 Introduction

Hydrogels are defined as polymer networks that have the ability to absorb and retain large amounts of water without dissolving. This retention is often connected to the ability of a hydrogel to simulate the surrounding tissue around them (Qiu et al, 2003) which means they are often considered as biomaterials: materials that are able to come into contact with human tissue without triggering an immunological response (Williams, 2009). Hydrogels are also used as membranes – hydrated porous media for a broad range of applications (Yazdi et al, 2020). The combination of the material's water-absorbing ability, biocompatibility and porous structure makes them highly valuable for use in separation techniques, such as in the food manufacturing industry, water desalination, and in the gas separation industry but they are also a key material in the biomedical devices industry.

Silicone-based hydrogels are most commonly used in contact lenses. The material was developed to address the need for a contact lens with increased oxygen transmission to the cornea of the eye. Conditions linked with hypoxia – a state in which oxygen is not available in sufficient amounts at tissue level to maintain adequate homeostasis (Bhutta et al, 2021) – at the surface of the eye were associated with contact lens wear at the time (Mandell & Polse, 1970).

The hydrogels synthesised and discussed in this thesis can be described as self-assembly hydrogels. These hydrogels are formed by the spontaneous self-assembly of monomeric components into polymeric structures via non-covalent interactions and such hydrogels have been considered to be more suitable for biomedical applications due to their biocompatibility (Rajbhandary & Nilsson, 2016).

Silicon itself is a chemical element, represented by the symbol Si. The element is ubiquitous in nature and forms the basis of the silicone polymer. Silicone is a synthetic polymer consisting of silicon, oxygen, carbon and hydrogen. This polymer has low intermolecular forces and the bonds between silicon and oxygen along the backbone are relatively unhindered (Clarson & Semlyen, 1993). This material is often referred to as silicone rubber. The high flexibility of the silicon-oxygen chain in the silicone polymer provides free volume through which gas can diffuse (Warrick et al, 1979). Gases are soluble in rubber/rubber-like materials. Dissolution of gases occurs at the surface of these materials and the dissolved gas molecules are able to diffuse through (Zhang & Cloud, 2006). The permeation of gases through silicone rubber membranes occurs in 3 steps: dissolution, diffusion, and evaporation out of the membrane. The hydrophobicity of the material is brought about by the hydrophobic methyl side groups along the chain that are in constant rotation (Holly & Refojo, 1975).

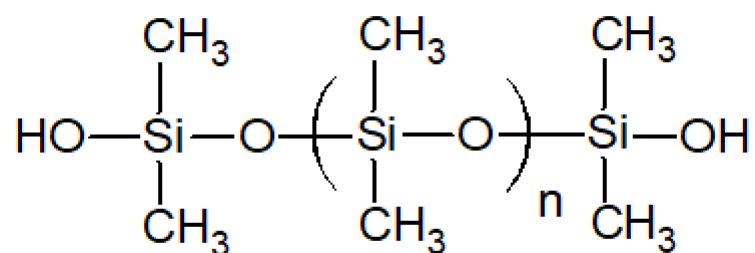


Figure 1.1 Structure of silicone polymer (Image source: Polymer Database)

Permeation studies on the silicone polymer often pertain to gas permeability as opposed to ion permeability, although studies are emerging in the area of the latter. It is still important to understand how gas permeation functions in these materials, with the hope of the mechanisms for the phenomena being applicable to ion permeation as well.

Biomedical applications refer to the use of technology and engineering to living beings, especially the design and employment of medical equipment (Khosrow-Poor, 2014). Two-dimensional materials have a high surface area-to-volume ratio and are able to facilitate interfacial phenomena such as the transport of solutes at the surface (Nguyen et al, 2020). Such a description could apply to a hydrogel, making them a promising candidate for use in biomedical technologies that rely on transport and separation principles.

The purpose of this PhD project was to synthesise multiple sets of silicone-containing hydrogels, inspired by formulations that are utilised in contact lens manufacturing. The use of specific monomer combinations and ratios is to ensure the self-assembly of the siloxy units does not extend in a manner that impairs optical clarity of the final hydrogel (Saez-Martinez et al, 2020). The characteristics of the hydrogels were experimentally determined, including permeation. Establishing the permeation behaviour of the hydrogels would begin to highlight their suitability for applications that operate on the basis of the separation and release of solutes.

This thesis consists of eight chapters: introduction, materials & methodology, water content, partition coefficient, single-salt permeation, multiple-salt permeation, membrane characteristics and summary & future works. The introductory chapter includes a literature review in which the fundamental principles and aspects of the project will be discussed, such as the parameters that the project sets out to investigate, as well as a brief history into hydrogels and their evolution. Developments with self-assembly hydrogels will also be discussed as well as certain biomedical applications that may be suitable for the synthesised hydrogels to be included in.

Chapter two describes the methods for experimental techniques used during hydrogel characterisation, an explanation of their synthesis, formulation and reagents utilised throughout the PhD project. Chapter three focuses on the water content of the hydrogels, the different types of water found within them and the relationships of these water types with the formulation of the hydrogels. Chapter four discusses the partitioning behaviour of the hydrogels against the different chloride salts, specific patterns of behaviour seen per hydrogel set/series and relationships between their partition coefficients and water content, formulation, etc.

Chapter five looks at the permeation patterns and behaviours of the hydrogels towards the chloride salts on a singular basis and how this could have been affected by previously established characteristics of the hydrogel. Chapter six analyses the permeation behaviours of selected hydrogels towards the same chloride salts but within a mixture, i.e., all the salts at once. Chapter seven discusses the elemental composition and imaging of selected hydrogels as seen derived from elemental analysis and

microscopic work. Lastly, chapter eight ties together all the results discussed throughout the thesis and makes suggestions for future works necessary to consolidate the outcome further.

1.1 Literature Review

1.1.1 Hydrogels

The term “hydrogel” was first seen in scientific literature in the early 1900s but it was used to describe a colloidal gel, which is a substance consisting of a solid particle network and a liquid solvent made from inorganic salts (Institute of Industrial Science, 2019). In 1960, Wichterle & Lim were the first to utilise the term in the context that it is known for today. They reported the synthesis of a polyhydroxyethyl methacrylate (pHEMA) hydrogel with the intended use of being in contact with human tissue (Wichterle & Lim, 1960). They discovered this polymer was able to produce hydrogels that met the fundamental requirements of synthetic materials that could be in contact with human tissue. Such a requirement included being permeable towards water-soluble substances like salts, proteins and oxygen as well as being resistant to enzymatic degradation (Mahon & Lipps, 1971). These hydrogels are considered to be the first generation of hydrogels.

Generally, the development of hydrogels can be categorised into three stages: the first, second and third generation. The first generation of hydrogels were synthesised to understand what combination of cross-linking procedures, monomers and initiator would develop a material with a high-water affinity and desirable mechanical properties. These hydrogels were synthesised via addition polymerisation, in which new monomer units are added onto the growing polymer chain through the double or triple bonds on a monomer (McKeen, 2015).

The first-generation hydrogels, made from pHEMA, began to be used widespread as contact lenses but, soon the *N*-vinyl-2-pyrrolidone (NVP) monomer was employed as a co-monomer alongside hydroxyethyl methacrylate (HEMA) due to its superior biocompatibility. This resulted in contact lenses with enhanced oxygen permeability and wettability, but this particular combination of monomers produced hydrogels that were inconsistent in their quality due to the large differences in the reactivity ratios of the monomers. These hydrogels tended to have varying water content and modulus/tensile stiffness (Lai, 1997). By the late 1970s, alternative monomer families were being tested for their suitability, including acrylamides and other methacrylate monomers (Buwalda et al, 2014).

The second generation of hydrogels were concerned with developing materials that could respond to stimuli such as temperature, pH and changes in concentration of substances in its surroundings (Kopeček, 2009). The intent behind this generation was to develop a suitable material for drug delivery processes (Chirani et al, 2015; Buwalda et al, 2014). The inspiration for such a hydrogel was brought about by the early works of Kuhn et al (1950), which contemplated the possibility of chemical energy transfer into mechanical work. It was theoretically predicted that the degree of swelling of a hydrogel could be changed by external conditions (Dušek & Patterson, 1968) which was later confirmed experimentally by other laboratories (Tanaka, 1978; Suzuki & Tanaka, 1990). Different monomers under different conditions showcased varying behaviours: hydrogels containing methacrylic acid showcased

G.Durowoju, PhD Thesis, Aston University 2022.

an increased permeability towards sodium chloride under alkaline conditions, whereas hydrogels containing *N,N*-dimethylaminoethyl methacrylate showed increased permeability under acidic conditions (Kopeček et al, 1971).

The third generation of hydrogel advancement aimed to develop complexed materials i.e., joining multiple polymer systems together via physical cross-linking methods to enhance certain characteristics of a polymer in conjunction with another (Chung et al, 2008). This was considered to be a progression from the second generation hydrogels as the cross-links in those gels were mainly via hydrophobic and ionic interactions. The third generation of hydrogels aimed to develop gels that were cross-linked via peptide interactions and metal-ligand coordination (Buwalda et al, 2014).

More specifically, silicone-based hydrogels can also be categorised into first and second generations. In the late 1970s, silicone rubber was included in contact lenses due to their high oxygen permeability – these were considered the first generation. However, the hydrophobicity of the material meant that any resulting contact lenses tended to have little to no water. This would cause the lens to stick to the surface of the eye, causing discomfort for the wearer (Chou, 2008). Second generation silicone-based hydrogels made use of silicone monomers and hydrophilic monomers such as HEMA to combine increased oxygen permeability with the fluid transport properties of the other monomers. This made contact lenses that were more comfortable for the wearer due to the increased water content of the hydrogels (Iskeleli et al, 2013).

The rate of gas permeation in silicone rubber is dependent on the solubility and diffusion rate of a given gas (Van Amerongen, 1951). Although the factors described below relate to gas permeability, they are applicable to ion permeability as well. Factors that could affect the permeability of silicone rubber include:

- The type of gas: as diffusivity depends on size and solubility, different types of gas will result in different levels of permeation. Diffusivity is related to size whilst solubility is related to the charge of both the gas and the silicone rubber matrix (Warrick et al, 1979).
- Formulation: silicone rubber has low intermolecular forces and the bonds that link silicon and oxygen together are relatively unhindered, allowing for a high degree of rotation of the polymer chain. However, the introduction of functional groups along the siloxane chain has been linked to a reduction in permeability as solubility of gases is considered to be more influential than diffusion (Polmanteer, 1981).
- Thickness & area: this relates to the silicone rubber membrane itself. A thicker membrane results in less gas diffusion whereas a smaller membrane area can also result in lesser diffusion (Zhang & Cloud, 2006).

Another definition used to describe a hydrogel is a water-swollen polymeric material that maintains a distinct three-dimensional (3D) structure due to cross-linking (Chai et al, 2017). They can be classified as natural, synthetic or hybrid based on the source of their polymer (Zhu & Marchant, 2011).

Examples of natural polymers include collagen, gelatine, chitosan and alginate. Hydrogels from natural sources often have increased levels of biocompatibility but lack mechanical strength (Singh et al, 2016). Synthetic monomers often utilised in hydrogel synthesis include ethylene oxide, acrylic acid & HEMA. Hydrogels from this source often have improved physicochemical and mechanical properties that can be adjusted by reaction conditions, but some monomers are known to lack biocompatibility (Aswathy et al, 2020).

Since hydrogels are described as cross-linked networks, any method used to develop a cross-linked polymer can be used to produce a hydrogel (Ahmed, 2015). Three methods are largely used in the preparation of such polymers:

- Polymerisation via chemical reactions.
- Radiation: includes the use of ionizing radiation to generate free radicals that can act as junctions for cross-linking to occur.
- Physical cross-linking: facilitated by interactions between polymers such as entanglements, electrostatic forces and crystalline formation.

A typical polymerisation reaction requires an initiator, a monomer and a cross-linking agent. Once the hydrogel has formed, it is washed thoroughly or post-cured to remove impurities such as unreacted reagents and unwanted by-products (Jenkins, 2015). Post-curing is the process of exposing a cured object to temperatures at or above the temperature at which it was synthesised for an extended period (Moller et al, 2020).

In the case of this project, the hydrogels were synthesised via free radical polymerisation, making use of 2,2'-azobis(2-methylpropionitrile) (AIBN) as the initiator. This technique is often used with monomers that possess vinyl groups (shown in Figure 1.2) and the hydrogels that are produced are oftentimes permanently cross-linked (Min et al, 2015). Monomers are added to the polymer chain by being turned into reactive radicals via the carbon double bond. The hydrogels are also considered to be self-assembled as they are built from co-polymers that are driven by hydrophobic interactions to create blocks along the polymer chain (Serero et al, 1998).

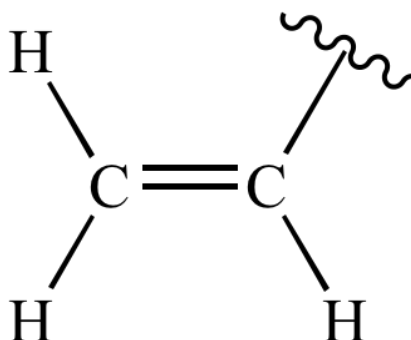


Figure 1.2 Vinyl functional group (Image source: UCLA Chemistry & Biochemistry)

One of the hydrophilic monomers included in the formulation of the synthesised hydrogels in this project was *N*-vinyl-2-pyrrolidone (NVP). This is a synthetically sourced monomer consisting of a 5-membered lactam ring with a vinyl group attached to the nitrogen on the ring. Its melting point is around 13.5°C and boiling point is between 90-93°C (Gerhartz, 1988).

The other hydrophilic monomer used was *N,N*-dimethylacrylamide (DMA). This is also a synthetic monomer consisting of a 2-carbon chain with an ester group on one end and an amine group on the other. Its boiling point is 171°C and it freezes at temperatures below -40°C (KJ Chemicals Corp., 2017).

Lastly, tris(trimethylsiloxy)-3-methylacryloxypropyl silane (TRIS) is the hydrophobic monomer and silicone component of the synthesised hydrogels. This compound is made up of methacrylate and siloxane groups. It has a boiling point between 112-115°C (Merck, 2022). TRIS is a commonly used monomer often added to hydrogel formulations as it maintains/improves oxygen permeability and reduces the modulus of the final hydrogel by reducing the cross-linking density (Lai, 1995).

The formulation of the synthesised hydrogels was heavily influenced by that of a typical contact lens formulation. Silicone-based hydrogels often include hydrophilic monomers in order to minimise the surface hydrophobicity as well as improve biocompatibility (Tighe, 2004). The material also has increased mechanical strength in addition to being a porous structure, which gives it an advantage over other biomaterials (Chai et al, 2017).

The synthesised hydrogels can also be described as self-assembled hydrogels, a way to describe “the spontaneous association and organisation of numerous individual units into well-defined structures without external participation” (Kopeček & Yang, 2012). This mechanism often informs the design of systems including biomaterials, which can be defined as natural, synthetic or hybrid polymers that have been designed to interact with a biological system whilst being non-toxic (Humphrey et al, 2014).

This particular type of hydrogels has been utilised heavily in drug delivery, specifically as injectables. As the hydrogels form in situ, they can be administered in a relatively non-invasive procedure to deliver therapeutic drug molecules or to transplant cells to a desired site (Chung & Park, 2009). As mentioned above, hydrogels can form from physical or chemical cross-links, but the former is considered to be more useful in this particular field due to their “mild” processing conditions and injectability (Hennink & Nostrum, 2002). Stimuli such as pH, light and temperature are used to trigger the cross-linking process and modifications can be made to monomers – such as the introduction of functional groups – to tailor the hydrogel forming process in situ (Nuttelman et al, 2008). Although these particular hydrogels exhibit stability with desirable drug release, they may contain toxic by-products such as unreacted monomers which poses an issue in terms of their clinical application (Chung & Park, 2009).

Lin et al (2015) modified a silicone-based hydrogel by incorporating chitosan and hyaluronic acid in a layer-by-layer self-assembly to improve the surface wettability and anti-protein adsorption. This technique has emerged as an efficient and versatile technique for developing biologically active surfaces in the biomedical engineering research sector, as opposed to relying on surface modification of

hydrogels. Analytical techniques such as atomic force microscopy and dyeing data was used to verify the progressive build-up of these layers on the silicone-based hydrogel.

Biodegradable self-assembled dextran-based hydrogels have been synthesised via radical polymerisation (Kim et al, 2000) with the aim of using them in drug delivery processes as well. Unlike silicone-based hydrogels, dextrans are hydrophilic and water soluble but they also display biocompatible abilities and they can be broken down by enzymes already existing in the human colon (Sery & Hehre, 1956).

These studies were highlighted to showcase the versatility of self-assembled hydrogels but it has been highlighted that their use is commonly seen in a specific industry – drug delivery and tissue engineering. It could be suggested that the hydrogels in this project could also be used in this realm as well as they fall under the umbrella of self-assembled. However, the hydrogels previously mentioned tend to be synthesised and utilised at the nano scale. A suggested application for the synthesised hydrogels of this project includes using them in a biomedical application that relies on the exchange of substances at a surface. The mechanism for gas permeation in silicone rubber as described above applies to ion permeability as well, suggesting a silicone-based hydrogel could be suitable for applications that rely on the exchange of ions, such as extracorporeal devices.

1.1.2 Biomedical Applications: Extracorporeal Devices

The intent of the study was to establish the suitability of hydrogels in biomedical applications that depend on the separation and release of substances in order to operate. This can be interpreted as an application that relies on permeating solutes within a mixture based on their size, charge, or other physical/chemical factors. An example of such an existing technology includes extracorporeal devices.

“Extracorporeal” is a medical term used to describe processes that exist outside of a body (Oxford Advanced Learner’s Dictionary, 2021). The main objective of extracorporeal devices is to provide an external replacement for a normally functioning organ and emulate its behaviour. They are designed to provide temporary relief or support to a patient if their body is unable to carry out the task on their own. The technique is able to remove toxins and waste products from the body by relying on activities such as diffusion, convection or adsorption (Lu & Xue, 2019). Usually, extracorporeal therapy is associated with renal replacement therapy (kidney support). However, advancements in technology have allowed this device to provide multiple organ support as the technique aims to treat the blood of a patient (Cruz et al, 2008). Liver disease can also be treated by using this technology and reports on therapeutic interventions for this particular disease are underreported. Based on this, liver disease will be discussed and the opportunities to improve existing extracorporeal technologies.

The liver is a major organ which serves several biological functions including detoxification of substances and metabolising drugs, the synthesis of albumin and blood clotting factors, storage of vitamins and minerals, the activation of enzymes as well as filtration of blood from the digestive tract. It is exposed to the most lethal chemicals that are ingested so it is most subject to injury but the largest internal organ in the human body has the ability to repair and regenerate itself when impaired. The liver

removes toxic substances from the body by breaking them down into smaller by-products that can be excreted from the liver via bile or blood which will eventually be filtered out of the body in urine or faeces (American Liver Foundation, 2022).

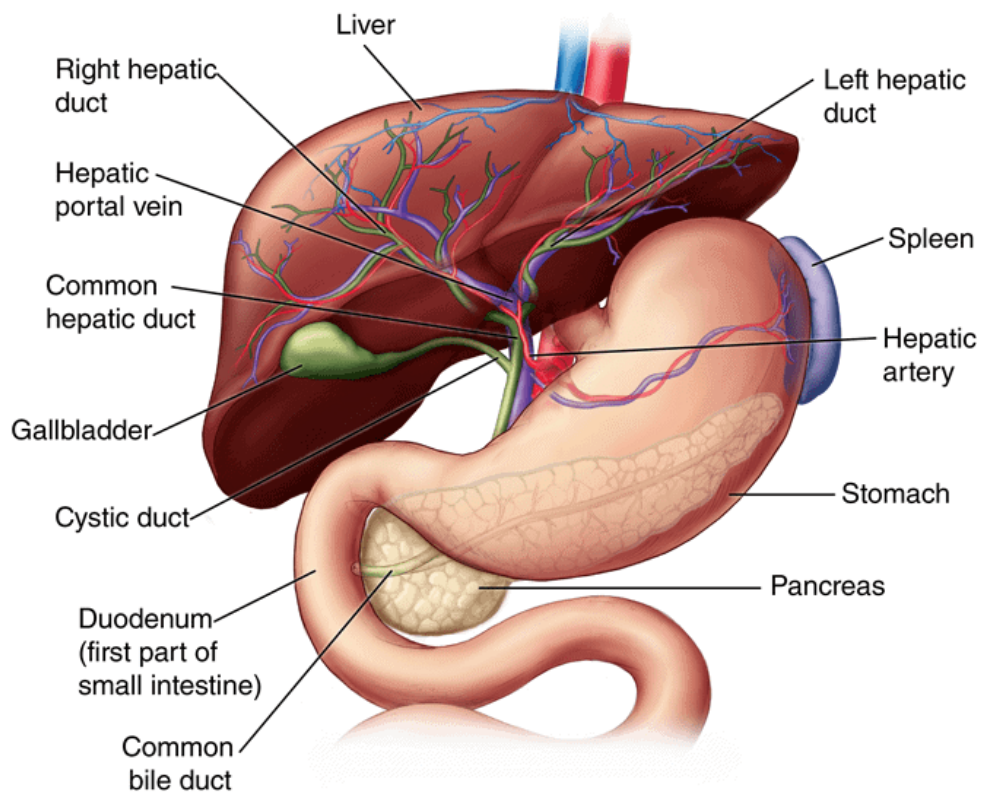


Figure 1.3 The Human Liver (Image Source: [American Liver Foundation](#), 2022)

Liver disease can be caused by several triggers including viral infection (hepatitis B/C), poor diet, autoimmune diseases, excessive consumption of alcohol and reactions to medications or toxic chemicals (Allen et al, 2016 & Tapper et al, 2018). Mortality from the disease in the United Kingdom has increased by 400% since 1970 and it is linked with increases in alcohol consumption, obesity and hepatitis C infections (Williams et al, 2014). Liver disease is also the leading cause of death in the 35-49 age group and is the third-leading cause of death in adults under the age of 65 (British Liver Trust, 2019). There is an economic impact from the disease as well – approximately 60,000 people have been diagnosed with cirrhosis in England and Wales, with 69,000 related admissions to hospital (Harris et al, 2017). In Scotland, approximately 35,000 people were admitted into hospital between 1991 and 2011 due to complications arising from the disease, costing £6664 per admission (Bouttell et al, 2016). As symptoms tend not to present until the disease has progressed, diagnosis is often late (Macpherson et al, 2022).

The progression of the disease can be broken down into four key stages (Germani et al, 2010):

1. Inflammation: at this stage, the liver becomes inflamed which is the bodily response to injury or a response to an overload in toxins.

2. Fibrosis: if inflammation is left untreated, this could lead to scarring and the excessive build-up of scar tissue on the liver is referred to as fibrosis. This scar tissue can prevent the liver from functioning as it should, and it could stop blood from flowing through the liver properly.
3. Cirrhosis: this occurs once the scar tissue starts to replace the healthy tissue of the liver. At this point, the damage that has occurred to the liver is irreversible.
4. End-stage liver disease: liver function has deteriorated to the point where the condition has become fatal unless the patient receives a liver transplant.

Treatment options for liver disease is dependent on the stage at which the intervention is made as well as the underlying cause of the disease, but options vary from medication, lifestyle changes, liver dialysis or a liver transplant.

Existing liver support technology are based on the fundamental principle of separation by size. It should not be confused with haemodialysis. The therapeutic aim of this intervention is to remove water and solutes from the blood of a patient, correct electrolyte abnormalities and acid-base disturbances (Hall & Fox, 2006). This can be achieved by hemodialysis, hemofiltration or hemodiafiltration. The key difference between each mechanism is the way solutes are removed: haemodialysis removes solutes in the blood by diffusion whilst hemofiltration relies on convection – the transport of solutes across a membrane along with the solvent (solvent drag). As a solvent is pulled across a membrane, the molecules dissolved within it are also pulled along. The driving force behind this is pressure.

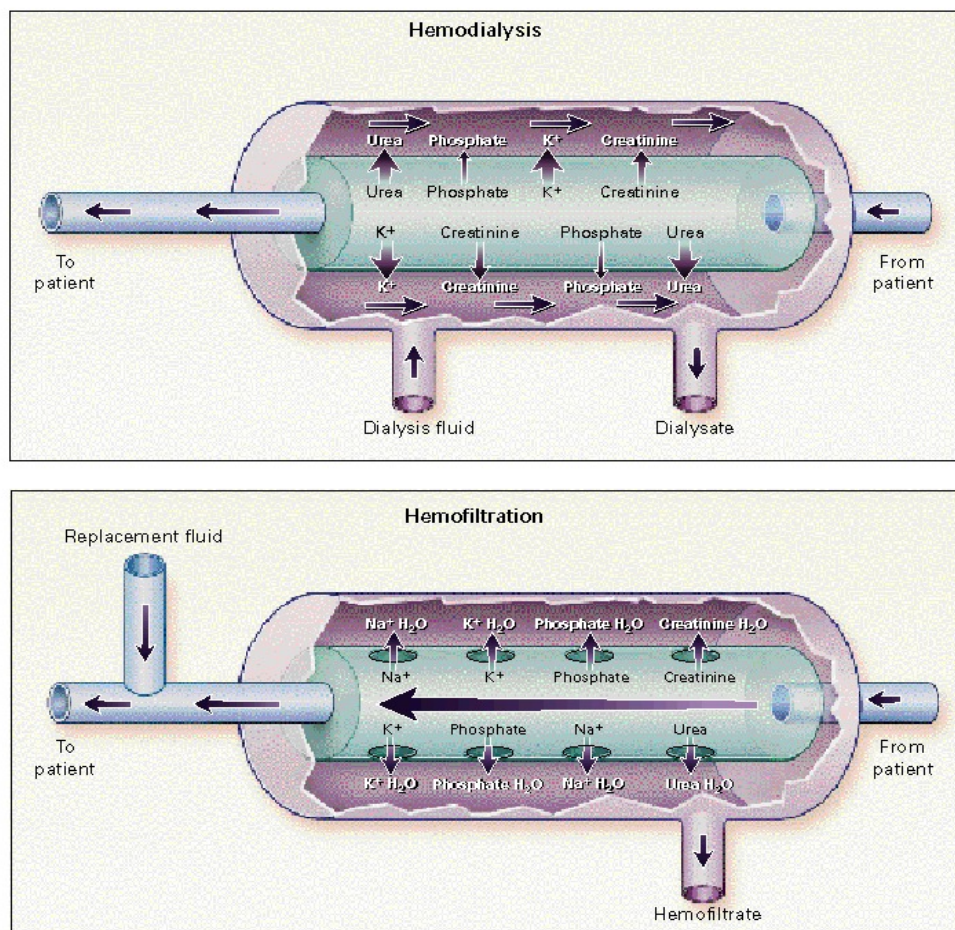


Figure 1.4 Hemodialysis vs hemofiltration (Image source: Forni & Hilton, 1997)

In the case of hemodialysis, solute clearance is dependent on concentration gradients. The solute within the blood will only leave if the fluid it is moving into has a low concentration of that particular solute. This can be affected by the size and weight of the molecule and the molecule's resistance to flow (Ledebø & Blankestijn, 2010). The membrane that facilitates movement is also said to be semi-permeable i.e., it has a criterion for the substances it will allow to pass through.

In the case of liver dialysis, the intervention is often referred to as albumin dialysis. Albumin is a globular protein that binds water, fatty acids, inorganic ions, hormones etc in the blood to regulate osmotic pressure and blood volume (Chien et al, 2017; Miller et al, 2001) and the aim is to remove toxins that a healthy liver would metabolise. Molecular Adsorbent Recirculation System (MARS) is a form of albumin dialysis that makes use of a membrane to separate the albumin solution – that has been filtered from a patient's blood – from albumin-bound toxins. The system makes use of a polysulfone hollow-fibre membrane that is 100 nm thick and flow is maintained by a concentration gradient (Boyle et al, 2004). This intervention has been established to work well at removing aromatic amino acids, fatty acids and bile acids but the larger molecules such as bilirubin, hormones and albumin-bound toxins are not removed as readily (Stange & Mitzner, 1996). The membrane also has a molecular cut-off of approximately 50 kilodaltons but the dilemma of being unable to remove larger toxins without removing vital albumin from the solution persists (Stange et al, 1999).

Another albumin dialysis intervention includes Single Pass Albumin Dialysis (SPAD). The key difference between this therapy and MARS is the “recycling” of albumin. In SPAD, the albumin is discarded after the patient's blood has been filtered whereas MARS cleanses the albumin so it can be reused by the patient (Pless, 2007). The key issue with this technique is the aspect of waste as it is more effective at reducing the amount of larger toxins from a patient's blood unlike MARS. The technique is also cheaper, costing approximately \$670 per session compared to MARS which costs around five times more (Lee et al, 2010).

Polysulfone is a polymer used in the development of thermoplastics (Sastri, 2010). They are largely used in the membranes of extracorporeal devices as they are very durable and are able to withstand the high temperatures of sterilization (Campo, 2008). However, the polymer has shown a reduced ability to remove larger toxins when used in dialysis-like settings (Stange, 2011). Current developments to extracorporeal technology are looking to increase the ease of administering the equipment to patients as well as determining what pump speeds would produce ideal clearance rates of toxins. However, it has been stated that the clearance rates of polysulfone membranes under convection or diffusion are limited (Costa et al, 2022).

Despite all of these interventions, no single system has demonstrated an effect on improving patient mortality (McKenzie et al, 2008). Structural and physicochemical changes to the membrane could possibly increase its ability to remove more toxins in an extracorporeal device setting. Although a certain type of membrane (polysulfones) is the preferred choice for these applications, it is important to suggest alternatives. Repurposing hydrogels, that are already used in biomedical applications, in a new manner could be beneficial. It also helps that silicone-based hydrogels, such as those used in contact lenses

and the basis for those developed in this project, have already demonstrated their biocompatibility. Trying different formulations and determining their characteristics could provide insight to how suitable such hydrogels would be in an extracorporeal setting. The next section of the literature review will discuss these characteristics and their importance when establishing the suitability of hydrogels in biomedical settings.

1.1.3 Characteristics Background: water content, partition coefficient, permeability, morphology

The main aim of this project was to utilise a well-known combination of synthetic polymers to create hydrogels that are commonly used in one particular biomedical application (contact lenses) and determine their suitability for another which depends on the principle of permeation (extracorporeal devices). The ability for hydrogels to be used in such applications is because they are classified as biomaterials, which are defined as synthetic or natural materials that can be used in medical applications with the intention of being the interface of biological systems, i.e., in contact with bodily fluids and/or tissues (Bandyopadhyay & Bose, 2013). Another definition of a biomaterial is a non-viable material that is used in a medical device intended to interact with biological systems to evaluate, treat, augment or replace any tissue, organ or function of the body. A biomaterial can also be a once-viable biological material that has been rendered sterile, non-immunogenic and acellular by some chemical intervention to prevent a biological response (Williams, 2009).

There are four main classes of biomaterials: polymers, metals, ceramics and composites. These materials range differently in terms of their chemical and physical structures. In the case of hydrogels, that fall under the umbrella of polymers, their ability to absorb or retain water, leading to their ability to simulate surrounding tissue gives them their biocompatibility (Hoffman, 2012). Literature often states that the water within a hydrogel can determine its permeation and solubilising ability towards solutes (Gun'ko et al, 2017) so it is important to understand the types of water present within the gels. When a newly synthesised hydrogel first comes into contact with water, the most hydrophilic groups along the polymer chains of its matrix are hydrated. Once these have been saturated, this causes the matrix to expand and the polymer chains to unwind. Unwinding of these chains exposes more groups, hydrophilic and hydrophobic, for water molecules to attach itself to. Water attached to these groups is considered to be the total bound water content of the hydrogel. Water will continue to penetrate the polymer matrix due to osmosis which causes the hydrogel to swell. However, osmosis will be opposed by the cross-links within the hydrogel structure and the hydrogel will reach a state of equilibrium swelling. This water is referred to as the equilibrium water content (EWC) of the hydrogel. EWC can be further categorised into freezing and non-freezing water, determined by the temperature at which the water freezes (Gun'ko et al, 2017). Freezing water, which freezes at 0°C, has the highest degree of mobility within a hydrogel as it is not bound to any groups along the chains of the polymer matrix.

A variety of analytical techniques can be used to estimate the different types of water within a hydrogel such as nuclear magnetic resonance, infra-red spectroscopy, x-ray powder diffraction and differential scanning calorimetry (DSC). Most of these methods depend on assumptions: in the case of DSC, it is assumed only freezing water can be frozen and the thermogram (see Figure 1.4, green section of the G.Durowoju, PhD Thesis, Aston University 2022.

graph) represents the melting of this water therefore, it represents the freezing water within the hydrogel. Bound water can then be calculated by subtracting the freezing water content (FWC) of a hydrogel from its EWC. The latter is often determined by gravimetric analysis, which is explained further in the materials & methodology chapter (2.4). The thermogram can also be used to calculate the different types of freezing water within the hydrogel such as polymer-associated water content (PAWC) and ice-like water content, which each have varying degrees of mobility but this is expanded upon in the water content chapter (3.3.2).

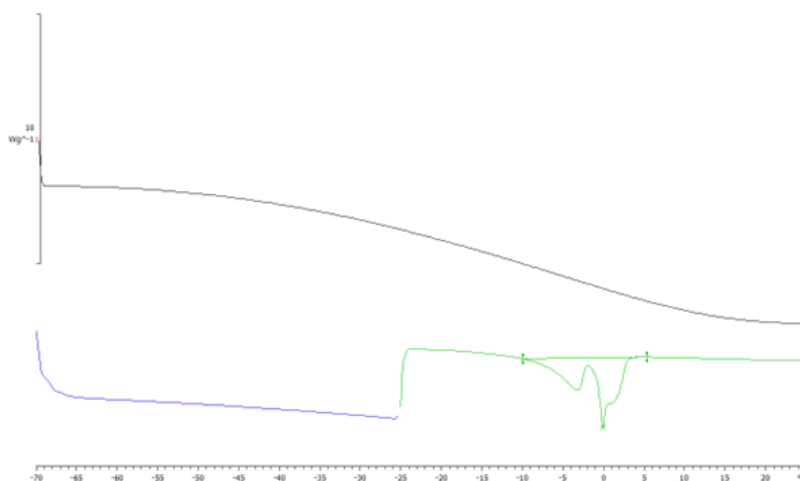


Figure 1.5 example DSC trace, thermogram representing freezing water in green (Image source: author's own)

Permeation was the next key attribute to determine with the hydrogels. These materials are already considered to be suitable for applications that depend on the diffusion of molecules due to their ability to facilitate this movement within itself (Vedadghavami et al, 2017). As the main use of silicone-based hydrogels are contact lenses, studies on their permeation behaviour often focus on gas permeability as opposed to solutes. The most commonly used technique to measure oxygen permeability in contact lenses was developed in 1971, which involved the flow of oxygen through a lens over time as pressure gradient was applied to both sides of the lens (Fatt, 1971). However, hydrogels made from other synthetic polymers are becoming more popular in tissue engineering and drug delivery applications (Kopeček, 2007) and scientists have developed techniques that can measure solute permeation.

Fujiyabu et al (2017) developed an apparatus that could measure water permeation in tetra-maleimide-terminated poly-ethylene glycol hydrogels (tetra-PEG) (see Figure 1.6). Other apparatus include the Franz diffusion cell (Salamanca et al, 2018) and the double-barrelled permeation cell (Singh et al, 2010) which was also used in this project, making use of receiver and donor cells to measure the permeation of solutes across the hydrogel. This apparatus has been described in further detail in the materials & methodology chapter (2.3.1).

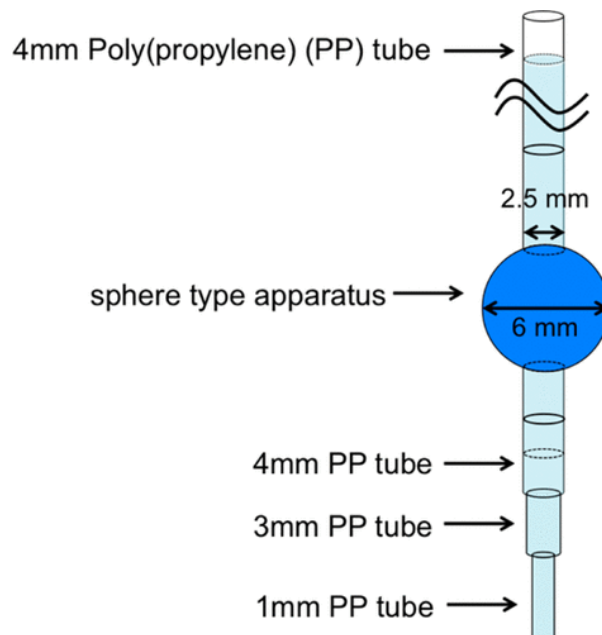


Figure 1.6 schematic of the apparatus used to measure water permeability (Image source: Fujiyabi et al, 2017)

Understanding the permeation behaviour of the hydrogels also provides insight to the pore size of the hydrogels. The molecules that are permeated through give an indication of what is able pass through the pores of the hydrogel. Probe solute permeation has been reported as a useful method for this very purpose, in which solutes within a range of molecular weights are labelled with fluorescent tags and are monitored as they travel through a hydrogel (Dong et al, 1994).

Mathematical models have been derived in a bid to explain how permeation occurs within hydrogels including hydrodynamic drag, free volume theory and obstruction effects (Amsden, 1998). Free volume theory assumes the interconnectivity of microporous structures within a hydrogel can influence solute permeability (Gun'ko et al, 2017). This ties into the morphology experiments that were conducted on the hydrogels using techniques such as environmental scanning electron microscopy (ESEM) to produce images of their surfaces, in the hope of providing evidence of these structures caused by phase separation at the micro-level (Hoffman, 2012).

Partition coefficient relays whether a species prefers to dwell within a hydrogel or in its environment (solution) (Dursch et al, 2014). This coefficient is often used when characterising hydrogels for inclusion in drug delivery systems to develop release profiles (Pimenta et al, 2016). Molecules could dwell within the hydrogel for several reasons:

- Adsorption
- Charge interactions between the molecule and the polymer matrix as well as hydrogen bonding and van der Waal forces (Su et al, 2019)
- Size exclusion due to the mesh size of the hydrogel network (Kotsmar et al, 2012, Russell & Carta, 2005)

The coefficient also relays evidence relating to the solubility of molecules within the polymer matrix of the hydrogel. Fluorescent tagging techniques have been reported to measure this coefficient but again, gravimetric analysis/back-end extraction is also suitable, and the procedure used has been documented in the materials & methodology chapter (2.5). However, this technique has been criticized for being unable to provide information about the spatial distribution of a solute throughout a hydrogel, i.e., whether the partition coefficient is representative of the entire hydrogel sample or just reports the accumulation of a solute in a particular section (Su et al, 2019).

1.1.4 Scope of Study

As detailed in the literature review, there is a need to contribute to knowledge relating to silicone-based hydrogels in regard to their solute permeability, further the understanding of their water structure, how phase separation occurs and the effects this can have on the hydrogel's overall morphology and partitioning abilities. The review also outlined how existing biomedical applications, such as extracorporeal devices that rely on the separation and release mechanisms of a membrane, also have shortcomings when it comes to the clearance of toxins, especially larger ones like albumin-bound toxins. Identifying the gaps in knowledge related to silicone-based hydrogels alongside recognising the need to improve the efficacy of extracorporeal devices presented an opportunity to fulfil two key tasks with this thesis:

- Demonstrate how differences in the formulation of silicone-based hydrogels could influence their characteristics such as water content & structure, partitioning behaviours, morphology, and their ability to permeate substances on the principle of size and/or charge.
- Deduce the suitability of these synthesised hydrogels for use as membranes in biomedical applications that depend on separation by size and/or charge to fulfil their purpose.

The core story of the thesis is to show how hydrogel formulations typically seen in contact lens manufacturing can produce hydrogels that are permeable to ionic salts and whether their size and/or charge will result in feasible differences in permeation from one to the other. Morphology studies on a selected range of hydrogels will show how differences in monomer combinations and reaction conditions can influence the appearance of phase separation or the expression of elements at the surface of the hydrogels. By understanding the parameters listed above, it will suggest whether the notion of repurposing hydrogels for different biomedical applications is a path worth pursuing.

The overarching aim is to demonstrate how alterations in the formulation of silicone-based hydrogels as well as the reaction conditions the hydrogels are exposed to during the polymerisation reaction, could bring about differences in their characteristics as mentioned above. Based on these observations, recommendations will be made for the suitability of specific hydrogels to be potentially used as membranes in biomedical applications like extracorporeal devices or other suitable uses. However, this thesis should be seen as the foundation for future endeavours that will lead to the ultimate goal of improving the clearance of toxins by membranes used in such devices, with suggestions for continuous experimentation that will further drive this research forward.

2 Materials & Methodology

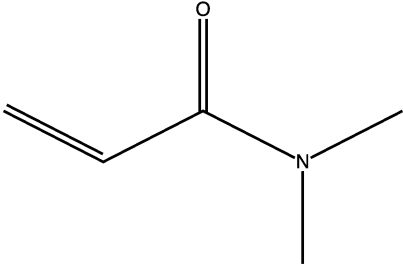
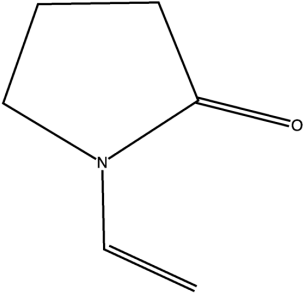
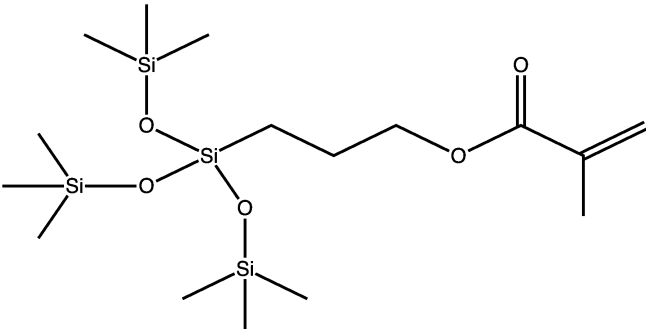
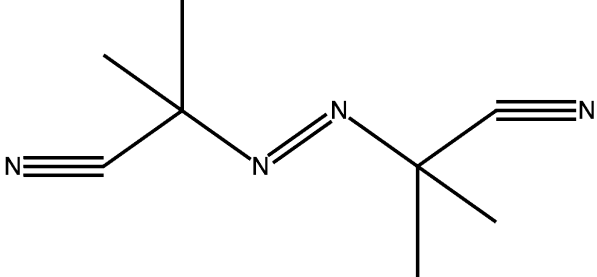
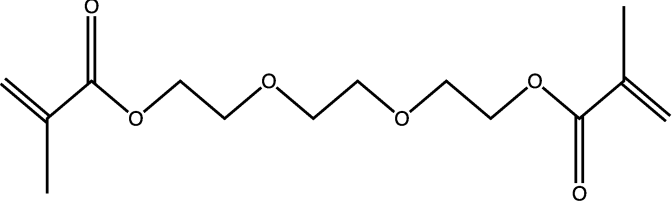
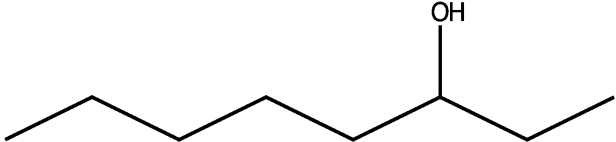
2.1 Chemicals

All reagents utilised are listed in Table 2.1. Their molecular structures, where applicable, can be found in Table 2.2. Chemicals were used as purchased. Monomers and components used in hydrogel synthesis were stored in a refrigerator until required. Salts were stored in a dark place at room temperature and atmospheric pressure. Deionised water used was sourced from a Purite™ Select Analyst Lab Deionisation Unit.

Table 2.1 Specifications of reagents & salts used

Reagent	Supplier	CAS No. / EC No.	Molecular Weight
2,2'-Azobis(2-methylpropionitrile) (98%)	Sigma-Aldrich	78-67-1	164.21
<i>N,N</i> -dimethylacrylamide (99%, contains 500 ppm monomethyl ether hydroquinone as inhibitor)		2680-03-7	99.13
<i>N</i> -vinyl-2-pyrrolidone (>99%, contains sodium hydroxide as inhibitor)		88-12-0	111.14
Tetraethylene glycol dimethacrylate (>90%, contains 0.006% hydroquinone as stabilizer)		109-17-1	330.37
3-octanol (>97%)		589-98-0	130.23
Calcium Standard for AAS		69349-250ML	n/a
Magnesium Standard for AAS		42992-250ML	n/a
Tris(trimethylsiloxy)-3-methylacryloxypropyl silane (high purity)	PCR Inc.	n/a	422.82
Calcium chloride (fused, granular, general purpose grade)	Fisher Chemical	10043-52-4	110.98
potassium chloride (>99%, laboratory reagent grade)		7447-40-7	74.55
Sodium chloride (>99.5%, laboratory reagent grade)		7647-14-5	58.44
Magnesium chloride (nitrogen flushed, pure)	ACROS Organics	7786-30-3	95.21
Potassium, AAS standard solution, Specpure, K 1000µg/ml liquid (KNO ₃ in 5% HNO ₃)	Alfa Aesar	231-714-2	n/a
Sodium, AAS standard solution, Specpure, Na 1000µg/ml liquid (Na ₂ CO ₃ in 5% HNO ₃)			

Table 2.2 Structures of chemicals

Chemical	Molecular Structure
<p><i>N,N</i>-Dimethylacrylamide (DMA)</p>	
<p><i>N</i>-vinyl-2-pyrrolidone (NVP)</p>	
<p>Tris(trimethylsiloxy)-3-methylacryloxypropyl silane (TRIS)</p>	
<p>2,2'-Azobis(2-methylpropionitrile) (AIBN)</p>	
<p>Tetraethylene glycol dimethacrylate (TEGDMA)</p>	
<p>3-octanol</p>	

2.2 Hydrogel Synthesis

Three sets of hydrogels were synthesised for study: set 1, set 2 and set 3. The key difference from one set to another was the use of a diluent and the inclusion of a 90 °C post-cure after the initial 60 °C synthesis cure. Table 2.3 details the exact conditions assumed under each set. The synthesised hydrogels were formulated from two hydrophilic monomers, a silicone monomer, a cross-linking agent, an initiator and a diluent (where applicable).

Table 2.3 Synthesis conditions for each hydrogel set

Condition	Set 1	Set 2	Set 3
72-hour synthesis @ 60 °C	Yes	Yes	Yes
3-hour post-cure @ 90 °C	No	Yes	Yes
Use of 3-octanol as diluent	E series – yes F series – no	No	Yes

Two sets of hydrogels were synthesised per set of reaction conditions: the E series and the F series. With the exception of hydrogels E1 and E7, the E series utilised both DMA and NVP as monomers in addition to TRIS. As DMA content increased down the series, NVP content decreased. Every other component of the hydrogel's formulation was kept constant. The F series made use of either DMA or NVP in addition to TRIS. Across both series, where applicable, AIBN was used as an initiator (0.05 g for E hydrogels, 0.1g for F hydrogels), TEGDMA as a cross-linking agent (0.1 g for E hydrogels, 0.2 g for F hydrogels) and 3-octanol as a diluent. The ratio of the monomers and diluent are listed in Table 2.4.

Table 2.4 Formulations of E & F hydrogels: set 1-3

Hydrogel	Formulations (wt. %)			
	DMA	NVP	TRIS	3-octanol
E1	0%	60%	35%	5% (in set 1 & 3 only)
E2	10%	50%		
E3	20%	40%		
E4	30%	30%		
E5	40%	20%		
E6	50%	10%		
E7	60%	0%		
F1	-	30%	65%	5% (in set 3 only)
F2	-	70%	25%	
F3	70%	-		

The hydrogels were prepared using bulk free radical polymerisation without the use of a solvent. The monomers, cross-linking agent and diluent (when applicable) were measured and added to a reaction vessel to be stirred until all the components had dissolved. Once dissolved, nitrogen was bubbled through the reaction mixture for 1 minute to displace oxygen. The reaction mixture was then injected into moulds consisting of two glass plates (measurements: 12.7 cm x 10 cm) onto which a Melinex® sheet was adhered on each plate. The plates were separated by a purpose-made polyethylene gasket and held together by a combination of spring clips, illustrated in Figure 2.1.

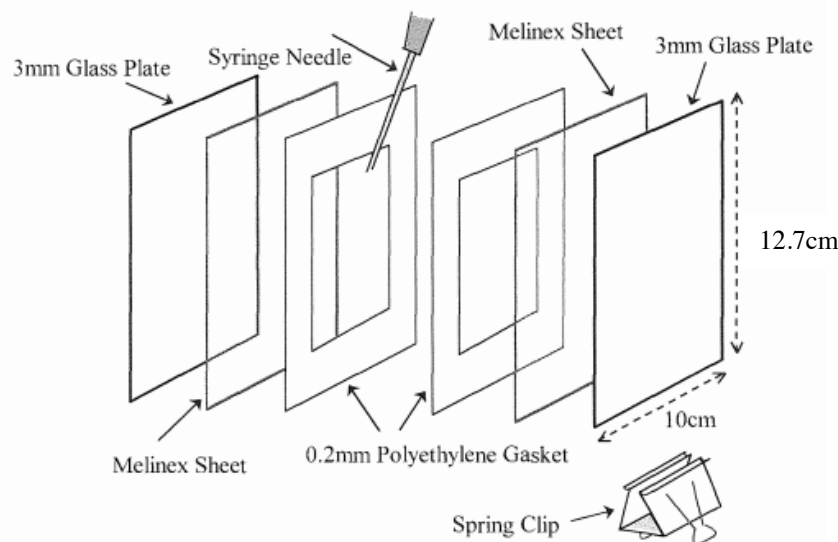


Figure 2.1 Schematic of mould used during hydrogel synthesis (Image source: author's own)

Whilst injecting, the moulds were tilted to a 45° angle to ensure the escape of air bubbles via the gap created by the needle. The moulds were placed upright in an oven pre-set to 60 °C for 72 hours. In the cases of set 2 and set 3 hydrogels, a post-cure was utilised. The moulds were removed from the oven after the initial 72-hour polymerisation period and placed in another oven pre-set to 90 °C for 3 hours to remove any unreacted monomer residue whilst increasing the likelihood of polymerisation between the monomers. After this, the hydrogels were carefully removed from their moulds and soaked in deionised water for a 14-day period, with the water being changed every day (except weekends). After this period, the hydrogels were stored in deionised water until required.

2.3 Permeation assays

2.3.1 Single-salt permeation assays

Principle: Understanding the permeation behaviour of the synthesised hydrogels was a tantamount objective of this project. Permeation is a characteristic that was essential to understand, considering the proposed application of said hydrogels. The approach to the study of permeation varies in terms of apparatus used. Mann et al (2018) made use of a Franz flow cell to conduct vertical permeation experiments on commercially available contact lenses. Fujiyabu et al (2017) used a purpose-built glass tube that was able to measure swelling of the tetra-PEG gel but also its permeation of water, shown in the literature review (section 1.1.3). The apparatus differs but the study of permeation is the overarching

end goal. The chloride salts – calcium, potassium, sodium and magnesium chloride – were selected for use in both the single and multiple-salt permeation assays for multiple reasons:

- The salts are water soluble, making it relatively simple to make up solutions for the experiments. This also proved advantageous when cleaning the permeation rig post-run, the process described in more detail below.
- Use of these salts presented an opportunity to pre-emptively gauge the permeation abilities of the hydrogels based on the principle of size and/or charge due to the properties of the salts. This notion is discussed in further detail in the partitioning chapter (4.3).
- Procurement of the salts was cost effective which was particularly helpful due to the amounts needed to conduct permeation assays and partitioning studies at the required level of repeats.

Permeation experiments were conducted on a purpose-built permeation rig, shown in Figure 2.2. This apparatus consisted of a horizontal permeability cell, a peristaltic pump, a conductivity probe connected to its meter and glass reservoirs for deionised water and salt solutions. The cylindrically shaped permeability cell was constructed of Perspex with a diameter of 9 cm and approximately 14 cm in length. Conductivity and temperature readings were measured using a Jenway Model 4510 Conductivity/TDS Meter.

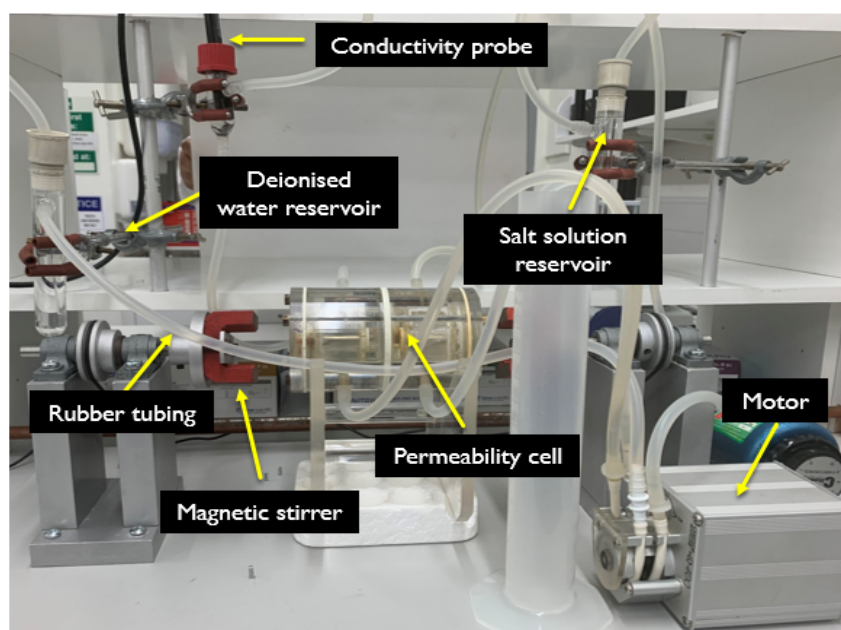


Figure 2.2 Permeation rig set-up, labelled (image source: author's own)

The entire rig set-up had to be thoroughly washed before the start of each experiment by pumping deionised water through the system. This was repeated until the conductivity meter showed a reading between 0-2 micro-Siemens (μS). A hydrogel sample was sandwiched between two custom o-ringed silicone washers which was further sandwiched in the permeation cell's deionised water and salt solution halves. A representation of the permeability cell can be seen in Figure 2.3. These chambers were bolted

together and each fluid inlet/outlet had its rubber tubing attached, connecting them to the deionised water and salt solution reservoirs respectively.

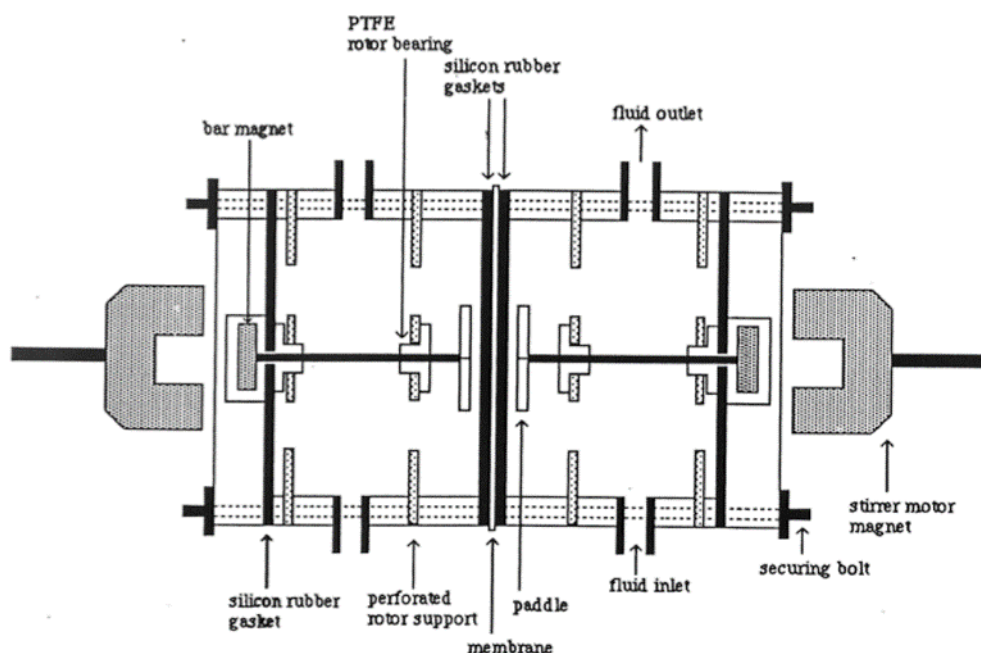


Figure 2.3 Schematic representation of permeability cell (Image source: Hamilton et al, 1988)

The left chamber of the cell held deionised water whilst the right chamber held the salt solution. A 250 mM solution of each chloride salt was made using 250 ml of deionised water and a calculated amount of a salt (3.65 g for a sodium chloride solution, 4.65 g for a potassium chloride solution, 5.95 g for a magnesium chloride solution and 6.93 g for a calcium chloride solution). The deionised water chamber was filled first to ensure there were no leaks in the system or the hydrogel sample had not torn. The peristaltic pump controlled this process, at a speed setting of four, which usually took a few minutes to complete. At this stage, it was important to physically manipulate the permeation cell to remove air bubbles within the chamber. This was to ensure the entire surface area of the hydrogel was in contact with the liquid. The salt solution chamber was filled afterwards, and the same bubble removal was conducted.

Once both chambers were filled with their respective liquids, the conductivity and temperature on the meter were noted for baseline measurement. During the first hour of the experiment, a reading was taken every ten minutes to show the progression of lag time. Every hour after this interval for the next 6 hours, the conductivity and temperature were recorded.

Upon completion of the experimental run, the volume of deionised water within its respective chamber was measured as this value is needed to calculate the permeability coefficient. The hydrogel sample was carefully removed, soaked in deionised water and labelled accordingly. The rig was then washed again as described earlier until the conductivity reading was between 0-2 μS . The cell was then dismantled, and each component soaked in deionised water until needed again. It should be noted that hydrogel samples were reused for each permeation experiment, with the samples being washed out by being soaked in deionised water in-between experimental runs.

2.3.2 Multiple-salt permeation assays

Principle: In real-life practice with biomedical applications, the hydrogels would be tasked with permeating and separating substances that contain many compounds. Multiple-salt permeation assays would help determine how well the hydrogels deal with the load of multiple compounds at once. Conductivity as a sole measure of permeation would not be adequate enough to understand what ion was being permeated the most. Inductively coupled plasma optical emission spectroscopy (ICP-OES) would be used on samples to measure the ratio of ions permeated over the duration of the 7-hour experiment.

The permeability rig set-up was the same as described in methodology section 2.3.1. A 250 mM salt solution was made using 1000 ml of deionised water and the calculated amounts of each chloride salt used to make their individual 250 mM salt solutions (3.65 g for a sodium chloride solution, 4.65 g for a potassium chloride solution, 5.95 g for a magnesium chloride solution and 6.93 g for a calcium chloride solution). Once both chambers had been filled up with their respective solutions (deionised water/salt solution), readings at 10-minute intervals were taken as was the case with the single-salt permeation assays. A 10 ml sample of fluid was collected from the left chamber of the permeability cell every hour to be analysed using Inductively Coupled Plasma Optical Emission Spectroscopy (ICP-OES) to measure the ratio of calcium, potassium, sodium, and magnesium ions that permeate through the hydrogel.

2.4 Water Content

2.4.1 Equilibrium Water Content

Principle behind EWC: Water within hydrogels plays an important role in determining their overall permeation behaviour as it is this water that facilitates the movement of components as well as providing the structural integrity of the hydrogels. Knowing the content of the synthesised silicone hydrogels can lend a hand in explaining its permeation behaviour towards different substances. When a newly synthesised hydrogel is first introduced to water, the negative charges along the polymer chain begin to repel and create space within the structure of the gel. Water molecules are polar; thus, they are attracted to these negative charges and in addition to these electrostatic attractions, hydrogen bonds also form. This process describes water uptake in hydrogels. However, there is a point in which the ability for the hydrogel to swell is directly opposed by the elongation of the cross-linked bonds between the monomers. Water absorbed by the hydrogel at this point is known as the equilibrium water content (EWC). EWC can be defined as the ratio of water contained in a hydrated sample compared to a dehydrated sample. This is usually determined by drying out a hydrogel and comparing its dry weight to its hydrated weight. This methodology is considered a static gravimetric method (Lutovska et al, 2017). This technique determines the amount of an analyte through the measurement of mass (Yoder, 2012).

The following equation is used to calculate EWC:

$$\text{EWC (\%)} = \frac{(\text{initial weight} - \text{final weight})}{\text{initial weight}} \times 100 \quad (2.1)$$

The hydrogel samples were prepared by using a cork-borer to cut out 0.8 cm (in diameter) discs. The surface water of these samples was removed by gently blotting with filter paper before the samples were then weighed. The samples were then placed on a glass plate, side by side, and kept in a vacuum oven set to 40 °C. The vacuum pressure was set to 140 millibar (mb) and the samples were left in the oven for 8 hours at a time. The weights of the samples were measured after this 8-hour period and placed back in the oven. This process was repeated over the course of 3-4 days, until the weight of the samples stabilised. Four samples were used as repeats per hydrogel.

2.4.2 Differential Scanning Calorimetry

Principle: There are different types of water within a hydrogel and it is determined by the interaction of water with the polymer backbone of the gel. The two main types are non-freezing and freezing water. Freezing water determines the permeation and sorption behaviour of a hydrogel as it dictates the movement of solutes through a hydrogel (Gun'ko et al, 2017). Differential Scanning Calorimetry (DSC) was used to understand the water structuring within the hydrogels. DSC is a form of thermal analysis that measures enthalpy.

There are two types of DSC: Heat Flux and Power Compensation. The type used in this experiment was the Heat Flux. Heat is supplied to both the sample and a reference material (often, an empty aluminium pan is used). Heat flow is proportional to the heat difference of the heat sink and holders. Whether the sample undergoes an exothermic or thermogravimetric change, the heat change is compensated by the heat sink so the temperature difference between the sample and the reference is kept constant throughout the experimental run (Hitachi, 2019). DSC functions as an analytical method to determine the ratio of water types in a hydrogel as it assumes only the freezing water within a hydrogel can be frozen. On this principle, the thermogram on a DSC figure represents the melting of freezing water so the value produced is the equivalent of the freezing water in the hydrogel (Hoffmann, 2002).

DSC experiments were conducted using a Mettler Toledo DSC1 instrument with a GC10 Star^e System Gas Controller, making use of liquid nitrogen to facilitate the freezing of the samples. The mass of each sample had to be between 5-15 mg so the samples were prepared using a scalpel and cutting board. The mass of each sample was recorded and the sample was placed in an aluminium pan that was sealed with a corresponding cover used specifically with the DSC equipment. Once the pan had been placed in its designated area, the hydrogel sample was rapidly frozen and then slowly warmed to determine the different types of water and their ratios.

Three distinct heating cycles were used in this experiment: the starting temperature of cycle one was 25 °C then the samples were cooled to -70 °C at a heating rate of -20 °C/min. The starting temperature

of cycle two was -70 °C then the samples were warmed up to -25 °C at a heating rate of 20 °C/min. The final cycle had a starting temperature of -25 °C then the samples were warmed back up to 25 °C at a heating rate of 5 °C/min.

2.5 Partition Coefficient

Principle: Partition coefficient is an empirically dimensionless property that describes how a chemical substance distributes itself between 2 phases (Tsai, 2007). The coefficient describes the solubility of the salt within the hydrogel's matrix. It should be noted that the partition coefficient takes into account the concentration of the unionized nature of the salt. Pharmacokinetic properties such as membrane transport and passive absorption can be directly affected by the partition coefficient, hence its importance.

The partition coefficient of each hydrogel was determined against all the salts used in the permeation experiment described previously and the 250 mM salt solutions were made using the same technique.

A cork-borer was used to cut out an approx. 0.8 cm (in diameter) sample of a hydrogel which was placed in a labelled container. 20 ml of each salt solution was poured into the containers. The samples were left to equilibrate for 24 hours at room temperature. After this period, the hydrogel sample was removed from its respective container, gently blotted with filter paper to remove surface water and weighed. Once weighed, the sample was transferred to a clean container containing 20 ml of deionised water, allowing the salt within the hydrogel sample to leach out. This was also left to equilibrate for 24 hours. The conductivity of each hydrogel's solution was measured and recorded. This process was repeated thrice per hydrogel/salt combination.

2.6 Membrane Characteristics

2.6.1 Environmental Scanning Electron Microscopy & Energy-dispersive X-ray Spectroscopy

Principle: Environmental Scanning Electron Microscopy (ESEM) makes use of an electron beam to create an image of a surface. Unlike Scanning Electron Microscopy (SEM), samples do not need to be coated in gold or any other conductive material in order for images to be made. Also, SEM is not suitable for imaging wet samples like hydrogels (Plieva et al, 2006). ESEM overcomes these issues by utilising a high vacuum environment at the electron gun whilst maintaining a steady pressure within the imaging chamber (Azo Materials, 2002). Primary electrons are emitted from the gun which push out secondary electrons from the specimen. It is these secondary electrons that are detected, resulting in the formation of a magnified image.

Energy-dispersive X-ray Spectroscopy (EDX) is an analytical technique that is used to identify the elemental composition of the surface of a material. The method works by bombarding a sample with x-rays which causes electrons to be displaced from a specimen. This displacement leaves behind a "hole"

which should be filled with an electron from a higher energy state. But in between that time, the “hole” emits energy while it relaxes. Each element has a unique relaxation energy which is detected and assigned to its respective element (Gaston & Protter, 2020).

Both the ESEM and EDX experiments were conducted using a Quattro S Electron Microscope (Thermo Fisher Scientific, USA) coupled with an EDS UltraDry 60M (129 eV) detector. The analysis of the hydrogels was conducted in wet mode.

The hydrogel samples were analysed in a hydrated state. A small section of the hydrogel sample was cut out with a PTFE-coated razor blade and then mounted onto a Peltier stage using copper tape to cool the samples during analysis. The Peltier stage was then placed in the centre of the chamber and the chamber was purged with several pumps of nitrogen gas to reach the desired pressure of 500 Pa. The chamber was also cooled to 2 °C. Initially, the chamber pressure was set to 700 Pa but upon beginning the imaging process, it was noted that 500 Pa produced the clearest images in which the morphology could be thoroughly appreciated. The Gaseous Secondary Electron Detector (GSED) was the selected detector for imaging due to its compatibility with a majority of materials and its ease of use. The chamber conditions were adjusted to produce images with the most clarity and although the equipment was mostly able to maintain these conditions, there was a degree of variability noted especially in temperature and pressure. The pressure of the chamber was kept at 500 Pa as this is what worked best whereas the humidity was varied between 78-99%. The acceleration voltage used was 24 kV and the spot size setting varied between 4 and 5. The samples were analysed at x35000 magnification. Under these conditions, high resolution imaging was achieved.

EDX was coupled with the microscope used during ESEM imaging. The Pathfinder 1.3 X-ray Microanalysis software was used to acquire and analyse all EDX data. Images were taken at a resolution of 512 x 384 pixels, an accelerating voltage of 25-30 kV with a spot size setting between 4-5. The collection time was kept short to an average of 58 seconds per sample as the electron beam was known to char or burn the samples.

2.6.2 X-ray Photoelectron Spectroscopy

Principle: This analytical technique makes use of x-ray beams to bombard the surface of a sample. This causes the excitation of the core electrons and this leads to an energy emission. The energy required to excite the core electrons of a specific element are unique to that element, which is why binding energy is the unit of measurement used. It should be noted that XPS only gives information about the surface of a sample, specifically the top 0-10 nm. The binding energy emitted from an element differs based on the environment in which said element is detected. This chemical shift allows for XPS to be used to determine the surface chemistry of a sample (Mathias, 2020).

The following describes the methodology as denoted by Dr. Marc Walker (Warwick University) who carried out the analysis: X-ray photoelectron spectroscopy (XPS) measurements were carried out using a Kratos Axis Ultra DLD spectrometer (Kratos Analytical, Manchester, UK). The hydrogel samples were dehydrated by being stored in a vacuum oven at 40 °C for a 7-hour period before being sent for analysis.

The hydrogel sample was mounted on electrically conductive carbon tape upon the sample bar and loaded into the spectrometer. Once an acceptable vacuum level had been reached, the samples were transferred to the main analysis chamber. The samples were illuminated by a monochromated Al K α x-ray source ($h\nu = 1486.7$ eV) and also flooded with low energy electrons from a charge neutraliser to prevent the surface from becoming positively charged during the experiment. Data was collected in a hemispherical analyser using a pass energy of 160 eV for survey spectra and 20 eV for high resolution core level spectra (resolution approx. 0.4 eV).

Data was analysed using the CasaXPS software package, using mixed Gaussian-Lorentzian (Voigt) lineshapes and Shirley backgrounds. The spectrometer was calibrated using the Ag 3d $_{5/2}$ peak and Fermi edge of clean polycrystalline Ag prior to the start of the experiments, with the transmission function determined using various clean metallic foils. The binding energies of the data were adjusted during the analysis, using the C-C/C-H component in the C 1s region at 284.6 eV as the reference point.

2.7 Calibration Curve Development

2.7.1 Single-salt calibration curve

Principle: Traditionally, calibration curves show the linear relationship between an independent variable and a dependent variable that was a response to the initial variable (Moosavi et al, 2018). Such a curve serves several purposes including predicting a value of the dependent variable by interpolation on the figure. In this case, the slope of the line provides the basis for the conversion of conductivity (mS) to concentration (ppm).

A linear calibration curve was established for the purpose of converting conductivity readings (ms) derived from each permeability experiment to concentration (ppm). Using 250 ml of deionised water, sodium chloride, potassium chloride, magnesium chloride and calcium chloride were used to make a 1000 ppm salt solution in a volumetric flask (CaCl $_2$ – 0.692 g, KCl - 0.473 g, NaCl - 0.635 g, MgCl $_2$ - 0.979 g). These weights were calculated by using the molar mass of the cation for each salt instead of the molar mass of the salt. Via serial dilution, a concentration series ranging between 2-1000 ppm was made, resulting in 13 data points. The conductivity for each solution was taken via immersion of the conductivity probe and recording the value shown on the meter. Between each reading, the probe was rinsed with deionised water and wiped dry. Also, the conductivity of water was also recorded between each concentrated solution. A reading was taken three times per solution/concentration.

2.8 ICP-OES Method Development

Principle: when electrons of a specific element are energised, they move from a lower to higher energy state. When these electrons relax to their ground state, photons are emitted and they possess wavelengths that are characteristic and specific to a particular element. With Inductively Coupled Plasma Optical Emission Spectroscopy (ICP-OES), plasma is used to bombard the electrons of a sample which ionise the sample. It is this ionisation process that releases photons that are later used to characterise the proportion of elements within a sample.

Elemental analysis of the multiple-salt permeation experiments was conducted using a Thermo-Scientific iCAP 7000 Series ICP Spectrometer coupled with an ASX-520 AutoSampler. The spectrometer was required to be kept between 17-20 °C, which was maintained by a chiller (Thermo-Scientific NESLAB ThermoFlex900). Using the purchased elemental standards, a calibration series for each element was developed at concentrations of 1, 2, 5, 10, 15 and 20 ppm using deionised water to dilute. A methodology was developed on the accompanying software to identify and quantify the concentration of the aforementioned elemental standards.

There were two options available for the collection of photons: axial and radial. The radial mode was utilised as it ensures a wide range of photons are detected by the equipment whilst maintaining the stability of the instrument. Axial mode is the preferred option when working with extremely low elemental concentrations.

Sample preparation of the multiple-salt permeation samples included diluting down the samples collected during the permeation experiments with deionised water and digesting the samples with 1 ml of 5 % nitric acid solution. This was necessary to prevent the salts from precipitating out during analysis which could potentially cause damage to the equipment. The 1 ml of 5 % nitric acid was deducted from the amount of deionised water required to dilute the solution to a concentration within 1-20 ppm. Analysis of the solutions provided the amount of each element in parts per million.

2.9 Statistical Analysis

Principle: It was important to determine the statistical validity of the data procured during this project – whether there was statistical significance to the data between hydrogel sets and to determine whether there was a significant difference in reproducibility between experimental repeats.

All statistical analysis in this project was carried out using the Microsoft Excel Data Analysis add-on. This function allows for a series of statistical tests to be calculated such as Analysis of Variance (ANOVA), t-test, F-test, etc. Two categories of statistical data were produced per hydrogel series and per reaction conditions set: category one focused on the statistical difference between the experimental runs of each hydrogel against the different chloride salts; whilst category two aimed to determine the statistical difference between the experimental runs of a particular hydrogel/salt combination. The rationale for category one was to determine whether the changes in the formulation of the hydrogels could produce a difference in their permeation behaviours towards the different chloride salts that was statistically significant. For category two, the rationale was to note the validity of the experimental runs, i.e., whether the data was reproducible between repeat runs on the permeation rig. Beyond those two categories, the standard deviations of the permeation, partition and diffusion coefficients were calculated to report how far the data swayed from the average.

The test used for category one was ANOVA: Single Factor, which produced a p-value. The p-value is used to validate a hypothesis (Grabowski, 2016). The null hypothesis for category one stated there was no significant difference between the experimental runs from one hydrogel to the next against each

chloride salt ($\text{CaCl}_2/\text{KCl}/\text{NaCl}/\text{MgCl}_2$). The same test was used for category two data and the null hypothesis stated that there was no significant difference between each experimental run from one specific hydrogel/salt combination ($\text{CaCl}_2/\text{KCl}/\text{NaCl}/\text{MgCl}_2$). ANOVA: Single Factor was the chosen form of statistical analysis due to the nature of data at hand – with the category one tests, comparisons were being made between 3-4 experimental runs whereas category two tests included up to 10 sets of data to compare at a time. Using the t-test would have been simpler but increased the chances of introducing greater error during analysis as this method is more suitable for comparing two data sets against each other (Voxco, 2021). The use of ANOVA: Single Factor in the statistical analysis of this thesis was to increase reliability.

The alpha level was set to 0.05, so if the p-value was more than 0.05 (>0.05), there was no statistically significant difference between the hydrogels, thus the null hypothesis would be accepted. If the p-value was less than 0.05 (<0.05), there was a statistically significant difference, and the null hypothesis would be rejected.

The summary tables of these workings can be found in appendix section 6 but for the category one tests of the hydrogels from sets 1-3, the null hypothesis was rejected, as hoped. With the category two tests, the majority of the hydrogels accepted the null hypothesis, also as hoped. However, there were exceptions – the p-value of hydrogel F1 was less than 0.05 repeatedly, regardless of the salt it was tested against or the set to which it belonged. This led to believing the borderline impermeability of the hydrogel against the salts could have caused this issue with the ANOVA test. The other exception was seen in set 3 with hydrogels E2 and E3. In the case of hydrogel E3, the null hypothesis was rejected but this is most likely due to the lack of reproducible runs as a result of tears during permeation experiments. But in the case of hydrogel E2, the reaction conditions of the set produced an impermeable version of the hydrogel, so it is thought the same issues encountered with hydrogel F1 were repeated.

3 Water Content

3.1 Introduction

Rationale: water content is often considered to be the most important characteristic of a hydrogel, hence why this is the primary chapter of the results section of this thesis. As mentioned in the introduction, the unique water-absorbing qualities of a hydrogel can be attributed to its ability to interact with bodily tissue without triggering an immunological response – enabling the hydrogel to be considered as a biomaterial. Literature offers conflicting viewpoints on the influence of water within hydrogels, with some studies stating there is not an explicitly clear link between the water content of a hydrogel and its ion permeation (Mann et al, 2019), whereas others state the type of water in a hydrogel can determine the permeation of substances in and out of it (Hoffmann, 2012). However, it is important to understand whether changes in the formulation (i.e., ratio of NVP and DMA monomer content) and reaction conditions used during the synthesis of the hydrogels can influence the different water types that can be found in a hydrogel. Determining the different types of water within the synthesised hydrogels as well as deducing the relationship between these water types and formulation provides the necessary foundation for understanding some of the remaining characteristics to be discussed such as partitioning and permeation.

Hydrophilic groups on the polymer chain are responsible for water absorption in hydrogels. In the case of this project, such groups include acrylamides introduced to the polymer network via the monomer dimethylacrylamide (DMA). Negative charges along the polymer chains of a hydrogel create spaces within its structure due to repulsions between the charges. They also attract water molecules. Water is a polar molecule as the oxygen atom on water is more electronegative than hydrogen, causing this attraction between the polymer chain and the water molecules (Brini et al, 2017). The presence of negatively charged groups increases the electrostatic repulsions between the polymer chains, increasing the amount of water that can enter the hydrogel (Pasqui et al, 2012) and attach to the polymer chain.

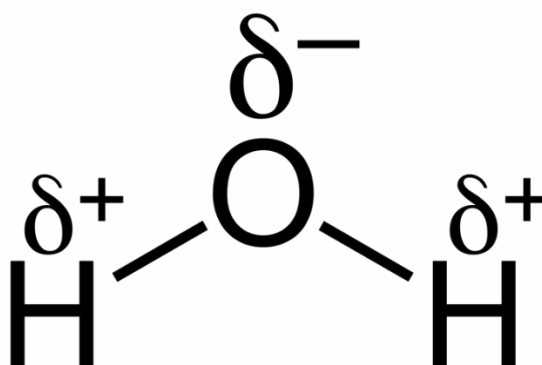


Image 3.1 Water molecule schematic (image source: author's own)

As water molecules attach themselves to the chain via hydrogen bonding, this also causes the polymer chains within the hydrogel to open itself up to more water absorption. The initial water that attaches itself to the polymer chain is referred to as primary bound water. Once the polymer chain has been fully extended, it exposes the hydrophobic groups along the chain but there is also interaction between these groups and water which leads to the formation of secondary bound water (Gulrez et al, 2011). Bound water can also be referred to as non-freezing water. The sum of primary and secondary bound water equates to and is referred to as the total bound water of the hydrogel. Generally, additional water is also absorbed after this step, but the absorption is hindered by the actions of osmosis and the chemical and physical cross-links of the hydrogel structure. This water is referred to as freezing water and it fills the gaps within the hydrogel, formed by the polymer network of cross-links (Hoffman, 2012).

The overall amount of water absorbed by a hydrogel is determined by a number of factors including temperature and the interactions between the polymer chains and the water molecules (Kołodziejka et al, 2016). This absorption may also be hindered by the formation of salt blocking channels. Calcium and magnesium ions are present in water and said ions can create electrostatic interactions between the polymer chain which inhibit the chain's ability to form hydrogen bonds with water (Shahid et al, 2012). However, this phenomenon can be minimised by utilising deionised water at every stage of the synthesis of a hydrogel, which was the case in this project.

In silicone-based hydrogels, clusters of hydrophobic and hydrophilic monomers tend to form along the polymer chain due to their difference in water attraction. It is the water found in these hydrophilic domains that can have a large effect on mechanical and transport properties such as aqueous solute uptake and ion permeability (Liu et al, 2015).

It is important to understand that the overall presence of equilibrium water improves the biocompatibility of a hydrogel. Water content has been directly related to solvent-free hydrophilic-phase volume fraction (ϕ) i.e., when there is an increased presence of hydrophilic monomers within a hydrogel, there is an increase in water content (Fujiyabu et al, 2019). However, this may not be directly applicable to the behaviours of self-assembled hydrogels, the category in which the synthesised hydrogels of this project fall in to.

Differential Scanning Calorimetry (DSC) is an analytical technique that was utilized in this project to determine the amount of freezing water content within the hydrogels. The methodology has been described in section 2.4.2 of the materials & methodology chapter. From the determination of freezing water, other water types within a hydrogel such as non-freezing water, polymer-associated water and ice-like water (Gun'ko et al, 2017) can be extrapolated. During an experiment, a hydrogel sample is frozen using liquid nitrogen then slowly heated to defrost it and 2 peaks are observed on the DSC trace: the thermogramic peak, which represents the freezing of the free water within the hydrogel and the exothermic peak, which is associated with the melting of the free water within the hydrogel. It is a generally accepted notion that the greater the amount of freezing water within a hydrogel, the greater its permeability, as freezing water has the highest mobility of all the water types present in a hydrogel (Bag & Valenzuela, 2017).

As explained above, there are different stages and mechanisms in which water is absorbed by a hydrogel upon its first contact with water. Once all the polar, non-polar and ionic groups are completely saturated with water, “extra” water fills the empty spaces within the polymer network and this water is referred to as free/freezing water (Hoffman, 2002). It is this free water that is referred to as freezing water and can also be classified into polymer-associated water and ice-like water. By determining the ratio of the water types present within the hydrogels, the relationship with their permeation coefficients can be established which can be used to determine whether the water types are influential in regard to permeation and diffusion behaviour which in turn, influences the movement of salts across the hydrogel membrane.

3.2 Results

3.2.1 Equilibrium Water Content Results: E & F Series

The key differences between the hydrogels of sets 1-3 included reaction conditions more so than formulation. As DMA monomer content increased down the set, NVP monomer content decreased whilst TRIS monomer content remained constant, this was the case of formulation for the E series hydrogels. The amounts of the NVP, DMA and TRIS monomers were intentionally altered largely within the F series hydrogels to determine the effects of having a more hydrophobic/hydrophilic formulation on the overall characteristics of the hydrogels as in shown in the formulation Table 3.1.

Table 3.1 Formulations of E & F Hydrogels

Hydrogel	Formulation (%)			
	DMA	NVP	TRIS	3-octanol
E1	0%	60%	35%	5% (used in sets 1 & 3 only)
E2	10%	50%		
E3	20%	40%		
E4	30%	30%		
E5	40%	20%		
E6	50%	10%		
E7	60%	0%		
F1	-	30%	65%	5% (used in set 3 only)
F2	-	70%	25%	
F3	70%	-		

As described in section 2.4.1 of the materials & methodology chapter, equilibrium water content was determined by placing hydrated hydrogel samples in a vacuum oven. Table 3.2 below includes the average EWC values of each E hydrogel from their respective set. The averages were derived from a total of four repeats per hydrogel sample. The data for each individual hydrogel can be found in the G.Durowoju, PhD Thesis, Aston University 2022.

appendix section 1.1. The standard deviation is reported alongside the averages of the different water types in each results table.

Table 3.2 EWC values for hydrogels E1 to E7 of sets 1-3 (n=4) (brackets indicate standard deviation)

	Set 1	Set 2	Set 3
E1	47.0% (0.02)	51.8% (0.02)	62.8% (0.005)
E2	58.9% (0.02)	61.1% (0.005)	60.5% (0.006)
E3	59.6% (0.03)	60.9% (0.01)	65.5% (0.006)
E4	61.3% (0.03)	57.6% (0.01)	57.0% (0.006)
E5	63.0% (0.01)	54.6% (0.01)	57.1% (0.002)
E6	64.8% (0.003)	56.2% (0.01)	51.6% (0.003)
E7	59.7% (0.04)	55.4% (0.002)	58.1% (0.002)

Overall, from sets 1-3, there was a significant change in EWC ($p < 0.05$). In set 1, the E hydrogels showed a gradual increase in their EWC which also corresponded with the aforementioned DMA monomer content increase. Hydrogel E1 did not contain any DMA which might suggest why its EWC is 47%, the lowest of the set. A similar phenomenon was seen with hydrogel E7 – a hydrogel that did not possess any NVP – which had an EWC of 59.7%, a decrease from the previous hydrogel, E6, which had the highest EWC of the set at 64.8%. There was not an obvious trend with the E hydrogels of set 2, although an initial increase was seen between hydrogels E1 and E2. Beyond this, there was a decline in EWC, albeit non-linearly, for the remaining hydrogels of the set. With the set 3 E hydrogels, an increase was seen between hydrogels E2 to E3 but there was also a lack of a trend development in the set beyond that point.

The EWC values of the F hydrogels can be found in Table 3.3. These hydrogels did not follow a definitive trend in terms of DMA/NVP/TRIS monomer content unlike the E hydrogels, however, a significant change ($P < 0.05$) was seen in their EWC from sets 1-3.

Table 3.3 EWC values for hydrogels F1-F3 of sets 1-3 (n=4) (brackets indicate standard deviation)

	Set 1	Set 2	Set 3
F1	25.4% (0.02)	27.3% (0.01)	32.5% (0.004)
F2	62.1% (0.002)	55.8% (0.02)	77.2% (0.009)
F3	88.5% (0.002)	70.7% (0.005)	65.9% (0.002)

The ethos behind their synthesis was to see the effects of drastically increasing the quantities of both the hydrophilic and hydrophobic monomers in their formulation. But instead of using both the DMA and NVP monomer, the formulations were limited to one hydrophilic monomer per hydrogel. With that in mind, hydrogel F1 represents the most hydrophobic hydrogel of the sets whilst hydrogels F2 and F3 represent the most hydrophilic. It was not entirely possible to draw exact comparisons from one hydrogel to the next as each hydrogel is fundamentally different. However, comparisons can be made from one set to another.

Hydrogel F3 showed a decrease in EWC from set 1 to set 3, having EWCs ranging from 88.5% to 70.7% and finally 65.9%, displayed in Figure 3.1.

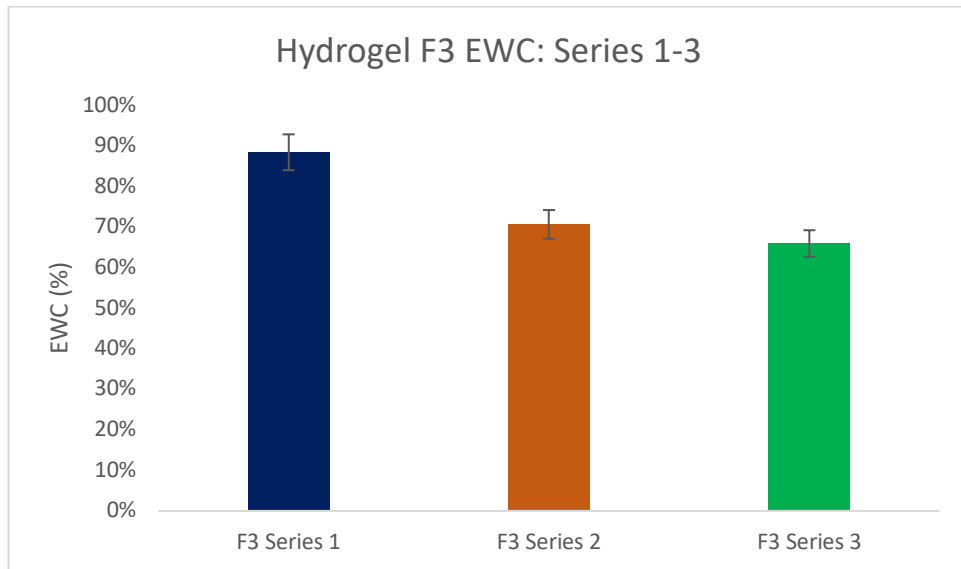


Figure 3.1 hydrogel F3 EWC from set 1-3

Hydrogel F1 displayed the exact opposite trend, with an increase in EWC from set 1 to 3. In set 1, its EWC was 25.4%, increasing to 27.3% in set 2 and 32.5% in set 3, shown in Figure 3.2.

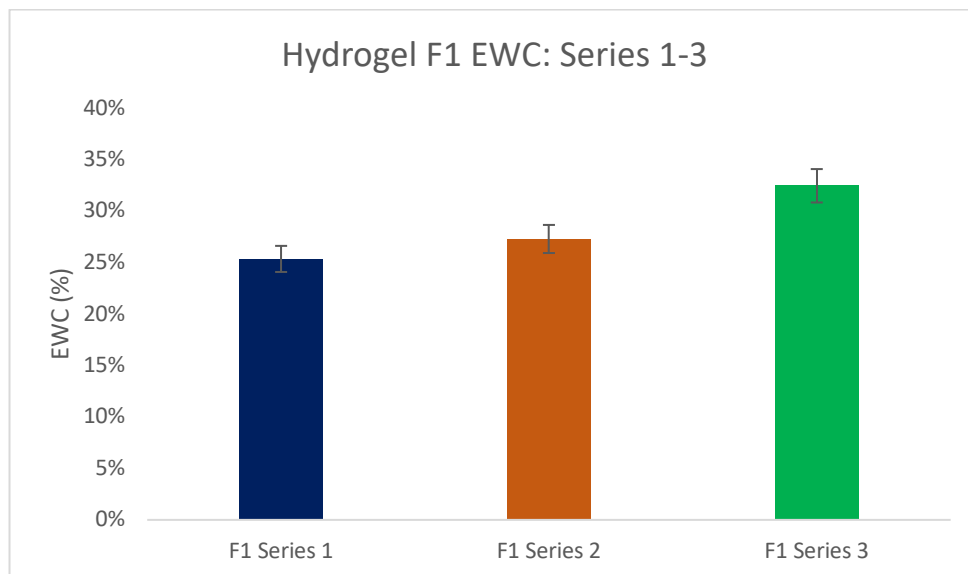


Figure 3.2 hydrogel F1 EWC from set 1-3

Hydrogel F2 saw a decrease in its EWC between sets 1 to 2 but there was an increase in set 3. In set 1, its EWC was 62.1% before decreasing to 55.8% in set 2. The EWC of hydrogel F2 increased to its highest value in set 3 at 77.2%, shown in Figure 3.3.

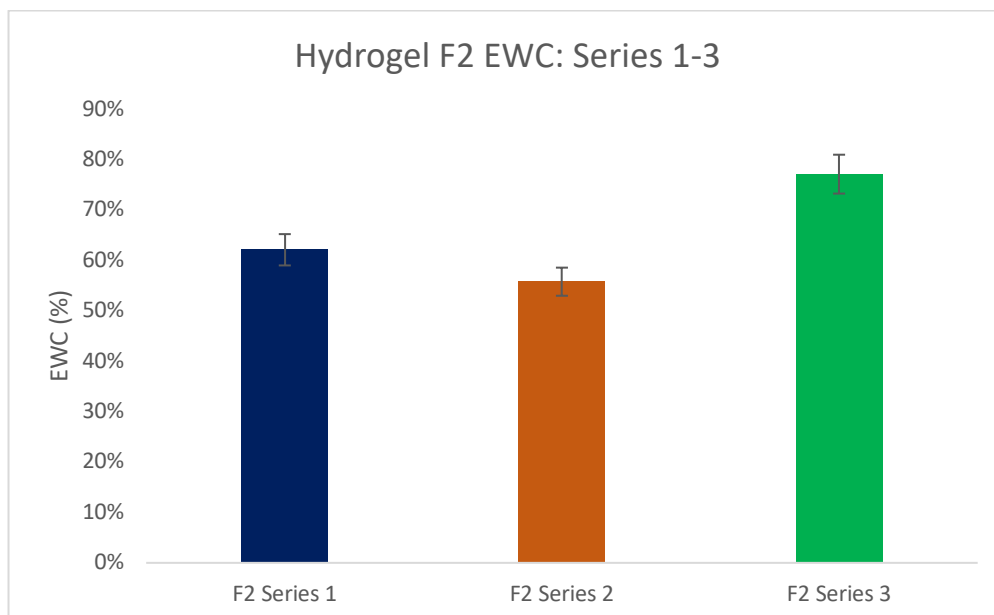


Figure 3.3 hydrogel F2 EWC from set 1-3

Hydrogels F2 and F3 had the same amounts of the TRIS monomer and their respective hydrophilic monomer in their formulations. However, in spite of that, hydrogel F2 had a significantly lower EWC than hydrogel F3 in both set 1 (62.1% vs 88.5%) and set 2 (55.8% vs 70.7%).

3.2.2 DSC Results: E & F Series

As mentioned in section 3.1, water in hydrogels can be divided into two main categories: freezing water (FW) and non-freezing water (NFW). DSC is used to analyse freezing water whilst the other water types are derived. Freezing water can be further divided into two sub-categories: polymer-associated water content (PAWC) and ice-like water content (ILWC).

It is the area of the thermogram that is used to calculate the freezing water content of a hydrogel. An example of a thermogram for hydrogel E6 from set 3 can be found in figure 3.4. Such calculations consider the weight of the sample used during the experiment as well as the heat of fusion of ice (333.7 J/g). The heat of fusion of ice is the amount of energy required to melt 1g of ice. This is also referred to as the latent heat of melting (Legates, 2005).

Using the following equations, the freezing water content of the hydrogels was determined:

$$FWC = \frac{\text{normalised area of endotherm } \left(\frac{J}{g}\right)}{\text{heat of fusion of ice } \left(\frac{J}{g}\right)} \quad (3.1)$$

$$\text{normalised area of endotherm} = \frac{\text{total area of endotherm (j)}}{\text{sample weight (g)}} \quad (3.2)$$

Non-freezing water is a derived value, making use of the freezing water content and equilibrium water content values. Non-freezing water cannot be frozen, even at temperatures as low as -100°C so it cannot be determined experimentally (Bag & Valenzuela, 2017).

$$NFWC = EWC - FWC \quad (3.3)$$

Polymer-associated water content and ice-like water content were also calculated using the thermogram derived from the experiment, but they were dependent on evident splitting of the thermogram peak. As shown in Figure 3.4, the thermogram formed between -5 to 5°C with a sharp peak forming at 0°C .

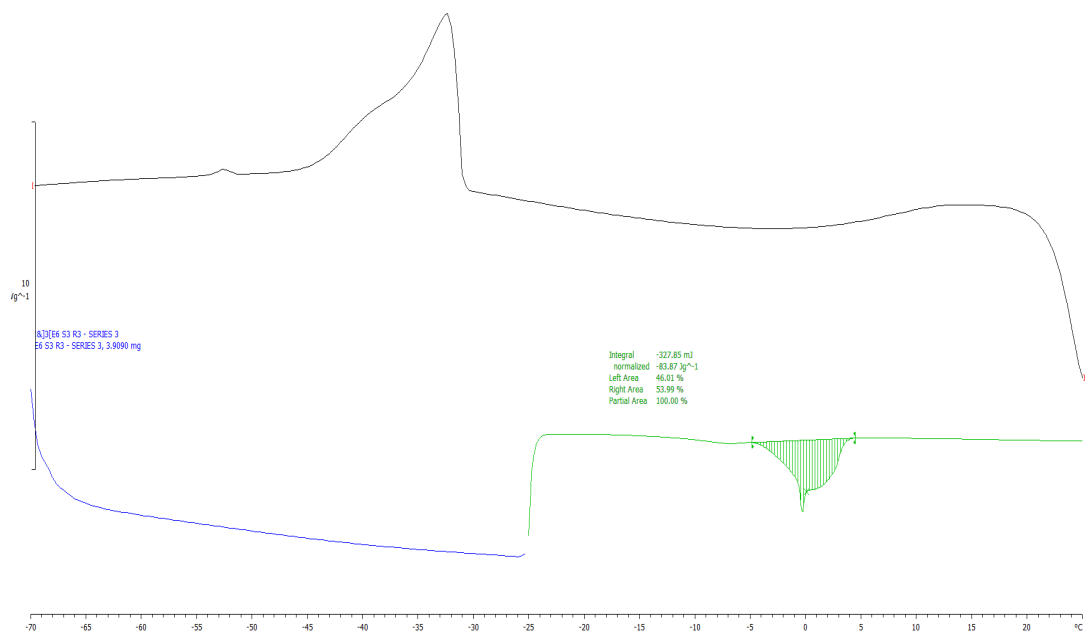


Figure 3.4 DSC thermogram for hydrogel E6 (set 3)

Any melting that occurred before this sharp peak (viewed from left to right) was considered to be polymer-associated water as it represents water with a lower melting point than water. The change in melting point could be attributed to impurities – or in this case, the polymer network that the water was bound to – that caused the melting point of the water within the hydrogel to change. Melting beyond 0°C was considered to be ice-like water. The thermograms for the hydrogels can be found in appendix II.

The amounts of freezing and non-freezing water for each hydrogel in their respective sets can be found in Tables 3.4 and 3.5.

Table 3.4 Freezing water contents of E hydrogels in sets 1-3 (n=9) (brackets indicate standard deviation)

	Set 1	Set 2	Set 3
E1	38.0% (0.02)	28.0% (0.09)	44.6% (0.01)
E2	37.8% (0.01)	13.5% (0.11)	29.0% (0.03)
E3	44.5% (0.02)	28.1% (0.14)	35.9% (0.05)
E4	39.2% (0.06)	34.2% (0.03)	40.4% (0.02)
E5	43.5% (0.02)	21.8% (0.02)	27.4% (0.02)
E6	40.0% (0.01)	30.5% (0.07)	19.9% (0.03)
E7	39.1% (0.02)	32.5% (0.03)	35.6% (0.04)

Table 3.5 Non-freezing contents of E hydrogels in sets 1-3 (n=9) (brackets indicate standard deviation)

	Set 1	Set 2	Set 3
E1	9.0% (0.02)	15.4% (0.01)	18.2% (0.01)
E2	23.5% (0.01)	30.2% (0.03)	31.5% (0.03)
E3	15.1% (0.02)	28.5% (0.05)	29.6% (0.05)
E4	22.1% (0.06)	15.8% (0.02)	16.6% (0.02)
E5	19.1% (0.03)	30.0% (0.02)	29.6% (0.02)
E6	24.7% (0.01)	32.1% (0.03)	31.7% (0.03)
E7	20.6% (0.02)	27.8% (0.04)	22.5% (0.02)

With the set 1 E hydrogels, there was not an obvious trend noticed in regards to changes in the hydrophilic monomer content being accompanied by a change in freezing water content. The hydrogel with the largest amount of freezing water was hydrogel E3 at 44.5% whilst the hydrogel with the lowest FWC was hydrogel E2 at 37.8%. The same can be said about the non-freezing water content of the set too: no obvious trend was seen. Hydrogel E6 had the most non-freezing water at 24.7% whilst hydrogel E1 had the lowest amount at 9%. Figure 3.5 showcases the ratio of these water types in each of the E hydrogels.

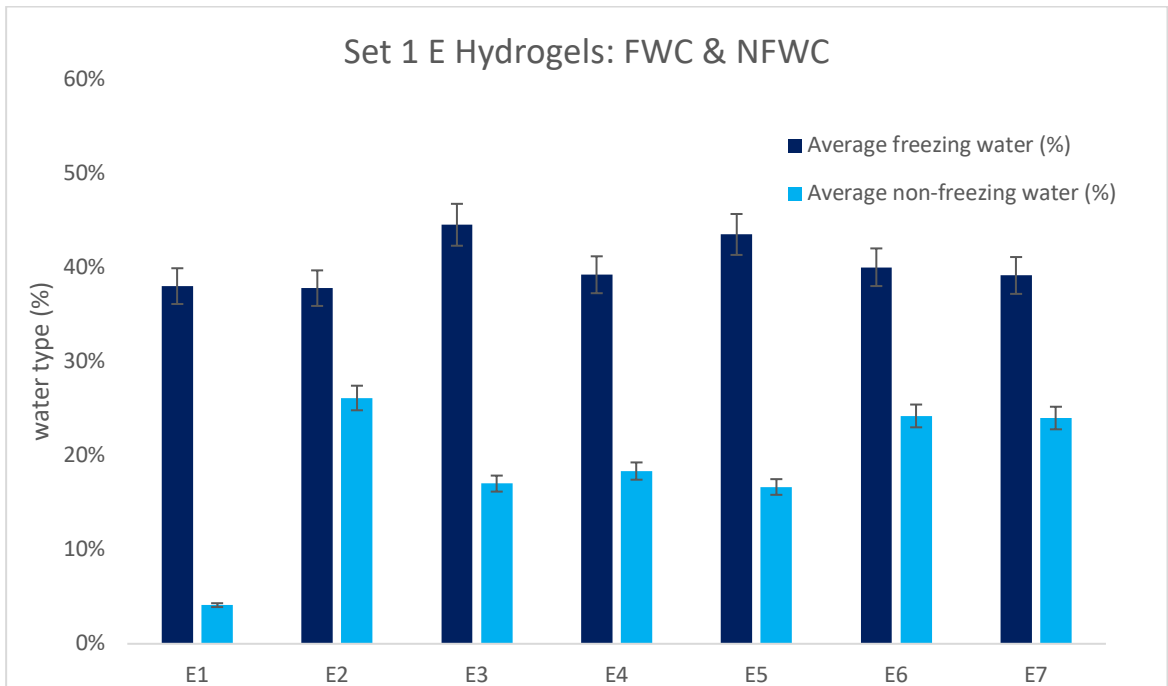


Figure 3.5 Freezing and non-freezing water contents of set 1 E hydrogels

The set 2 E hydrogels also did not display an obvious relationship or trend with either freezing water or non-freezing water and their ratios are displayed in Figure 3.6 below. The hydrogel with the largest amount of freezing water was hydrogel E4 at 34.2% whilst hydrogel E2 has the lowest at 13.5%. This hydrogel also had the highest non-freezing water content at 47.6%, suggesting almost half of the water within the hydrogel is unable to participate in permeation, the aspects of which will be discussed in the next chapter.

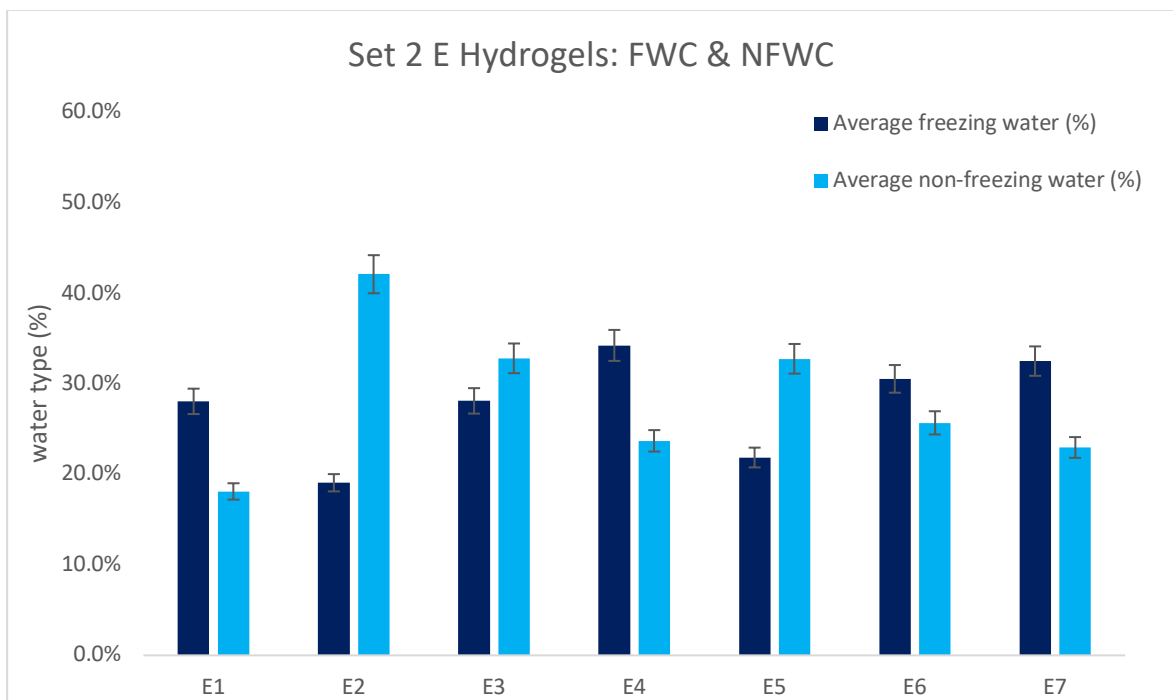


Figure 3.6 Freezing and non-freezing water contents of set 2 E hydrogels

A similar situation was seen with the set 3 E hydrogels as well – no obvious trend was noticed across the set, shown in Figure 3.7. Hydrogel E1 had the highest FWC at 44.6%. Hydrogel E6 had the lowest FWC of the set at 19.9% and it also had the highest NFWC of the set at 31.7%. The hydrogel with the lowest NFWC was hydrogel E4 at 16.6% which had the second highest FWC of the set at 40.4%.

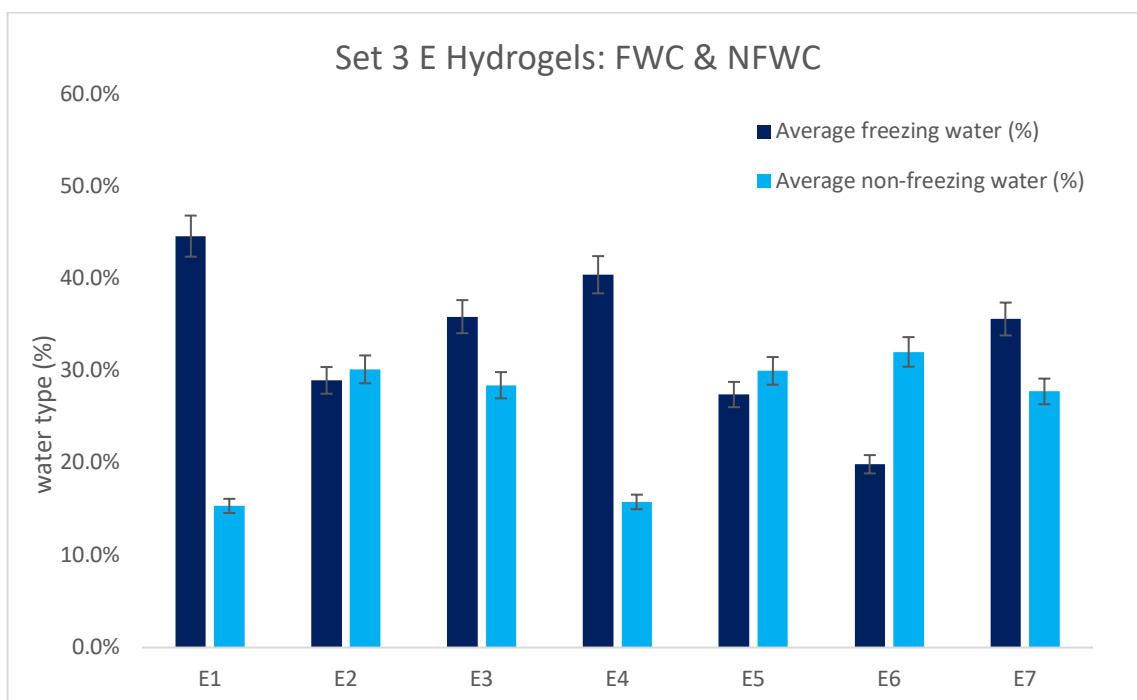


Figure 3.7 Freezing and non-freezing water contents of set 3 E hydrogels

Tables 3.6 and 3.7 show the freezing and non-freezing water contents of the F hydrogels from sets 1-3. In set 1, hydrogel F2 had the highest FWC of the set at 43.2% followed by hydrogel F3 at 36%. Hydrogel F1 had the lowest FWC in all the sets, with contents of 13%, 12.6% and 13.2% from sets 1-3, respectively. Hydrogel F3 had the most NFWC of all the sets and overall for both the E and F hydrogels at 52.5%.

Table 3.6 Freezing water contents for the F hydrogels sets 1-3 (n=9) (brackets indicate standard deviation)

	Set 1	Set 2	Set 3
F1	13% (0.02)	12.6% (0.03)	13.2% (0.02)
F2	43.2% (0.02)	38.2% (0.02)	57.2% (0.03)
F3	36% (0.02)	46.5% (0.03)	37.2% (0.03)

Table 3.7 Non-freezing water contents for the F hydrogels set 1-3 (n=9) (brackets indicate standard deviation)

	Set 1	Set 2	Set 3
F1	12.3% (0.02)	14.7% (0.03)	19.3% (0.02)
F2	19% (0.02)	17.7% (0.02)	20% (0.03)
F3	52.5% (0.02)	24.2% (0.03)	28.7% (0.03)

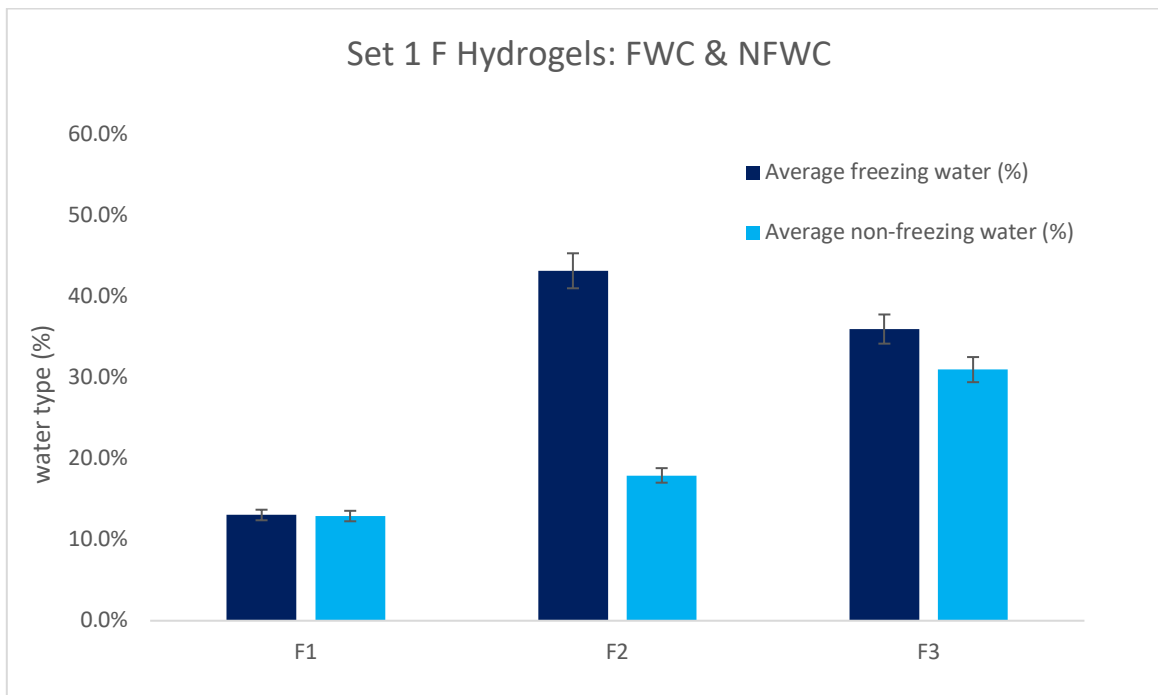


Figure 3.8 FWC & NFWC of F hydrogels: set 1

The F hydrogels of set 2 were the only set of hydrogels that displayed a gradual increase in both FWC and NFWC as seen in Figure 3.9. However, this trend did not follow a definitive formulation trend. As stated earlier, the key differences between the F hydrogels were the hydrophilic monomer used in its formulation as well as the amounts of TRIS in each hydrogel's respective formulation. Hydrogels F2 and F3 had the same quantity of a hydrophilic monomer but hydrogel F2 contained NVP whilst hydrogel F3 made use of DMA.

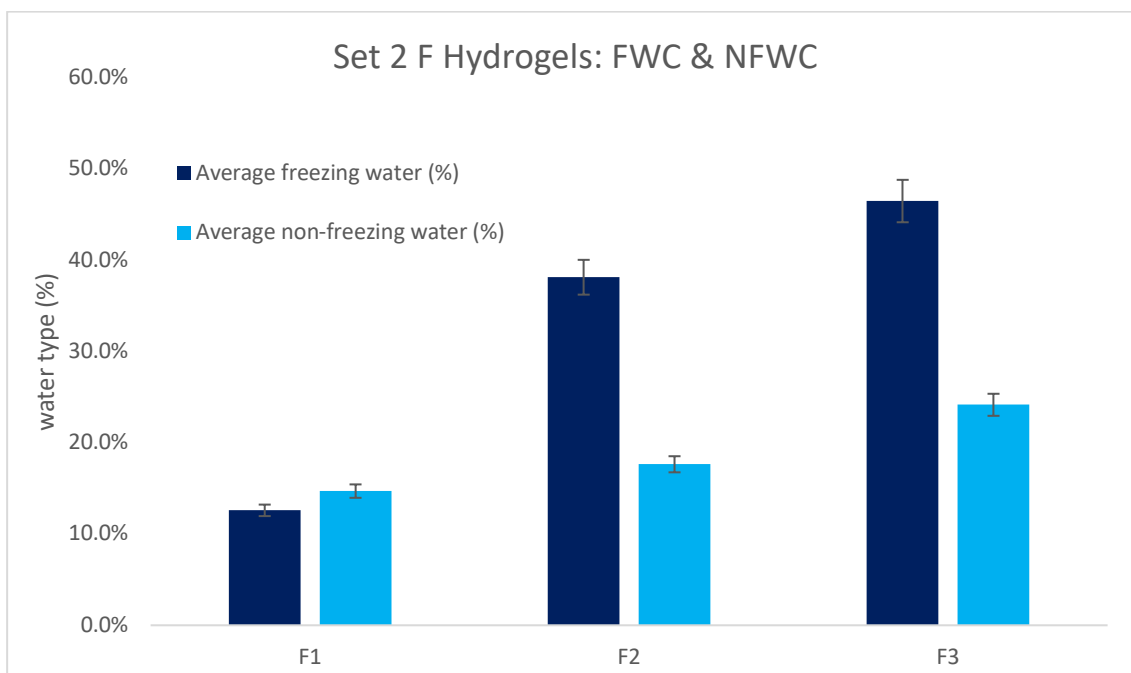


Figure 3.9 FWC & NFWC of F Hydrogels: set 2

Hydrogel F3 had the highest FWC of set 2 at 46.5% and a NFWC of 24.2%, suggesting a 2:1 ratio of freezing to non-freezing water within the hydrogel. Hydrogel F2 followed with a FWC of 38.2% then hydrogel F1 at 12.6%. Between sets 1 and 2, hydrogel F1 maintained an almost 1:1 ratio of freezing and non-freezing water content.

Lastly, set 3 brought about the largest increase in FWC for hydrogel F2 at 57.2%, shown in Figure 3.10. Hydrogel F1 maintained a low FWC at 13.2% whilst the FWC of hydrogel F3 was at 37.2%, the closest to the group's average FWC of 36.5%. Also, hydrogel F2 then had an almost 2:1 ratio of FWC to NFWC at 57.2% to 20%. However, a steady increase in NFWC was seen from hydrogels F1-F3.

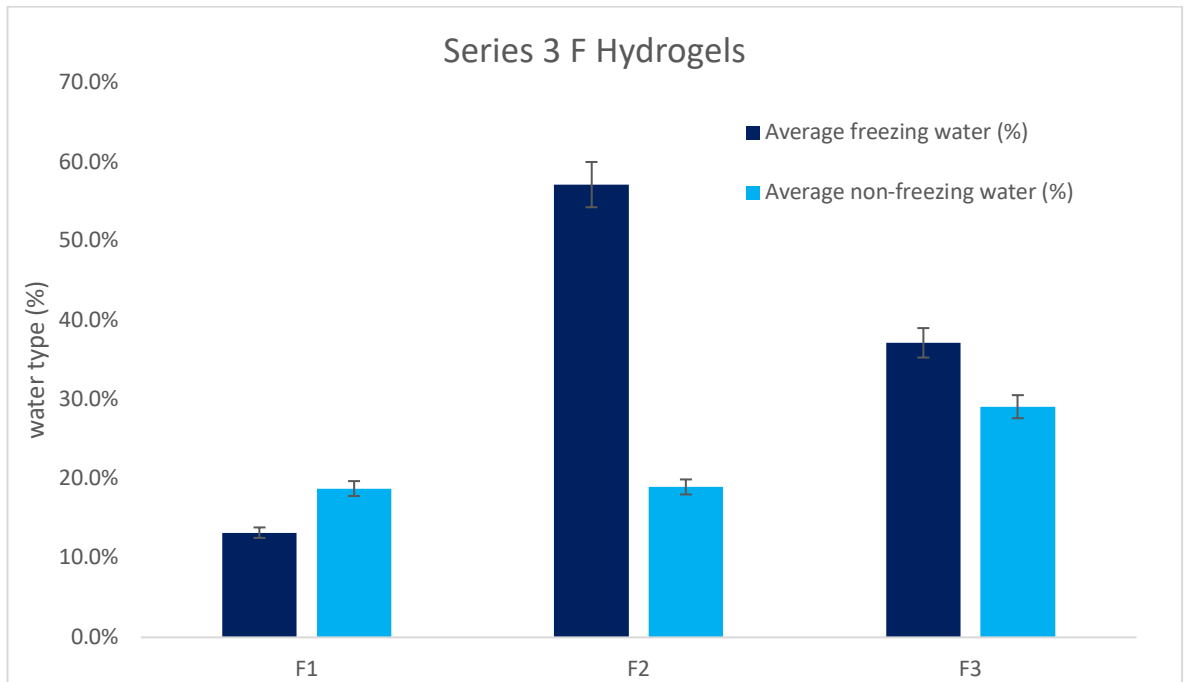


Figure 3.10 FWC & NFWC of set 3 hydrogels

3.3 Discussion

3.3.1 Relationship between water content & formulation

It is thought that as the hydrophilic components of a hydrogel formulation increases, it would be correlated with an increase in water content, specifically equilibrium water and freezing water content. Water-solubilising groups such as hydroxyl groups, carbonyl groups, ester groups and amide groups found along the polymer chain contribute greatly to the hydrophilicity of a hydrogel (Gun'ko et al, 2017). These groups attract and retain water molecules by forming hydrogen bonds and electrostatic attraction between the O-H bonds of the water molecule and the functional group.

A key reason behind the formulation of the hydrogels was to identify whether a change in monomer ratio would have a direct impact on the water content of the hydrogels and whether a specific monomer would have a greater effect on this content than the other.

In all of the E hydrogels from sets 1-3, a trend was noticed between the EWC and DMA/NVP content. However, the trends were not consistent between sets, but a change was definitive.

Starting with the set 1 E hydrogels, a trend was noticed between the DMA monomer content of the gels and their equilibrium water content. As DMA increased, there was an increase in the EWC of the hydrogels as well, as shown in Figure 3.11.

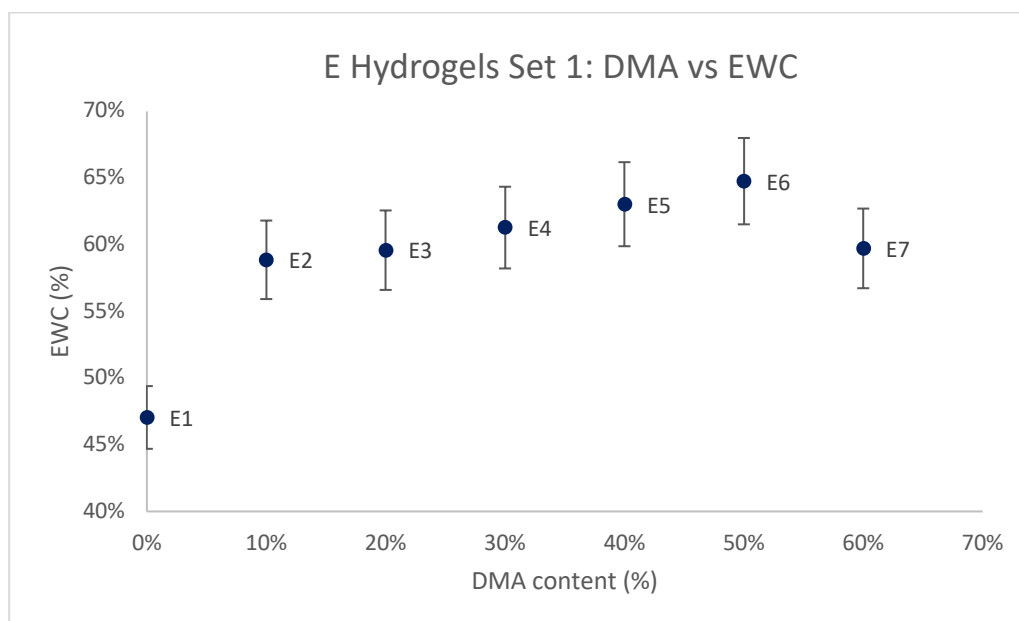


Figure 3.11 DMA content (%) vs EWC (%) – E hydrogels of set 1

Therefore, when EWC was plotted against NVP content for the same set of hydrogels, a decrease in EWC was seen.

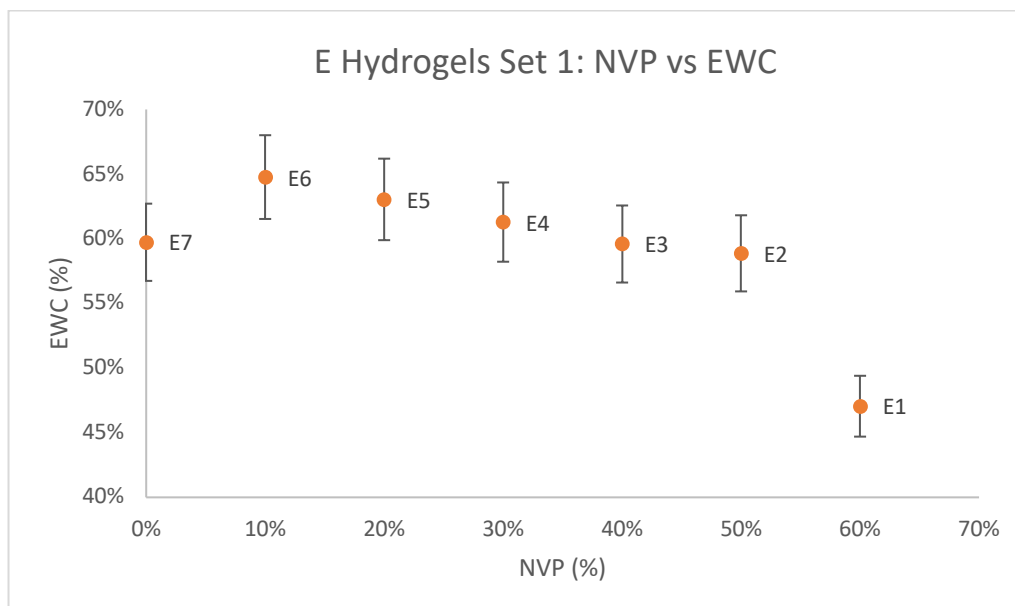


Figure 3.12 NVP content (%) vs EWC (%) – E hydrogels of set 1

The trend seen suggests that not all hydrophilic monomers bear the same degree of water-attracting properties but it also suggests that the hydrophobic monomer, which was thought to be the most influential factor in determining the EWC of the hydrogel may not be as impactful, in the case of these particular hydrogels. When charted, the EWC of the hydrogels changed despite the fact that TRIS content remained constant, suggesting the hydrophobic monomer was not significant to determining the EWC of the hydrogels. This may speak to the reactivity ratios of each monomer used in the formulation of the hydrogels and their incorporation into the polymer microstructure, which is discussed in further detail in the discussion section of the membrane characteristics chapter (7.5.4). However, it could also be argued that the lack of trends associated with the TRIS monomer content and EWC are because of this constant value.

In the E hydrogels of set 2, the opposite trend is seen. As DMA content within the hydrogels increased, the EWC decreased as shown in Figure 3.13. There is an increase in the EWC between hydrogels E1 and E2 before declining between hydrogels E3 to E5 before increasing again in hydrogels E6 and E7. Despite this, there is an overall decline in the EWC of the hydrogels as DMA content increases across the set. The key difference between set 1 and set 2 is the use of a post-cure and the use of a diluent. The set 2 hydrogels do not have a diluent in their formulation but the hydrogels were exposed to a post-cure. The set 1 E hydrogels have a diluent in their formulation and but were not exposed to a post-cure.

The decrease in EWC as NVP content increased (see Figure 3.12) demonstrated by hydrogels E7 and E1 may be as a result of the lack of the other hydrophilic monomer, DMA, in their formulations.

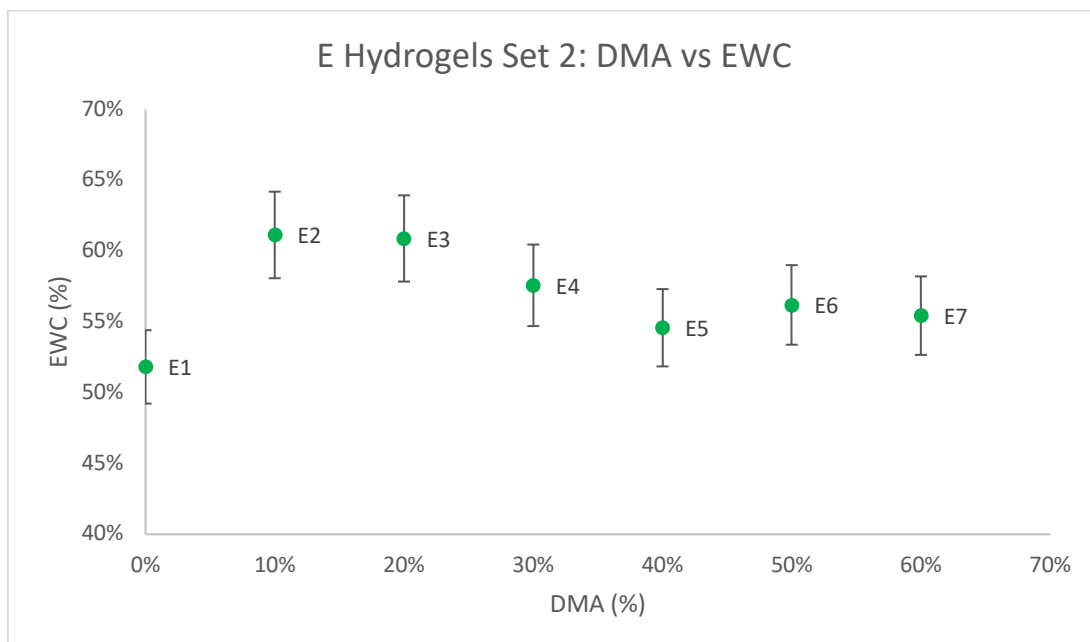


Figure 3.13 DMA content (%) vs EWC (%) – E hydrogels of set 2

Plotting the same hydrogels' EWC against NVP content shows an upward trend as NVP content increases (Figure 3.14 below).

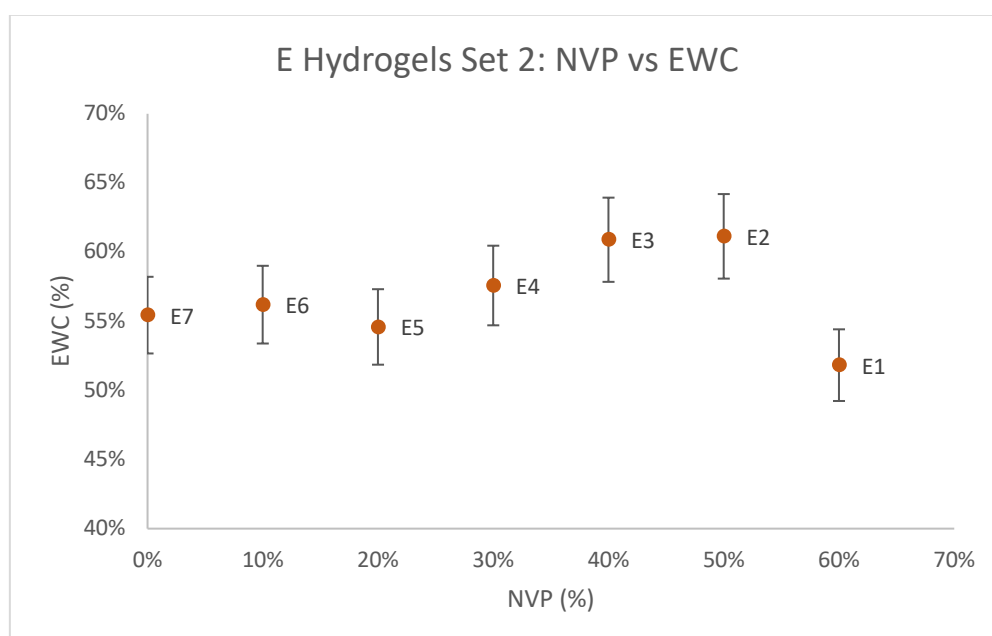


Figure 3.14 NVP content (%) vs EWC (%) – E hydrogels of set 2

With the E hydrogels of set 3, although a trend is seen, it is more ambiguous than the previous sets. But it can be said that as DMA increases, a decrease in EWC is noticed, shown in Figure 3.15.

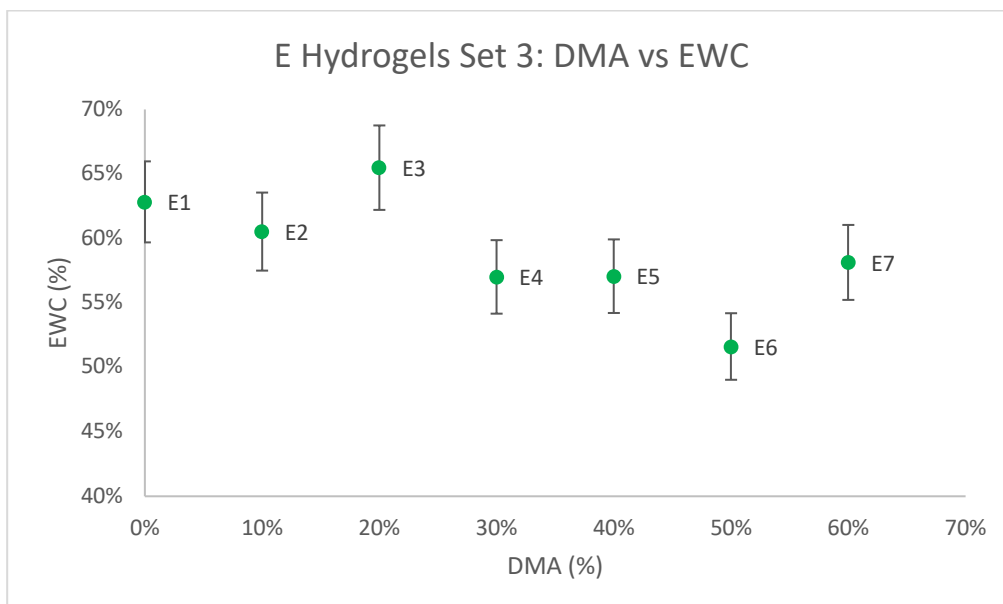


Figure 3.15 DMA content (%) vs EWC (%) – E hydrogels of set 3

And the opposite was seen when NVP monomer content was plotted against EWC, shown in Figure 3.16.

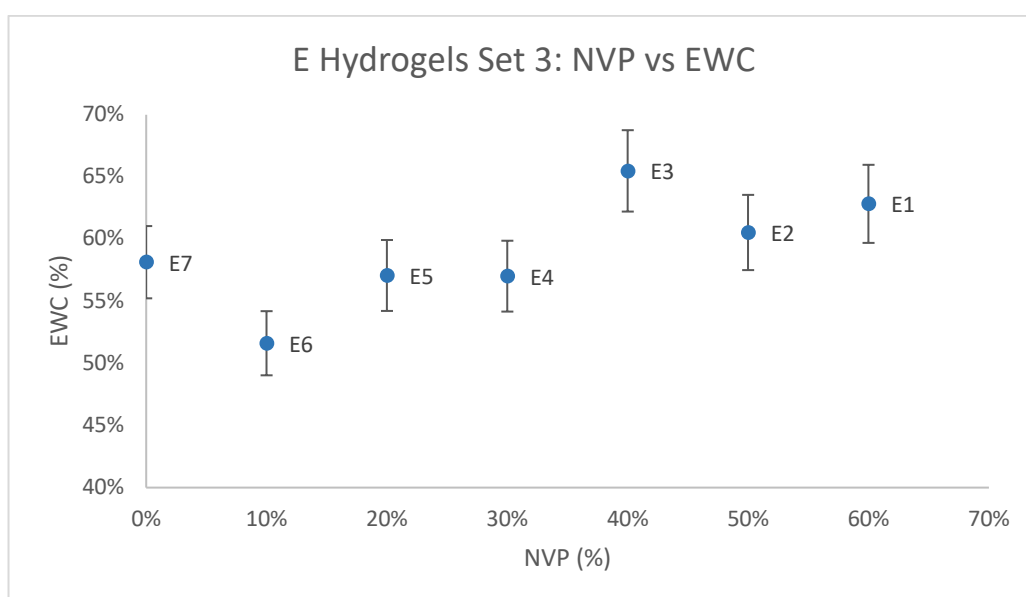


Figure 3.16 NVP content (%) vs EWC (%) – E hydrogels of set 3

It was hypothesised that a post-cure could improve the incorporation of low reactivity monomers into the final polymer structure, such as NVP. If true, the effects of the post-cure on the E hydrogels of set 3 are shown in Figure 3.16 – the hydrophilic ability of the NVP monomer becomes more evident across the set as its quantity increases. This notion could speak to the synergistic properties of both DMA and NVP and how they increase the hydrophilic nature of a formulation when used in tandem. Wan et al (2005) synthesised a series of polyacrylonitrile (PAN) & NVP films in which they varied the amount of NVP in the formulation and they found that the films with a higher NVP content had a higher water content which they attributed to the presence of the carbonyl group on NVP being able to bind to more stable water molecules (Bag & Valenzuela, 2017). Nie et al (2003) found that the biocompatibility of a PAN hydrogel

increased when NVP was incorporated into the formulation and biocompatibility of silicone-based hydrogels is often attributed to its ability to absorb and retain water (Pedley et al, 1980).

Analysis was carried out to understand the relationship between the formulation of the hydrogels and their freezing and non-freezing water content. However, a clear correlation was not established. With the E hydrogels of set 1, as DMA content increases, the FWC of the hydrogels remains in a similar region. The same is seen when FWC was plotted against NVP (see appendix section 1.3).

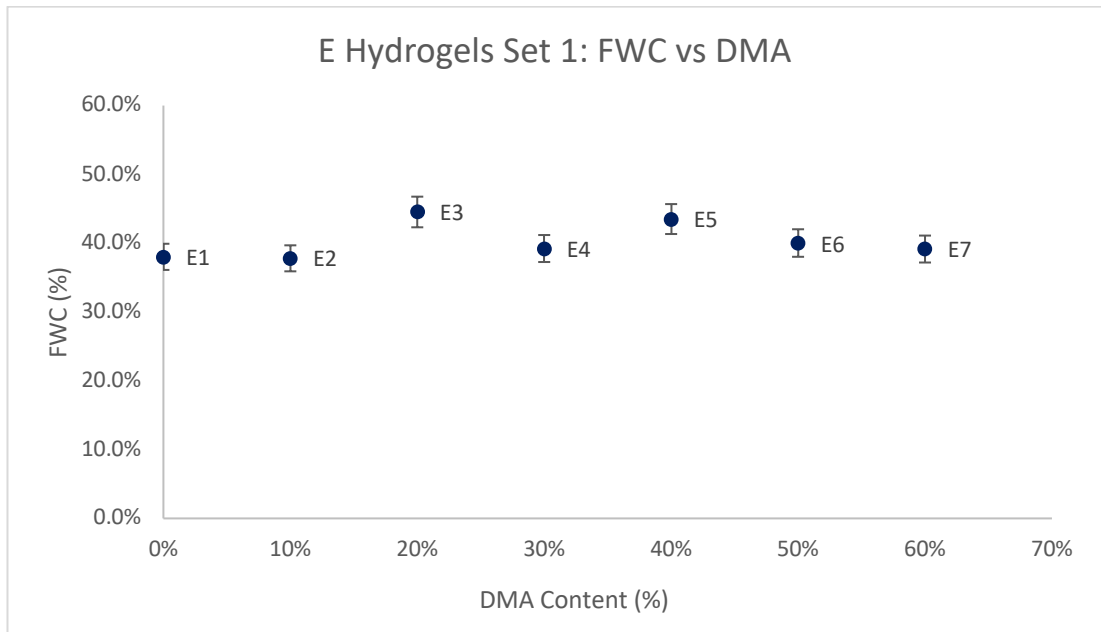


Figure 3.17 DMA content (%) vs FWC (%) – E hydrogels of set 1

The correlation with the set 2 hydrogels is more sporadic, seen below in Figure 3.18. Here, the relationship between FWC and DMA can be seen.

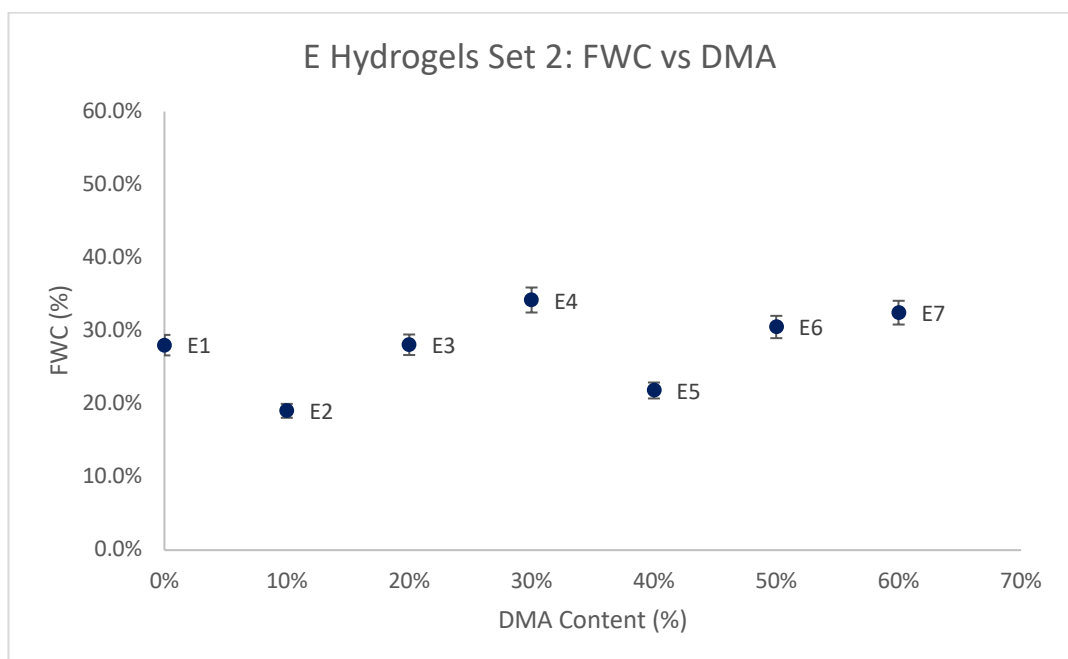


Figure 3.18 DMA content (%) vs FWC (%) – E hydrogels of set 2

It appears as if the FWC increases between hydrogels E2 to E4 before decreasing at E5 then increasing until hydrogel E7. This may appear to be a phenomenon, but it also could be coincidental. The inverse is seen when FWC is plotted against NVP, shown in appendix section 1.3.1.

In regards to the set 3 hydrogels, a similar pattern seen with the set 2 hydrogels was noticed in Figure 3.18. However, the trend is more exaggerated in the set 3 hydrogels. From hydrogels E2-E4, there was an increase in FWC then from hydrogels E4-E7, there was a clear decline in FWC as DMA content increased. The inverse was seen when correlating NVP content with FWC, shown in appendix section 1.3.1.

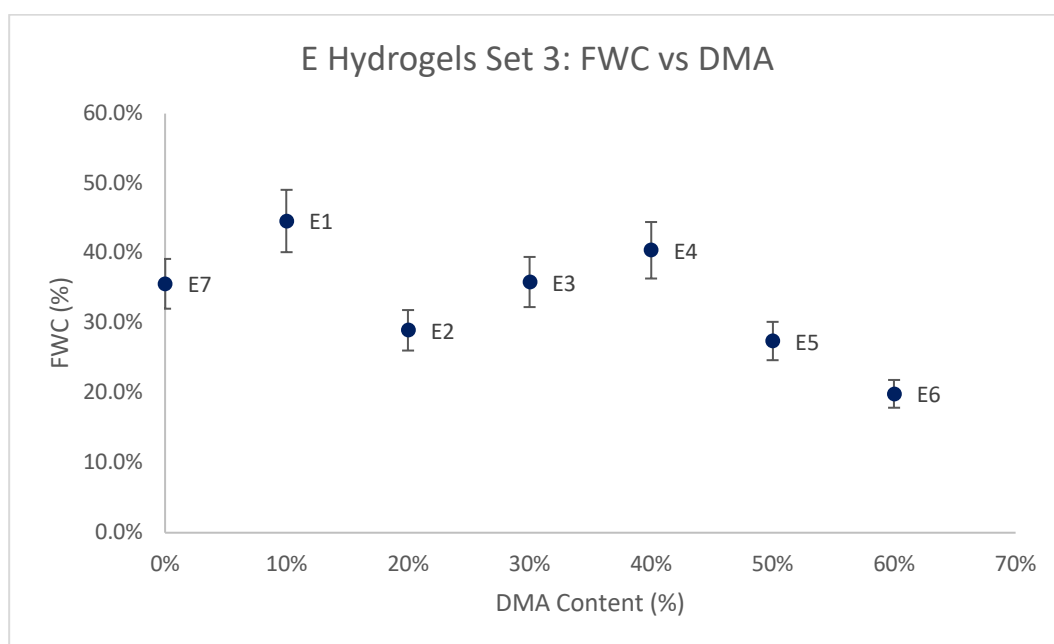


Figure 3.19 DMA Content (%) vs FWC (%) – E hydrogels of set 3

As mentioned previously, there was not a definitive formulation trend in the synthesis of F hydrogels so a clear relationship between NVP/DMA content and the FWC/NFWC content of the hydrogels cannot be established as clearly as it is for the E hydrogels.

In regards to non-freezing water content, none of the E or F series hydrogels in any set exhibited a definitive trend between NVP/DMA content and an increase or decrease in NFWC. The only hydrogels that alluded to a possible trend were the E hydrogels of set 3. Shown in Figure 3.20, there was an increase in hydrogels E7 to E5 and another increase from hydrogels E4 to E2 as NVP content increased up the set.

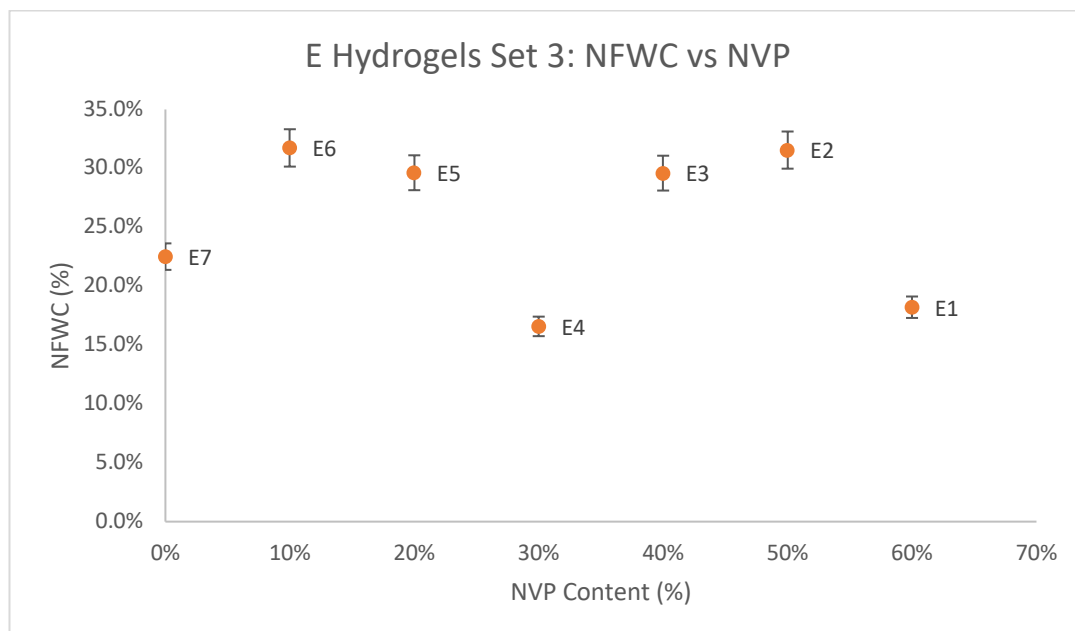


Figure 3.20 NVP Content (%) vs NFWC (%) – E hydrogels of set 3

With DMA content, a decrease was seen from hydrogels E2 to E4 and again from hydrogels E5 to E7, although less steep as seen in Figure 3.21.

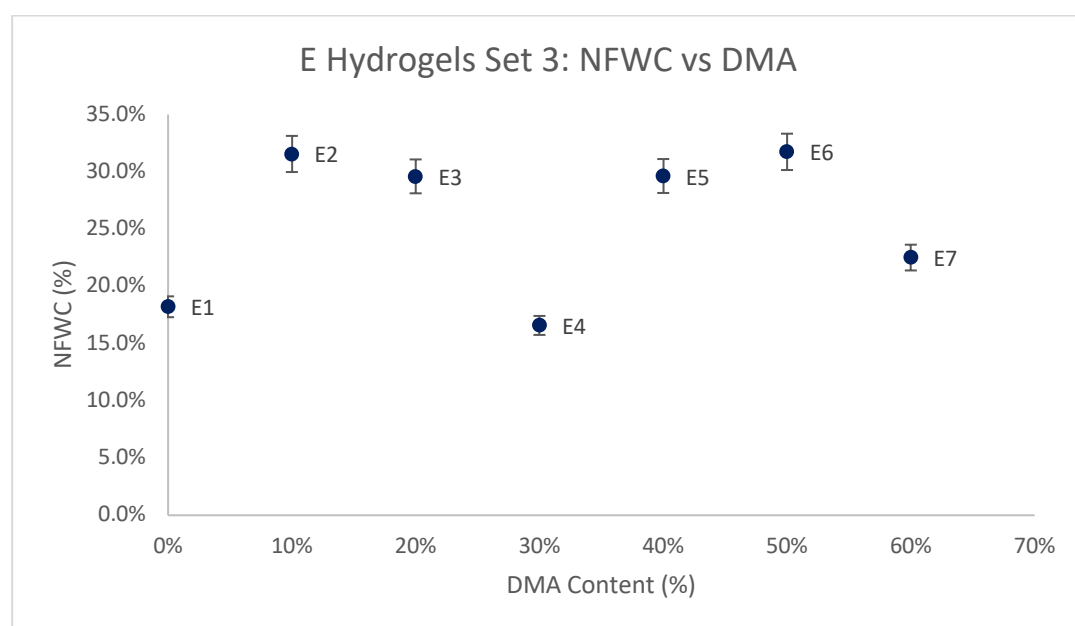


Figure 3.21 DMA Content (%) vs NFWC (%) – E hydrogels of set 3

In the case of the F hydrogels from all sets, it is more difficult to identify a trend or relationship between the different water types and the formulation as there was not an incremental change in either hydrophilic monomers or the hydrophobic monomer from hydrogel F1 to hydrogel F3. The hydrogels of the F series should be viewed and analysed as independent hydrogels as opposed to those of the E series which can be seen as a collective with a commonality between them.

The morphology of the hydrogels also contributes to the water content, specifically the occurrence of phase separation which will be discussed in further detail in the membrane characteristics chapter G. Durowoju, PhD Thesis, Aston University 2022.

(7.5.1). During co-polymerisation between the hydrophilic monomers and silicone monomer, it is thought that the short but flexible silicone chains are able to disperse the hydrophilic domains along the polymer chain to reduce interaction tension between water molecules and these hydrophilic regions. With this, water is able to disperse itself freely along the chain and throughout the polymer network resulting in relatively average EWCs of the hydrogels but higher levels of freezing/free water (Tao et al, 2017). This phasing has a direct effect on water content, which in hand affects the permeation abilities of the hydrogel. Another factor that could affect this phenomena would be the cross-linking chain length but seeing as the cross-linker was kept constant in the formulation of the hydrogels, this effect can be discounted.

3.3.2 Peak Splitting & Water Structuring

Beyond the water types that have already been identified (FWC & NFWC), DSC thermograms with evident splitting of the thermogram peak suggests there are phases within these water types that are present within the hydrogel. For the sake of easing this explanation, freezing water can be subdivided into two distinct “categories”: polymer-associated water content (PAWC) and ice-like water content (ILWC). Ice-like water is not bound to the polymer matrix and has a high degree of mobility. The melting point of this water type is very similar to freezing water so it can be identified as the part of the thermogram peak that occurs after 0 °C (Mann et al, 2019). Polymer-associated water, also referred to as freezing bound water (Wan et al, 2005; Bag & Valenzuela, 2017) has a lower melting point than pure water due to it being loosely bound to the polymer chain. The melting point of pure water can be changed if impurities are introduced (S.P Forsey, N.D). This water “type” behaves similarly to free water but its mobility is reduced and it can be identified as part of the thermogram peak that occurs before 0°C.

Typically in literature relating to hydrogels, the general consensus states there are three types of water present: freezing water, intermediate water and bound water (Sekine et al, 2004, Bag & Valenzuela, 2017). Intermediate water is often described as having weak interactions with the polymer matrix and exists in a state between free (freezing) and bound (non-freezing) water.

The existence of these water types can be explained by understanding the way water behaves: structurally, a water molecule consists of two hydrogen atoms covalently bonded to an oxygen atom. An oxygen atom bears four electron pairs, two pairs are used in the covalent bonding between the two hydrogen atoms. The remaining pairs allow a water molecule to form its (unique) tetrahedral structure by electron repulsion.

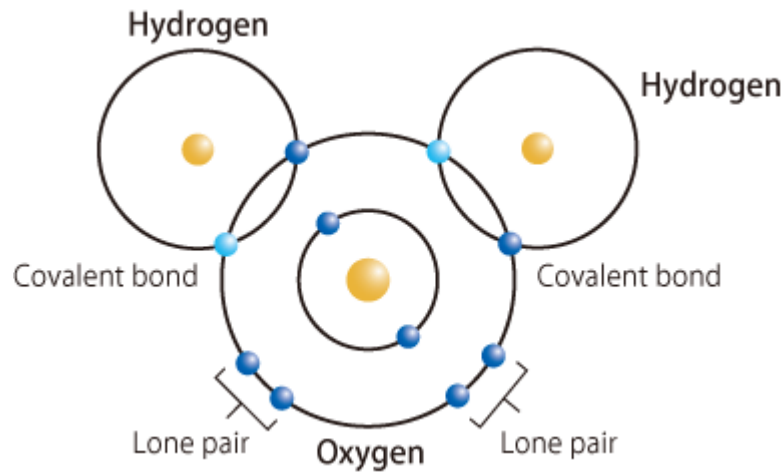


Figure 3.22 Water molecule & its electron pairs (source: Honda, (N.D))

The electrostatic force between the oxygen atom in one water molecule and the hydrogen atom of another water molecule is referred to as a hydrogen bond (Elangannan et al, 2011). In ice, a single water molecule is able to form 4 hydrogen bonds with neighbouring water molecules whereas, in water, an averaged 3.4 hydrogen bonds are able to form (Jhon & Andrade, 1973). This is due to the crystal lattice between the molecules being broken in order to allow the water molecules to move around as a fluid. In a system that contains both hydrophobic and hydrophilic regions, water would hydrate the hydrophilic regions and exclude the hydrophobic sections. In the context of a hydrogel, hydrophobic regions of the polymer chains would lead to imperfections within the crystal lattice of ice upon freezing, influencing the melting points of the water along the chain (Saez-Martinez et al, 2021), arising in the different water types that can be identified based on the different temperatures at which they melt.

The thermogram for hydrogel E3 of set 2 has been included to demonstrate an instance of this peak splitting, shown in figure 3.23.

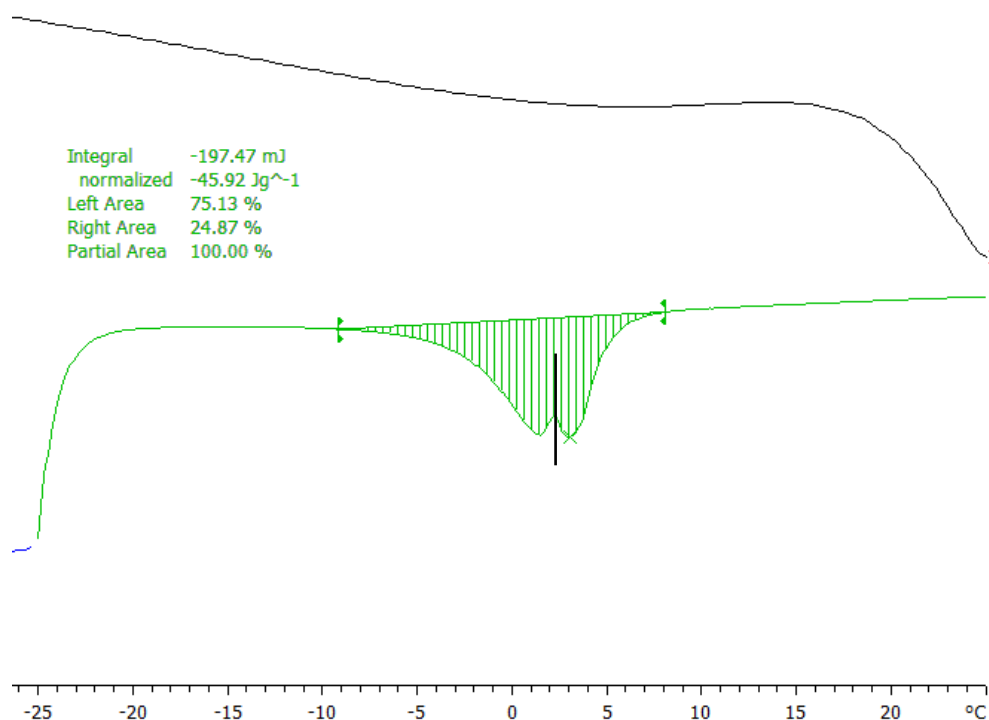


Figure 3.23 DSC thermogram of hydrogel E3 (set 2). Thermogram shown, black line separating peaks. G.Durowoju, PhD Thesis, Aston University 2022.

The entire thermogram spans across -9 to 8 °C, representing freezing water. The peak divides into two halves at 2 °C. The first half of this thermogram represents polymer-associated water whilst the second half represents ice-like water. Peak-splitting analysis was conducted on all the DSC thermograms derived for each E & F hydrogel in their respective sets. Figure 3.23 showcases the ratio of polymer-associated water (PAW) and ice-like water (ILW) within the E & F hydrogels of set 1.

Noticeably, hydrogel F1 – the hydrogel with the lowest EWC and highest amount of the silicone monomer in its formulation – has the lowest amount of ILW at 2.8%. Hydrogel E3 possesses the largest amount of both ice-like and polymer-associated water but this occurs at a 1:1 ratio, as shown in Figure 3.24. With the F series, hydrogel F3 had the highest levels of both ILW and PAW.

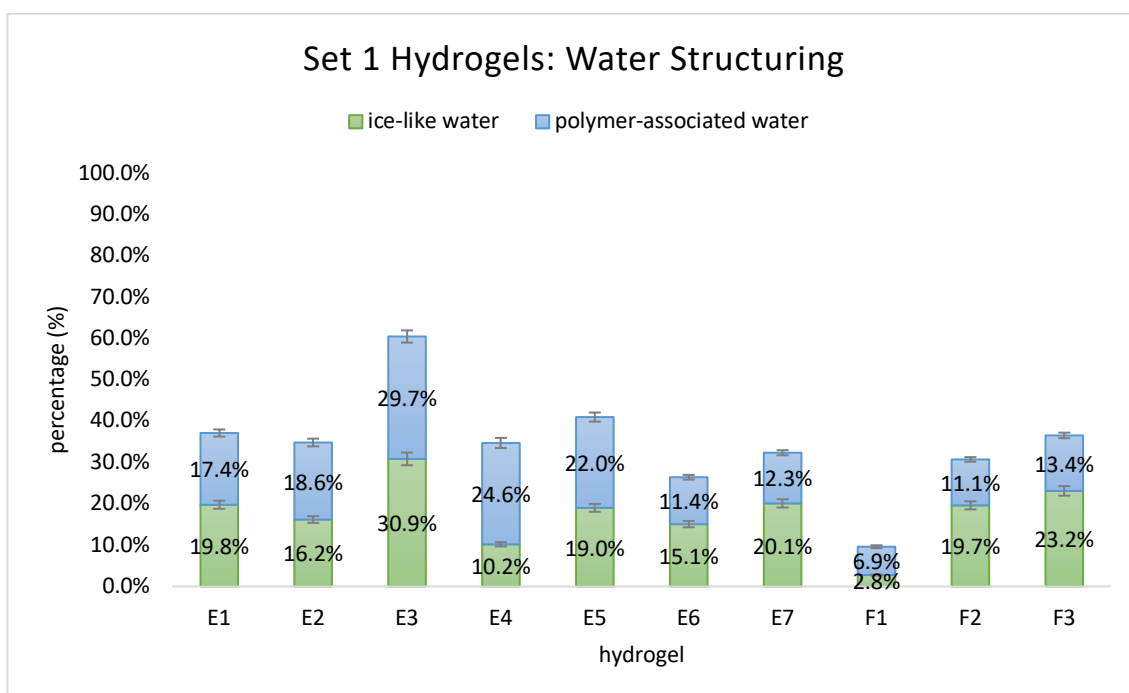


Figure 3.24: Set 1 Hydrogels: Water Structuring

With the set 2 hydrogels, hydrogel F1 also had the lowest ILWC and PAWC at 3.6% and 9.4% respectively. Hydrogel F3 had the highest ILWC of all the E & F hydrogels at 28.3%, increasing from its set 1 version. Hydrogels E1, E6 and E7 had similar ILWCs within the 20% range. Hydrogel E1 also had the lowest PAWC of the set at 8%, as seen in Figure 3.25.

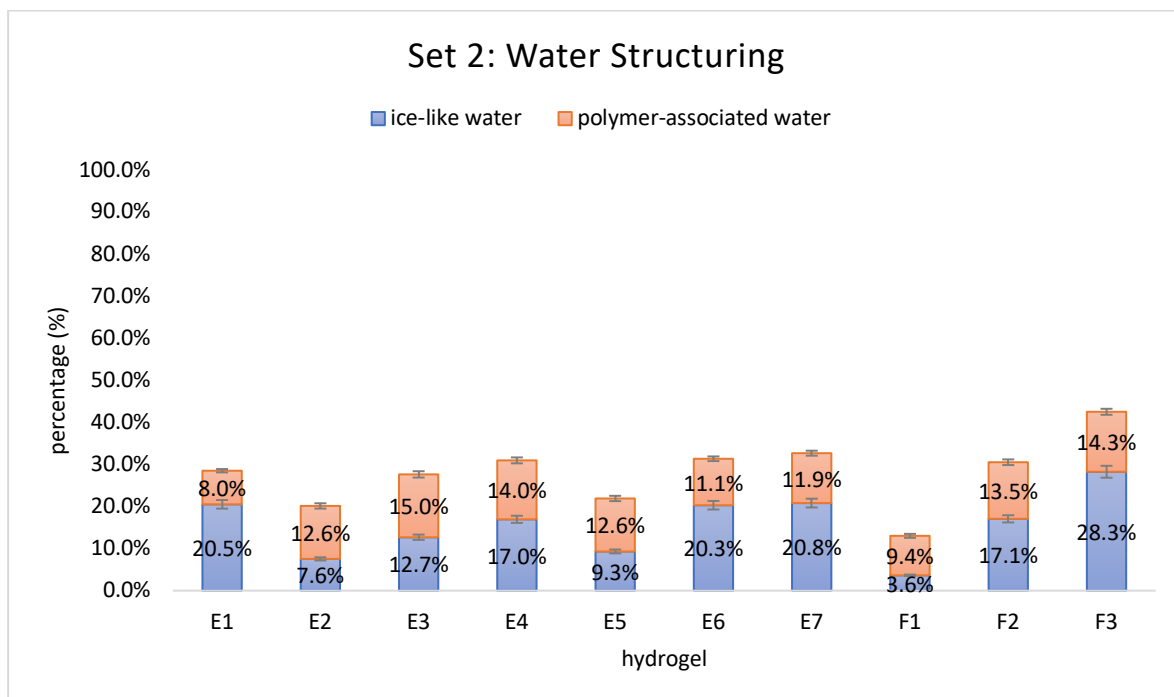


Figure 3.25: Set 2 Hydrogels: Water Structuring

Referring to figure 3.26, the ILWC of the set 3 E & F hydrogels, were higher when compared to those of set 1 and 2, suggesting the reaction conditions of the set in addition to the formulation were capable of producing hydrogels with increased levels of the water “type” with increased mobility. Hydrogel F2 had the largest ILWC of all the hydrogels at 44.2%, followed by hydrogel E1 at 36.2%. Both of these hydrogels did not include the hydrophilic monomer DMA in their formulation, they were made up of NVP-TRIS in addition to a diluent. Hydrogel F1 had the lowest ILWC of all the hydrogels from sets 1-3 in set 3 at 0.2% whereas hydrogel E5 had the lowest PAWC of both the E & F hydrogels at 8.5%.

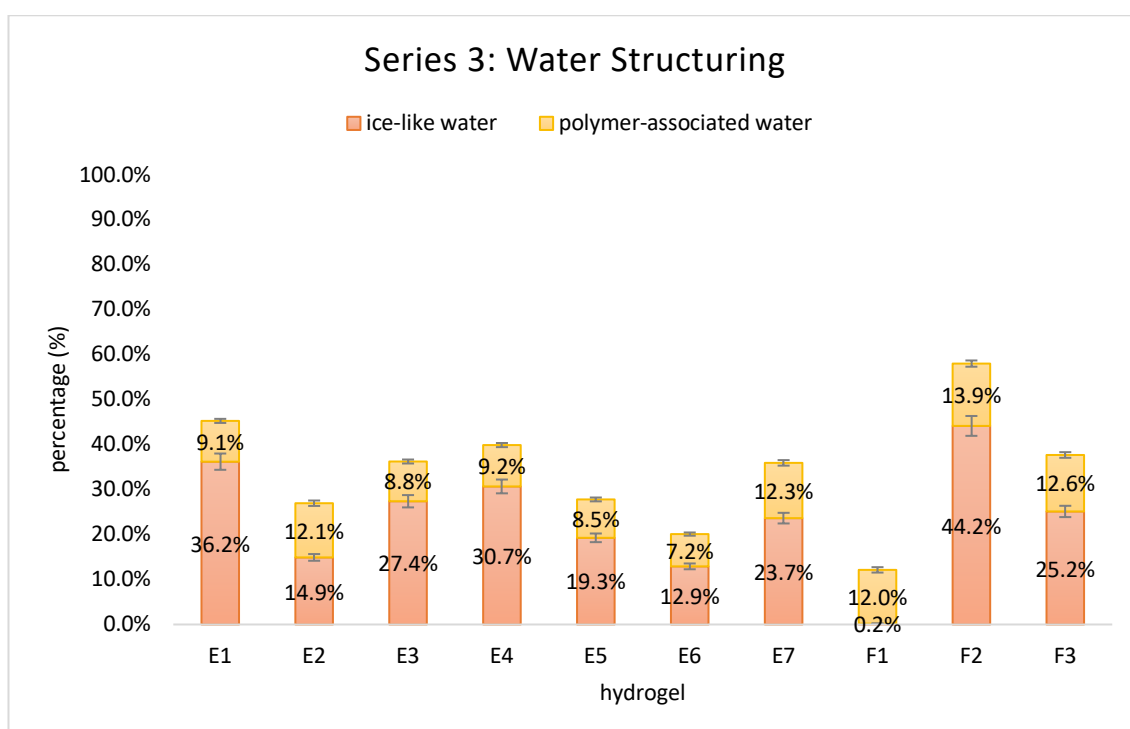


Figure 3.26: Set 3 Hydrogels: Water Structuring

3.3.2 Relationship between water content & synthesis conditions

As previously mentioned, three sets of hydrogels were synthesised. The formulations between each set were kept constant in regards to monomers DMA, NVP and TRIS, however, the conditions that were purposely altered were the presence of a diluent and the inclusion of a post-cure. The reaction conditions for each set synthesised are as follows:

- Set 1: a diluent was included but the hydrogels were not post-cured.
- Set 2: no diluent included but the hydrogels were post-cured.
- Set 3: a diluent was included and the hydrogels were post-cured.

The main aim behind manipulating these conditions was to understand how important their inclusion or lack thereof would affect the overall characteristics of the hydrogels, especially in terms of their permeation behaviour and water content. Typically, diluents are included in the formulation of a hydrogel to fulfil two main purposes: to prevent the silicone monomer from precipitating out during polymerisation therefore ensuring its incorporation into the macrostructure of the hydrogel, and secondly, to fill in the spaces that water would otherwise occupy during the polymerisation reaction and provide a structure to the developing hydrogel arrangement.

A post-cure is the act of heating the hydrogels immediately after their synthesis has reached completion. takes place at 60 °C and the post-cure occurs at 90 °C. The ethos behind a post-cure is to remove residual, unreacted monomer from the macrostructure of the hydrogel.

Diluents such as 3-octanol have been found to increase the pore volume of cross-linked hydrogels and produce pores with a relatively large diameter. Also, the pore distribution of hydrogels with such diluents are characterised by having a large proportion of meso- and macropores (Okay, 2000). It has been noted that the majority of water present within macropores is bulk water, a general water type present in hydrogels that freezes at 0°C that is capable of solvating substances within a hydrogel (Savina et al, 2011).

With that in mind, it was thought that there would be a trend seen within the hydrogels in which a diluent was utilised (the set 1 E hydrogels and the set 3 E & F hydrogels) and their equilibrium water content - it was thought that their EWCs would be generally higher than those of set 2 which did not contain a diluent. However, that was not explicitly the case. In three instances, an increase in EWC in both set 1 and set 3 was seen in hydrogels E5, E7 and F2. In hydrogels E1, E3 and F1, a steady increase in EWC from set 1 to 3 was seen. Meanwhile in hydrogels E4, E6 and F3, a decrease in EWC from set 1 to 3 was witnessed.

It was hypothesised that the interaction between DMA and NVP monomers during the early stages of polymerisation sets the tone for the behaviour of a hydrogel towards water. During polymerisation, the monomers form individual clusters which organise themselves to form the polymer backbone with alternating blocks of DMA and NVP. NVP is said to have low reactivity, which means it is reluctant to incorporate itself into the chain. DMA ushers these NVP clusters and encourages its incorporation before silicone (TRIS) clusters begin to insert themselves along this chain, creating hydrophobic regions.

During polymerisation, the order that monomers organise themselves into sequences, whether random or ordered, along the polymer chain is dependent on their reactivities.

If the product of reactivities (r_1, r_2) is equal to zero, the order of the sequence is in an ordered manner between the two monomers. If the product is equal to one, the radicals of each monomer has no preference and the order of the sequence is random. In such circumstances, one monomer is usually more reactive than the other. In this case, this monomer will make up a greater proportion of the repeat units along the chain. Methyl acrylate and styrene are often used as a standard for reference against another monomer to present in a ratio. The reactivity ratios are still applicable in the case of this project despite the presence of 3 monomers. However, this phenomenon will be discussed in further detail in chapter 5 – the morphology chapter.

3.4 Conclusion

Overall, the results discussed showed that a TRIS-NVP-DMA monomer formulation is capable of producing silicone-based hydrogels with equilibrium water contents in the range of 50-60% regardless of the use of a diluent which is known to influence the absorption of bulk water within a hydrogel.

An increase in the equilibrium water content of the E hydrogels of set 1 as DMA monomer content increased was observed whilst a decrease in this water content was seen as NVP content increased. An influence on EWC by these same monomers was not witnessed with the F hydrogels also of the same set. Meanwhile, the E hydrogels of set 2 demonstrated an increase in equilibrium water content as NVP monomer content of the hydrogels increased. Conversely, a decrease in EWC was noticed as DMA content increased. Trends seen with the set 3 E hydrogels were not as clear-cut as was the case with the E hydrogels of set 1 and 2 but overall, there was an increase in the equilibrium water content of the hydrogels as NVP monomer content increased. This observation suggests the effects of a post-cure increased NVP incorporation into the polymer network, allowing for its hydrophilic properties to influence water absorption more so than the other hydrophilic monomer, DMA.

The F series of hydrogels were analysed separately from the E series due to the difference in formulation between the sets. Hydrogel F1, the hydrogel with the least amount of all water types and the highest amount of the hydrophobic monomer TRIS, saw an increase in EWC from sets 1-3, suggesting the effects of a post-cure and inclusion of a diluent were favourable to its water absorption abilities. The reverse was seen in hydrogel F3 who saw a decrease in EWC from sets 1-3, despite it having the highest DMA content of all the hydrogels from both the E and F series.

The E hydrogels of sets 1-3 did not show a noticeable trend in terms of formulation or synthesis conditions affecting its freezing or non-freezing water content. Meanwhile the F hydrogels showed that non-freezing water increased from hydrogel F1-F3 in set 1 and both freezing and non-freezing water increased from hydrogel F1-F3 in set 2. In set 3, non-freezing water content increased from hydrogel F1-F3. A trend was not established between the F hydrogels and their freezing water content but there was an increase in non-freezing water content from hydrogel F1-F3 across all sets.

A post-cure is meant to remove unreacted monomers from the hydrogel structure whilst a diluent creates spaces within the hydrogel microstructure during polymerisation that will later be filled with water upon hydration. From sets 1-3, hydrogels E1 and E7 showed a deviation from whatever trend was occurring when equilibrium water content was plotted against the NVP or DMA content of the hydrogels. These hydrogels demonstrated what can occur if the monomers are not used in tandem and suggests there is a synergistic nature to these hydrophilic monomers that has a direct influence on the water-absorbing abilities of hydrogels that utilise them. The hydrophobic nature of TRIS is documented clearly in hydrogel F1 as this hydrogel remained the lowest in all water types, regardless of synthesis conditions.

The lack of a relationship between freezing water content and hydrophilic monomer content that was seen across the hydrogels from sets 1-3 suggests the absorption of this specific water type does not rely solely on the amount of hydrophilic monomer but other factors may also influence its presence such as reaction conditions (post-cure and the use of a diluent).

4 Partitioning

4.1 Introduction

Rationale: the partition coefficient is referred to as a thermodynamic property (Peng & Chauhan, 2012), meaning it is a measurable feature of a system that can be used to describe the state of a physical system (Cengal et al, 2011). In this case, a partition coefficient can be used as a 'snapshot' of the microstructure of a hydrogel, by describing a solute's preference on where it will dwell – within the hydrogel or in water surrounding the hydrogel. This coefficient also provides insight on the distribution of hydrophilic and hydrophobic regions throughout the hydrogel which can be used, in conjunction with diffusion and permeation studies, to understand transport behaviours of ions. Seeing as the intended aim of the hydrogels synthesised and characterised in this thesis is to be included in biomedical applications that rely on the transport of substances, this information is vital. Determining relationships between partitioning and the different water types as well as formulations is vital to further understand factors that can influence the partition coefficient of silicone-based hydrogels towards certain ionic salts.

The partition coefficient of a hydrogel describes the distribution of a solute between a hydrogel and its surrounding environment (solution) at equilibrium (Gehrke et al, 1997).

Uptake and release processes in relation to hydrogels are heavily dependent on the interaction between a solute and the hydrogel network and this can be investigated by understanding the partition coefficient of a hydrogel against a specific solute. This coefficient, often represented as K , is calculated using the following equation:

$$K = \frac{\text{concentration of solute in hydrogel}}{\text{concentration of solute in solution}} \quad (4.1)$$

As stated in the introductory chapter of this thesis, hydrogels are described as cross-linked polymer networks that are made up of a mesh-like network with the spaces in between this network being filled with water (Bahram et al, 2016). Solutes such as salt ions partition and diffuse through this mesh but this is dependent on several factors, including the size and charge of the solute, the amount of water within these spaces as well as the size of the spaces of the polymer network. The solute may also adsorb to the polymer chain of the hydrogel which reduces its diffusion through the hydrogel but results in larger partition coefficients (Liu, 2016), illustrated in Image 4.1.

In the case of silicone-based hydrogels, there are different phases within the network of the hydrogel due to the hydrophilic and hydrophobic monomers used during their synthesis. As a result of this, it is thought that the hydrophilic regions of the gel would facilitate the movement of aqueous-solute transport whilst the silicone-rich regions would facilitate the movement of the lipophilic substances. However, the overarching aim of this project focuses on the transport behaviour of aqueous salt solutions and how this differs depending on the formulation of a particular hydrogel.

The suggested application for these hydrogels leans towards processes that include and depend on the separation and release of solutes. Understanding the partitioning and diffusion of molecules in the gels provides insight to the physical microstructure of the hydrogel as well as understanding the interaction between said molecules and the matrix of the hydrogel. Factors that can affect how a solute partitions into a hydrogel include the strength of the interacting forces between the solute and the hydrogel network (hydrogen bonding, electrostatic forces, Van der Waal forces), the radius of the polymer chains, the size and shape of the solute as well as the volume fraction (ϕ) of the hydrogel (Tong & Anderson, 1996).

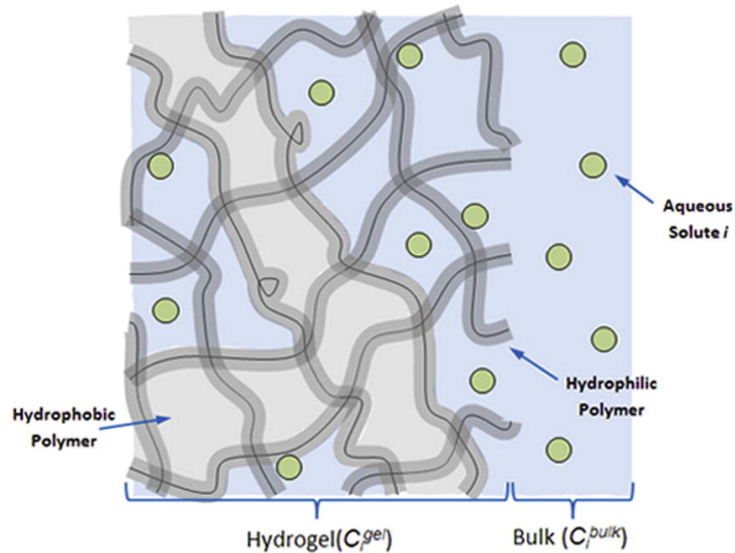


Image 4.1 schematic representing a hydrogel polymer matrix and how an aqueous solute could interact with the network (Image source: Liu et al, 2015)

Determining the partition coefficient of a hydrogel is also not limited to salt solutions. Studies have been conducted that load the hydrogel with a drug to determine its usefulness as a drug delivery system (Kim et al, 2008 & Dursch et al, 2014). Partitioning provides information about how a hydrogel interacts with certain solutes which indicates its suitability for certain applications such as being included in drug delivery systems and contact lens wear.

4.2 Results

Four salts were utilised in the partition coefficient experiments: calcium chloride, potassium chloride, sodium chloride and magnesium chloride. Each of the experimental sets were repeated a minimum of three times per salt/hydrogel combination. The following Tables detail the average equilibrium partition coefficient for each hydrogel in tandem to each chloride salt. As with previous data reporting, the tables (4.1 - 4.6) have been split into hydrogel series (E or F) and the synthesis conditions sets (1, 2 and 3). The figures in brackets represent the standard deviation.

Table 4.1 Partition Coefficients for E Hydrogels of Set 1 (brackets indicate standard deviation)

	E1	E2	E3	E4	E5	E6	E7
CaCl₂	0.14 (0.02)	0.16 (0.02)	0.13 (0.03)	0.19 (0.02)	0.18 (0.01)	0.15 (0.02)	0.16 (0.01)
KCl	0.19 (0.02)	0.31 (0.05)	0.25 (0.07)	0.17 (0.05)	0.24 (0.01)	0.25 (0.04)	0.40 (0.3)
NaCl	0.21 (0.02)	0.22 (0.03)	0.18 (0.06)	0.22 (0.04)	0.20 (0.02)	0.25 (0.02)	0.28 (0.06)
MgCl₂	0.19 (0.06)	0.23 (0.03)	0.26 (0.03)	0.25 (0.07)	0.22 (0.003)	0.21 (0.06)	0.15 (0.04)

Table 4.2 Partition Coefficients for F Hydrogels of Set 1 (brackets indicate standard deviation)

	F1	F2	F3
CaCl₂	0.10 (0.01)	0.17 (0.02)	0.16 (0.02)
KCl	0.08 (0.01)	0.26 (0.01)	0.15 (0.01)
NaCl	0.07 (0.04)	0.22 (0.01)	0.15 (0.04)
MgCl₂	0.02 (0.003)	0.08 (0.02)	0.31 (0.07)

Table 4.3 Partition Coefficients for E Hydrogels of Set 2 (brackets indicate standard deviation)

	E1	E2	E3	E4	E5	E6	E7
CaCl₂	0.67 (0.08)	0.87 (0.09)	1.21 (0.011)	1.36 (0.07)	1.05 (0.03)	0.55 (0.01)	1.47 (0.22)
KCl	1.26 (0.02)	0.99 (0.05)	2.21 (0.08)	0.79 (0.004)	1.07 (0.09)	0.62 (0.15)	0.85 (0.18)
NaCl	0.53 (0.03)	0.51 (0.08)	0.50 (0.05)	0.51 (0.12)	0.52 (0.17)	0.94 (0.07)	0.56 (0.08)
MgCl₂	0.51 (0.12)	0.87 (0.02)	1.44 (0.15)	0.41 (0.004)	1.27 (0.02)	0.35 (0.04)	0.56 (0.13)

Table 4.4 Partition Coefficients for F Hydrogels of Set 2 (brackets indicate standard deviation)

	F1	F2	F3
CaCl₂	0.19 (0.03)	1.01 (0.02)	1.50 (0.37)
KCl	0.92 (0.08)	0.70 (0.17)	1.90 (0.05)
NaCl	1.18 (0.09)	0.56 (0.001)	0.69 (0.04)
MgCl₂	0.26 (0.04)	1.07 (0.16)	0.50 (0.07)

Table 4.5 Partition Coefficients for E Hydrogels of Set 3 (brackets indicate standard deviation)

	E1	E2	E3	E4	E5	E6	E7
CaCl₂	1.21 (0.06)	0.68 (0.05)	0.31 (0.09)	0.65 (0.03)	0.79 (0.03)	0.58 (0.06)	0.82 (0.06)
KCl	1.54 (0.11)	0.87 (0.02)	0.71 (0.03)	0.75 (0.08)	0.56 (0.01)	0.85 (0.05)	0.64 (0.08)
NaCl	0.64 (0.06)	0.46 (0.002)	0.57 (0.04)	0.27 (0.08)	0.51 (0.02)	0.74 (0.03)	0.59 (0.01)
MgCl₂	0.54 (0.01)	0.74 (0.01)	0.51 (0.04)	0.57 (0.04)	0.53 (0.01)	0.37 (0.03)	0.44 (0.06)

Table 4.6 Partition Coefficients for F Hydrogels of Set 3 (brackets indicate standard deviation)

	F1	F2	F3
CaCl₂	0.18 (0.11)	0.92 (0.02)	0.97 (0.07)
KCl	0.46 (0.05)	1.14 (0.07)	0.94 (0.07)
NaCl	0.37 (0.01)	0.59 (0.01)	0.62 (0.02)
MgCl₂	0.15 (0.04)	0.48 (0.02)	0.46 (0.05)

Set 1: With the E hydrogels of Set 1, calcium chloride produced the overall lowest partition coefficients with hydrogel E4 having the highest coefficient at 0.19 and hydrogel E3 with the lowest at 0.13.

There was an increase in overall partitioning with potassium chloride compared to those against calcium chloride with hydrogel E7 producing the largest coefficient at 0.40 and the lowest being hydrogel E1 at 0.19. Sodium chloride saw a slight trend, with there being an increase in the coefficients down the set: hydrogel E7 produced the largest coefficient at 0.31 and hydrogel E3 produced the lowest at 0.18. Lastly, hydrogel E3 produced the largest coefficient against magnesium chloride at 0.26 whilst hydrogel E7 produced the lowest at 0.15.

With the F hydrogels of the same set, hydrogel F1 consistently produced the smallest partition coefficient against all the salts. Hydrogel F2 also produced the largest coefficient against all the chloride salts, except for magnesium chloride in which hydrogel F3 was highest at 0.31.

Set 2: Generally, the partition coefficients from this set were all considerably larger than those determined from the other sets. There was little to no trend seen in the coefficients going across this set against any of the chloride salts, although, a slight upward trend was seen with the coefficients of calcium chloride along the set, but this trend ended at hydrogel E5 before decreasing again. The highest partition coefficient of calcium chloride was produced by hydrogel E7 at 1.47 and the lowest coefficient was produced by hydrogel E6 at 0.55.

The highest coefficient for potassium chloride was produced by hydrogel E3 at 2.21 and its lowest was by hydrogel E6 at 0.62. Hydrogel E6 produced the largest coefficient against sodium chloride at 0.94 whilst the lowest against the same salt was produced by hydrogel E3 at 0.50. Meanwhile, hydrogel E6 produced the lowest partition coefficient for magnesium chloride at 0.35 whilst the highest was made by hydrogel E3 at 1.44.

In this set, hydrogel E3 was responsible for the largest coefficients against potassium and magnesium chloride. Meanwhile, in set 1, hydrogel E3 was responsible for the lowest coefficients against calcium and sodium chloride. The same formulation showcased differing behaviours against the same salts but the key difference between sets 1 and 2 that may be responsible for this noticeable change is the use of both a diluent and a post-cure for the hydrogels. Set 2 does not make use of a diluent but a post-cure was utilised, sparking a question as to how a diluent may influence a hydrogel's partitioning behaviour and whether a post-cure, which is meant to improve NVP incorporation into a hydrogel's final matrix, can impact partitioning as well. The differences in partitioning behaviour between sets 1 and 2 suggests the reaction conditions could be influential.

Regarding the F hydrogels of the same set, a trend was noticed against calcium chloride. There was a general increase in the partition coefficients from hydrogel F1 (0.19) to F3 (1.50). Hydrogel F1 generally had the lowest coefficient but there was an exception with sodium chloride as it came the highest at 1.18 whilst hydrogel F2 was the lowest at 0.56.

Set 3: Similar to set 2, there was little to no trend seen in the partition coefficients of the E hydrogels against the differing chloride salts except in the case of potassium chloride which saw a slight decrease in the partition coefficients from hydrogel E1 to E7. Hydrogel E1 produced the largest coefficient for calcium chloride at 1.21 with hydrogel E3 producing the smallest at 0.31. Hydrogel E1 also produced potassium chloride's largest coefficient at 1.54 and hydrogel E5 with the smallest at 0.56.

Hydrogel E6 produced the largest coefficient for sodium chloride at 0.74 whilst hydrogel E4 was responsible for the smallest value at 0.27. The largest coefficient of magnesium chloride was produced by hydrogel E2 at 0.74 as well and hydrogel E6 produced the smallest coefficient at 0.37.

Both calcium and sodium chloride saw an upward trend in partition coefficients from hydrogels F1 to F3. In this set, hydrogel F1 was once again responsible for the smallest coefficients against all salts. Hydrogel F2 produced the largest coefficient for potassium chloride and magnesium chloride at 1.14 and 0.48 respectively.

4.3 Discussion

Tables 4.1 to 4.6 report the measured equilibrium partition coefficients of the E and F hydrogels against the calcium, potassium, sodium and magnesium ions across sets 1-3.

Liu et al (2015) found that there was a linear increase in the aqueous-solute partition coefficients as the amount of hydrophilic monomer within a silicone hydrogel increased. It was not as straightforward to establish such a correlation in this project as more than one hydrophilic monomer is included in the formulation of the hydrogels. However, a recent study (Wu et al, 2021) suggested the oxygen permeability of silicone hydrogels is not directly related to the EWC of the hydrogel due to their complicated morphology caused mainly by the phase separation of hydrophilic and siloxane regions. It is possible that this hypothesis could be extended and applied to the solute permeability through silicone-based hydrogels, which could be reflected in their partitioning behaviour as well.

When determining partition coefficient, the solute distributes itself in the hydrogel and in the solution until the chemical potential of the solute is equal in both places (Gehrke et al, 1997). The chemical potential of a substance is a representation of its energy intensity in a given system (Chen, 2019). Partitioning depends on a number of chemical and physical properties of both the solute and the hydrogel such as polarity, size and shaping. Electrostatic interactions between the polymer network and the solution can also influence partitioning. If the solute and the polymer matrix are similarly charged, it could lead to repulsion and exclusion which would result in a lower partition coefficient whilst oppositely charged ions could lead to attraction between the solute and the matrix, causing an increase in partitioning.

The E hydrogels of set 3 showcased how the same hydrogel can have different interactions against the different chloride salts. Hydrogel E6 (50% DMA, 10% NVP) of the set was responsible for the largest partition coefficient against sodium chloride whilst also producing the smallest coefficient against magnesium chloride. This could be an illustration of how the charge of an ion influences interactions between the solute and the polymer matrix, causing an effect on the partition coefficient. The sodium ion is a monovalent ion, meaning it has the ability to form one ionic/covalent bond whereas the magnesium ion is a divalent ion, meaning it has the ability to form two ionic/covalent bonds (Veerman & Vermaas, 2016). These differences in partitioning can also be used to demonstrate the effects of ion size as well, as the size of an ion and how it interacts with the pores of the hydrogel can influence partitioning. The degree of an ion's hydration is dependent on the strength of the electrostatic forces between the ion and the surrounding water molecules (Hribar et al, 2002). When hydrated, the magnesium ion is the largest ion in comparison with the potassium, sodium, calcium and chlorine ions, shown in Image 4.2. Systematically, partition coefficients for the hydrogels against magnesium chloride were the smallest of set 2 and 3 whilst calcium chloride was the smallest for set 1. The size of a hydrated magnesium ion is 0.43nm whilst that of a calcium ion is 0.41nm (Israelachvili, 2011). The hydrated potassium ion is the smallest at 0.33nm followed by the sodium ion at 0.36nm.

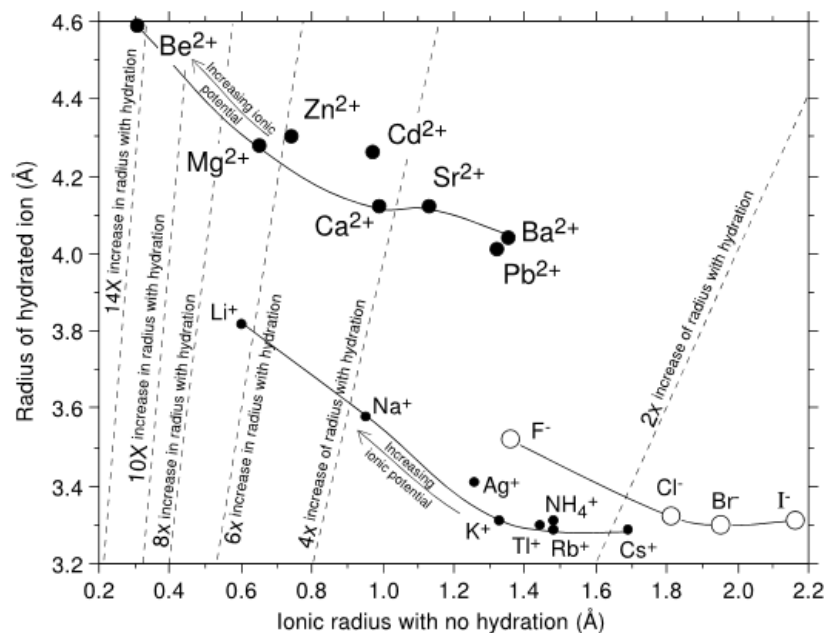


Image 4.2: Variations in hydrodynamic radii of ions (Image source: Railsback, 2006)

Size exclusion is a factor that can also influence partitioning and it depends on the size of the solute and the size of the hydrogel's pores. Within the matrix of the hydrogel, a solute has lower entropy so it has a lower amount of possible orientations when compared to how it would behave in a solution. Due to this, a solute tends not to enter the hydrogel even if it is not obstructed from doing so. This hindrance worsens as the solute size gets closer to that of the hydrogel mesh, meaning size exclusion would increase as the size of the solute increases (Gehrke et al, 1997). That is, salt ions that are similarly sized as the pores of the hydrogel may not partition inside the matrix of the hydrogel, resulting in a lower partition coefficient.

As mentioned in the results section of this chapter, the set 2 partition coefficients were considerably larger in comparison to the coefficients of the other sets. Magnesium chloride produced the smallest coefficients across the different sets yet the average coefficient against this salt from the set 2 E hydrogels was 0.77 whilst its average from the set 1 E hydrogels was 0.22 and 0.53 from the set 3 E hydrogels. The factors listed above including the attractive forces between the solute and the hydrogel as well as electrostatic interactions could have been considerably greater between the varying chloride salt solutions and the set 2 E hydrogels. This may have been due to the reaction conditions that these hydrogels were exposed to that the others were not, such as the use of a post-cure or the lack of a diluent, as described in the methodology chapter (2.2). It is possible these reaction conditions could influence the pore size of the hydrogels which would contribute to their differing partitioning behaviours.

4.3.1 Relationship between water content & partition coefficient

Yasuda et al (1968) found that the diffusion, permeation and partition coefficients of cross-linked hydrogels against sodium chloride depended on water content. The study found that the partition coefficients "varied linearly" with the water content of the hydrogel. Liu et al (2015) also stated that equilibrium partition coefficients of silicone-hydrogel soft contact lenses increased as the water content G.Durowoju, PhD Thesis, Aston University 2022.

of the hydrogel increased, however, they attributed this to the majority of the water within the hydrogel being present in the hydrophilic domains.

This correlation between partitioning and water content may stem from a hydrogel's feed composition, particularly the influence of the hydrophilic monomers. In a characterisation study, Peng et al (2012) found that the partition coefficient of silicone-based hydrogels was linked to composition: as DMA content increased, so did the partition coefficients against sodium chloride whilst the coefficients decreased as TRIS monomer content increased. They stipulated that this correlation occurred because of the change in water content as the composition of the gels changed i.e., as the hydrophilic monomer content increased, so did water content due to the water-attracting abilities of the monomer. This correlation fits the narrative, as a salt will partition within the water phase of a hydrogel matrix. If a hydrogel possesses more water, there is more water for a salt to be solubilised by, thus increasing the amount of salt that can be held within the hydrogel. Based on this reasoning, it was hypothesised that the partition coefficient of the hydrogels in this project against sodium chloride would also increase as water content increased. However, the study found that this trend was not what occurred. The conductors of the study attributed this deviation from the hypothesised trend to the negative thus repulsive interactions between the polymer chains and the salt ions, assuming the charges along the polymer chain were also negative.

It is important to understand whether there would be a relationship between equilibrium water content and the partitioning behaviour of the E hydrogels of the different sets. Seeing as the hydrophilic monomer content of these hydrogels was from both DMA and NVP in alternating quantities, determining such trends provides information that is necessary to further understand these novel hydrogels. It was also of interest to see if this theory could be extended to the other water types present in a hydrogel, as determined and detailed in the water content chapter (2.4), such as polymer-associated water, ice-like water, freezing and non-freezing water.

4.3.1.1 The relationship between partitioning & equilibrium water content

From sets 1 to 3, the partition coefficients produced by calcium, potassium, sodium and magnesium chloride were plotted against the equilibrium water content of each respective E hydrogel. Figures not shown in this section can be found in appendix 2.2.2.

Set 1 E Hydrogels: Initially, it appeared that there was little to no relationship between the partition coefficients of the set 1 E hydrogels and equilibrium water content due to the lack of trends shown in Figures 4.1 to 4.4. From calcium to magnesium chloride, the hydrogels formed a cluster in the EWC region of 50 - 70%, regardless of the partition coefficient of the hydrogel. However, once those clustered trends were expanded, a trend emerged against each salt. Repeatedly, hydrogels E3, E4, E5 and E6 were included in the trends seen.

With the set 1 E hydrogels, there was a downward trend in partitioning against calcium chloride between hydrogels E3 - E5 as equilibrium water content increased, seen in Figure 4.1 below.

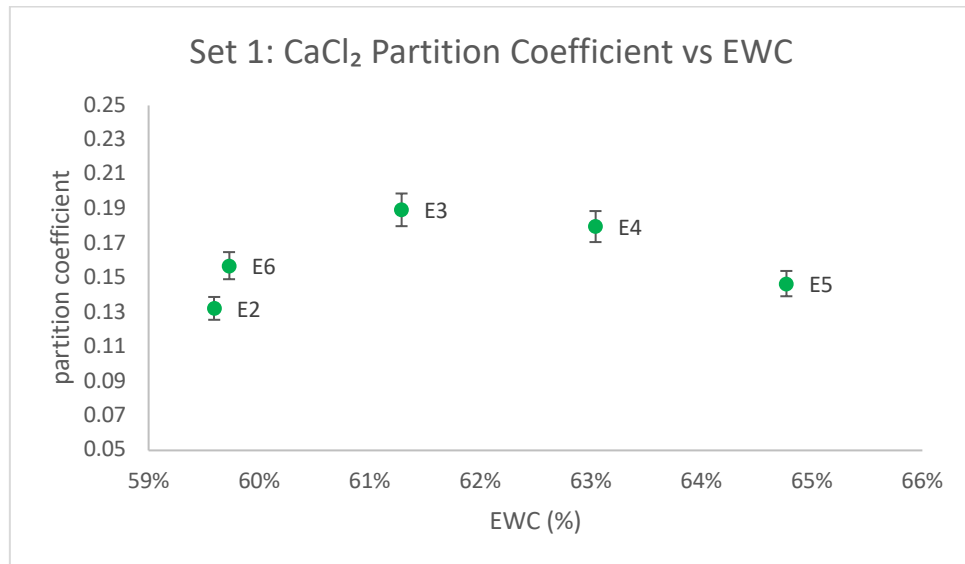


Figure 4.1 Set 1 - CaCl₂ Partition Coefficient vs EWC (expanded view)

Potassium chloride brought about the opposite trend but with the same set of hydrogels as previously mentioned with calcium chloride. There was a slight increase in partitioning against this salt between hydrogels E3 - E5 as equilibrium water content increased, as seen in Figure 4.2.

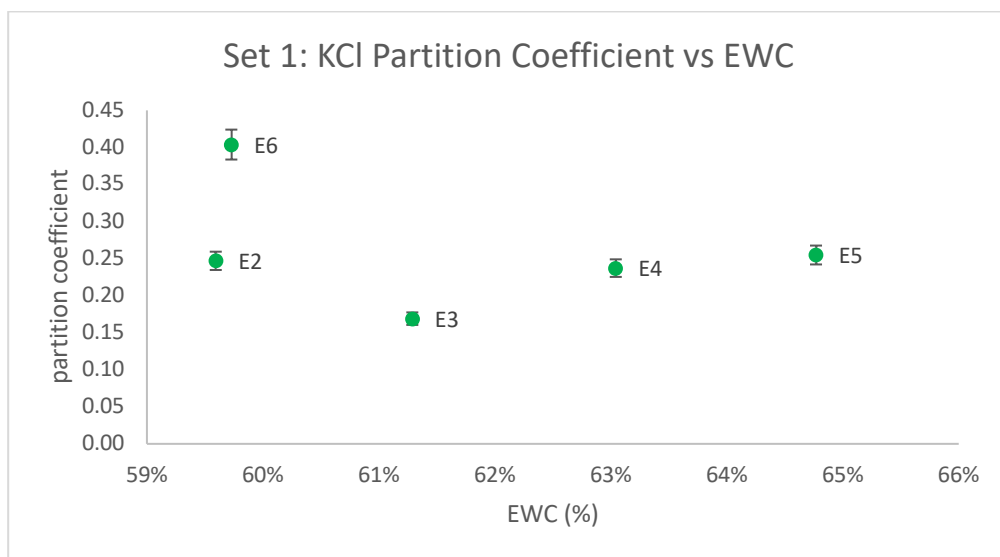


Figure 4.2 Set 1 - KCl Partition Coefficient vs EWC (expanded view)

With sodium chloride, a minor U-shaped trend was noticed between hydrogels E3-E5 as previously seen in addition to hydrogel E6, as seen in Figure 4.3. Hydrogel E6 followed by hydrogel E3 saw a decrease in partitioning as EWC increased but there was an increase in partitioning between hydrogels E4 and E5.

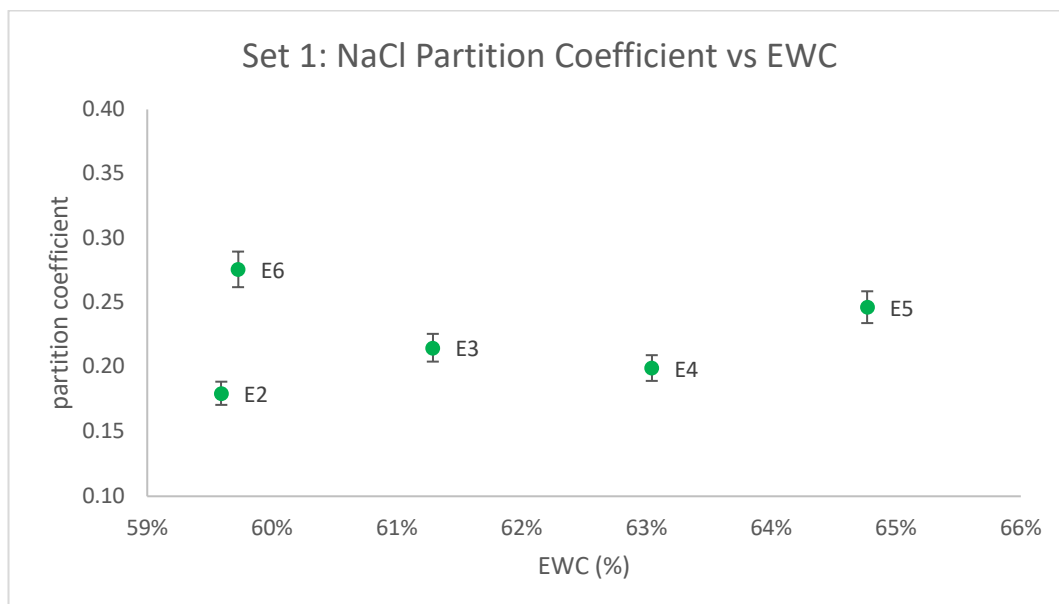


Figure 4.3 Set 1 - NaCl Partition Coefficient vs EWC (expanded view)

Hydrogels E3-E6 were included in the downward trend between the magnesium chloride partition coefficients and equilibrium water content, shown in Figure 4.4. As the EWC of the hydrogels increased between 60 - 65%, there was a gradual decrease in partitioning between those hydrogels. Hydrogel E7 was excluded from this trend.

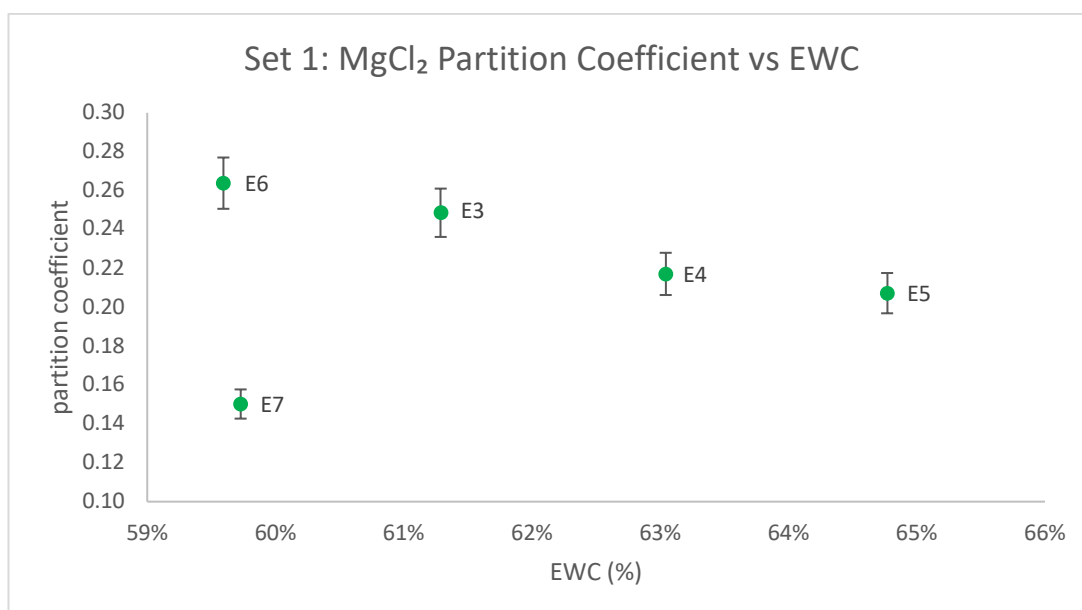


Figure 4.4 Set 1 - MgCl₂ Partition Coefficient vs EWC (expanded view)

Hydrogel E7 did not follow any trends that were seen with the chloride salts, it often behaved as an outlier – a reason for its non-appearance in the expanded view of trends. Overall, each salt brought about a different trend of behaviour in the partition coefficients of the set 1 E hydrogels but an effect was established.

Set 2 E Hydrogels: When investigating the link with the set 2 E hydrogels, the trends became less evident or were not present at all. Clusters also formed between the hydrogels when initially plotted G.Durowoju, PhD Thesis, Aston University 2022.

against EWC but upon expansion of these clusters, there was little to no pattern between the hydrogels, suggesting there is no relationship between equilibrium water content and the partitioning behaviours of these hydrogels against the chloride salts. When looking at the relationship between the sodium chloride partitioning behaviour of the same hydrogels and EWC, all the set 2 E hydrogels, except hydrogel E6, showed that their partition coefficients remained in the same region despite an increase in EWC across the set.

Set 3 E Hydrogels: Similarly to the set 2 E hydrogels, there were little to no trends established with the partition coefficients against the different chloride salts and their EWC. From calcium to magnesium chloride, the partition coefficients of the hydrogels remained somewhat constant despite changes in their EWC. At first, the trends are represented as clusters but even when they were expanded, the hydrogels remained relatively constant.

Set 1-3 F Hydrogels: As is the case with the F hydrogels, it is impossible to determine a trend between them due to the lack of relationship each F hydrogel has with each other, in terms of the formulation from one hydrogel in the set to another. Unlike the E hydrogels that have a consecutive increase/decrease in the hydrophilic monomers, changes in formulation were independent of the next hydrogel in the set. Because of this, comparisons can only be made between each hydrogel from sets 1 - 3 and note the differences in both water content and partitioning as the set change.

When the partition coefficients produced by the different chloride salts for the hydrogels were compared from sets 1 - 3 against their EWCs, hydrogels F1, F2 and F3 did not display a trend. The hydrogels did not follow a discernible sequence in relation to partitioning as EWC changed across the sets.

In the context of conventional contact lenses, hydrophilic-domain water uptake greatly influences the loading and release of water-soluble drugs (Dursch et al, 2014). The mechanism of drug delivery depends on the partitioning behaviour of the hydrogel: the uptake, hold and release of solutes within the matrix of a hydrogel. Hydrogels with high water contents mean they have more water-filled hydrophilic domains, providing more spaces for water-soluble ions to interact and partition within the gel (Liu et al, 2015). This is why it is thought that the relationship between a hydrogel's formulation and partitioning behaviour was tied to water content as the ratio of hydrophilic to hydrophobic monomers in a hydrogel can determine its water content, just as they influence other parameters relating to the hydrogel. However, this trend depends on the majority of the water within a hydrogel dwelling within its hydrophilic polymer domains.

In addition to relationships with EWC, it is thought there could also be a relationship between the partitioning behaviours of silicone-based hydrogels and their non-freezing water content (Guan et al, 2011).

By definition, the partition coefficient represents the concentration of a salt within the membrane phase of a polymer matrix (Hamilton et al, 1988). Seeing as salt dissolution requires water, it can also be assumed that all the salt in the membrane phase has been solvated by water within the hydrogel. Based on this, the amount of salt found in the hydrogel is linked to the amount of water in the hydrogel too.

Even though literature does not state that there is a connection between partitioning behaviours of silicone-based hydrogels and the water types beyond EWC and NFWC, it is still important to investigate the links between partitioning and all the water types present in a hydrogel.

In hydrogels with a larger water content, it is possible to suggest that the water within the hydrogel is held in large clusters within the polymer matrix. Such clusters may also be capable of solvating the salt ions, thus minimising the salt ion interaction with the polymer network which could result in a reduced partition coefficient (Yasuda et al, 1968). This theory assumes all the water within the hydrogel is able to participate in interacting with the salts, but it is known that water within hydrogels can be categorised into different types including freezing and non-freezing water content. Freezing water can be further categorised into ice-like and polymer-associated water. Therefore, understanding potential links between these water types and partitioning could provide more insight into their effects on these characteristics.

4.3.1.2 The relationship between partitioning & freezing/non-freezing water content

In the case that partition coefficients do not follow a trend with equilibrium water content, Guan et al (2011) suggested determining the trend between partitioning and non-freezing water content to rationalise results. Non-freezing water may be unable to participate in permeation or diffusion, but it is still capable of solvating the ions of salts within the hydrogel, thus, influencing the partition coefficient. Freezing water is essential to permeation, as discussed in the water content chapter of this thesis. Increased levels of this water type within a hydrogel should increase the mobility of solutes within and through the hydrogel.

From sets 1 to 3, the partition coefficients produced by calcium, potassium, sodium and magnesium chloride were plotted against the freezing, non-freezing, ice-like and polymer-associated water content of each respective E hydrogel to determine whether there was a relationship. Figures not displayed below can be seen in appendix section 2.2.3.

Freezing Water

Set 1 E Hydrogels: with these hydrogels, there were no evident trends noticed between their freezing water contents and the partition coefficients against all the chloride salts.

Set 2 E Hydrogels: these hydrogels displayed trends with their partition coefficients against calcium chloride and their FWC. With calcium chloride, there was an increase in partitioning for the majority of the hydrogels as FWC increased between 20 - 35%, shown below in Figure 4.5. As the FWC of the hydrogels did not increase consecutively along the set, the upward trend was also not in the order of the hydrogel set, i.e., from hydrogel E1 - E7.

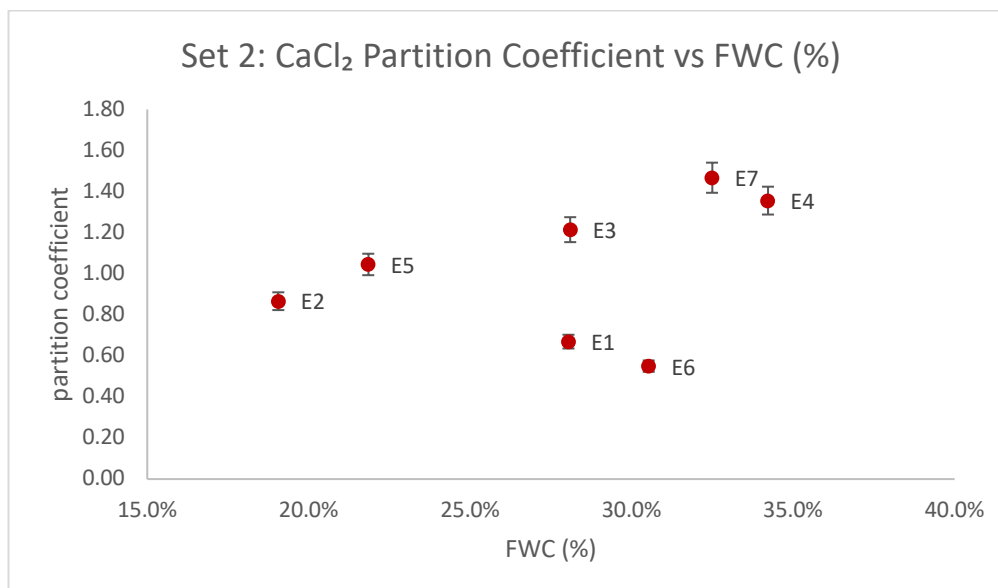


Figure 4.5 Set 2 – CaCl₂ Partition Coefficient vs FWC (%)

The partition coefficients of the same hydrogels against sodium chloride saw the coefficients remaining constant despite increases in FWC. Both the coefficients of potassium and magnesium chloride partition coefficients did not follow an evident trend.

Set 3 E Hydrogels: The partition coefficients of the set 3 E hydrogels against calcium chloride showed an increase as their FWC increased. Between potassium and sodium chloride, the trends showed that the partitioning of the hydrogels remained constant despite changes to FWC across the set. Lastly, magnesium chloride was the only salt to not showcase a correlation between its partition coefficients of the set 3 E hydrogels and FWC.

Non-Freezing Water

Figures relating to the relationship between the partition coefficient of the hydrogels and their NFWC can be found in appendix section 2.2.4.

Set 1 E Hydrogels: with the set 1 E hydrogels, NFWC did not seem to impact the calcium and sodium chloride partition coefficients as they remained constant despite increases in this particular water content. With potassium and magnesium chloride, there was no discernible trend between their partition coefficients and the NFWC of the hydrogels.

Set 2 E Hydrogels: the general trend seen was the formation of clusters as opposed to clear declines or inclines, when compared against the set 1 trends seen. The non-freezing water contents of these hydrogels remained in a specific region which corresponded with the hydrogels having their partition coefficients within a similar region as well. This distinct behaviour could be a characteristic of hydrogels that were post-cured but lack a diluent, as is the case with set 2 hydrogels.

A clear case of this clustering was seen between the calcium chloride coefficients and non-freezing water, as shown in Figure 4.6. Three distinct clusters formed between certain pairs of hydrogels. These

clusters suggest a hydrogel with a particular non-freezing water content is only capable of producing a specific partition coefficient.

For example, hydrogels E4 and E7 have a non-freezing water content of 23.7% and 23% and they produced a partition coefficient of 1.36 and 1.47 respectively. Another cluster formed between hydrogels E3 and E5, with a non-freezing water content of 32.8% and 32.7%. They each produced a partition coefficient of 1.21 and 1.05. The last cluster formed was between hydrogels E1 and E6 which have a non-freezing water content of 23.8% and 25.7% respectively. They also produced partition coefficients that were in a similar range of 0.67 and 0.55. The only un-clustered hydrogel was hydrogel E2 which had the largest non-freezing water content of the hydrogels at 42.1% and a partition coefficient of 0.87.

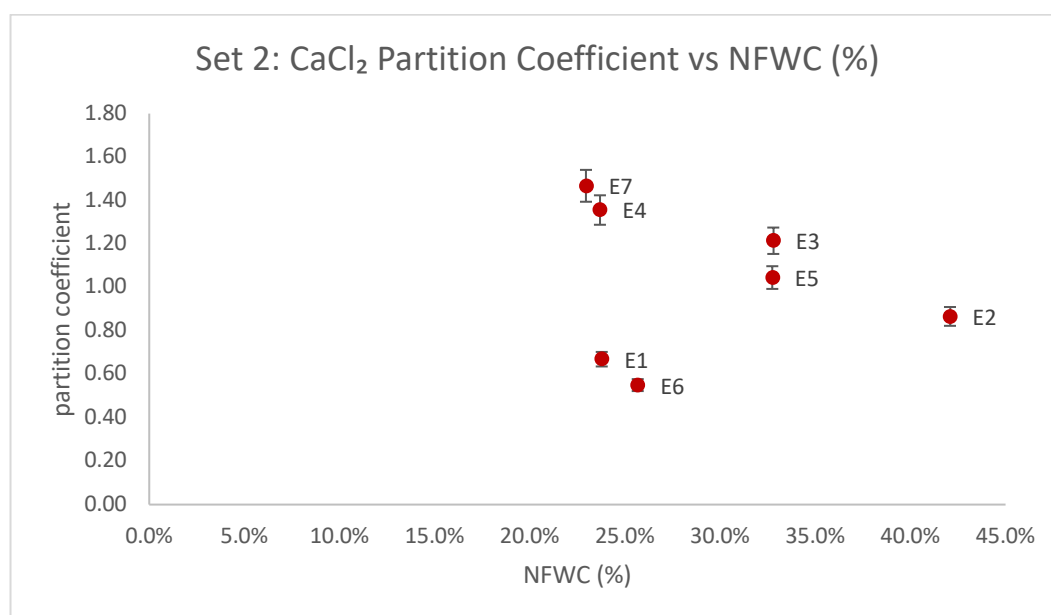


Figure 4.6 Set 2 E Hydrogels – CaCl₂ Partition Coefficient vs NFWC (%)

The remainder of the chloride salts did not display trends within the clusters they formed, suggesting NFWC did not have an effect on their partition coefficients.

Set 3 E Hydrogels: With the set 3 E hydrogels, the partition coefficients against sodium chloride decreased as NFWC increased across the set. The coefficients of magnesium chloride showcased an increase as NFWC increased but with both the partition coefficients against calcium and potassium chloride, a clear trend was not established.

F Hydrogels: As previously mentioned, determining trends in the F series of hydrogels is not entirely straightforward due to the nature of their formulation: unlike the E hydrogels that follow incremental changes to their hydrophilic and hydrophobic monomer content, the F hydrogels do not contain both hydrophilic monomers in their formulation nor do they possess the same amount of TRIS. However, it is still possible to draw connections from each individual hydrogel in the different sets.

The partition coefficients of hydrogels F1 and F2 did not demonstrate a noticeable trend as their non-freezing water contents changed from set 1 to 3. However, with hydrogel F3, there was a downward trend seen in the order of set 2 → set 3 → set 1 that showed the partition coefficients against all the

chloride salts decreased as non-freezing water content increased. With this same hydrogel, its largest partition coefficients against each chloride salt were produced by its set 2 version. This set also possessed the largest NFWC for this particular hydrogel.

In the event that a trend was seen with both the E & F hydrogels when studying the relationship between non-freezing water and partitioning behaviour, majority of the trends showed that as non-freezing water increased, it was accompanied by a decrease in the partition coefficient of the hydrogel. Non-freezing water is somewhat dependent on the ratio of hydrophilic to hydrophobic monomers in the formulation of a hydrogel as it is the water that binds to the polymer chain initially and it is also the water that interacts with the hydrophobic groups along the chain as well (Hoffman, 2002).

4.3.1.3 The relationship between partitioning and ice-like/polymer-associated water content

Ice-like Water

Ice-like water within silicone-based hydrogels has been attributed to increasing their permeation towards solutes. This water type is not hindered from moving within the hydrogel unlike non-freezing water and this mobility is what allows the water to participate in permeation more so than other water types (Bag & Valenzuela, 2017).

Although existing literature does not suggest ice-like water could influence the partitioning behaviour of the hydrogels, establishing a connection is still important in the characterisation of these novel silicone-based hydrogels. Figures not shown below can be found in section 2.2.5.

Set 1 E Hydrogels: initially, the set 1 E hydrogels formed clusters when the partition coefficients against the different chloride salts was plotted against ice-like water content. Upon expanding these clusters, the partition coefficients produced by calcium, potassium and sodium chloride did not reveal a trend between the hydrogels, their figures can be found in the appendix section 2.2.5. However, with potassium chloride, trends were identified between certain hydrogels.

In the case of potassium chloride, there was a clear trend between the partition coefficients of the hydrogels and their ILWC: as this water type increased, the partitioning of these hydrogels also increased, shown in Figure 4.7.

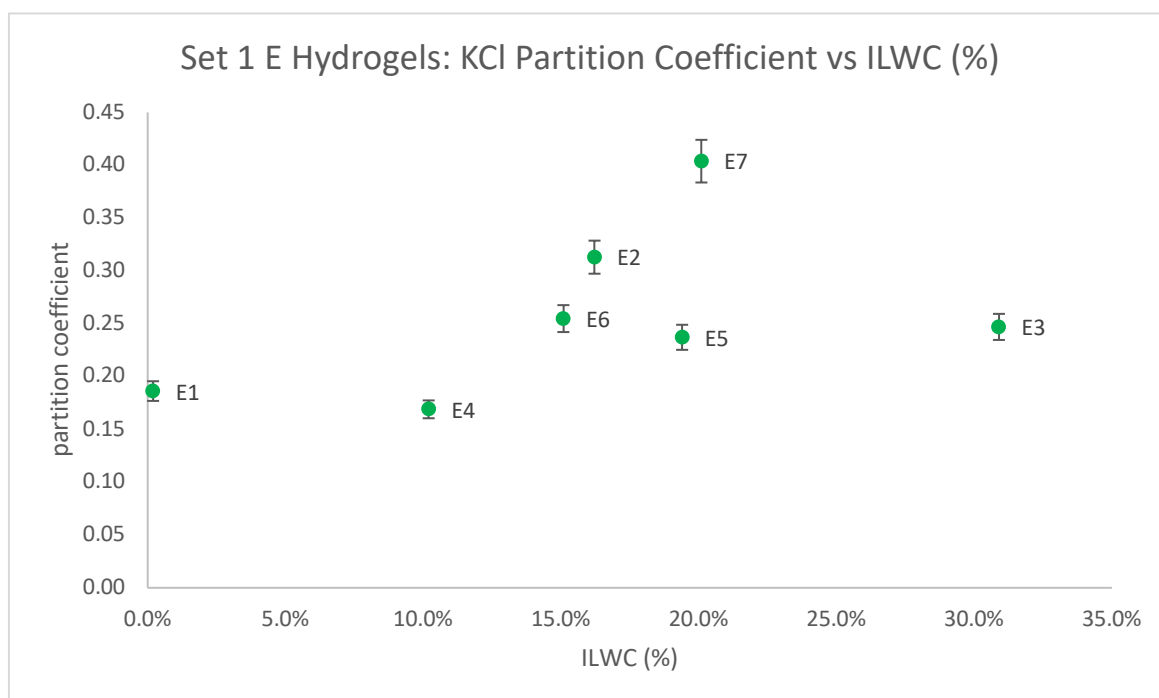


Figure 4.7 Set 1 E Hydrogels – KCl Partition Coefficient vs ILWC (%)

Except for hydrogel E3, there was a decrease in the partition coefficient of these hydrogels against magnesium chloride as ILWC increased across the set.

Set 2 E Hydrogels: trends between partitioning and ILWC were more evident across most of the chloride salts, except for those against potassium chloride.

Against calcium chloride, the coefficients displayed an upward trend in partitioning as ILWC increased. Noticeably, as seen in set 1 as well, the trends do not follow the consecutive order that the E hydrogels follow i.e., ILWC did not increase consecutively from E1 to E2 to E3 etc. This is shown in Figure 4.8. This may suggest formulation is not directly linked to this water content trend, unlike when investigating the link between partitioning and equilibrium content that saw the partitioning of the hydrogels descending or ascending with EWC but in the order of the set.

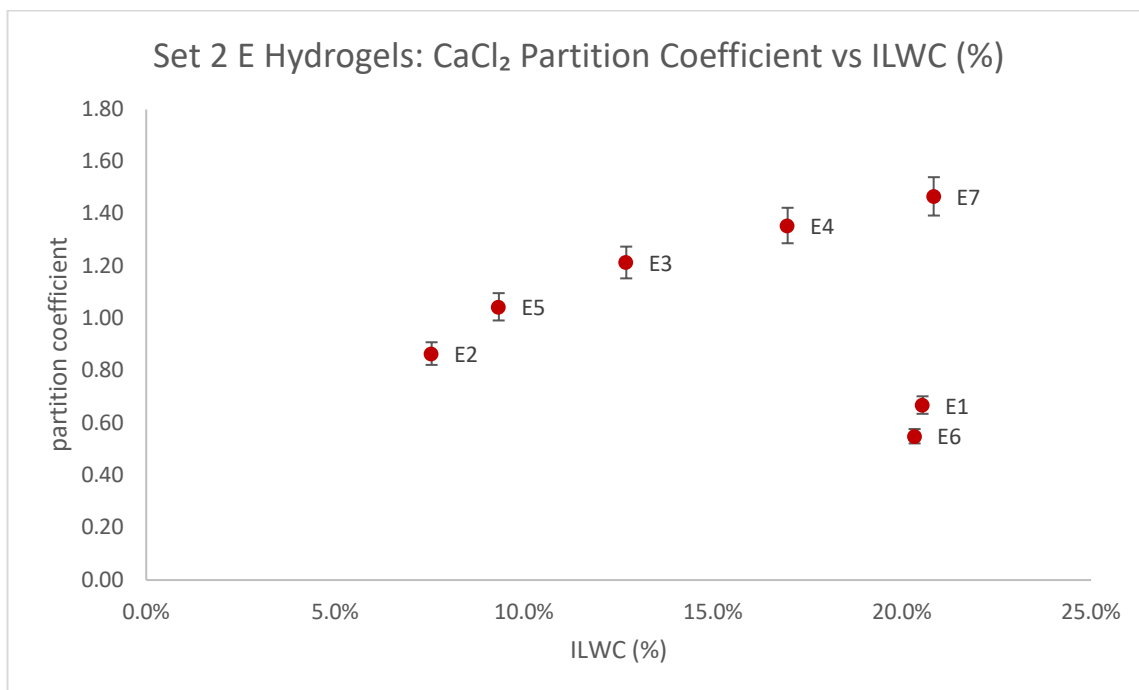


Figure 4.8 Set 2 E Hydrogels – CaCl₂ Partition Coefficient vs ILWC (%)

The partition coefficients of sodium chloride remained constant despite changes in ILWC whilst those of magnesium and potassium chloride did not demonstrate a trend despite ILWC increasing.

Set 3 E Hydrogels: clear trends were seen that denoted a relationship between their partitioning behaviour and ILWC. Out of the different sets of E hydrogels, both set 1 and set 3 demonstrated trends although the E hydrogels of set 3 showed the strongest correlations.

With the partition coefficients against calcium chloride, the set 3 E hydrogels experienced an increase as their ILWC increased between 12-36%, suggesting the effect of ILWC on the ability of a solute to partition in these silicone-based hydrogels was greater when there was an increased amount of this water type. The same was seen with the partition coefficients of potassium, sodium and magnesium chloride: as ILWC increased, so did the coefficients. The relationship between the magnesium chloride partition coefficients of these hydrogels and their ILWC content is shown in Figure 4.9.

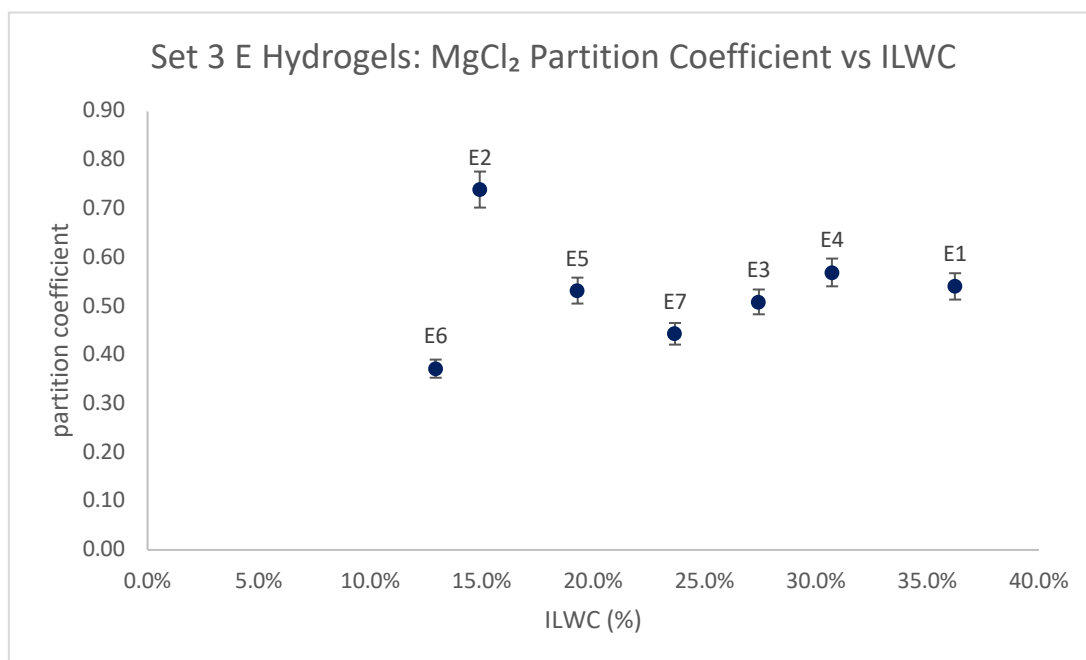


Figure 4.9 Set 3 E Hydrogels – MgCl₂ Partition Coefficient vs ILWC (%)

F Hydrogels: As previously stated when analysing the relationship between the water types and the partitioning of the F hydrogels against the different chloride salts, it is not possible to directly compare one hydrogel to another due to their formulation. Therefore, comparisons can be made between the same hydrogel against itself in each set. Each set represents different reaction conditions (post-cure/use of diluent), but the formulation of the hydrogel remains the same.

Similarly seen with other water types, hydrogels F1 and F2 did not display any trends with their partition coefficients against the varying chloride salts as ILWC changed across the sets. Hydrogel F3 displayed a trend which saw an increase in the partition coefficients against all the chloride salts as ILWC increased in the order of set 1 → set 3 → set 2. This was the same trend seen when determining its partitioning relationship with EWC.

Polymer-Associated Water

Polymer-associated/intermediate water is also a sub-category of freezing water. It possesses a degree of mobility but it is much lower than that of ice-like water as it is still attached to the polymer chain (Pissis & Kyritsis, 2012) and so it is considered detrimental to the permeation abilities of silicone-based hydrogels. Establishing a trend between this water type and partitioning consolidates how all the different water types in a silicone-based hydrogel could be influential. Figures relating to the hydrogels and their relationship with this water type can be seen in appendix section 2.2.6.

Set 1 E Hydrogels: for the set 1 E hydrogels, there was an effect seen across all the partition coefficients against the chloride salts, with the greater general effects seen against the partition coefficients of sodium and magnesium chloride. Similarly to the trends seen with ice-like water content and non-freezing water content, the hydrogels did not follow these trends in their consecutive set orders.

The coefficients against calcium and potassium chloride increased as the PAWC of the hydrogels also increased. Those against sodium chloride remained relatively constant despite changes in PAWC whilst the partition coefficients of magnesium chloride also demonstrated an increase as PAWC increased across the set – this can be seen in Figure 4.10.

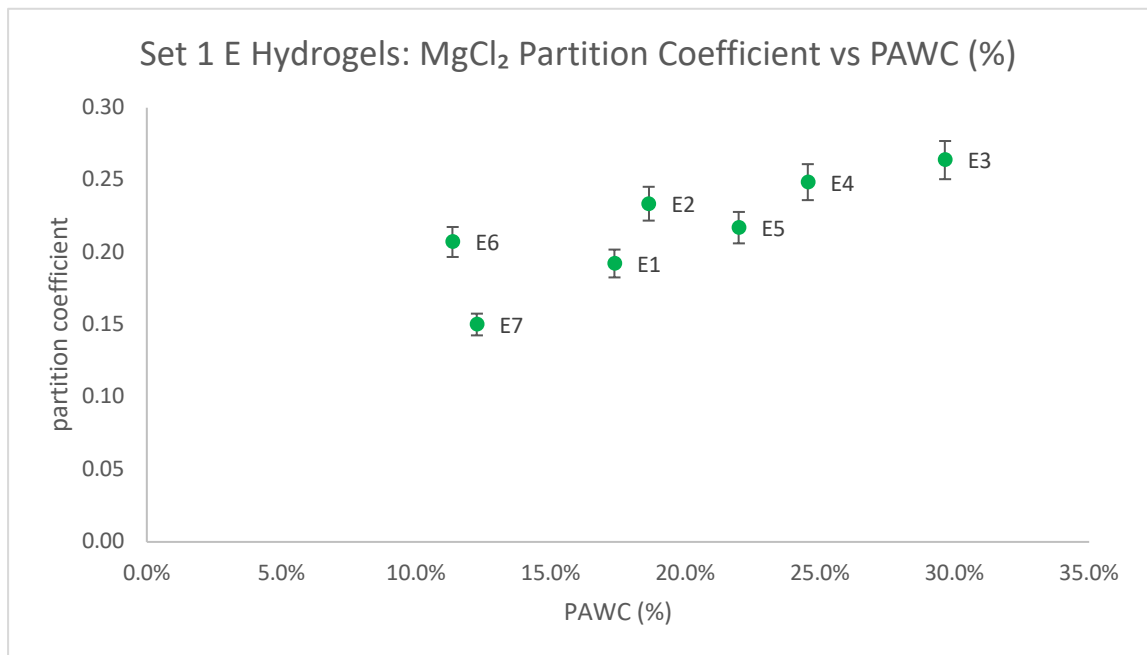


Figure 4.10 Set 1 E Hydrogels – MgCl₂ Partition Coefficient vs PAWC (%)

Set 2 E Hydrogels: The partition coefficients of the set 2 E hydrogels also displayed a trend although they were less widespread. Both the coefficients of calcium and potassium chloride generally increased as the PAWC of the hydrogels increased whilst those of sodium chloride remained constant. The coefficients against magnesium chloride did not demonstrate a trend with PAWC. The relationship with the potassium chloride coefficients is shown in Figure 4.11.

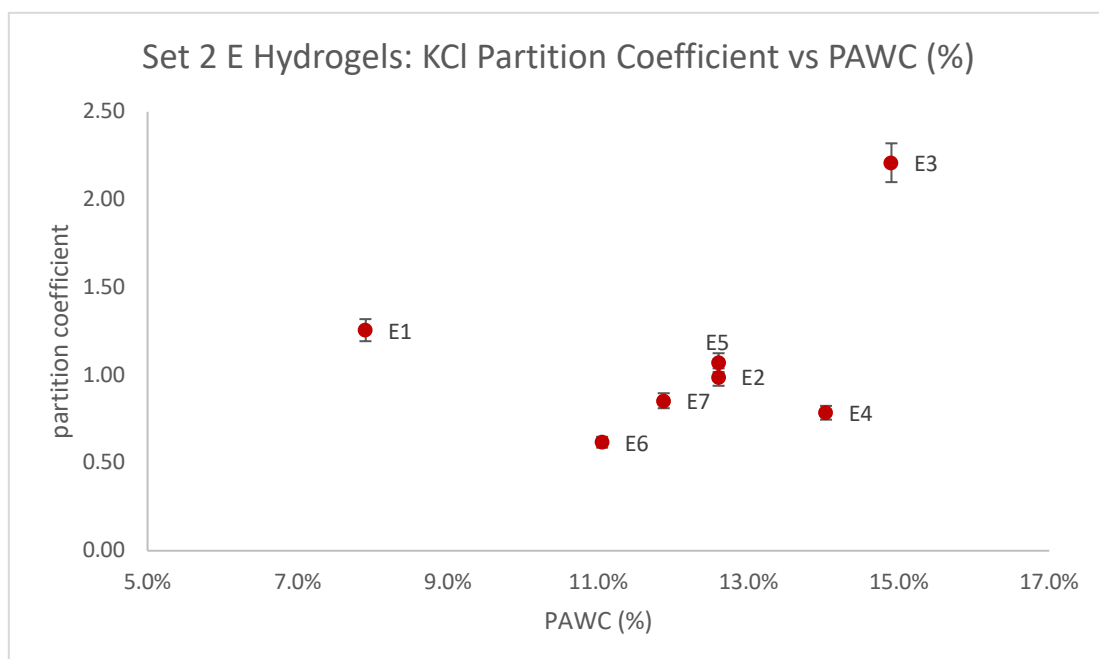


Figure 4.11 Set 2 E Hydrogels – KCl Partition Coefficient vs PAWC (%)

Set 3 E Hydrogels: Lastly, the set 3 E hydrogels had the weakest links between this particular water type and their partitioning behaviour across all the chloride salts. Overall, the PAWC of the hydrogels from this set was the lowest of sets 1 to 3. It was not possible to establish clear patterns of a relationship between the partition coefficients of the E hydrogels and their PAWC.

F Hydrogels: The F hydrogels were also compared to the differing versions of themselves from sets 1 to 3, as was done against the other water types. With hydrogels F1 and F3, none of the partition coefficients against the different chloride salts displayed a trend. However, in two instances with hydrogel F2, there was an upward trend seen with both the divalent salts: calcium and magnesium chloride in the order of set 1 → set 3 → set 2.

4.3.2 Relationship between formulation & partition coefficient

Silicone-based hydrogels tend to include hydrophilic monomers in their formulation to promote ion permeability which would otherwise be non-existent if silicone was the sole monomer. This is due to its hydrophobic nature (Peng & Chauhan, 2012). In the context of a contact lens, ion permeation is essential, in order to allow the lens to move as the human eye moves as well (Pozuelo et al, 2014). However, in other biomedical applications, such as inclusion in a liver dialysis system, ion permeation would be the mechanism responsible for removing toxic by-products from the human body via blood.

Generally, siloxane-based monomers are immiscible with hydrophilic monomers and so a diluent is used to increase the solubilisation of the monomers. Such hydrogels are often described as isotropic materials with a dispersed microstructure and a polymer network in which both the hydrophobic and hydrophilic phases are continuous i.e., there are regions of hydrophobicity just as there are regions of hydrophilicity (Peng & Chauhan, 2012). This allows ions to interact with either the silicone-rich or hydrophilic regions of the hydrogels, meaning formulation should have a direct relationship and effect on partitioning. The morphological structure of the synthesised hydrogels is discussed in further detail in the membrane characteristics chapter (7).

Typically in a formulation system that makes use of a singular hydrophilic monomer and a singular hydrophobic monomer, the relationship between an increase in either monomer and the partition coefficient is linear: as one monomer increases/decreases, there is an increase/decrease in partition coefficient (Liu et al, 2015). However, in the case of the synthesised hydrogels being discussed in this project, linking the formulation directly to the partition coefficients is not as easy to establish due to the nature of the formulations, in which there are two hydrophilic monomers in use and the quantities of these monomers are juxtaposed against each other, with one ascending as the other descends.

Set 1 E Hydrogels: Beginning with the set 1 E hydrogels, an increase in DMA content from hydrogel E1 to E7 down the set did not result in a linear increase in the partition coefficients against calcium chloride. The coefficients remain in a similar region despite the incremental increase in DMA content. The same trend but in the reversed order of hydrogels (E7 → E1) was seen when the same coefficients were plotted against NVP content. This was expected to be seen in the case of all the chloride salts due

to the nature of the formulations of the hydrogels. The figures for this trend can be found in the appendix 2.2.1.

When the partition coefficients of the set 1 E hydrogels for sodium chloride were plotted against DMA content, a similar situation was observed (seen in Figure 4.12). The coefficients remained in a similar reason despite an increase in DMA content across the set. However, an increase in partitioning was noticed from hydrogel E5 to E7 as DMA content increased between 40% to 60%.

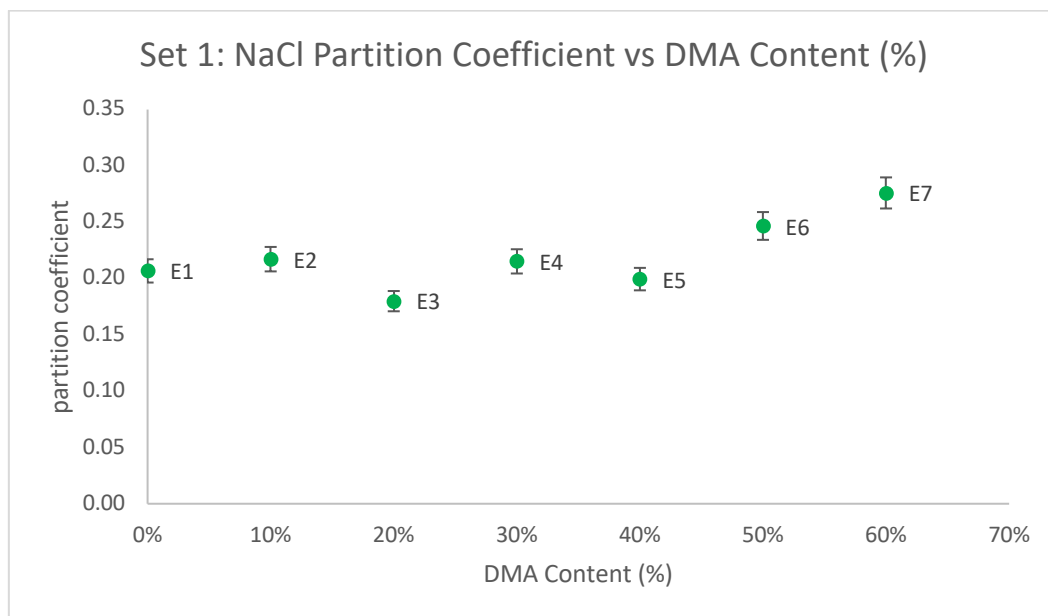


Figure 4.12 Set 1 E Hydrogels – NaCl Partition Coefficient vs DMA Content (%)

When determining the relationship between DMA content and the potassium chloride partition coefficients, there was a decline in partitioning between hydrogels E2 to E4 as DMA content increased between 10-30%. This was followed by an increase in partitioning between hydrogels E4 to E7, with a slight plateau occurring between hydrogels E5 and E6. This can be seen in Figure 4.13.

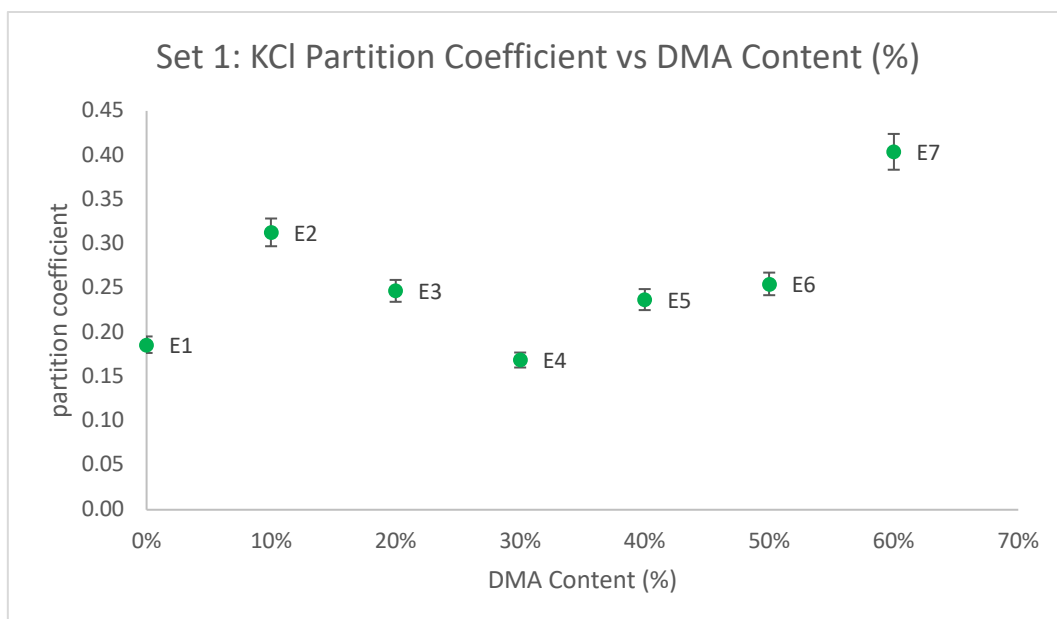


Figure 4.13 Set 1 E Hydrogels – KCl Partition Coefficient vs DMA Content (%)

With magnesium chloride, the opposite effect is seen. There was an increase in partitioning between hydrogels E1 to E3 at which a peak was reached. From hydrogel E4 onwards, there was a decrease in the partition coefficient of the hydrogels as DMA content increased, as shown in Figure 4.14.

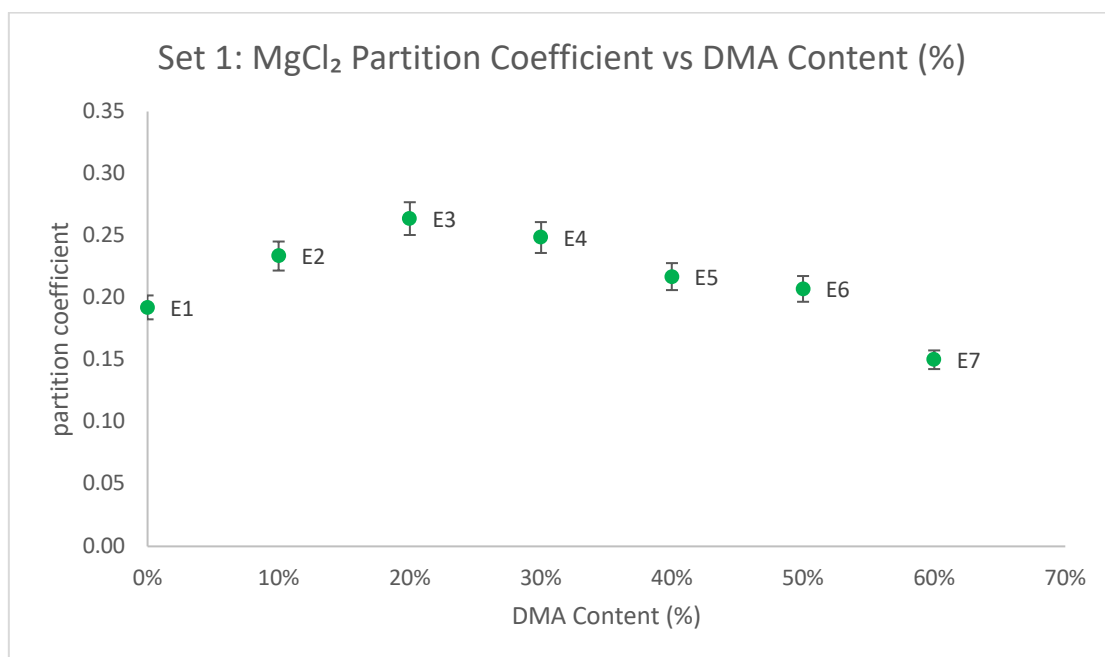


Figure 4.14 Set 1 E Hydrogels – MgCl₂ Partition Coefficient vs DMA Content (%)

Set 2 E Hydrogels: With the set 2 E hydrogels, there was less of a trend seen when pairing DMA/NVP content against the partition coefficients of the different chloride salts. However, in comparison to the set 1 and 3 hydrogel partition coefficients, the coefficients of these sets were considerably higher against each respective salt, as previously mentioned in the results section of this chapter. The key differences between this set and the other two are the lack of diluent in its formulation and these hydrogels were subjected to a post-cure.

As was the case with the set 1 E hydrogels, the links between the partitioning behaviour of the set 2 E hydrogels and NVP content were the exact mirror images of the trends seen with DMA content, as expected. Therefore, the figures illustrating the relationships between the partition coefficients against the different chloride salts and NVP content can be found in the appendix section 2.2.1.

The partition coefficients of potassium chloride remained constant as the DMA content of the hydrogels increased across the set. This was the same situation with the sodium chloride coefficients. With the coefficients against magnesium chloride, the trends seen were more sporadic, suggesting there was no relationship between the DMA content of the hydrogels and their partitioning behaviour. In the case of calcium chloride, the partition coefficients demonstrated a linear increase from hydrogels E1 to E4 as DMA content increased which was followed by a decrease until hydrogel E6, as shown in Figure 4.15. There was a sudden increase in the partition coefficient of hydrogel E7, the only hydrogel of the set to have DMA as the sole hydrophilic monomer alongside TRIS.

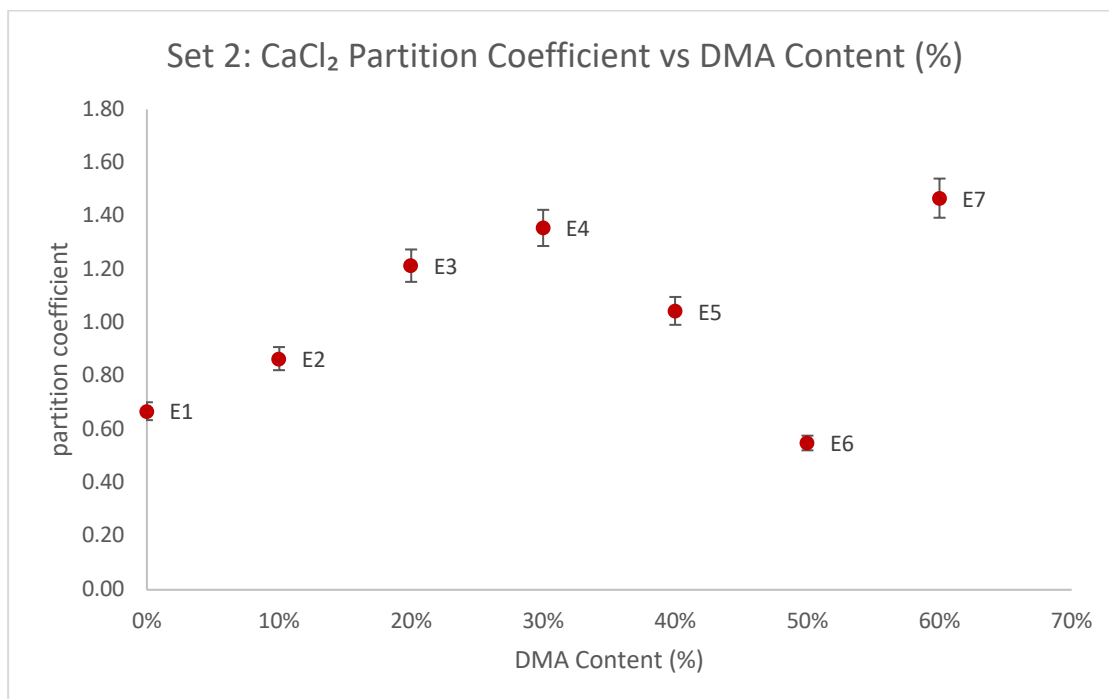


Figure 4.15 Set 2 E Hydrogels – CaCl₂ Partition Coefficient vs DMA Content (%)

Set 3 E Hydrogels: Generally, with the set 3 E hydrogels, differing trends were identified from calcium chloride to magnesium chloride in regards to their partition coefficients and DMA content. In terms of size, the coefficients were similar to those of set 1, suggesting there is a considerable effect on partitioning behaviour caused by the reaction conditions of a post-cure and use of a diluent in the synthesis of these hydrogels. As was the case with the set 1 and 2 E hydrogels, trends seen when stating the relationship between NVP content and partitioning behaviour were mirror images of the trends seen with DMA content for the same reasons that were stated earlier. For this reason, all figures detailing the relationships between NVP content and the partitioning of the set 3 E hydrogels can also be found in the appendix 2.2.1.

With the calcium chloride partition coefficients, there was a linear decline in partitioning as DMA content increased from hydrogel E1 to hydrogel E3. This was followed by an increase from hydrogel E4 to E5 but beyond that, the trend was lost as shown in Figure 4.16.

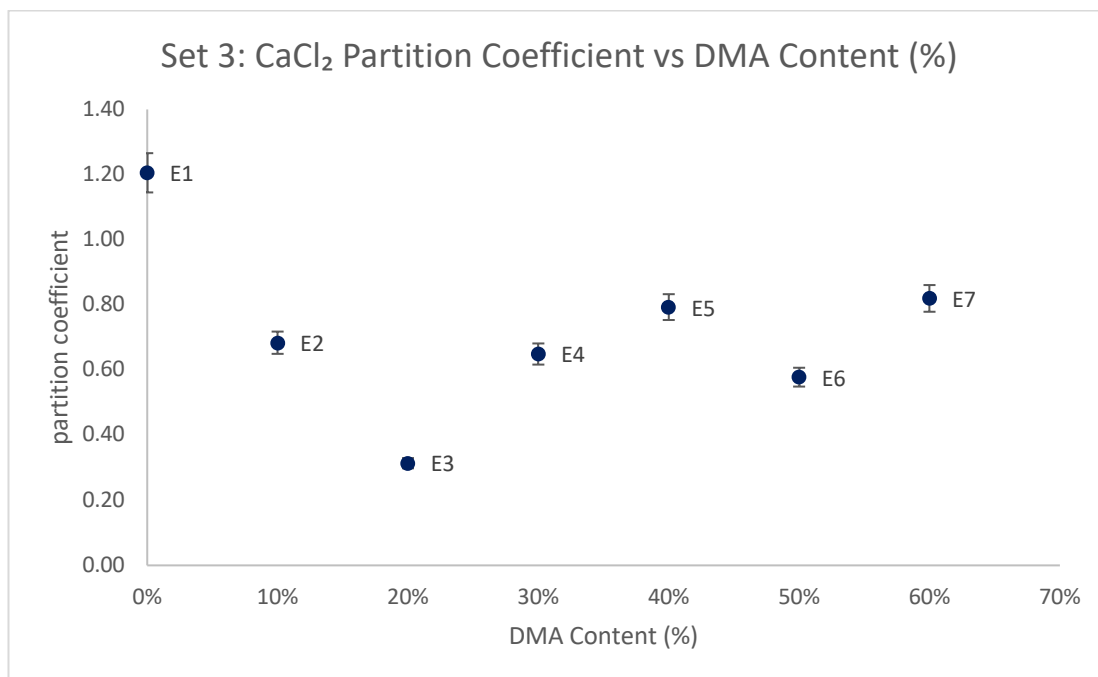


Figure 4.16 Set 3 E Hydrogels – CaCl₂ Partition Coefficient vs DMA Content (%)

The partition coefficients against potassium chloride also saw a decline as DMA content increased between hydrogels E1 to E3 but beyond this point, the coefficients remained constant despite an increase in DMA content, seen in Figure 4.17.

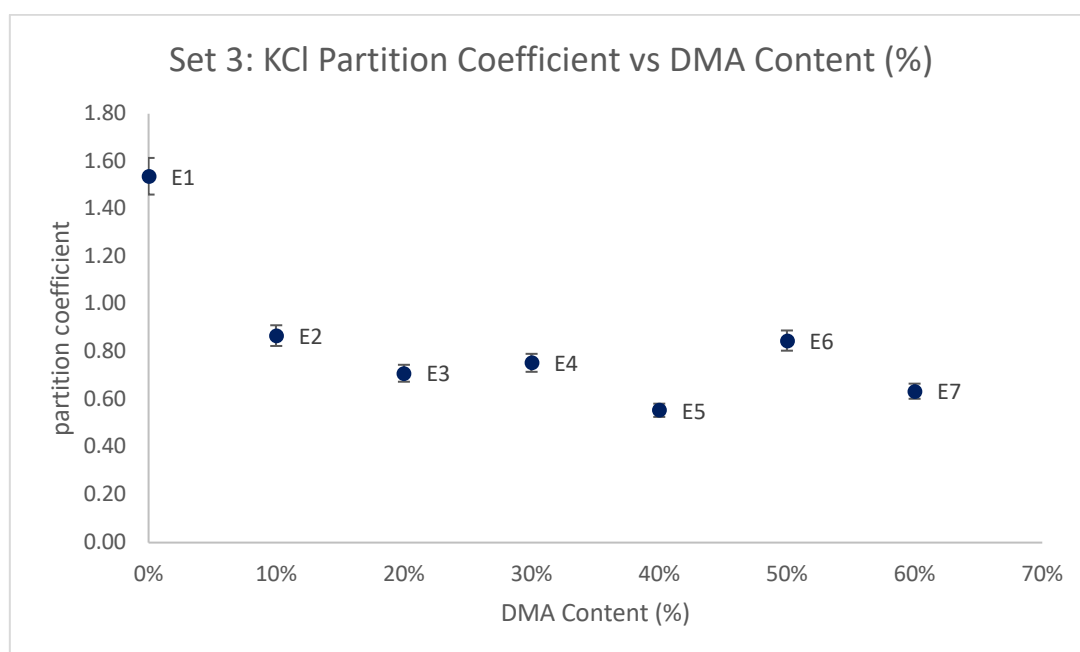


Figure 4.17 Set 3 E Hydrogels – KCl Partition Coefficient vs DMA Content (%)

The coefficients of sodium chloride did not demonstrate a clear trend with DMA content unlike potassium and calcium chloride whilst those of magnesium chloride remained relatively constant as DMA content increased across the set.

F Hydrogels: it is not possible to establish a relationship between the hydrophilic monomers and the partitioning patterns of the F hydrogels as there was not a standardised incremental change to their formulation unlike the system used with the E series hydrogels. However, it is possible to see how the partitioning patterns of the F series hydrogels changed from set 1 to set 3, depending on the synthesis conditions the gels were exposed to. Noticeably, every hydrogel of the F series had their largest partition coefficients produced by their set 2 versions, similar to those of the E series hydrogels.

The formulation of hydrogel F1 consisted of 70% TRIS and 30% NVP, making it the most hydrophobic formulation of all the hydrogels from both the E and F series. This hydrogel was also responsible for the lowest partition coefficients of all the hydrogels, its lowest values occurring in set 1. Against all the chloride salts, the largest coefficient was produced in set 2 followed by set 3 then set 1. The Figure demonstrating differences between the potassium chloride coefficients in all the sets of this particular hydrogel has been shown in Figure 4.18. The remaining figures can be found in the appendix section 2.3.

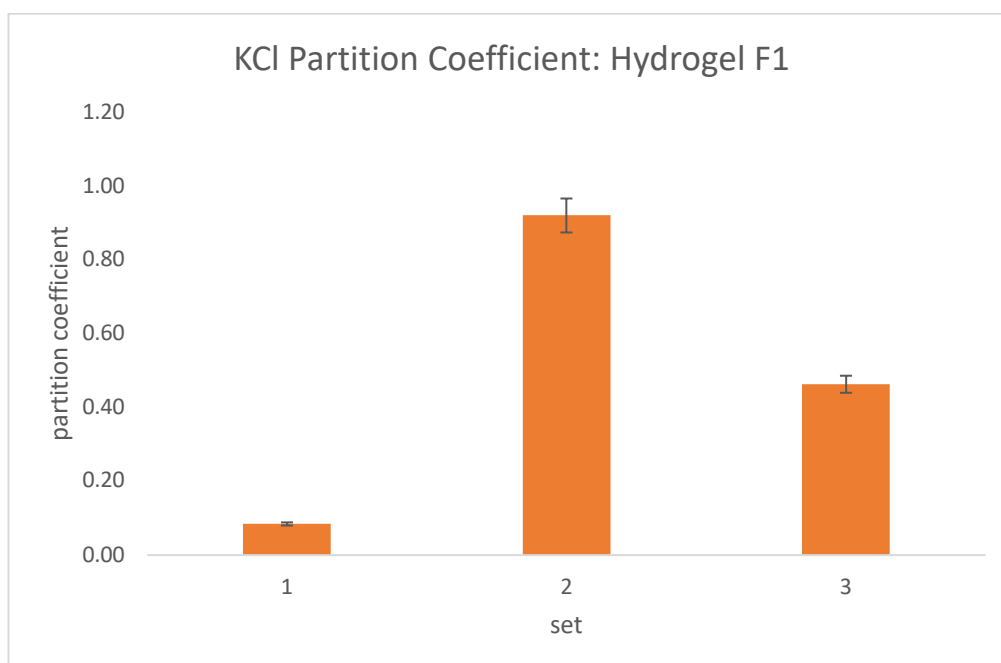


Figure 4.18 KCl Partition Coefficient: Hydrogel F1 – all sets

The formulation of hydrogel F2 consisted of 70% NVP and 30% TRIS. Calcium and magnesium chloride followed the same partitioning pattern seen with the other E & F hydrogels in which the set 2 version of the hydrogels was responsible for the largest coefficients out of all the sets.

The ratio of hydrophilic and hydrophobic monomers within hydrogel F3 was the same as hydrogel F2: 70% hydrophilic monomer and 30% hydrophobic monomer. The main difference between them was the hydrophilic monomer used: F2 utilised NVP whilst F3 utilised DMA. The partitioning behaviour of this hydrogel also followed the trend in which set 2 produced the largest coefficients out of all the sets and set 1 produced the smallest. This was seen with the partition coefficients of each chloride salt.

4.4 Conclusion

Overall, the partition coefficients of the set 2 E hydrogels (the hydrogels were post-cured and diluent was not used) were the highest in direct comparison to the E hydrogels of sets 1 (a diluent was included but the hydrogels were not post-cured) and 3 (the hydrogels were post-cured and a diluent was used). This was maintained by all the chloride salts utilised (calcium, potassium, sodium and magnesium).

In addition to this, individual hydrogel partitioning behaviours differed in-between each sets, emphasising the effect that reaction conditions such as a post-cure or use of a diluent can have on the microstructure of the hydrogels, thus influencing their partitioning characteristics. Hydrogel E3 produced the largest partition coefficients of the set 2 hydrogels against potassium and magnesium chloride whilst its set 1 version produced the lowest coefficients against calcium and sodium chloride.

It was hypothesised that the hydrogels would follow the trend in which the larger salt ions such as calcium and magnesium would partition less than the smaller ions due to size exclusion. This was the case the majority of the time, with magnesium chloride producing the smallest coefficients in set 2 and 3 and calcium chloride in set 1.

When investigating the connection between equilibrium water content and partitioning, no actual trends were initially determined due to the formation of clusters and this was the case against all the salts. However, once these clusters were expanded upon, trends emerged in all the different E hydrogels although, some trends were more widespread than others. The F hydrogels, when compared between the different sets, did not display a trend.

The relationship between freezing water content and partitioning varied between the different sets and chloride salts. The set 1 E hydrogels generally did not demonstrate a relationship with this particular water type but the E hydrogels of sets 2 and 3 did. As mentioned previously, freezing water can be further categorised into ice-like water and polymer-associated water. Trends were present for both of these water types but they were weak when compared to those seen with EWC. Despite this, trends were seen from sets 1-3.

In terms of the effects of formulation on partitioning, literature stated that an increase in the hydrophilic monomer in a hydrogel would be accompanied by an increase in partitioning. In the case of the E hydrogels, two hydrophilic monomers – DMA and NVP – were used in the formulations of the hydrogels alongside a sole hydrophobic monomer, TRIS. Each set displayed a different type of trend but overall, there was a correlation between the amount of NVP/DMA in the formulation of the hydrogel and its partitioning. In set 1, the trends differed between salts. Against calcium chloride, there was no correlation seen whilst in the remaining salts, any trends noticed were not widespread across all the gels, suggesting certain ratios of the hydrophilic monomers brings about a specific behaviour. With set 2, there were no trends seen with the different chloride salts whilst the set 3 hydrogels also demonstrated a range of trends.

Overall, clear differences in partitioning behaviour were witnessed between the E and F hydrogels from sets 1-3, further showcasing how reaction conditions and the ratio of hydrophilic monomers in a hydrogel can have a profound effect on how the hydrogel interacts with a salt ion. The lack of trends can be seen as a reflection of the complexity of the silicone-based hydrogels and how their microstructure affects these parameters, disallowing the determination of clearly established trends between aspects such as water content and formulation.

Regardless of this, the data can be used to determine suitable uses for the hydrogels in relation to biomedical applications that can make the best use of each hydrogel's unique partitioning characteristics.

5 Single-salt Permeation

5.1 Introduction

Rationale: when reviewing literature for studies on permeation in silicone-based hydrogels, they are often focused on oxygen permeability as the inclusion of silicone enhances this ability. However, understanding how similar formulations can influence the permeation of ions in these hydrogels is of importance too. This chapter sets out to understand the permeation behaviours of a series of chloride salts through the synthesised hydrogels as well as determining whether there are relationships between this parameter and other defining characteristics of a hydrogel including water content, partitioning and whether the size/charge of eluting ions is influential. Often, an increase in the hydrophilic monomer content of a hydrogel is attributed to an increase in permeation and this chapter examines the relationship between the hydrophilic/hydrophobic monomer content and permeation per salt as well. The intended aim of use for the hydrogels being studied in this thesis is inclusion in biomedical applications, as a membrane, via the mechanism of uptake and release. Not only will the work related to this chapter contribute to the general knowledge ion transportation in silicone-based hydrogels, it is hoped to further understand how all the characteristics being studied in the thesis influence ion transport of these particular hydrogels.

Permeability is the measure of the rate at which a certain component is transported through a membrane under specific conditions of concentration, temperature, pressure and/or electric field (Chai et al, 2017). Transportation rate across a membrane is determined by the structure of the membrane, the driving force of this transportation, the chemical composition and the charge of the membrane and lastly, the size and the charge of the components being permeated (Gulrez et al, 2011).

Permeation studies pertaining to silicone hydrogels often focus on oxygen transportation. This is due to the fact that the current and most significant use of these hydrogels in biomedical applications is their use as contact lenses. It is important for any biomedical device that comes into contact with the cornea of the eye to be permeable to gases, specifically oxygen, to ensure the survival of the eye (Bahram et al, 2016). This is one of the main reasons why the TRIS monomer is included in the formulation of a hydrogel as silicone is known to increase the permeability of a hydrogel to oxygen (Tran et al, 2019).

Typically, ion permeation of contact lenses is of concern as a lack of it is attributed to the adhering of the lens to the human eye as ions have to travel through the lens to maintain a fluid hydrodynamic boundary layer between the lens and the cornea (Peng & Chauhan, 2012). However, this project focuses on utilising a silicone-based hydrogel for other biomedical applications, including but not limited to liver support devices, as discussed in the literature review.

A general rule of thumb is that high ion permeabilities can be obtained by including hydrophilic monomers in a formulation and in this project, this notion has been investigated by alternating the amounts of either hydrophilic monomers – NVP and DMA – whilst keeping the hydrophobic monomer – TRIS – constant. The synthesis conditions are also thought to have an effect on a hydrogel's permeation

abilities and so each set has been analysed separately as each set represents a different set of reaction conditions in regards to the use of post-cure and inclusion of a diluent in a hydrogel's formulation.

Permeation studies are conducted in a variety of ways but the most common method at present makes use of Franz Cells, shown in image 5.1. Such cells are often used to evaluate the in-vitro drug permeation of hydrogels (Ng et al, 2010).

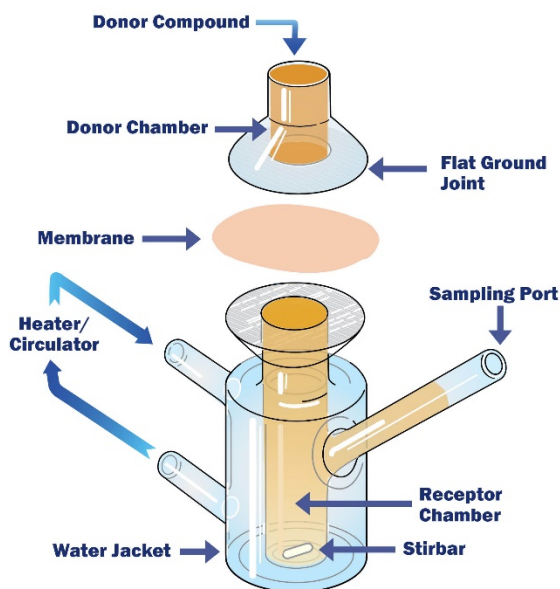


Image 5.1 Schematic of Franz Cell (image source: PermeGear, Inc., 2015)

However, this project makes use of a dual chamber permeation cell, as described in methodology chapter 2.3. This type of cell is also referred to as a Side-Bi-Side cell, as shown in image 5.2. The Franz cell focuses on vertical diffusion whilst the Side-Bi-Side cell focuses on horizontal diffusion (Tamas et al, 2015).

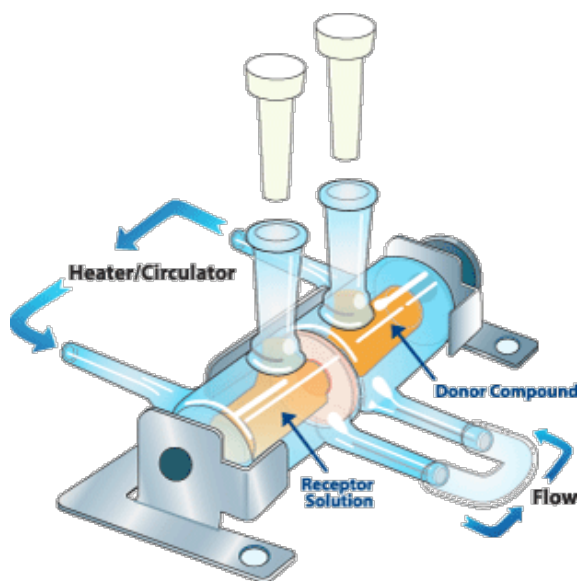


Image 5.2 Schematic of Side-Bi-Side Cell (image source: PermeGear, Inc., 2019)

Both are used for in-vitro permeation studies, but some studies have shown that one cell is more suitable for certain applications than others. For example, Bartos et al (2021) found that the Side-Bi-Side cell was more suited for studying the permeation of drugs in powder, liquid and suspension formats whilst drugs in a gel format were less suited for the apparatus.

Permeability experiments provide the information required to calculate two very important coefficients that provide insight to the permeation behaviour of the hydrogels: the permeability coefficient and the diffusion coefficient.

Permeation is made up of three aspects: solution (absorption), diffusion and release (desorption). The permeating species must first be absorbed into the hydrogel matrix and this process is often facilitated by a concentration gradient or pressure. In the permeation studies conducted, the concentration gradient is the driving force. Once the species has entered the matrix, the solute has to spread and move through the hydrogel – this process is known as diffusion. Lastly, the permeating species must be released from the gel. The diffusion coefficient describes the rate at which the eluting/permeating species moves within the hydrogel whilst the permeability coefficient describes the rate at which the entire process of permeation occurs (Polymer Properties Database, 2015).

In this chapter, the permeation behaviours of the different hydrogels will be reported and discussed, examining the effects of formulation and reaction conditions on the permeation and diffusion coefficients as well as understanding relationships between this coefficient and other parameters that have been experimentally established in this project, such as partitioning and water content.

5.2 Results

5.2.1 Permeation Coefficient

Permeation experiments were conducted using four chloride salts: calcium chloride, potassium chloride, sodium chloride and magnesium chloride. Each of the permeation experiments were repeated a minimum of three times per salt/hydrogel, as described in the methodology chapter 2.3.

Tables 5.1 to 5.6 detail the average permeation coefficients for each hydrogel against each respective salt, excluding misrepresentative runs. As with previous data reporting, the Tables have been split into the synthesis conditions sets (1, 2 or 3) and hydrogel series (E or F). Standard deviation figures are reported in the brackets next to the coefficients.

Table 5.1 Permeation Coefficients for E hydrogels of Set 1 (brackets indicate standard deviation)

	E1	E2	E3	E4	E5	E6	E7
CaCl₂	4.67x10 ⁻¹⁰ (1.80x10 ⁻¹⁰)	4.63x10 ⁻¹⁰ (2.72x10 ⁻¹⁰)	3.77x10 ⁻¹⁰ (8.22x10 ⁻¹⁰)	9.09x10 ⁻¹¹ (7.90x10 ⁻¹¹)	6.47x10 ⁻¹⁰ (7.22x10 ⁻¹⁰)	5.46x10 ⁻¹⁰ (9.05x10 ⁻¹⁰)	7.72x10 ⁻¹⁰ (2.74x10 ⁻¹⁰)
KCl	4.04x10 ⁻¹⁰ (1.80x10 ⁻¹⁰)	4.33x10 ⁻¹⁰ (2.72x10 ⁻¹⁰)	1.96x10 ⁻⁹ (8.22x10 ⁻¹⁰)	2.47x10 ⁻¹⁰ (1.90x10 ⁻¹¹)	2.35x10 ⁻⁹ (7.22x10 ⁻¹⁰)	2.59x10 ⁻⁹ (9.05x10 ⁻¹⁰)	3.36x10 ⁻⁹ (2.74x10 ⁻¹⁰)
NaCl	3.87x10 ⁻¹⁰ (2.24x10 ⁻¹⁰)	6.96x10 ⁻¹⁰ (8.63x10 ⁻¹¹)	7.14x10 ⁻¹⁰ (6.53x10 ⁻¹¹)	1.76x10 ⁻¹⁰ (1.12x10 ⁻¹¹)	3.49x10 ⁻¹⁰ (3.92x10 ⁻¹¹)	8.36x10 ⁻¹⁰ (7.38x10 ⁻¹¹)	1.16x10 ⁻⁹ (9.81x10 ⁻¹⁰)
MgCl₂	3.57x10 ⁻¹⁰ (3.25x10 ⁻¹⁰)	4.90x10 ⁻¹⁰ (2.46x10 ⁻¹⁰)	9.50x10 ⁻¹⁰ (8.62x10 ⁻¹⁰)	5.91x10 ⁻¹¹ (3.51x10 ⁻¹¹)	6.19x10 ⁻¹⁰ (2.32x10 ⁻¹⁰)	5.16x10 ⁻¹⁰ (3.58x10 ⁻¹⁰)	7.86x10 ⁻¹⁰ (3.30x10 ⁻¹¹)

Table 5.2 Permeation Coefficients for F hydrogels of Set 1 (brackets indicate standard deviation)

	F1	F2	F3
CaCl₂	4.04x10 ⁻¹² (3.44x10 ⁻¹²)	6.66x10 ⁻¹⁰ (3.49x10 ⁻¹⁰)	1.71x10 ⁻⁹ (1.27x10 ⁻⁹)
KCl	3.68x10 ⁻¹² (3.68x10 ⁻¹²)	1.30x10 ⁻⁹ (3.49x10 ⁻¹⁰)	3.62x10 ⁻⁹ (1.27x10 ⁻¹⁰)
NaCl	3.55x10 ⁻¹² (2.17x10 ⁻¹²)	5.61x10 ⁻¹⁰ (4.50x10 ⁻¹⁰)	1.17x10 ⁻⁹ (1.07x10 ⁻⁹)
MgCl₂	1.39x10 ⁻¹² (1.39x10 ⁻¹²)	4.21x10 ⁻¹⁰ (1.22x10 ⁻¹⁰)	8.95x10 ⁻¹⁰ (8.46x10 ⁻¹⁰)

Table 5.3 Permeation Coefficients for E hydrogels of Set 2 (brackets indicate standard deviation)

	E1	E2	E3	E4	E5	E6	E7
CaCl₂	9.01x10 ⁻¹⁰ (1.06x10 ⁻¹⁰)	1.42x10 ⁻¹⁰ (2.28x10 ⁻¹¹)	2.471x10 ⁻⁹ (2.24x10 ⁻¹⁰)	1.44x10 ⁻⁹ (9.55x10 ⁻¹¹)	2.04x10 ⁻⁹ (6.19x10 ⁻¹⁰)	1.35x10 ⁻⁹ (2.62x10 ⁻¹⁰)	1.91x10 ⁻⁹ (1.53x10 ⁻¹⁰)
KCl	1.55x10 ⁻⁹ (6.22x10 ⁻¹¹)	4.40x10 ⁻¹⁰ (2.23x10 ⁻¹⁰)	4.38x10 ⁻⁹ (6.48x10 ⁻¹⁰)	2.60x10 ⁻⁹ (3.49x10 ⁻¹⁰)	3.31x10 ⁻⁹ (1.50x10 ⁻⁹)	2.33x10 ⁻⁹ (7.42x10 ⁻¹⁰)	3.30x10 ⁻⁹ (2.53x10 ⁻¹⁰)
NaCl	8.19x10 ⁻¹⁰ (2.61x10 ⁻¹¹)	3.19x10 ⁻¹⁰ (8.24x10 ⁻¹¹)	2.76x10 ⁻⁹ (3.03x10 ⁻¹⁰)	1.64x10 ⁻⁹ (2.15x10 ⁻¹⁰)	4.30x10 ⁻⁹ (1.84x10 ⁻⁹)	1.98x10 ⁻⁹ (2.19x10 ⁻¹⁰)	2.41x10 ⁻⁹ (2.38x10 ⁻¹⁰)
MgCl₂	4.67x10 ⁻¹⁰ (1.26x10 ⁻¹¹)	6.73x10 ⁻¹¹ (1.17x10 ⁻¹³)	1.57x10 ⁻⁹ (8.46x10 ⁻¹¹)	1.02x10 ⁻⁹ (3.39x10 ⁻¹¹)	2.17x10 ⁻⁹ (6.99x10 ⁻¹⁰)	7.99x10 ⁻¹⁰ (7.73x10 ⁻¹¹)	1.32x10 ⁻⁹ (1.09x10 ⁻¹⁰)

Table 5.4 Permeation Coefficients for F hydrogels of Set 2 (brackets indicate standard deviation)

	F1	F2	F3
CaCl₂	4.90x10 ⁻¹³ (2.61x10 ⁻¹³)	1.89x10 ⁻⁹ (5.39x10 ⁻¹⁰)	2.735x10 ⁻⁹ (1.53x10 ⁻¹⁰)
KCl	8.67x10 ⁻¹⁴ (-)	2.50x10 ⁻⁹ (1.61x10 ⁻¹¹)	4.84x10 ⁻⁹ (3.28x10 ⁻¹⁰)
NaCl	6.41x10 ⁻¹² (1.04x10 ⁻¹¹)	1.78x10 ⁻⁹ (2.36x10 ⁻¹⁰)	3.34x10 ⁻⁹ (1.81x10 ⁻¹⁰)
MgCl₂	1.34x10 ⁻¹³ (3.98x10 ⁻¹⁴)	8.81x10 ⁻¹⁰ (9.36x10 ⁻¹¹)	2.11x10 ⁻⁹ (1.05x10 ⁻¹⁰)

Table 5.5 Permeation Coefficients for E Hydrogels of Set 3 (brackets indicate standard deviation)

	E1	E2	E3	E4	E5	E6	E7
CaCl₂	1.25x10 ⁻⁹ (1.96x10 ⁻¹¹)	2.19x10 ⁻¹² (8.36x10 ⁻¹³)	5.35x10 ⁻⁹ (3.80x10 ⁻⁹)	1.92x10 ⁻⁹ (2.68x10 ⁻¹⁰)	2.02x10 ⁻⁹ (1.81x10 ⁻¹⁰)	3.13x10 ⁻⁹ (5.52x10 ⁻¹⁰)	2.90x10 ⁻⁹ (1.31x10 ⁻⁹)
KCl	2.41x10 ⁻⁹ (1.21x10 ⁻¹⁰)	3.69x10 ⁻¹² (3.24x10 ⁻¹⁰)	3.76x10 ⁻⁹ (7.28x10 ⁻⁹)	3.63x10 ⁻⁹ (2.82x10 ⁻¹⁰)	3.27x10 ⁻⁹ (6.92x10 ⁻¹¹)	6.91x10 ⁻⁹ (4.25x10 ⁻¹⁰)	3.90x10 ⁻⁹ (5.07x10 ⁻¹⁰)
NaCl	1.40x10 ⁻⁹ (7.96x10 ⁻¹²)	2.96x10 ⁻¹² (5.15x10 ⁻⁹)	6.93x10 ⁻⁹ (1.16x10 ⁻⁸)	2.31x10 ⁻⁹ (1.32x10 ⁻¹⁰)	2.00x10 ⁻⁹ (2.11x10 ⁻¹⁰)	1.33x10 ⁻⁸ (1.67x10 ⁻⁸)	2.53x10 ⁻⁹ (1.45x10 ⁻¹⁰)
MgCl₂	8.37x10 ⁻¹⁰ (7.42x10 ⁻¹¹)	7.11x10 ⁻¹³ (7.43x10 ⁻¹³)	4.25x10 ⁻⁹ (3.76x10 ⁻⁹)	1.28x10 ⁻⁹ (6.48x10 ⁻¹¹)	1.30x10 ⁻⁹ (2.60x10 ⁻¹⁰)	2.22x10 ⁻⁹ (2.12x10 ⁻¹⁰)	1.40x10 ⁻⁹ (1.24x10 ⁻¹⁰)

Table 5.6 Permeation Coefficients for F hydrogels of Set 3 (brackets indicate standard deviation)

	F1	F2	F3
CaCl₂	7.61x10 ⁻¹³ (1.79x10 ⁻¹³)	2.34x10 ⁻⁹ (2.10x10 ⁻¹⁰)	2.641x10 ⁻⁹ (2.10x10 ⁻¹⁰)
KCl	1.90x10 ⁻¹² (4.72x10 ⁻¹³)	4.19x10 ⁻⁹ (1.16x10 ⁻¹¹)	4.42x10 ⁻⁹ (1.93x10 ⁻¹⁰)
NaCl	8.34x10 ⁻¹³ (1.43x10 ⁻¹³)	2.59x10 ⁻⁹ (3.80x10 ⁻¹¹)	2.80x10 ⁻⁹ (6.75x10 ⁻¹¹)
MgCl₂	3.09x10 ⁻¹² (4.09x10 ⁻¹²)	1.59x10 ⁻⁹ (3.92x10 ⁻¹¹)	1.68x10 ⁻⁹ (1.75x10 ⁻¹⁰)

5.2.2 Diffusion Coefficient

Diffusion coefficients were calculated using the following equation:

$$\text{diffusion coefficient (cm}^2/\text{s)} = \frac{\text{permeation coefficient (cm}^2/\text{s)}}{\text{partition coefficient}} \quad (5.1)$$

Tables 5.7 to 5.12 detail the diffusion coefficients of the hydrogels per set, as shown with the permeation coefficients.

Table 5.7 Diffusion Coefficients for E Hydrogels of Set 1 (brackets indicate standard deviation)

	E1	E2	E3	E4	E5	E6	E7
CaCl₂	3.37x10 ⁻⁹ (9.16x10 ⁻¹⁰)	2.49x10 ⁻⁹ (1.04x10 ⁻⁹)	4.43x10 ⁻⁹ (7.42x10 ⁻¹⁰)	4.80x10 ⁻¹⁰ (8.71x10 ⁻¹¹)	5.14x10 ⁻⁹ (1.48x10 ⁻⁹)	7.01x10 ⁻⁹ (1.23 x10 ⁻⁹)	6.90x10 ⁻⁹ (1.22x10 ⁻⁹)
KCl	2.35x10 ⁻⁹ (1.01x10 ⁻⁹)	1.90x10 ⁻⁹ (1.46x10 ⁻⁹)	7.92x10 ⁻⁹ (3.33x10 ⁻⁹)	1.46x10 ⁻⁹ (1.12x10 ⁻¹⁰)	1.27x10 ⁻⁸ (4.25x10 ⁻⁹)	6.42x10 ⁻⁹ (4.24x10 ⁻⁹)	1.32x10 ⁻⁸ (1.07x10 ⁻⁹)
NaCl	3.54x10 ⁻⁹ (1.81x10 ⁻⁹)	3.21x10 ⁻⁹ (3.98x10 ⁻¹⁰)	1.67x10 ⁻⁸ (3.63 x10 ⁻¹⁰)	8.16x10 ⁻¹⁰ (5.19x10 ⁻¹¹)	3.79x10 ⁻⁹ (3.64x10 ⁻⁹)	4.07x10 ⁻⁹ (3.83x10 ⁻⁹)	5.38x10 ⁻⁹ (2.35x10 ⁻⁹)
MgCl₂	5.95x10 ⁻¹⁰ (3.40x10 ⁻¹⁰)	1.45x10 ⁻⁹ (1.29x10 ⁻⁹)	3.60x10 ⁻⁹ (3.27x10 ⁻⁹)	2.38x10 ⁻¹⁰ (1.41x10 ⁻¹⁰)	3.09x10 ⁻⁹ (1.43x10 ⁻⁹)	1.86x10 ⁻⁹ (1.70x10 ⁻⁹)	3.85x10 ⁻⁹ (1.47x10 ⁻¹⁰)

Table 5.8 Diffusion Coefficients for F Hydrogels of Set 1 (brackets indicate standard deviation)

	F1	F2	F3
CaCl₂	4.20x10 ⁻¹¹ (4.20x10 ⁻¹¹)	3.52x10 ⁻⁹ (3.52x10 ⁻⁹)	1.11x10 ⁻⁸ (1.11x10 ⁻⁸)
KCl	1.10x10 ⁻¹¹ (6.95x10 ⁻¹²)	1.53x10 ⁻⁸ (4.13x10 ⁻⁹)	1.40x10 ⁻⁸ (4.92x10 ⁻⁹)
NaCl	2.30x10 ⁻¹¹ (1.41x10 ⁻¹¹)	9.93x10 ⁻⁹ (5.75x10 ⁻⁹)	4.29x10 ⁻⁹ (2.12x10 ⁻⁹)
MgCl₂	1.19x10 ⁻¹¹ (7.18x10 ⁻¹²)	3.15x10 ⁻⁸ (1.72x10 ⁻⁸)	1.92x10 ⁻⁸ (7.66x10 ⁻⁹)

Table 5.9 Diffusion Coefficients for E Hydrogels of Set 2 (brackets indicate standard deviation)

	E1	E2	E3	E4	E5	E6	E7
CaCl₂	1.71x10 ⁻⁹ (6.42x10 ⁻¹⁰)	1.64x10 ⁻¹⁰ (2.64x10 ⁻¹¹)	2.03x10 ⁻⁹ (1.85x10 ⁻¹⁰)	1.10x10 ⁻⁹ (5.36x10 ⁻¹¹)	1.95x10 ⁻⁹ (5.93x10 ⁻¹⁰)	2.46x10 ⁻⁹ (4.76x10 ⁻¹⁰)	1.30x10 ⁻⁹ (1.04x10 ⁻¹⁰)
KCl	1.24x10 ⁻⁹ (4.95x10 ⁻¹¹)	4.45x10 ⁻¹⁰ (2.26x10 ⁻¹⁰)	1.98x10 ⁻⁹ (2.93x10 ⁻¹⁰)	3.31x10 ⁻⁹ (4.44x10 ⁻¹⁰)	3.09x10 ⁻⁹ (1.40x10 ⁻⁹)	3.77x10 ⁻⁹ (1.20x10 ⁻⁹)	3.86x10 ⁻⁹ (2.97x10 ⁻¹⁰)
NaCl	1.69x10 ⁻⁹ (2.58x10 ⁻¹⁰)	6.29x10 ⁻¹⁰ (1.63x10 ⁻¹⁰)	5.56x10 ⁻⁹ (6.11x10 ⁻¹⁰)	3.18x10 ⁻⁹ (4.18x10 ⁻¹⁰)	8.29x10 ⁻⁹ (3.55x10 ⁻⁹)	2.09x10 ⁻⁹ (2.32E10)	4.31x10 ⁻⁹ (4.26x10 ⁻¹⁰)
MgCl₂	9.09x10 ⁻¹⁰ (2.46x10 ⁻¹¹)	7.71x10 ⁻¹¹ (1.33x10 ⁻¹³)	1.09x10 ⁻⁹ (5.87x10 ⁻¹¹)	2.25x10 ⁻⁹ (4.15x10 ⁻¹⁰)	1.72x10 ⁻⁹ (5.52x10 ⁻¹⁰)	2.25x10 ⁻⁹ (2.19x10 ⁻⁹)	2.35x10 ⁻⁹ (1.95x10 ⁻¹⁰)

Table 5.10 Diffusion Coefficients for F Hydrogels of Set 2 (brackets indicate standard deviation)

	F1	F2	F3
CaCl₂	3.78x10 ⁻¹² (2.21x10 ⁻¹²)	1.87x10 ⁻⁹ (5.33x10 ⁻¹⁰)	1.83x10 ⁻⁹ (1.02x10 ⁻¹⁰)
KCl	9.42x10 ⁻¹⁴ (-)	3.57x10 ⁻⁹ (1.65x10 ⁻¹¹)	2.55x10 ⁻⁹ (1.73x10 ⁻¹⁰)
NaCl	3.32x10 ⁻¹³ (3.44x10 ⁻¹³)	3.20x10 ⁻⁹ (4.24x10 ⁻¹⁰)	4.83x10 ⁻⁹ (2.62x10 ⁻¹⁰)
MgCl₂	5.06x10 ⁻¹³ (1.51x10 ⁻¹³)	8.22x10 ⁻¹⁰ (8.73x10 ⁻¹¹)	4.27x10 ⁻⁹ (2.12x10 ⁻¹⁰)

Table 5.11 Diffusion Coefficients for E Hydrogels of Set 3 (brackets indicate standard deviation)

	E1	E2	E3	E4	E5	E6	E7
CaCl₂	1.03x10 ⁻⁹ (1.63x10 ⁻¹¹)	3.20x10 ⁻¹² (1.22x10 ⁻¹²)	1.71x10 ⁻⁸ (1.21x10 ⁻⁸)	2.96x10 ⁻⁹ (4.13x10 ⁻¹⁰)	2.08x10 ⁻⁹ (8.26x10 ⁻¹⁰)	5.41x10 ⁻⁹ (9.55x10 ⁻¹⁰)	3.54x10 ⁻⁹ (1.59x10 ⁻⁹)
KCl	1.03x10 ⁻⁸ (1.52x10 ⁻⁸)	4.24x10 ⁻¹² (3.10x10 ⁻⁹)	6.40x10 ⁻⁸ (3.13x10 ⁻⁸)	2.97x10 ⁻⁸ (4.30x10 ⁻⁸)	4.77x10 ⁻⁸ (7.25x10 ⁻⁸)	4.05x10 ⁻⁸ (5.58x10 ⁻⁸)	3.51x10 ⁻⁸ (5.06x10 ⁻⁸)
NaCl	2.21x10 ⁻⁹ (1.77x10 ⁻¹¹)	6.44x10 ⁻¹² (9.25x10 ⁻⁸)	1.48E-07 (7.53x10 ⁻⁸)	8.28x10 ⁻⁹ (4.56x10 ⁻¹⁰)	3.92x10 ⁻⁹ (4.14x10 ⁻¹⁰)	5.43x10 ⁻⁸ (1.49x10 ⁻⁸)	4.31x10 ⁻⁹ (3.40x10 ⁻¹⁰)
MgCl₂	1.55x10 ⁻⁹ (1.37x10 ⁻¹⁰)	9.61x10 ⁻¹³ (1.00x10 ⁻¹²)	8.35x10 ⁻⁹ (7.38x10 ⁻⁹)	2.23x10 ⁻⁹ (8.79x10 ⁻¹¹)	2.44x10 ⁻⁹ (4.88x10 ⁻¹⁰)	5.97x10 ⁻⁹ (5.71x10 ⁻¹⁰)	3.17x10 ⁻⁹ (2.79x10 ⁻¹⁰)

Table 5.12 Diffusion Coefficients for F Hydrogels of Set 3 (brackets indicate standard deviation)

	F1	F2	F3
CaCl₂	4.23x10 ⁻¹² (9.93x10 ⁻¹³)	2.54x10 ⁻⁹ (2.28x10 ⁻¹⁰)	2.719x10 ⁻⁹ (2.17x10 ⁻¹⁰)
KCl	3.58x10 ⁻¹¹ (4.58x10 ⁻¹¹)	2.54x10 ⁻⁸ (3.76x10 ⁻⁸)	3.39x10 ⁻⁸ (5.07x10 ⁻⁸)
NaCl	6.40x10 ⁻¹¹ (5.05x10 ⁻¹¹)	4.46x10 ⁻⁹ (1.26x10 ⁻¹¹)	4.58x10 ⁻⁹ (6.67x10 ⁻¹¹)
MgCl₂	1.34x10 ⁻¹¹ (2.11x10 ⁻¹¹)	3.24x10 ⁻⁹ (8.09x10 ⁻¹¹)	3.58x10 ⁻⁹ (3.82x10 ⁻¹⁰)

Set 1: For both the E & F hydrogels of this set, potassium chloride was responsible for the largest permeability coefficients whilst magnesium chloride was responsible for the lowest coefficients with the exception of hydrogels E2 and F1. Sodium chloride was responsible for the largest permeability coefficient of hydrogel E2 ($6.96 \times 10^{-10} \text{ cm}^2/\text{s}$) whilst calcium chloride was responsible for the largest permeability coefficient of hydrogel F1 ($4.04 \times 10^{-12} \text{ cm}^2/\text{s}$). Also, hydrogel E7 saw its smallest permeability coefficient brought about by calcium chloride ($7.72 \times 10^{-10} \text{ cm}^2/\text{s}$).

Overall, hydrogel F3 was the most permeable hydrogel against calcium, potassium and sodium chloride whilst hydrogel E3 was the most permeable against magnesium chloride ($9.5 \times 10^{-10} \text{ cm}^2/\text{s}$). Hydrogel F1 was consistently the least permeable hydrogel against all the salts. Beyond that, hydrogel E1 was the second least permeable hydrogel against calcium, potassium and magnesium chloride whilst hydrogel E5 was the least permeable against sodium chloride ($3.49 \times 10^{-10} \text{ cm}^2/\text{s}$).

The diffusion coefficients brought about a range of activity in the varying hydrogels. Hydrogels E1-E3 saw their largest diffusion coefficients brought about by sodium chloride. Hydrogels E4, E5 and E7 saw their largest coefficients brought about by potassium chloride. Hydrogels E6 and F1 had their largest coefficients caused by calcium chloride whilst hydrogels F2 and F3 saw their largest coefficients being caused by magnesium chloride. All the E hydrogels saw their smallest diffusion coefficients being

G.Durowoju, PhD Thesis, Aston University 2022.

caused by magnesium chloride. Each F hydrogel of this set had a different salt responsible for its smallest coefficients: hydrogel F1 was potassium chloride, F2 was calcium chloride whilst F3 was sodium chloride. None of the F series saw their lowest diffusion coefficients being brought about by magnesium chloride.

Set 2: with the exception of hydrogels E5 and F1, potassium chloride was responsible for the largest permeability coefficients of the set 2 E & F hydrogels. Hydrogels E5 ($4.30 \times 10^{-9} \text{ cm}^2/\text{s}$) and F1 ($6.41 \times 10^{-12} \text{ cm}^2/\text{s}$) saw their largest coefficients being caused by sodium chloride. The same was seen with the minimum permeability coefficients: all the hydrogels except hydrogels E5 and hydrogel F1 had their smallest coefficients caused by magnesium chloride. For hydrogel E5, this was brought about by calcium chloride (2.04×10^{-9}) whilst hydrogel F1 was caused by potassium chloride ($8.67 \times 10^{-14} \text{ cm}^2/\text{s}$).

Similarly to the set 1 hydrogels, the diffusion coefficients did not see one salt being solely responsible for the largest or smallest coefficients. Both hydrogels E1 and F1 saw their largest diffusion coefficient being caused by calcium chloride at $1.71 \times 10^{-9} \text{ cm}^2/\text{s}$ and $3.78 \times 10^{-12} \text{ cm}^2/\text{s}$ respectively. Hydrogels E2, E3, E5 and E7 saw their largest coefficient being caused by sodium chloride. Hydrogels E4, E6 and F2 were caused by potassium chloride. With the minimum coefficients, hydrogels E1-E3, E5 and F2 were caused by magnesium chloride. Hydrogels E4, E7, and F3 were caused by calcium chloride. Hydrogel E6 was the sole hydrogel of the set to see sodium chloride causing its smallest diffusion coefficient at 2.09×10^{-9} whilst hydrogel F1 was also the only hydrogel of the set that saw potassium chloride being responsible for its smallest coefficient at 9.42×10^{-14} .

Set 3: with the exceptions of hydrogels E3, E6 and F1, potassium chloride was responsible for the largest permeation coefficients of the E and F hydrogels. Both hydrogels E3 ($6.93 \times 10^{-9} \text{ cm}^2/\text{s}$) and E6 ($1.33 \times 10^{-8} \text{ cm}^2/\text{s}$) had their largest permeation coefficient caused by sodium chloride whilst magnesium chloride was responsible for that of hydrogel F1 ($3.09 \times 10^{-12} \text{ cm}^2/\text{s}$). Magnesium chloride caused the smallest coefficients for all of the E and F hydrogels except those of hydrogel E3 and F1. Hydrogel E3's smallest coefficient was caused by potassium chloride ($3.76 \times 10^{-9} \text{ cm}^2/\text{s}$) whilst that of hydrogel F1 was by calcium chloride ($7.61 \times 10^{-13} \text{ cm}^2/\text{s}$).

In sets 1 and 2, hydrogel F1 was responsible for the lowest permeation coefficients against all the chloride salts. However, the set 3 version of hydrogel E2 demonstrated low levels of permeability towards all the chloride salts, producing coefficients in the range of $\times 10^{-12}$ and $\times 10^{-13} \text{ cm}^2/\text{s}$. When directly compared against the coefficients of hydrogel F1, those of hydrogel E2 were consistently lower. Its previous set versions had permeation coefficients comparable to the majority of the E hydrogels, which performed in the region of $\times 10^{-9}$ and $\times 10^{-10} \text{ cm}^2/\text{s}$.

Although magnesium chloride was responsible for majority of the hydrogels' lowest diffusion coefficients, sodium chloride was responsible for the largest diffusion coefficients of all the hydrogels except hydrogel E1 whose largest coefficient was caused by potassium chloride. This same salt was responsible for the largest diffusion coefficients of hydrogels E3 ($3.76 \times 10^{-9} \text{ cm}^2/\text{s}$) and F1 ($1.90 \times 10^{-12} \text{ cm}^2/\text{s}$).

5.3 Discussion

The permeability behaviour of hydrogels is one of the most important factors to determine and understand when synthesising hydrogels for applications in biomedical settings as the ability of a hydrogel to permeate and diffuse molecules forms the basis for its usage within such a system, especially when the intended use includes the separation and release of different molecules.

As mentioned in the introduction to this chapter, permeation is dependent on diffusivity and partitioning as seen in the equation used to incorporate all three coefficients:

$$P = KD \tag{5.2}$$

where P is the partition coefficient, K is the permeation coefficient (cm^2/s), and D is the diffusion coefficient (cm^2/s).

If a solute partitions at a greater rate within a hydrogel, it will be diffused slower through the matrix and thus have a lower permeation rate and vice versa (Kanduč et al, 2020). Understanding how these parameters influence permeation is necessary but also establishing how other characteristics such as formulation and water content influence permeation is just as important.

The principles that can affect permeation include pore size of the hydrogel and the driving force behind the transport of the solute across the membrane such as pressure or a concentration gradient (Offeddu et al, 2018). Permeability is also linked to the morphological structures of the hydrogels, which in turn can be influenced by the incorporation of a diluent in the synthesis of the hydrogel, especially by influencing the mesh size of the polymer network.

Transport of solutes can also be affected by the transport paths within a hydrogel. These can be influenced by the hydrophilic/hydrophobic monomers within a hydrogel (Offeddu et al, 2018), with the hydrophilic monomers producing paths that would facilitate ion permeation and the hydrophobic monomers facilitating oxygen permeation (Pozuelo et al, 2014).

The exact mechanism behind ion mobility within hydrogel structures is not entirely understood but it is assumed that the process involves the dissociation of the ions of a salt within water and its diffusion through the water/water channels within the polymer matrix (Pozuelo et al, 2014). Due to this, the water content of the hydrogel is thought to have a high level of influence on the overall process of permeation.

Unlike the partition coefficient which depends on the (total fraction of) the two phases within a hydrogel: the hydrophilic and hydrophobic phases, diffusion depends on the connectivity between these two phases – whether the morphology of the hydrogel is dispersed or bi-continuous (Peng & Chauhan, 2012). More insight is provided on the morphology of the hydrogels in the membrane characteristics chapter (7).

Due to these factors, the relationship between permeation and the formulation of the hydrogels will be discussed, the influence of the varying water types within the hydrogels on their permeation will be investigated and the relationship between diffusion, partitioning and permeation will be discussed. The difference in permeation performance between the chloride salts will also be discussed as well as trends between the E & F hydrogels from sets 1-3.

5.3.1 Effects of formulation & reaction conditions on permeation

In previous chapters, it has been established that the synthesised hydrogels have both hydrophobic and hydrophilic regions due to the monomers included in their formulation. This notion is discussed further in the membrane characteristics chapter (7). Due to this, they are considered to be biphasic polymers (Austin & Kumar, 2005). Such hydrogels possess “channels” that facilitate oxygen permeation via the hydrophobic but oxygen-loving regions attributed to TRIS content and ion permeation through the hydrophilic regions established by DMA and NVP content.

As was the case with the relationship between partitioning and formulation, determining a relationship between the formulation of the hydrogels and permeation would be easier to establish if the formulation was based on a singular hydrophilic monomer and hydrophobic monomer (Liu et al, 2015). As one monomer increases/decreases, there would be a direct increase/decrease in permeation. However, seeing as there are three monomers to consider, establishing a relationship with all three is just as important.

Three different sets of E & F hydrogels were synthesised and characterised for the permeation behaviour towards the four different chloride salts. The differences between the synthesis conditions of each set are described in Table 5.13.

Table 5.13 Reaction conditions between sets

Set Name	Post-cure @ 90°C	Diluent included
Set 1	No	Yes (E hydrogels only)
Set 2	Yes	No
Set 3	Yes	Yes

Post-cures are included in the synthesis of silicone-based hydrogels to remove unreacted monomers from the hydrogel matrix whereas diluents are included to increase the solubility of the monomers if there is a degree of immiscibility between them (Peng & Chauhan, 2012) and to also increase the pore formation of the polymer network (Okay, 2000). It was of interest to see whether altering these conditions between the hydrogel sets would influence their characteristics, including permeation.

In addition to the reaction conditions, the influence of the monomer ratio on permeation behaviour was of interest. This would involve establishing if the amount of the hydrophilic monomers within the hydrogels has a relationship with their permeation behaviour. The TRIS monomer may be less influential

on permeation than DMA and NVP because its ratio within the monomers has been kept constant and it is also hydrophobic in nature.

Relationships between the permeation coefficients of the hydrogels of sets 1-3 and the different monomers included in their formulation have been considered. Mirrored trends between the monomers DMA and NVP are expected due to the intentional juxtaposition of their content in the hydrogels. If an increase in a parameter was seen as DMA content increased in the hydrogels, the order of the trend would be reversed as NVP content also increased. Due to this, trends from one monomer will be shown per set and the trends not shown can be found in the appendix 3.3.6.

Set 1 E Hydrogels: as stated earlier, one monomer will be showcased per set due to the mirroring effect of the monomer relationships. For set 1, NVP content and its relationship with the permeation coefficients from the different chloride salts will be discussed.

There was no relationship between the different chloride salt permeation coefficients of the E hydrogels of set 1 and their TRIS monomer content. As TRIS content was kept constant and the monomer is hydrophobic in nature, it was thought the monomer would either have a negative or neutral effect on permeation but it was confirmed that there was no effect.

For all the salts, trends were noticed between the NVP content of the hydrogels and their permeation coefficients. In the case of potassium chloride permeation coefficients, the departure of hydrogel E4 from the trend line, shown in Figure 5.1, may be a result of error – a lack of a sizeable sample for this particular hydrogel led to only two permeation experiments being conducted as opposed to five/six like the remainder of the hydrogels for this set. However, the Figure reveals the closeness in permeation coefficient between hydrogels E2 and E1 despite the difference in their formulation. Against potassium chloride, they produced permeation coefficients of $4.33 \times 10^{-10} \text{ cm}^2/\text{s}$ and $4.04 \times 10^{-10} \text{ cm}^2/\text{s}$, respectively.

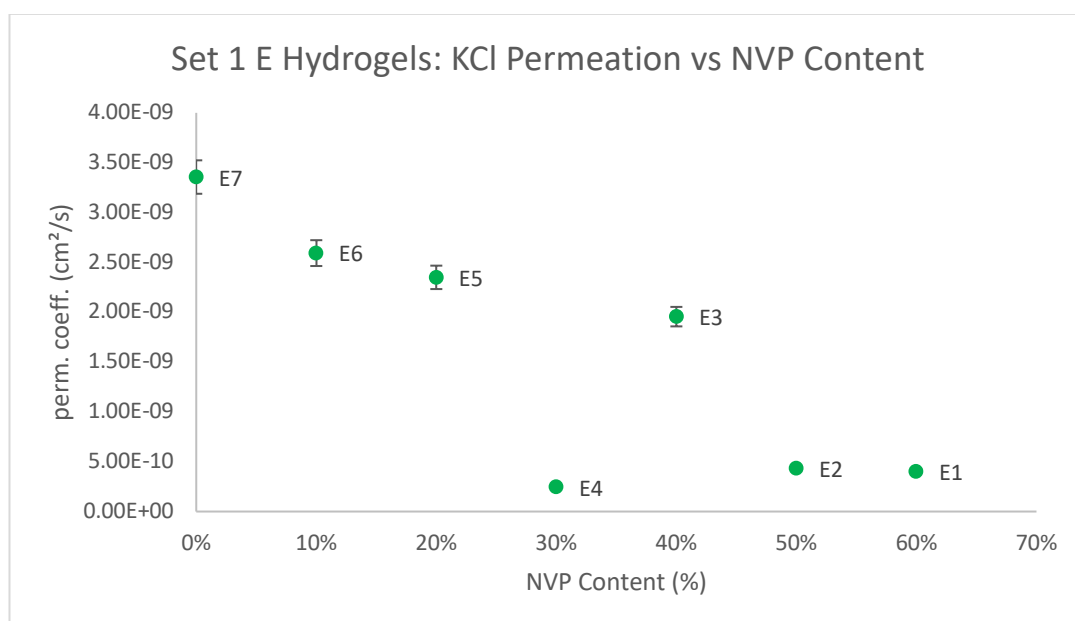


Figure 5.1 Set 1 E Hydrogels – KCl Permeation vs NVP Content (%)

With the divalent salts, calcium and magnesium chloride, a clear relationship between NVP content and the permeation of these salts was not established. However, with the mono-chloride salts, potassium and sodium chloride, there was a decrease in the permeation coefficients of the E hydrogels as their NVP content increased across the set.

Set 2 E Hydrogels: with this set, the NVP monomer content of the hydrogels will be discussed. For all the salts, a relationship was established, and trends were noticed between the DMA and NVP content of the hydrogels and their permeation coefficients. Again, no trends were established between the set 2 permeation coefficients and their TRIS content. The permeation coefficients changed independently of the static TRIS content. Trends between DMA content and permeation coefficients were less evident with the set 2 E hydrogels than with set 1 and this was the case against all the salts.

At an initial glance, it appears there is no trend between the permeation coefficients of the hydrogels against calcium chloride and NVP content, as shown in Figure 5.2. However, the trend derived shows sequential decreases and increases between the hydrogels as NVP content increased across the set, seen in Figure 5.2. The permeation coefficients between hydrogels E3-E7 remained between the ranges of $1.4 - 2.5 \times 10^{-9} \text{ cm}^2/\text{s}$.

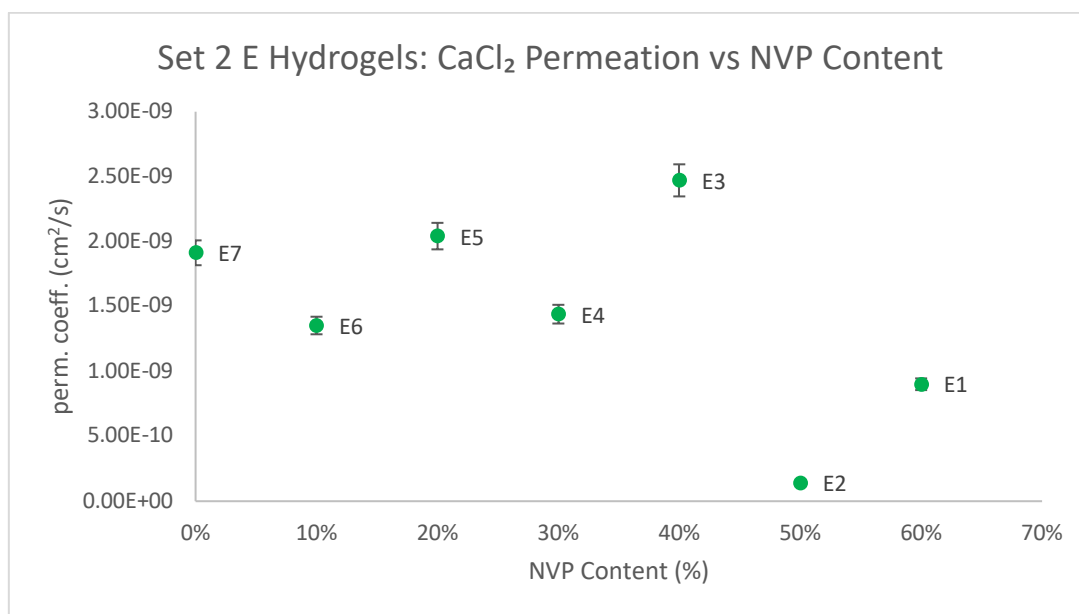


Figure 5.2 Set 2 E Hydrogels – CaCl₂ Permeation vs NVP Content

This type of trend was seen again with potassium chloride. There were sharp increases and decreases between all the E hydrogels as NVP content increased between 0-60%. With sodium chloride and magnesium chloride, there was a split in the trend with the hydrogels, the trend with sodium chloride shown in Figure 5.3. Both splits saw the permeation coefficients of the hydrogels decreasing as NVP content increased.

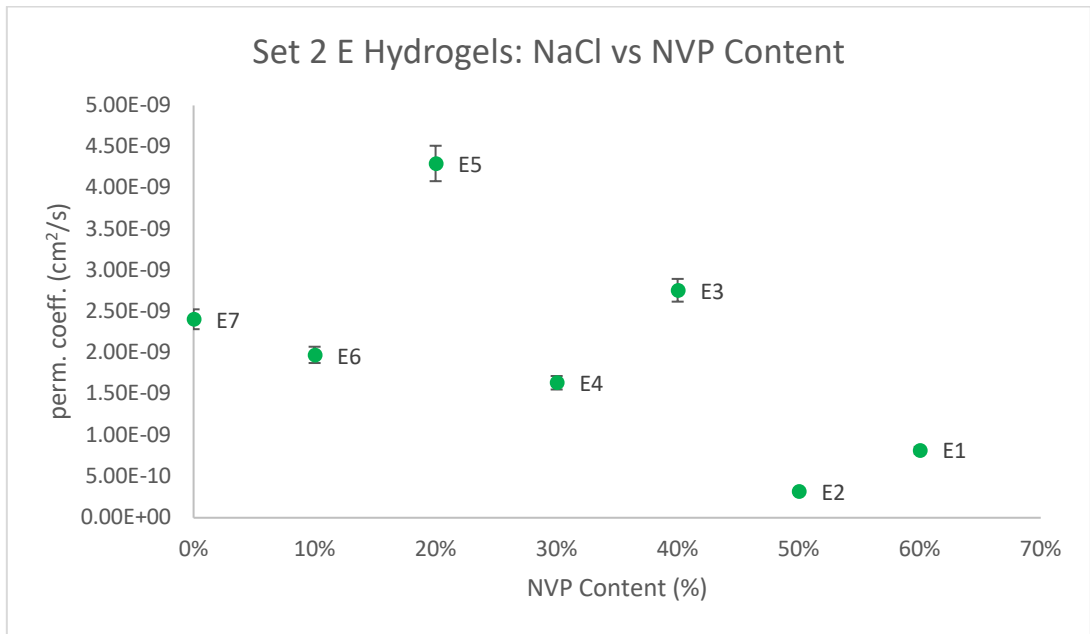


Figure 5.3 Set 2 E Hydrogels – NaCl Permeation vs NVP Content (%)

Set 3 E Hydrogels: when investigating the relationship between NVP content and the permeation coefficients of the set 3 E hydrogels, the most prominent trend was a decline in permeation as NVP content increased across the set. Apart from those against sodium chloride, the permeation coefficients of the different set 3 E hydrogels declined as the NVP content of the hydrogels increased. With the exception of hydrogels E6 and E3, the coefficients of these hydrogels remained relatively constant despite increases in NVP content.

A continuous exception from the trends seen against the different chloride salts for this particular set was hydrogel E3. This hydrogel produced the largest permeation coefficient of both the E & F hydrogels against calcium and magnesium chloride, the calcium chloride relationship shown in Figure 5.4.

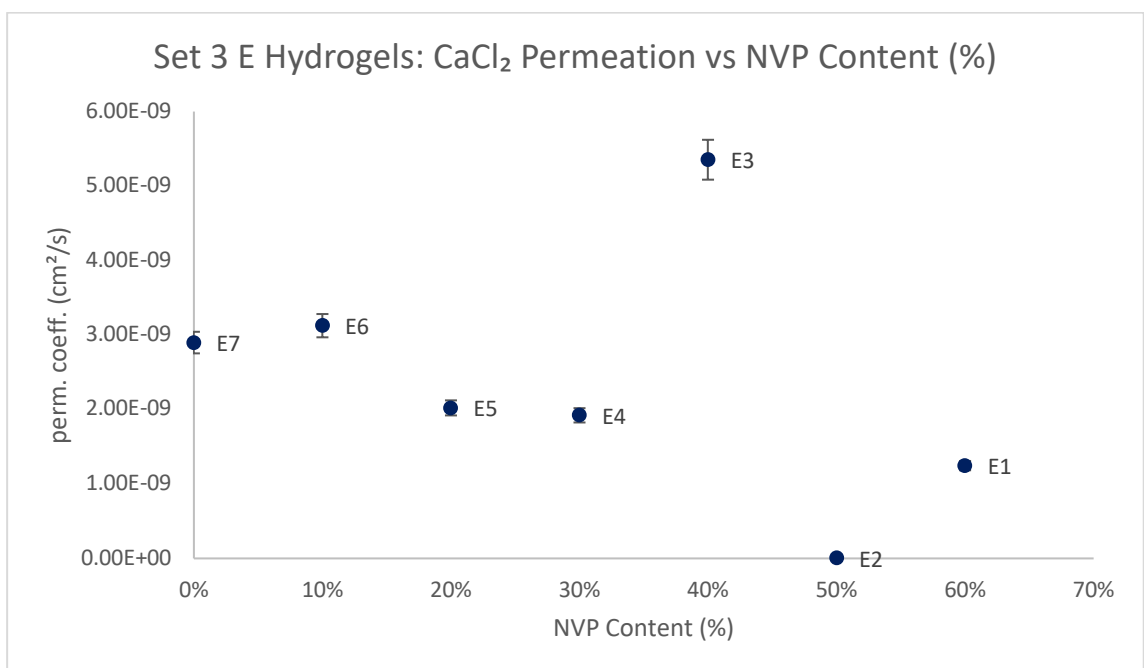


Figure 5.4 Set 3 E Hydrogels – CaCl₂ Permeation vs NVP Content (%)

Set 1-3 F Hydrogels: Unlike the E hydrogels, it is not possible to establish trends between the F hydrogels of the different sets due to the nature of their formulation. Referring to Table 5.14, which lists the formulation of the F hydrogels, the F hydrogels do not follow a descending/ascending order with NVP or DMA content. These hydrogels were synthesised with the aim of seeing how parameters such as permeation, partitioning and water content could be changed if larger amounts of TRIS, DMA and NVP were included in their formulation. The side-by-side comparisons for these hydrogels can be seen in appendix section 3.5.

Table 5.14 Formulations of the F hydrogels

Hydrogel	Formulations (wt. %)			
	DMA	NVP	TRIS	3-octanol
F1	-	25%	65%	5% (in set 3 only)
F2	-	65%	25%	
F3	65%	-		

Due to this, the permeation coefficients of the F hydrogels have been compared against the different versions of themselves from sets 1-3, to showcase the effects of the reaction conditions on their permeation coefficients against all the chloride salts.

Hydrogels F2 and F3 followed a specific order of changes in their permeation coefficients against all the chloride salts used in the permeation experiments. Hydrogel F2 followed the sequence of set 3 having the largest permeation coefficients followed by set 2 → set 1. Below is a Figure (5.5) of the permeation coefficients of the aforementioned hydrogel under the calcium chloride (CaCl_2) salt.

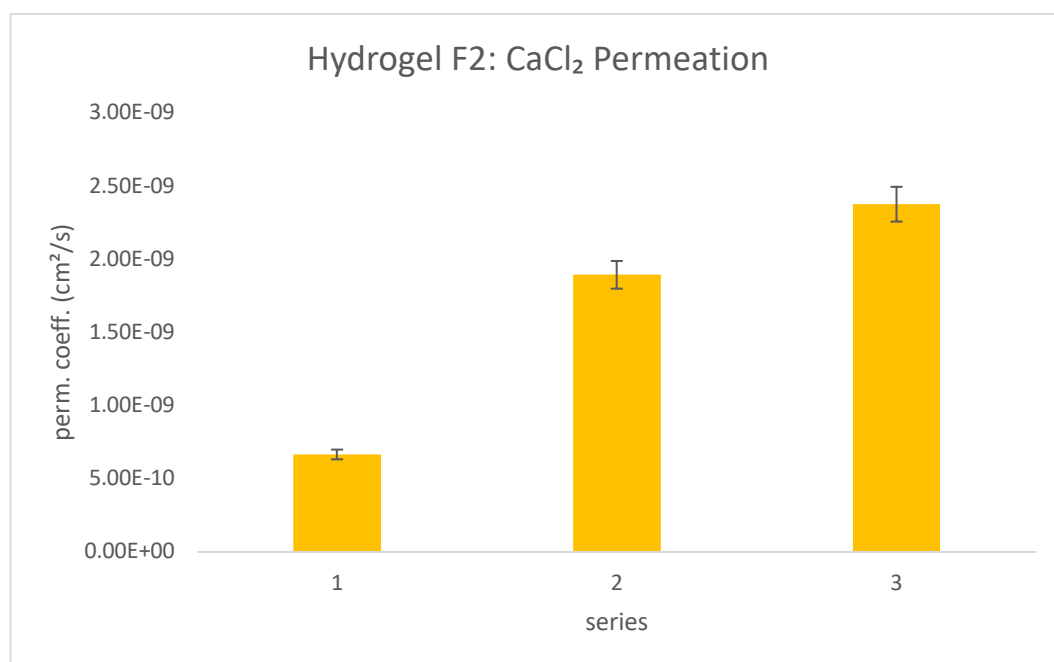


Figure 5.5 Hydrogel F2 Permeation Coefficients (set 1-3): CaCl_2

This was also the case with the potassium, sodium and magnesium chloride coefficients of these hydrogels. For calcium and sodium chloride, the set 1 F hydrogels produced coefficients to the order of $\times 10^{-10}$ whilst sets 2-3 were in the order of $\times 10^{-9}$. Calcium chloride brought about only the set 1 version of hydrogel F2 having a permeation coefficient of $\times 10^{-10}$ whilst magnesium chloride brought about the sets 1-2 versions of the hydrogel having coefficients to the power of $\times 10^{-10}$.

With hydrogel F3, its set 2 version was responsible for its largest permeation coefficients followed by set 3 \rightarrow set 1. This was the format seen for all of the permeation coefficients of the chloride salts. With the only exception of the set 1 coefficient produced against magnesium chloride, all of the permeation coefficients for hydrogel F3 from set 1-3 produced against the chloride salts remained in the order of $\times 10^{-9}$ cm²/s.

Hydrogel F1 did not follow a sequence with the increase/decrease in its permeation coefficients across sets 1-3 against the chloride salts with the exception of its coefficients against calcium and potassium chloride which both followed the order of set 1 \rightarrow set 3 \rightarrow set 2 whilst sodium chloride followed the sequence of set 2 \rightarrow set 1 \rightarrow set 3. The same hydrogel's permeation coefficient against magnesium chloride brought about set 3 having the largest coefficient followed by set 1 \rightarrow set 2. A commonality drawn between the behaviour of hydrogel F1 and the different chloride salts is that set 2 produced the lowest coefficients of the hydrogel (with the exception of sodium chloride whose lowest coefficient was with set 3).

5.3.2 Differences in permeation between chloride salts

In the previous sub-chapter (5.3.1), the permeation coefficients of the hydrogels from sets 1-3 have been discussed. The effects of formulation on their permeation behaviours across the different sets have also been discussed. However, it is important to understand how each hydrogel permeates the varying chloride salts and whether the same permeation patterns were maintained between sets/series.

It was initially thought that the monovalent salts – potassium and sodium chloride – would be permeated the most whilst the divalent salts – calcium and magnesium chloride – would be permeated the least due to the size of their ions. This concept has previously been discussed in the partition coefficient chapter (4.3), but the principle remains important in relation to permeation. When hydrated, the magnesium ion is the largest in comparison to the potassium, sodium, calcium and chlorine ions. The size of a hydrated magnesium ion is 0.43 nm whilst that of a calcium ion is 0.41 nm. The hydrated potassium ion is the smallest at 0.33 nm followed by the sodium ion at 0.36nm (Israelachvili, 2011). The degree of an ion's hydration is dependent on the strength of the electrostatic forces between the ion and the surrounding water molecules (Hribar et al, 2002). Based on this, the expected permeation pattern for the synthesised hydrogels, irrespective of set, was *potassium chloride* \rightarrow *sodium chloride* \rightarrow *calcium chloride* \rightarrow *magnesium chloride*.

Permeation profiles were drawn up for all the E & F hydrogels from sets 1-3 to showcase their permeation behaviours towards the different chloride salts. The majority of the hydrogels across the sets

followed the permeation order of *potassium chloride* → *calcium chloride* → *sodium chloride* → *magnesium chloride*. These profiles can be found in the appendix section 3.4.

Set 1: It should be noted that all of the E & F hydrogels in set 1 permeated potassium chloride the most and magnesium chloride the least and followed the most commonly seen trend that was highlighted above. In the case of hydrogel E6 of set 1, potassium chloride was permeated at a higher rate than the remainder of the salts, although the aforementioned permeation pattern was maintained. The permeation coefficient of this hydrogel for potassium chloride was $2.59 \times 10^{-9} \text{ cm}^2/\text{s}$ whilst the remainder of the salts had coefficients to the power of $\times 10^{-10}$.

However, hydrogels E2, E5 and E7 of set 1, followed the permeation order of *potassium chloride* → *sodium chloride* → *calcium chloride* → *magnesium chloride*, the originally hypothesised permeation order. The permeation profile for hydrogel E5 can be found below in Figure 5.6. Similarly to hydrogel E6, this hydrogel permeated potassium chloride at a higher rate than the remaining salts and it was reflected in its permeation coefficients. Its coefficient for potassium chloride is $2.35 \times 10^{-9} \text{ cm}^2/\text{s}$ whilst the remaining salts were in the power of $\times 10^{-10}$.

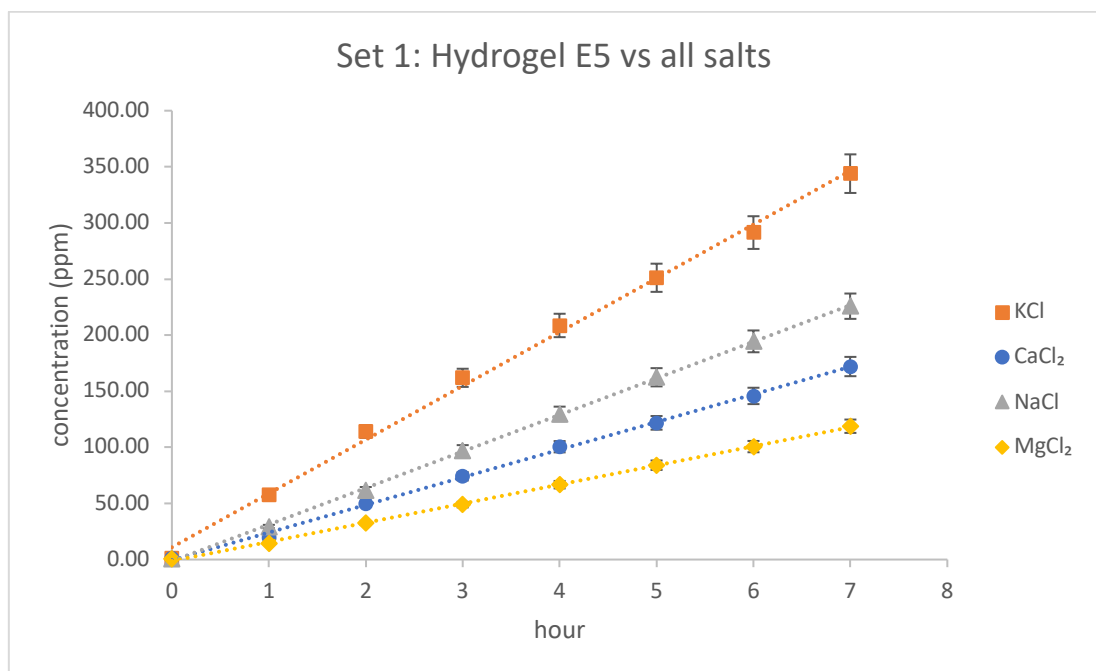


Figure 5.6 Permeation profile of hydrogel E5 – set 1

Set 2: With the set 2 hydrogels, hydrogels E1-E4 and all of the F hydrogels permeated potassium chloride the most. Within this, hydrogels F1 and E4 permeated sodium chloride the least, following the permeation order of *potassium chloride* → *calcium chloride* → *magnesium chloride* → *sodium chloride*. The permeation profile of hydrogel E4 is shown in Figure 5.7.

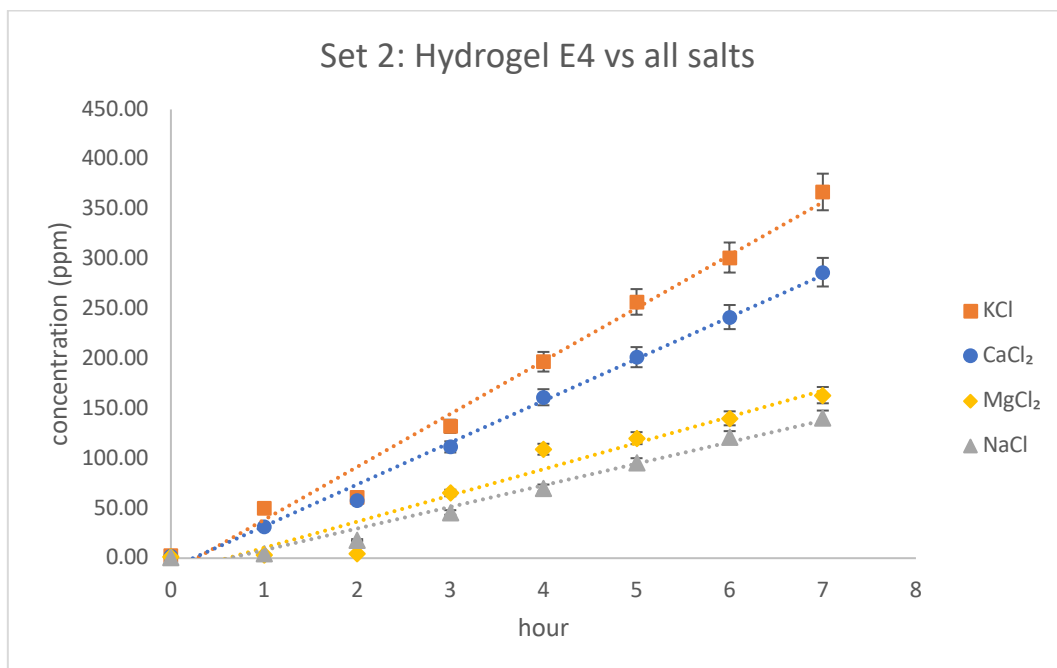


Figure 5.7 Permeation profile of hydrogel E4 – set 2

With hydrogels E5-E7 of set 2, calcium chloride was also permeated the highest, however, the permeation order of these particular hydrogels was *calcium chloride* → *potassium chloride* → *sodium chloride* → *magnesium chloride*. The permeation profile for hydrogel E7 of set 2 can be found in Figure 5.8. The end concentration for the salts were very similar and formed pair-like trends. Calcium and potassium chloride formed a pair, with end concentrations of 257.6ppm and 239.5ppm respectively, whilst the pairing between sodium and magnesium chloride had end concentrations of 156ppm and 150.11ppm respectively.

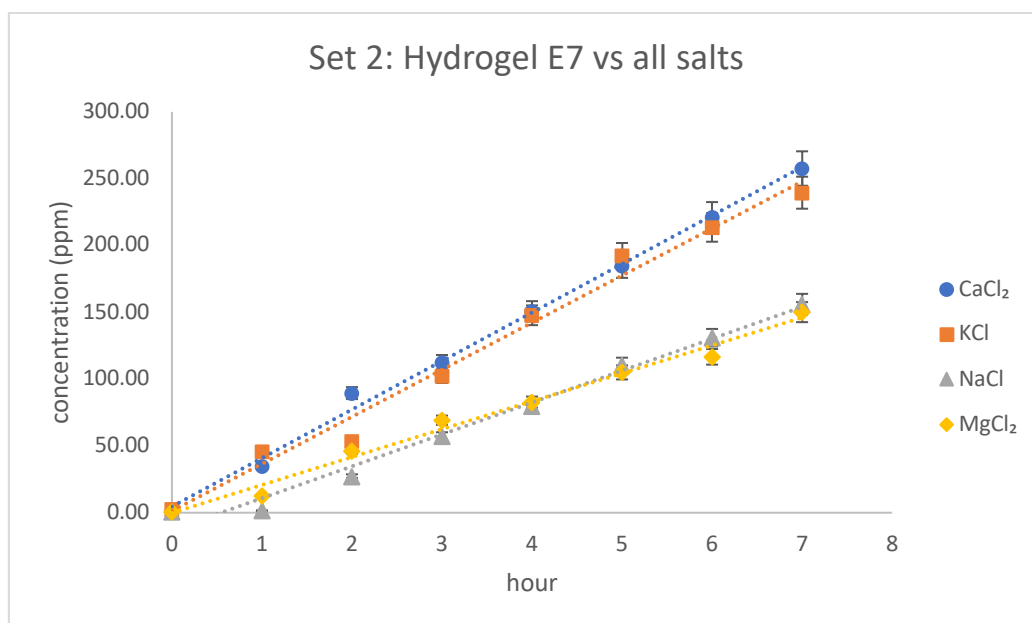


Figure 5.8 Permeation profile of hydrogel E7 – set 2

Set 3: The set 3 E & F hydrogels saw potassium chloride being the most permeated salt with the only exception to this being hydrogel E3. This hydrogel followed the permeation sequence of *calcium chloride*

→ *magnesium chloride* → *sodium chloride* → *potassium chloride*. This was the only instance in which the divalent ions which are also the larger ions, were permeated more than the smaller ions. The permeation profile of this hydrogel can be found below in Figure 5.9.

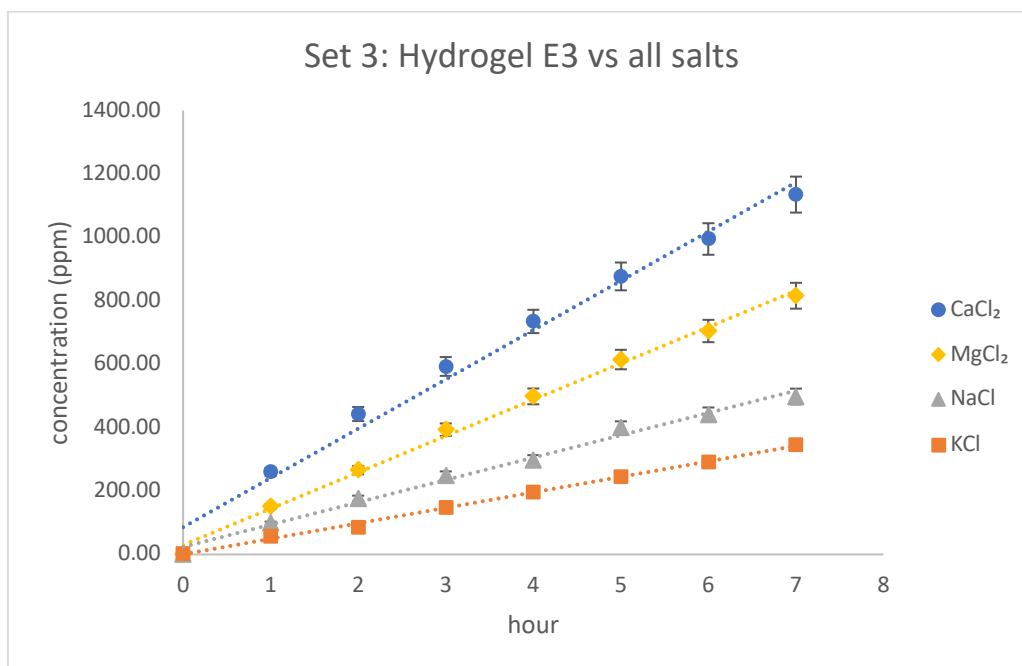


Figure 5.9 Permeation profile of hydrogel E3 – set 3

Also from set 3, hydrogels E1, E2 and F1 permeated sodium chloride the least and these particular hydrogels followed the permeation sequence of *potassium chloride* → *calcium chloride* → *magnesium chloride* → *sodium chloride*. The permeation profile for hydrogel E1 can be found below in Figure 5.10.

This data set demonstrated that the size of the salt ions may not be entirely influential in determining permeation rates as the smallest ions were permeated both the most and the least with these particular hydrogels of this particular set.

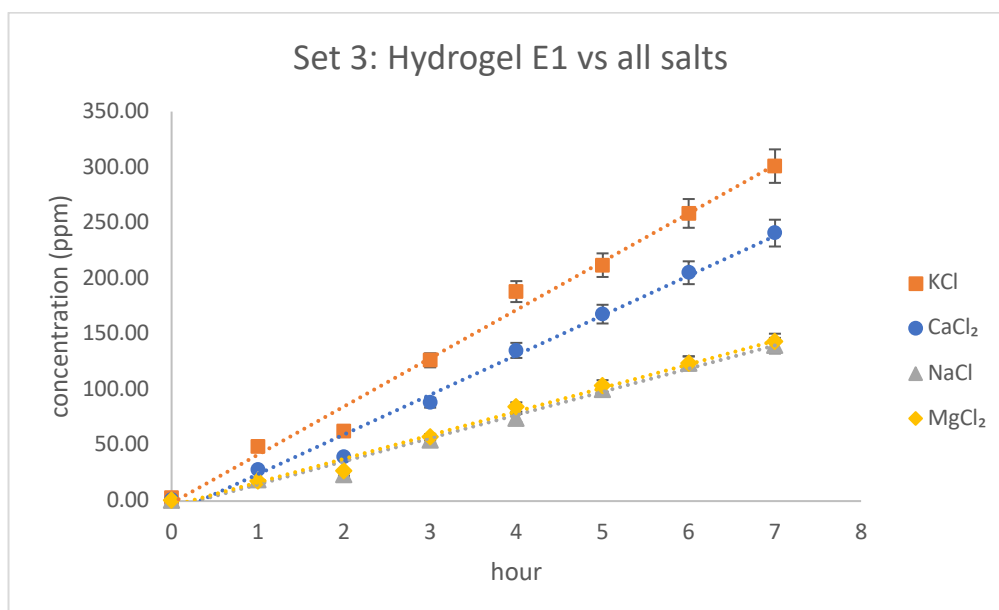


Figure 5.10 Permeation profile of hydrogel E1 – set 3

All the versions of hydrogel F1, from sets 1-3, were the least permeable hydrogel of them all. Its permeation profile from set 2 can be found in Figure 5.11 below. This hydrogel maintained a low permeation rate across all salts and continuously permeated potassium chloride the most.

In set 2 and 3, this hydrogel permeated sodium chloride the least but in set 1, it permeated magnesium chloride the least. Hydrogel F1 in set 1 was the only occurrence for this particular hydrogel in which its permeation pattern saw potassium chloride being permeated the most and magnesium chloride the least.

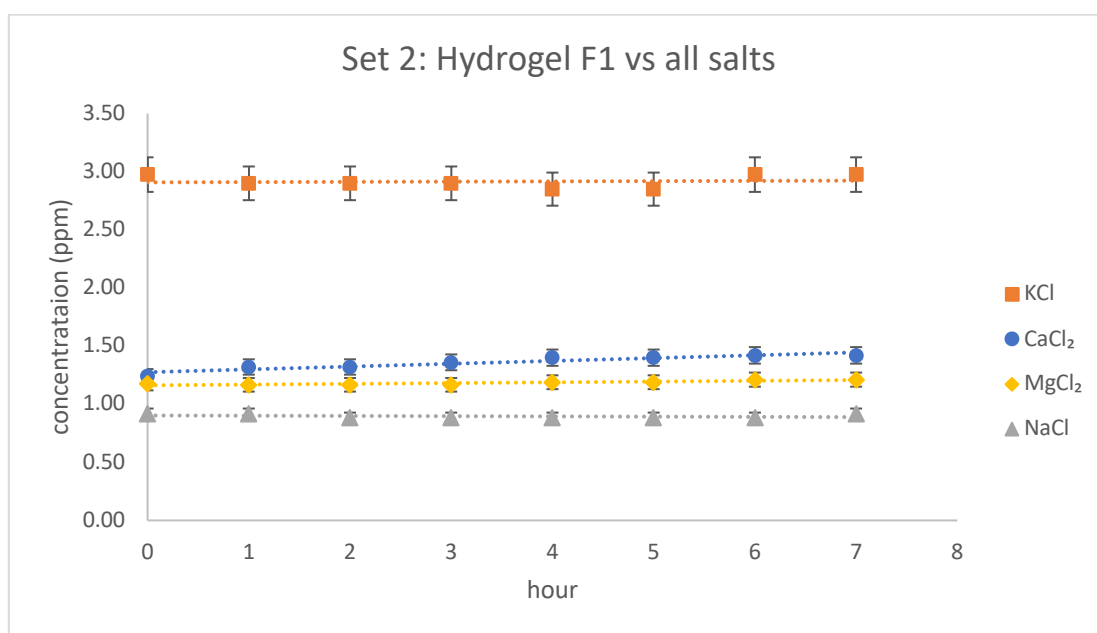


Figure 5.11 Permeation profile of hydrogel F1 – set 2

Hydrogel F1 had the lowest permeation coefficients across sets 1-3 but its lowest coefficients were produced in set 2. The coefficients of this hydrogel in set 1 ranged between 4.04×10^{-12} – 1.39×10^{-12} cm^2/s but declined to ranges of 6.41×10^{-12} – 8.67×10^{-14} cm^2/s in set 2 then to 3.09×10^{-12} – 7.61×10^{-13} cm^2/s in set 3.

Hydrogel F1 possessed the largest amount of the TRIS monomer compared to all of the hydrogels synthesised in the project. However, hydrogel E1 had the same DMA/NVP monomer ratio as hydrogel F1 – 0% DMA and 60% NVP – yet hydrogel E1 did not display the same permeation patterns towards the different chloride salts. However, the low permeation exhibited by hydrogel F1 could be attributed to its TRIS monomer levels, a monomer that is hydrophobic in nature.

No other hydrogel behaved in a similar nature to hydrogel F1 except hydrogel E2 of set 3 and noticeably, its permeation declined between the different set. From set 1, hydrogel E2 produced permeation coefficients that ranged between 6.96×10^{-10} – 4.33×10^{-10} cm^2/s . The permeation profile of hydrogel E2 (set 1) is shown in Figure 5.12. The permeation order for hydrogel E2 in set 1 was *potassium chloride* → *sodium chloride* → *calcium chloride* → *magnesium chloride*.

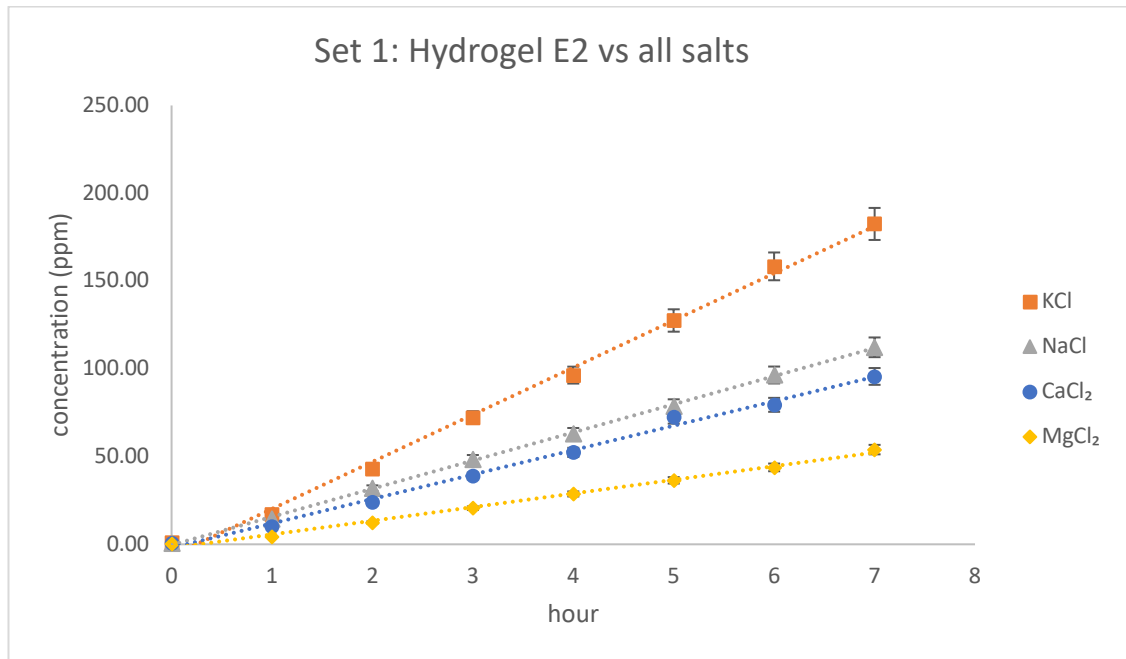


Figure 5.12 Permeation profile of hydrogel E2 – set 1

In the set 2 version of the hydrogel, permeation coefficients ranged between 4.4×10^{-10} – 6.73×10^{-11} cm^2/s , decreasing slightly in comparison to set 1. The permeation order shown in its set 1 version was maintained although potassium chloride permeated at a higher rate than the remaining chloride salts, however, the hydrogel demonstrated an evident lag time in the first 2 hours of the experiment, which can be seen in the permeation profile in Figure 5.1.

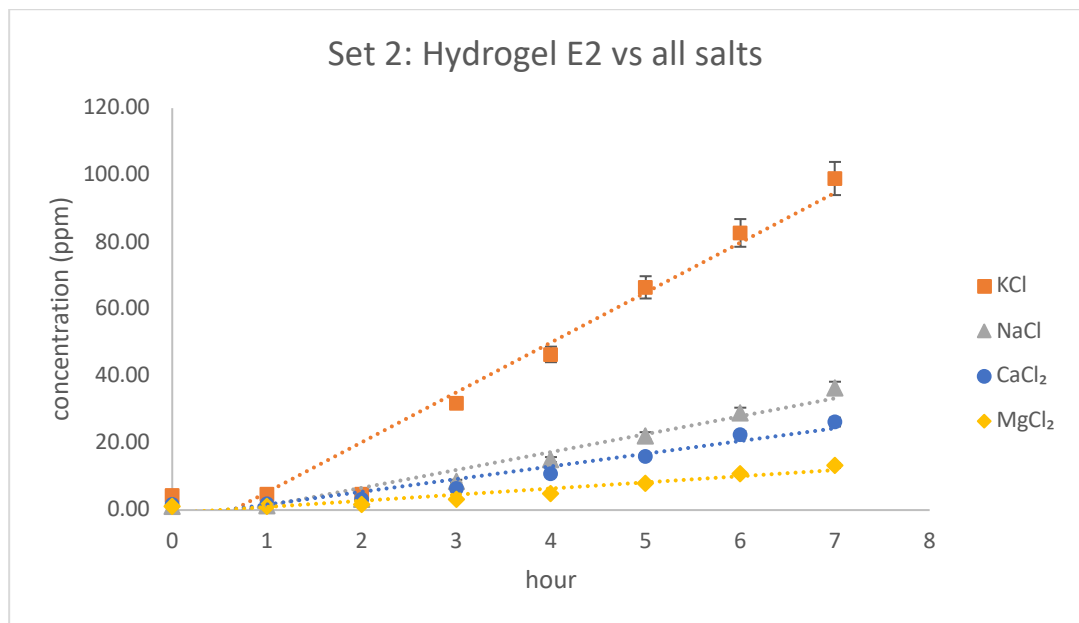


Figure 5.13 Permeation profile of hydrogel E2 – set 2

With its set 3 version, the permeation coefficients ranged between 3.69×10^{-12} – 1.24×10^{-12} cm^2/s , the lowest out of them all. The permeation profile for this hydrogel can be seen below in Figure 5.14. Here, the permeation order changed to *potassium chloride* → *calcium chloride* → *magnesium chloride* → *sodium chloride*.

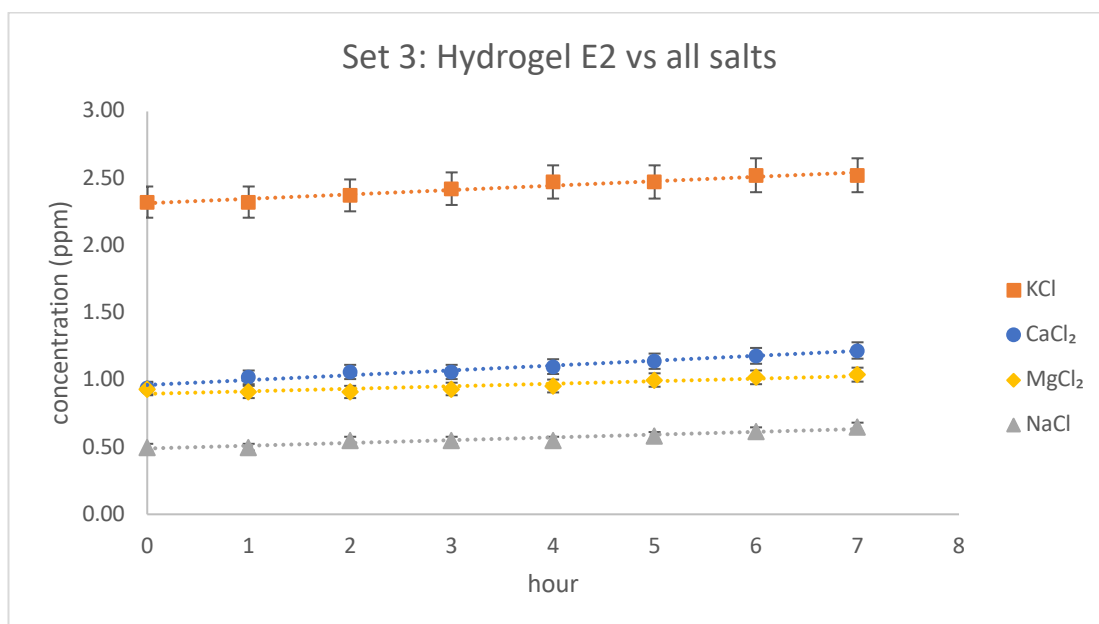


Figure 5.14 Permeation profile of hydrogel E2 – set 3

Between sets 1 and 2, the permeation order for hydrogel E2 was *potassium chloride* → *sodium chloride* → *calcium chloride* → *magnesium chloride*. In set 3, sodium chloride was permeated the least. The reaction conditions of the different set can be found in Table 5.15. The key difference between sets 1 and 2 was the use of a diluent and post-cure.

Table 5.15 Reaction conditions of set 1, 2 & 3

Set Name	Post-cure @ 90°C	Diluent included
Set 1	No	Yes (E hydrogels only)
Set 2	Yes	No
Set 3	Yes	Yes

The change in the permeation behaviour of hydrogel E2, in addition to its formulation (10% DMA, 50% NVP & 35 % TRIS), suggests the use of a diluent in addition to a post-cure is capable of reducing the permeation of a hydrogel more so than either of these conditions being used on an individual basis, as was done between sets 1 and 2.

5.3.3 The relationship between water content & permeation

The movement of solutes across a hydrogel membrane can occur via two known mechanisms: bulk flow or diffusion (Gavara & Compañ, 2017). Bulk flow includes the movement of the solute through the hydrogel when there is a difference in the hydrostatic pressure across the hydrogel membrane. Hydrostatic pressure is the force per unit area exerted by a liquid at equilibrium on an object

([EDinformatics](#), 1999) and it is caused by the force of gravity. Diffusion includes the movement of a solute across a membrane but it is facilitated and dependent on the solubility of the solute within the hydrogel and how well it diffuses within the membrane, which is illustrated by the diffusion coefficient. Diffusion is controlled by thermodynamic activity which in turn, depends on there being a difference in water content on either side of the membrane (Gavara & Compañ, 2017).

According to the majority of previously cited literature, permeability of silicone-based hydrogels should increase as the water content of the hydrogels increases. The ion size and interactions between salt ions and the polymer matrix can influence water structure, which will also lead to effects on salt permeability (Hamilton et al, 1987). Sodium chloride diffusion increased monotonically with membrane water content in agreement with free-volume theory (Yasuda et al, 1968). Willis et al found that hydrogels with a EWC below 15% have a low to zero permeation rate, suggesting a lack of phase connectivity of water in the hydrogel (Guan et al, 2011). Another rule suggests that with an increase in EWC, there should be an increase in solute partitioning caused by an increased presence of larger hydrophilic domains within the hydrogel (Fujiyabu et al, 2019). However, the synthesised hydrogels are considered to be self-assembled hydrogels which refer to the spontaneous association and organisation of numerous individual units into rational and well-defined structures without external participation (Kopeček & Yang, 2012). The behaviour of these hydrogels may be different when compared to those discussed in literature as the basis of the synthesis differs. The effect of reaction conditions also have to be taken into account.

The links between the different water types such as equilibrium water content (EWC), freezing & non-freezing water content (FWC & NFWC) as well as polymer-associated (PAWC) and ice-like water content (ILWC) and the permeation coefficients of the different E & F hydrogels from sets 1-3 were investigated.

5.3.3.1 Equilibrium Water Content

Set 1 E Hydrogels: when investigating the link between the permeation coefficients of the set 1 E hydrogels and their EWC, it was not possible to determine a relationship between the two parameters for all of the hydrogels as trends did not emerge. However, with the permeation coefficients of calcium, magnesium and potassium chloride, certain sets of hydrogels participated in linear changes in their permeation coefficients as EWC increased.

With calcium and magnesium chloride, hydrogels E5, E6 and E7 were the only hydrogels that demonstrated a consecutive decrease in their permeation coefficients as their EWC changed from 63%, 65% and 60% respectively. This can be seen in Figure 5.15 below. Hydrogels E3, E5 and E6 saw their permeation coefficients against potassium chloride increase as EWC increased from 60%, 63% and 65% respectively.

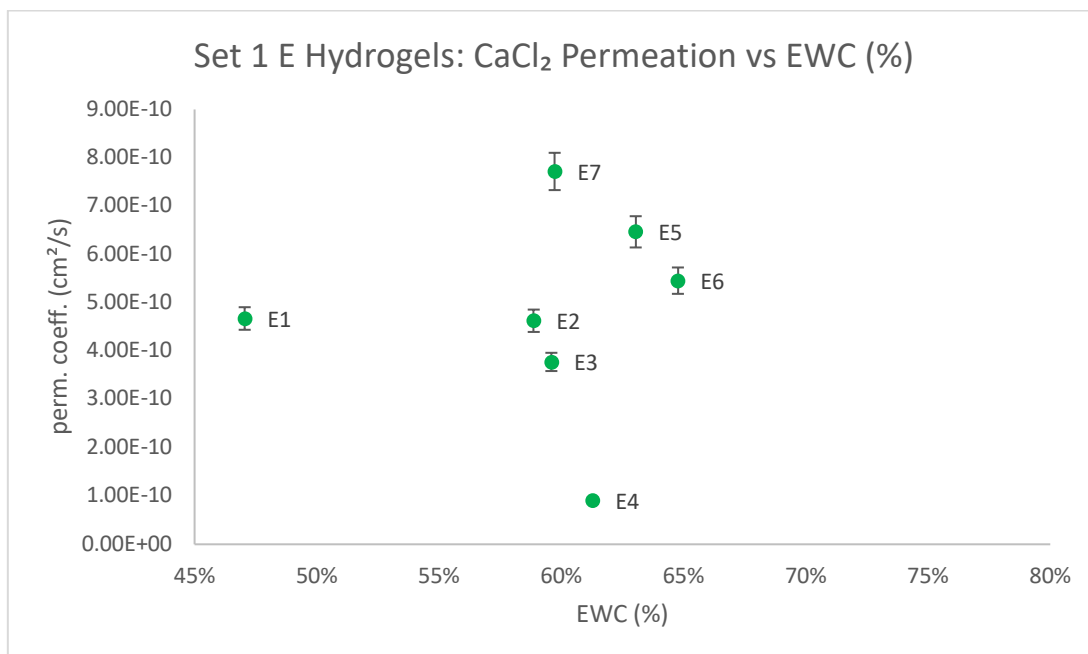


Figure 5.15 Set 1 E hydrogels – CaCl₂ Permeation vs EWC (%)

This analysis showed that even though the effects were not widespread, increases in permeation coefficient as EWC increased was seen specifically with the monovalent salt – potassium chloride. Decreases in permeation coefficient occurred only with the divalent salts – calcium and magnesium chloride. This was unique to the set 1 E hydrogels.

Set 1 F Hydrogels: it is possible to denote trends between the F hydrogels and their equilibrium water contents in their respective sets. In this set, the EWC of the hydrogels increased consecutively from F1-F3 and for the permeation coefficients against all the chloride salts, there was an increase in the permeation coefficients in that order as well. For calcium chloride, the coefficients of the F series hydrogels increased as their EWCs increased from 26%, 62% to 88%.

This was the exact format seen when investigating the link between the permeation coefficients of the different salts and so the remaining figures can be found in appendix 3.4. Unlike the E hydrogels, increases in equilibrium water content in the F hydrogels resulted in increases with their permeation coefficients and the increases occurred regardless of the size of the salt ion or their charge.

Set 2 E Hydrogels: Generally, the EWC of these hydrogels were slightly lower than those of set 1, ranging between 52-61% and the average EWC of the set being 57% whilst that of set 1 was 62% (excluding hydrogel E1 with an EWC of 47%). Trends seen with the set 2 E hydrogels were more definitive than those from the set 1 E hydrogels. Hydrogels E1 and E3 were constant outliers from any trend demonstrated but hydrogel E2 was consistently the lowest performing hydrogel against all the salts.

Against calcium, potassium and magnesium chloride, there was a general decrease in the permeation coefficient of the hydrogels as their EWC increased across the set. The order of the permeation decrease was also not in a consecutive order but in this set again, the EWC of the hydrogels did not

increase in the consecutive order of the hydrogels. However, the decrease in permeation coefficient against calcium chloride occurred as the EWC of the hydrogels increased between 55-61%.

The permeation coefficients of sodium chloride demonstrated a decrease as the EWC of the hydrogels increased, shown in Figure 5.16.

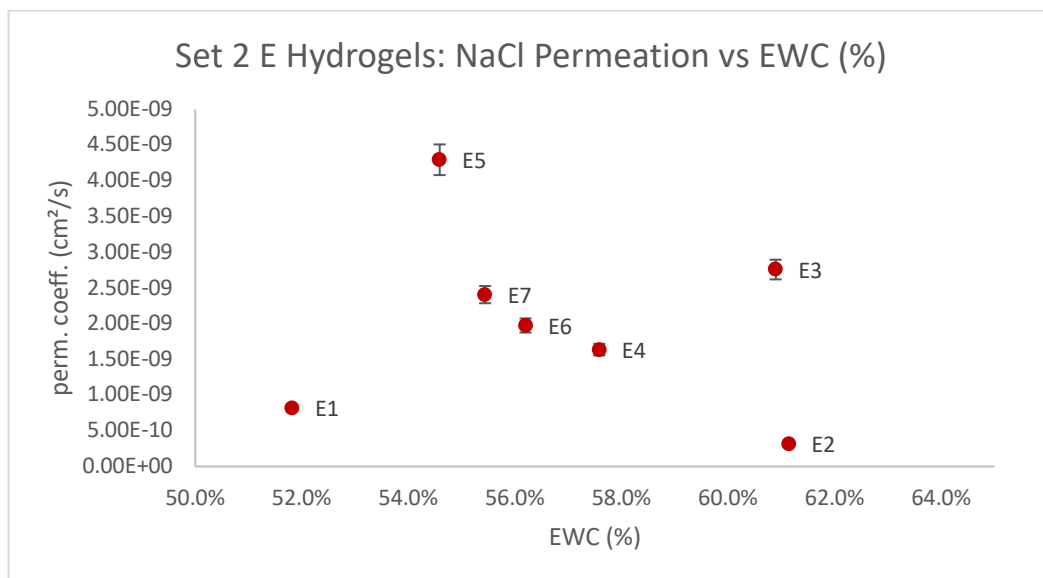


Figure 5.16 Set 2 E hydrogels – NaCl Permeation vs EWC (%)

Set 2 F Hydrogels: the EWC of most of the F hydrogels of this set were also lower in comparison to the set 1 F hydrogels, with hydrogel F2 being at 55% and F3 being 70%. However, regardless of the changes in EWC between set 1 and 2, the F hydrogels maintained the pattern of an increase in their permeation coefficients as EWC increased across the sets. This was the case between all the chloride salts.

Set 3 E Hydrogels: the EWC of the E hydrogels of this set ranged between 52-65%, closer to those of the set 1 E hydrogels than of set 2. Generally, the permeation coefficients of the hydrogels declined as their EWC increased across the set, with the exception of sodium chloride which did not demonstrate a clear trend. However, there was a recurring occurrence between hydrogels E1, E2 and E3 in which they deviated from the declining trendline with the rest of the hydrogels. These hydrogels would showcase an increase in their permeation coefficients in the order of E2 → E1 → E3 and this occurred with all the chloride salts. The relationship between the magnesium chloride permeation coefficients and EWC is shown in Figure 5.17.

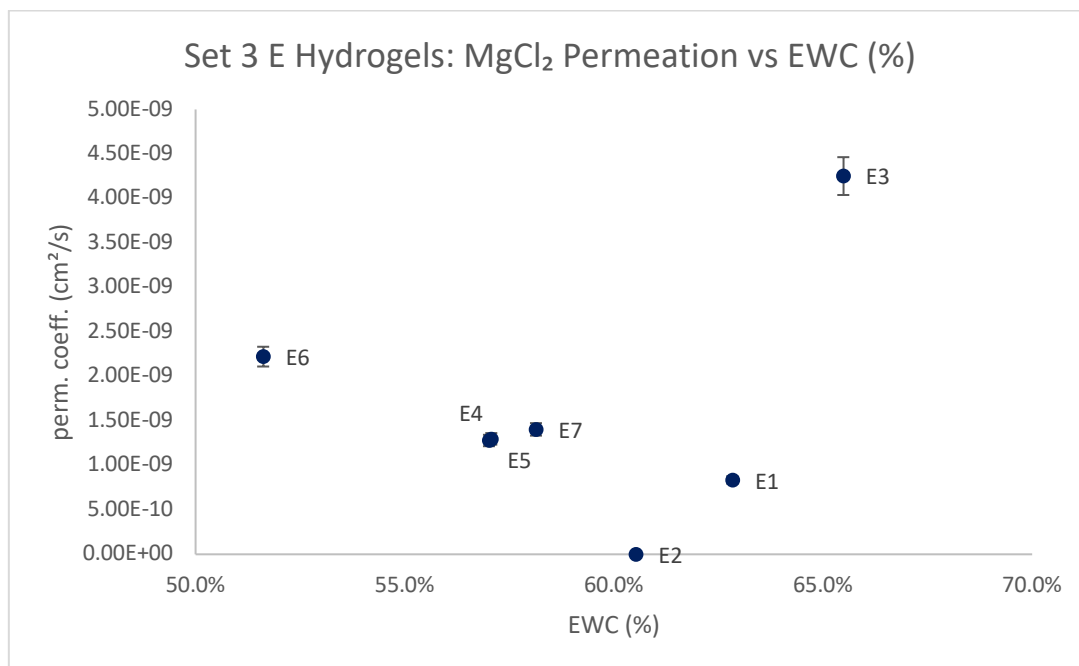


Figure 5.17 Set 1 E hydrogels – MgCl₂ Permeation vs EWC (%)

Set 3 F Hydrogels: hydrogels F1 and F2 of set 3 had the highest EWCs out of their previous versions in set 1 and 2. Hydrogel F1 reached an EWC of 32% and hydrogel F2 reached an EWC of 77%. Hydrogel F3 experienced a decrease in its EWC in this set, dropping to 66%. Despite these changes, there was not a clear relationship between the EWC of these hydrogels and their permeation coefficients against the different chloride salts. However, despite hydrogel F3 having the lowest EWC of the set, it was responsible for the largest permeation coefficients of the F hydrogels and this was seen with all the salts.

5.3.3.2 Freezing Water Content

Freezing water is a water type present in hydrogels that is determined experimentally using DSC, as described in the methodology chapter (2.8), and also spoken about extensively in the water content chapter (3.3). It has been established that this water is considered to be an advantage to the permeation of solutes across the hydrogel membrane as this water has an increased degree of mobility to the other water types present (Bag & Valenzuela, 2017) so increased amounts of this water within a hydrogel should be accompanied by an increase in permeation.

The relationship between freezing water and the permeation coefficients of the different hydrogels against the various chloride salts have been established.

Set 1 E Hydrogels: the freezing water content of the set 1 E hydrogels ranged between 37-44% and the increase in this water type did not occur consecutively from hydrogel E1-E7, as has been the case with the other water types previously discussed. Regardless of that, trends seen with the hydrogels were not widespread across the set or in most cases, did not occur, suggesting freezing water was not that influential in the determination of the permeation rates of these particular hydrogels. Repeatedly, hydrogel E4 had the lowest permeation coefficient despite its FWC being in the median of the set but

this may be due to its lack of experimental repeats as previously mentioned when discussing other relationships in this chapter.

The permeation coefficients of calcium, sodium and magnesium chloride did not demonstrate a clear pattern of change as their FWC increased across the set. However, with those of potassium chloride, there was a clear trend of a decline as the FWC of the hydrogels increased across the set. However, the trend appeared to split between the hydrogels although both demonstrated a decline.

Hydrogels E2, E1 and E4 showed a slight downward trend as their FWC content increased between 37-39%. The second trend which included hydrogels E7, E6, E5 and E3 showed a decreasing trend as the FWC of these hydrogels increased between 39-44%. The state of the two trends differed, with the first trend between hydrogels E2, E1 and E4 being more linear.

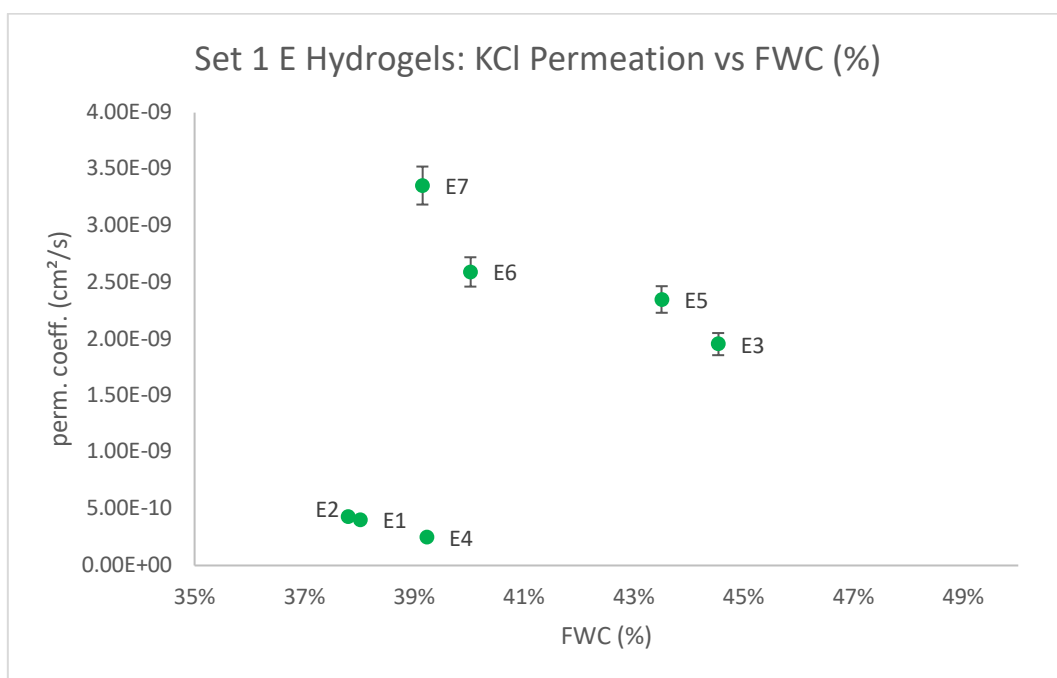


Figure 5.18 Set 1 E hydrogels – KCl Permeation vs FWC (%)

Set 1 F Hydrogels: unlike the trends seen with EWC – which saw a consecutive increase in the permeation coefficients of the hydrogels increased as their EWC also increased consecutively – trends with the FWC of these hydrogels did not follow suit. For all the chloride salts, despite having the largest freezing water content of the set at 43%, hydrogel F2 did not come atop any trendline between the three hydrogels. Hydrogel F3 consistently had the largest permeation coefficient against all the salts despite its FWC being slightly lower at 36% whilst hydrogel F1 had the smallest coefficients against all the salts with the lowest FWC of the set at 13%.

Set 2 E Hydrogels: again, the FWC of these hydrogels was lower than set 1, ranging between 19-34%. Trends between the permeation coefficients of the different chloride salts were much more evident with this set, with a majority of the hydrogels participating in them. With this set, hydrogel E2 had the smallest permeation coefficient against all the chloride salts and this hydrogel also had the lowest FWC of the set at 19%. Hydrogel E3 and E5 were amongst the peaks of each trend seen with the different salts but the FWC of these hydrogels were not the highest of the set at 28% and 21% respectively.

With calcium and potassium chloride, the permeation coefficients of the hydrogels generally increased as their FWC increased. In the case of both salts, the increase did not occur in a linear line and splits occurred between the hydrogels, but the general direction of the trend was upward. The permeation coefficients of the hydrogels against sodium chloride demonstrated a decrease as the FWC of the hydrogels increased across the set. Those of magnesium chloride demonstrated both an increase and decrease as the FWC of the hydrogels increased, shown in Figure 5.19. The downward trend occurred between hydrogels E5, E3 and E7, with their coefficients decreasing as their FWC increased between 22%, 28% and 32%. The intersection of the two trends occurred at hydrogel E4 and the upward trend included hydrogels E2, E1 and E6, showing an increase in their permeation coefficients as their FWC increased between 19%, 28% and 31%.

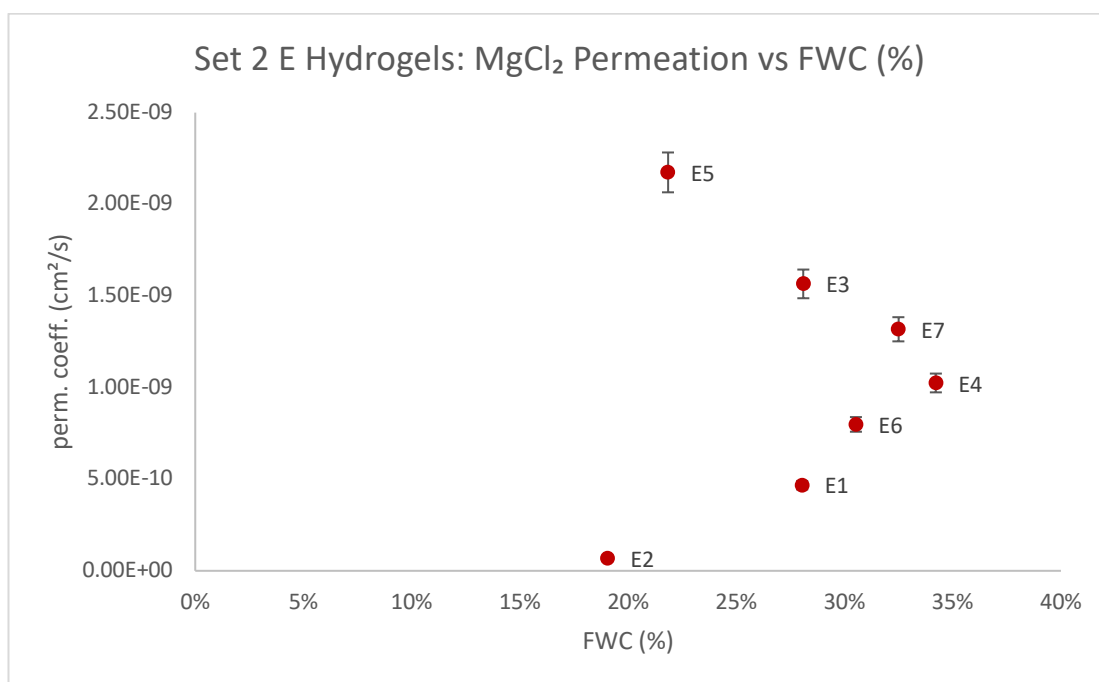


Figure 5.19 Set 2 E hydrogels – MgCl₂ Permeation vs FWC (%)

Set 2 F Hydrogels: unlike the set 1 F hydrogels, the FWC of these hydrogels increased consecutively in the set, with hydrogel F1 having the lowest FWC at 12.6%, a decrease from its set 1 version, hydrogel F2 with a FWC of 38.2% which also decreased from set 1, then hydrogel F3 with a FWC of 46.5%, the only hydrogel of the set that exhibited an increase in its FWC between set 1 and 2. When determining the link between the permeation coefficients of these hydrogels and their freezing water contents, there was a consecutive increase in the coefficients of the F hydrogels as their FWC increased across the set.

Set 3 E Hydrogels: the FWC of these hydrogels demonstrated an increase when compared to those of set 2, ranging between 19-44%. All of the permeation coefficients of the different chloride salts showcased a trend, unlike those from the previous sets but the trend seen was a decrease. As the FWC of the hydrogels increased, also not in a consecutive order across the set, the permeation coefficients of the E hydrogels decreased steadily. A constant outlier from the trends seen was hydrogel E2, which as previously stated, demonstrated low levels of permeation towards all the salts unlike its versions in G.Durowoju, PhD Thesis, Aston University 2022.

the previous set. Another recurring outlier, in the case of the divalent salts, was hydrogel E3 which demonstrated high levels of permeation towards these particular salts. The relationship between the permeation coefficients against potassium chloride and FWC of the set 3 E hydrogels is shown in Figure 5.20.

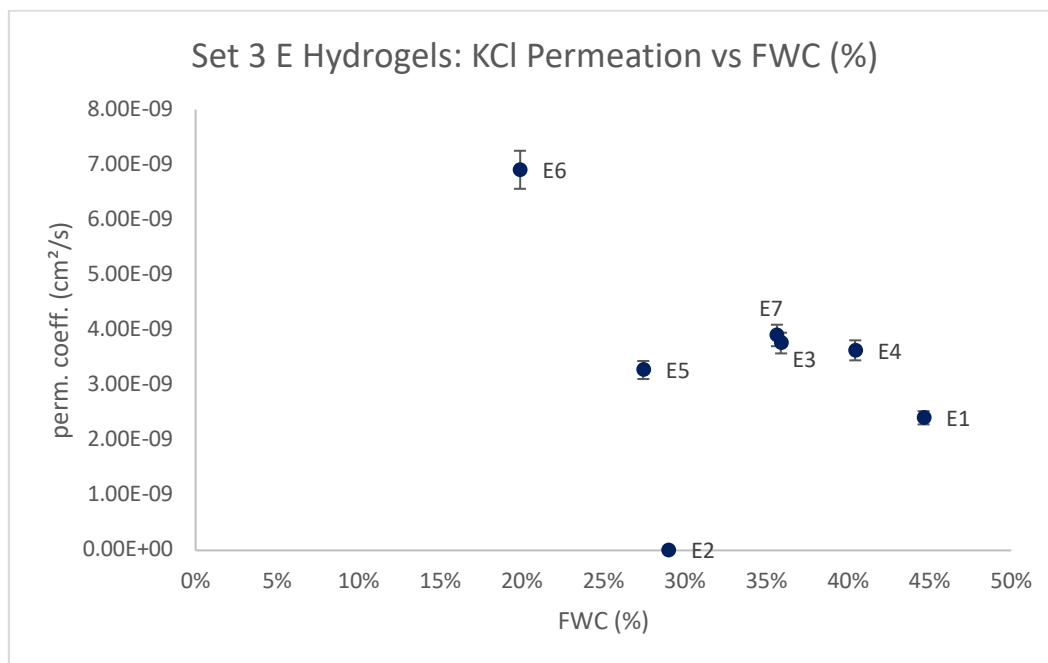


Figure 5.20 Set 3 E hydrogels – KCl Permeation vs FWC (%)

Set 3 F Hydrogels: the FWC of hydrogels F1 and F2 reached their highest in set 3, increasing to 13% and 57% respectively whilst that of hydrogel F3 decreased to 37%. Despite this decrease, hydrogel F3 was responsible for the largest permeation coefficients against all the chloride salts so the permeation of the F hydrogels did not increase as their FWC increased, suggesting there is no relationship between these two parameters.

The difference in relationships between the sets 1/3 and 2 E & F hydrogels suggests the reaction conditions of the different sets have the ability to alter the influence of water types on their permeation behaviour. The set 1 and 3 E hydrogels were synthesised with a diluent whereas those from set 2 did not make use of a diluent in its formulation. Polymer networks that made use of a diluent in their formulation have been seen, via electron microscopy, to have “agglomerates” of various sizes i.e., masses of different shapes and sizes making up the polymer whereas polymers synthesised without it have a continuous polymer phase (Okay, 2000). The lack of trend between the permeation of the set 1 E hydrogels and FWC as well as the decline in permeation of the set 3 E hydrogels could suggest the agglomeration of the hydrogel would depend less on freezing water to facilitate permeation across the hydrogel unlike the set 2 hydrogels whose continuous polymer phase would be dependent/conductive to water being the main source of mobility.

5.3.3.3 Non-Freezing Water Content

Non-freezing water is considered to be a hindrance to permeation as it has the lowest degree of mobility of any of the water types present within a hydrogel (Bag & Valenzuela, 2017) as it is tightly bound to the polymer chain (Ostrowska-Czubenko et al, 2011) unlike freezing water which is known to behave like bulk water. It is thought that there should be a negative relationship between the permeation coefficients of the hydrogels and their non-freezing water contents (NFWC) i.e. as NFWC increases, the permeation coefficient of the hydrogels would decrease.

Set 1 E Hydrogels: as was the case with the other water types discussed previously in this chapter, the non-freezing water content of the hydrogels did not change consecutively down the set. The NFWC ranges of these hydrogels were between 4-26%. However, across the different chloride salts, little to no relationships were formed between the permeation coefficients and their NFWCs. There were no evident trends denoted and this was the case across all the salts. As the remainder of the chloride salts did not showcase a trend, their figures can be found in appendix 3.3.3. Notably, hydrogel E1 had the lowest NFWC of the set at 4% and was amongst the hydrogels with the lowest permeation coefficients of the hydrogels.

Set 1 F Hydrogels: unlike the E hydrogels, the non-freezing water contents of the F hydrogels from set 1 increased consecutively down the set, with hydrogel F1 having the least amount of this particular water type at 13% and hydrogel F3 having the most NFWC at 31%. When the permeation coefficients and their non-freezing water contents were investigated to determine a link, it was shown that the coefficients of these hydrogels increased in a linear manner as their NFWC also increased. This was the case across all the chloride salts.

Set 2 E Hydrogels: The non-freezing water contents of the set 2 E hydrogels were considerably larger than those from set 1, ranging between 18-42% across the set. From calcium to magnesium chloride, trends did emerge between the permeation coefficients of the hydrogels and their non-freezing water contents. For all of the salts, there were general increases in the permeation coefficients of the hydrogels as their NFWC increased. The constant between each of these salts was that hydrogel E2, with the largest NFWC of the set at 42%, had the lowest permeation coefficient of all the salts. Seeing as the pattern of increase was the same against all the carrying chloride salts, the figure for sodium chloride has been included whilst the remaining figures can be found in the appendix 3.3.3.

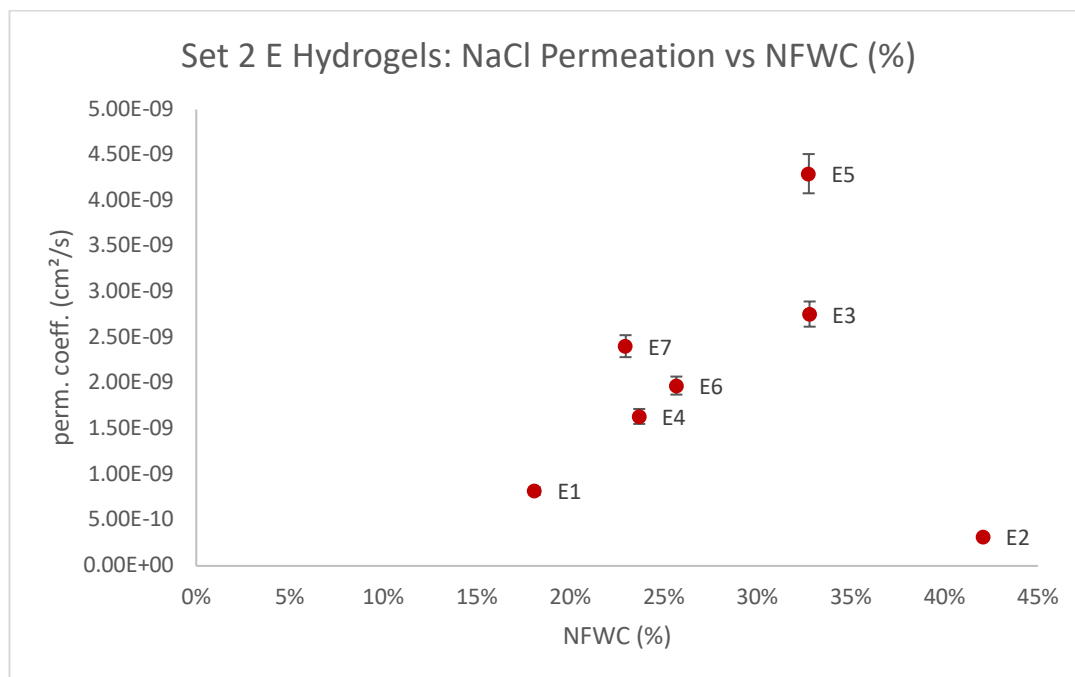


Figure 5.21 Set 2 E hydrogels – NaCl Permeation vs NFWC (%)

Set 2 F Hydrogels: Hydrogels F1 and F2 showcased increases in their NFWC in set 2 when compared to their set 1 versions, reaching NFWCs of 14.7% and 17% respectively. Hydrogel F3 was the only hydrogel to show a decrease in its NFWC in set 1 at 24%. Despite these changes, the F hydrogels yet again exhibited an increase in their permeation coefficients as the NFWC of the hydrogels increased across the set and this was the case with the permeation coefficients against all the chloride salts.

Set 3 E Hydrogels: the NFWC of these E hydrogels ranged between 14-32%, decreasing from those of set 2. However, when the relationship between the permeation coefficients of these hydrogels and their NFWC was investigated, no trends emerged.

Set 3 F Hydrogels: the NFWC of hydrogels F1 and F2 were very similar in this set, reaching 18.8% and 19.1% respectively. Despite this, the permeation coefficients of hydrogel F2 were considerably larger than those of hydrogel F1. The NFWC of hydrogel F3 was 29%, reducing slightly from its set 2 version. Despite the NFWC of the F hydrogels increasing consecutively, there was no relationship between their permeation coefficients and their water content.

5.3.3.4 Ice-like Water

The relationship between the permeation coefficients of each E set hydrogel and their ice-like water content (ILWC) was investigated.

Set 1 E Hydrogels: the ILWC of these hydrogels ranged between 10-31%. The permeation coefficients of these hydrogels against the monovalent salts (KCl & NaCl) did not demonstrate a relationship as ILWC increased across the set. In the case of the divalent salts (CaCl₂ & MgCl₂), there was an upward trend exhibited in the permeation coefficients as the ILWC of the hydrogels increased across the set.

The figure for the magnesium chloride coefficients has been included (see Figure 5.22) whilst the remaining figures can be found in appendix 3.3.4.

The trends seen could suggest the need for ice-like water to aid the larger salt ions such as Ca^{2+} and Mg^{2+} in permeating across the hydrogel membrane. The divalent ions are larger than the monovalent ions and have a larger charge. They may have a higher dissolution rate in ILWC in comparison to K^+ and Na^+ and thus, a stronger relationship.

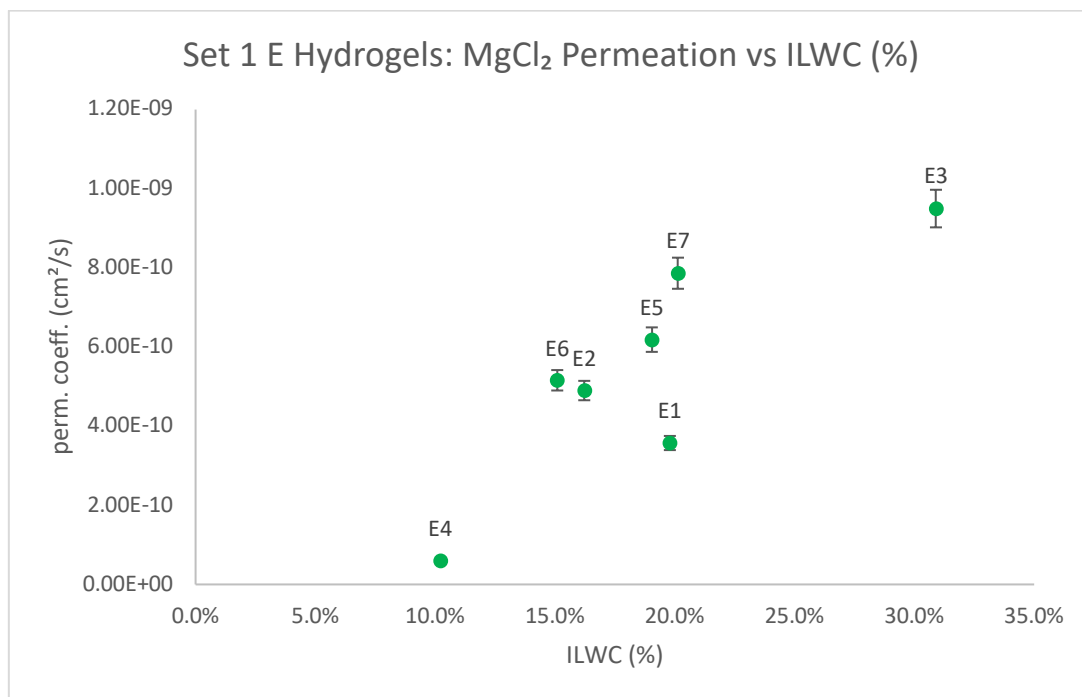


Figure 5.22 Set 1 E hydrogels – MgCl_2 Permeation vs ILWC (%)

Set 1 F Hydrogels: the ILWC of the hydrogels increased in order of the hydrogels of this set and the trends between their permeation coefficients and their ILWC followed suit as well. Against each of the chloride salts, there was a consecutive increase in the permeation coefficients of the F hydrogels as their ILWC increased across the set.

Set 2 E Hydrogels: The set 2 E hydrogels also showed a wide variety of trends in regards to their permeation coefficients and ILWC. With the permeation coefficients of calcium and potassium chloride, the trends were more ambiguous, however, those with the coefficients of sodium and magnesium chloride demonstrated a clear decline as ILWC increased across the set.

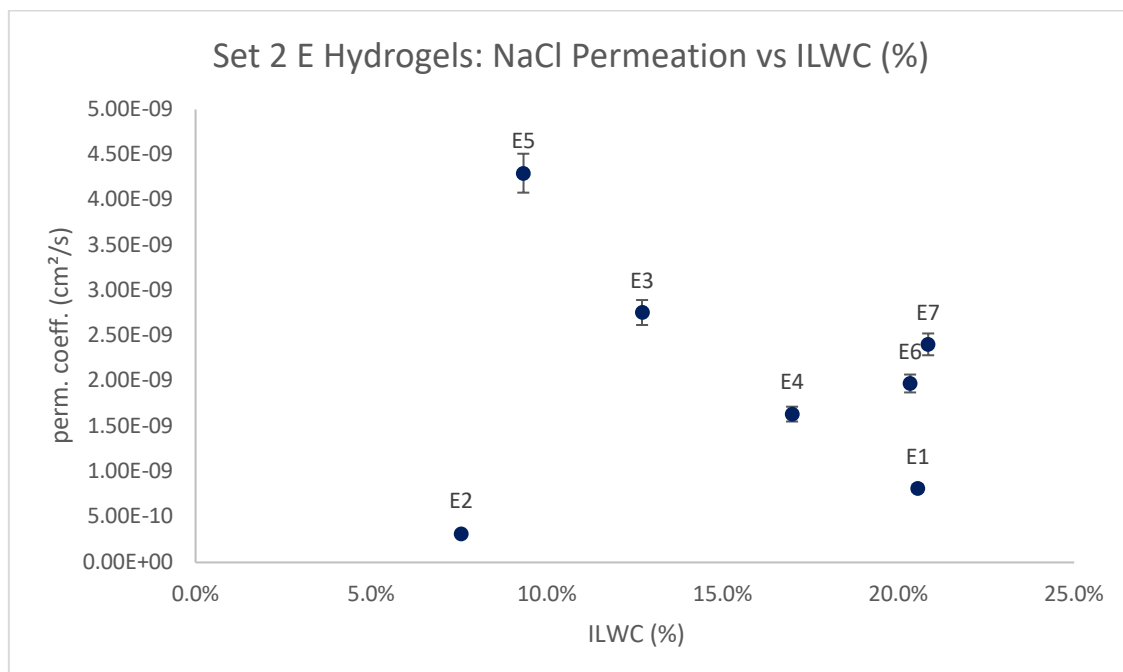


Figure 5.23 Set 2 E hydrogels – NaCl Permeation vs ILWC (%)

Set 2 F Hydrogels: as seen with the set 1 F hydrogels, the ILWC of these hydrogels increased in the order of the hydrogels in the set. And this consecutive increase was accompanied by upward trends in the permeation coefficients of these hydrogels against all the chloride salts.

Set 3 E Hydrogels: trends with the permeation coefficients of these hydrogels and their ILWC were less straightforward than those seen with the other E hydrogels. For both the divalent salts, the permeation coefficients of the hydrogels demonstrated a decline as their ILWC increased across the set. However, in the case of the monovalent salts, the trendline seen was almost identical between the permeation coefficients against them both. The relationship between the coefficients of potassium chloride and their ILWC is shown in Figure 5.24. In the case of both potassium and sodium chloride coefficients, hydrogel E6 was an outlier from this trend but the order of the hydrogels remained the same.

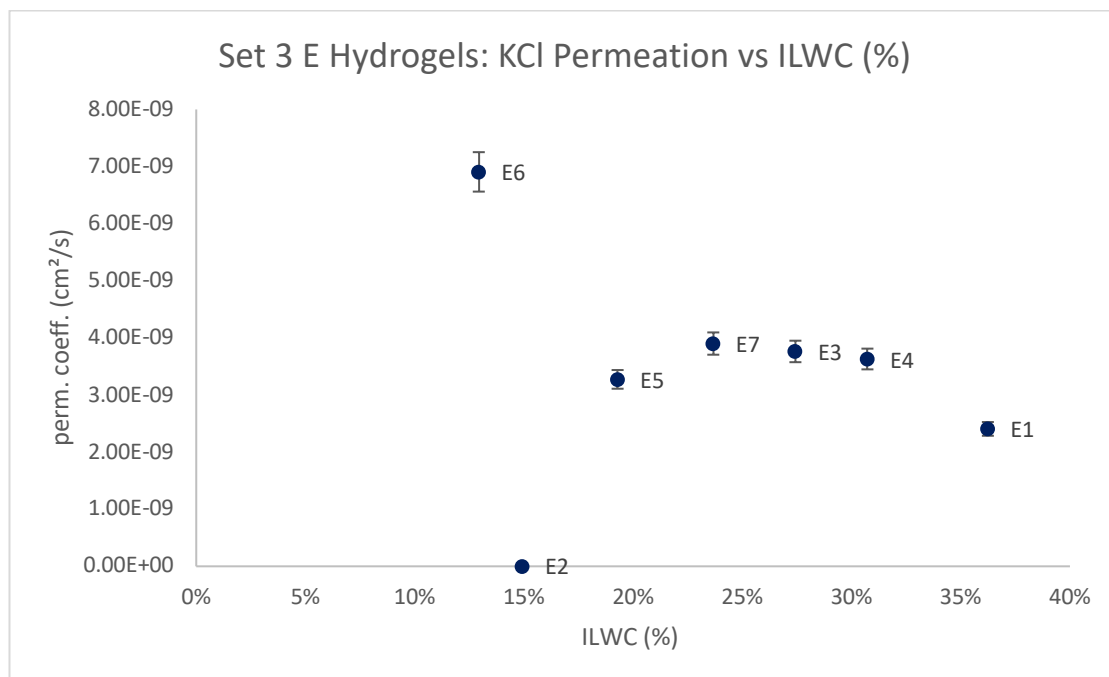


Figure 5.24 Set 3 E hydrogels – KCl Permeation vs ILWC (%)

Set 3 F Hydrogels: unlike previous set, hydrogel F2 had the highest ILWC of the set but in spite of that, hydrogel F3 was responsible for the largest permeation coefficients against all the chloride salts. due to this, there was not a successive trend between the coefficients of these hydrogels and their ILWC.

5.3.3.5 Polymer-associated Water

This water type is considered to be a sub-category of freezing water that is somewhat still attached to the polymer chain, thus, reducing its mobility in comparison to ice-like water. Based on this, it would be considered an interference to the permeation abilities of the hydrogels towards the different chloride salts.

Set 1 E Hydrogels: Relationships with PAWC were less defined and patterns seen were not limited to either mono or divalent ions with these hydrogels. The PAWC of these hydrogels ranged between 12-30%. However, the permeation coefficients of the hydrogels against all the chloride salts showed general decreases as the PAWC of the hydrogels increased across the set, suggesting the reduced mobility of this water type negatively affected their permeation across the hydrogel membrane. The relationship between this water type and the permeation coefficients against sodium chloride are shown in Figure 5.25.

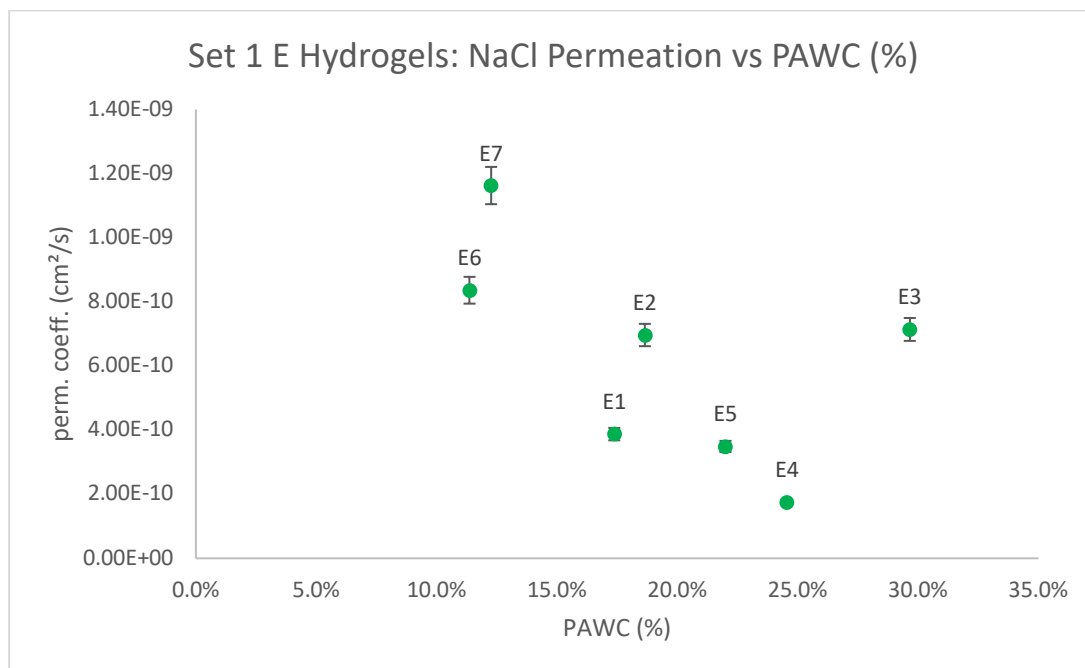


Figure 5.25 Set 1 E hydrogels – NaCl Permeation vs PAWC (%)

Set 1 F Hydrogels: again, the polymer-associated water content of the hydrogels did not increase in a consecutive order. Hydrogel F2 had the highest amount of this water content at 43% followed by hydrogel F3 at 36% then hydrogel F1 at 13%. With that, there was no trend between the permeation coefficients of these hydrogels and their PAWC.

Set 2 E Hydrogels: there was a decrease in the PAWC of these hydrogels compared to set 1, ranging between 8-15%. However, trends between the permeation coefficients of these hydrogels and their PAWC were seen. With all the chloride salts, the permeation coefficients increased as the PAWC of the hydrogels also increased across the set. Again, trends seen were not linear and splits did occur between the trendlines that were seen but generally, there were increases. The relationship between the permeation coefficients of the hydrogels against calcium chloride and their PAWC is shown in Figure 5.26.

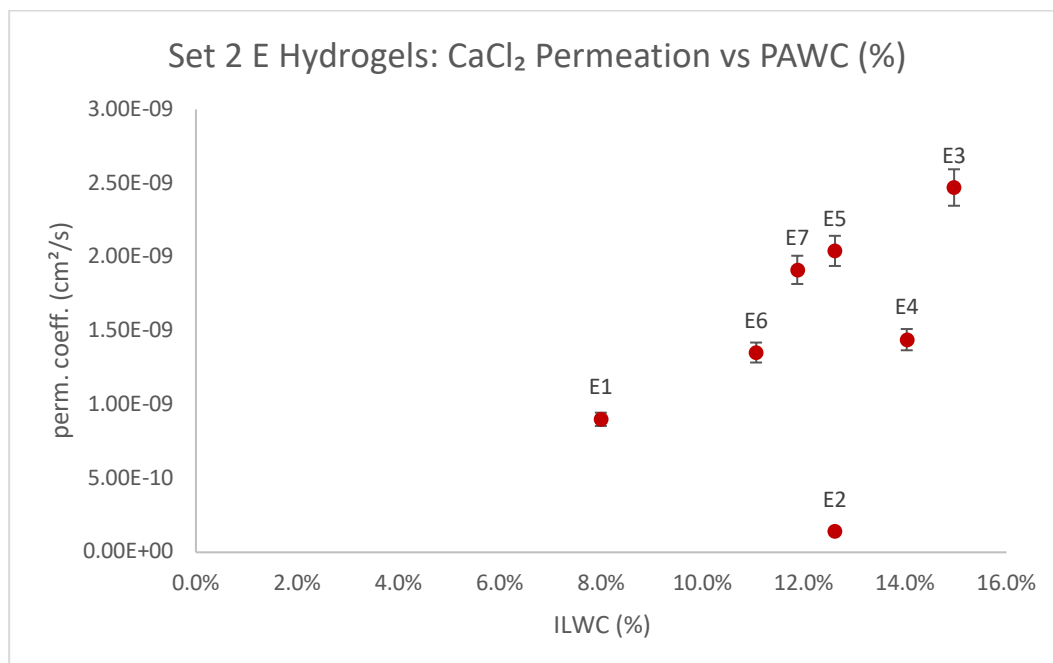


Figure 5.26 Set 2 E hydrogels – CaCl₂ Permeation vs PAWC (%)

Set 2 F Hydrogels: the PAWC of these hydrogels also exhibited a decrease when compared to their set 1 versions. Hydrogel F1, however, showed an increase in PAWC, rising to 9% in set 2. Here, the permeation coefficients of these hydrogels also increased as their PAWC increased across the set and this remained true for all the chloride salts.

Set 3 E Hydrogels: the PAWC of these hydrogels were the lowest of all the set, ranging between 7-12%, not increasing consecutively across the set which has been the case for all the water types thus discussed. The hydrogels demonstrated a decline in their permeation coefficients against each chloride salt as their PAWC generally increased across the set. This is the first instance in which the hypothesised notion regarding the effect of PAWC on permeation has been seen by a set of hydrogels synthesised in this project. As was the case with ILWC, hydrogel E3 was an outlier with the trends seen with the divalent salts.

Set 3 F Hydrogels: Lastly, the F hydrogels of this set also did not demonstrate a consecutive increase in PAWC from hydrogel F1 to F3 nor did the permeation coefficients of the hydrogels demonstrate a consecutive change as PAWC changed across the set.

5.3.4 The relationship between partitioning, diffusion & permeation

A number of factors are known to affect diffusion in hydrogels including: the mesh size of the hydrogel, the solute size in comparison to the mesh size, hydrogel swelling, solute to solute interactions within the hydrogel (aggregation), solute to hydrogel interactions via ionic or covalent bonding and also the microstructure of the hydrogel's matrix (Zustiak et al, 2010). A number of these factors can be associated with reaction conditions and the partitioning behaviour of the hydrogels.

Diffusion of aqueous solutes happens mainly through the water-filled porous structures of the polymer network. This diffusion can also be reduced by interactions between the solute and the polymer chains by way of steric hindrance and hydrodynamic resistance. Complexation between the eluting solute and the polymer network can also reduce diffusivity by way of adsorption to the polymer chain (Liu, 2016).

Solute to hydrogel interactions are described via partition coefficients whilst diffusion behaviours are described using diffusion coefficients. Bringing these together with the permeation coefficient will elucidate the connections and dependencies that each coefficient has on each other, as the equation used to calculate the partition coefficient describes (see equation 4.1).

Per set, the relationships between the permeation coefficients of the E & F set hydrogels and their respective partition and diffusion coefficients were determined.

5.3.4.1 Permeation & Partitioning

Based on the phenomenon that is partitioning, it was expected that there would be a decline in permeation as the partition coefficients of the hydrogels increased. A high partition coefficient means the solute prefers to dwell within the matrix of the hydrogel than the solution. It was thought that this action would prevent the movement of solutes through the hydrogel, reducing its permeation.

Set 1 E Hydrogels: the set 1 E hydrogels had the lowest partition coefficients towards all the chloride salts when directly compared to those of the set 2 and 3 E hydrogels. Despite that, these hydrogels displayed a general increase in their permeation coefficients as partitioning increased across the set for all the chloride salts. It should be noted that none of the trends occurred in an entirely linear manner. As was seen with previously discussed permeation relationships, hydrogel E4 behaved as an outlier. The reason for this remains the same. The figure for the sodium chloride permeation coefficients against the sodium chloride partition coefficients of the set 1 E hydrogels has been included and shown in figure 5.27 whilst the remaining figures can be found in appendix 3.6.

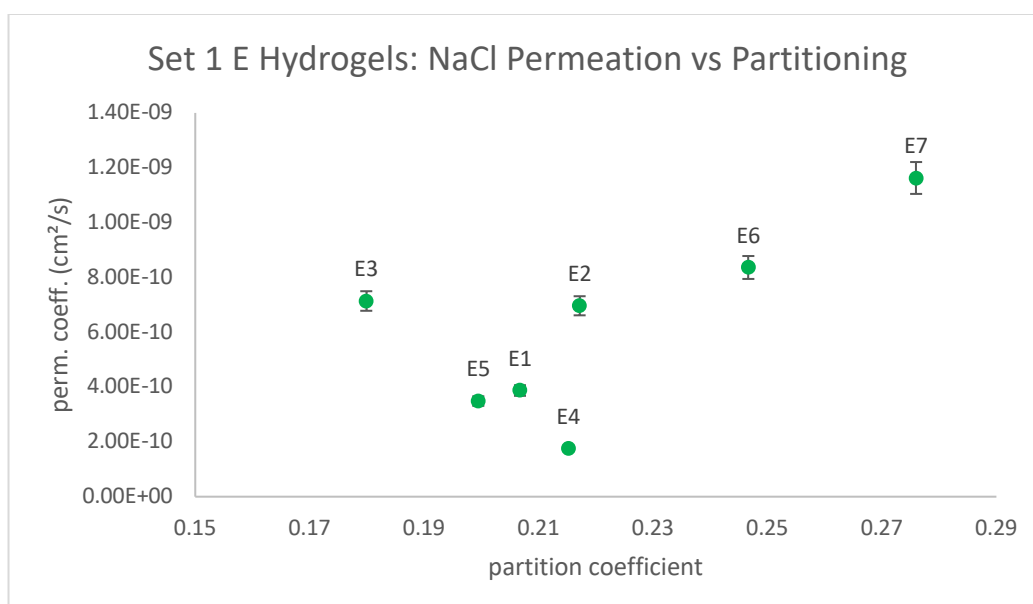


Figure 5.27 Set 1 E hydrogels – NaCl Permeation vs Partitioning

Set 1 F Hydrogels: In regards to the F hydrogels of set 1, there was no trend between permeation and partitioning for majority of the salts, the exception being magnesium chloride. In the case of this divalent salt, the permeation coefficients of the hydrogels increased as their partition coefficients increased across the set from hydrogel F1 → F2 → F3. Hydrogel F1 had both the lowest permeation and partition coefficient whilst hydrogel F3 had the largest of both coefficients in set 1.

Set 2 E & F Hydrogels: As stated in the partition coefficient chapter (4), the set 2 hydrogels, both the E & F sets, had the largest coefficients of all the sets developed, suggesting the reaction conditions of a 90°C post-cure without the use of a diluent are capable of producing silicone-based hydrogels with the behaviours that have been displayed. No clear trends were established between the partition and permeation coefficients of the E hydrogels of this set. The same can be said about the F hydrogels of the set, with the exception of calcium chloride. Against this salt, there was an increase in the permeation coefficients of the hydrogels as their partition coefficients also increased across the set. As was the case with the set 1 F hydrogels, hydrogel F1 was responsible for both the lowest partition and permeation coefficient of the set whilst hydrogel F3 had the largest of both these coefficients.

Set 3 E Hydrogels: the partition coefficients of this set showcased a wide range across the different chloride salts. When determining the link between these two coefficients, clear trends were not entirely established except in the case of the permeation coefficients against magnesium chloride. In this instance, there was a clear decline in the permeation of this salt as the partition coefficients of the hydrogels increased across the set, with the exception of hydrogel E3.

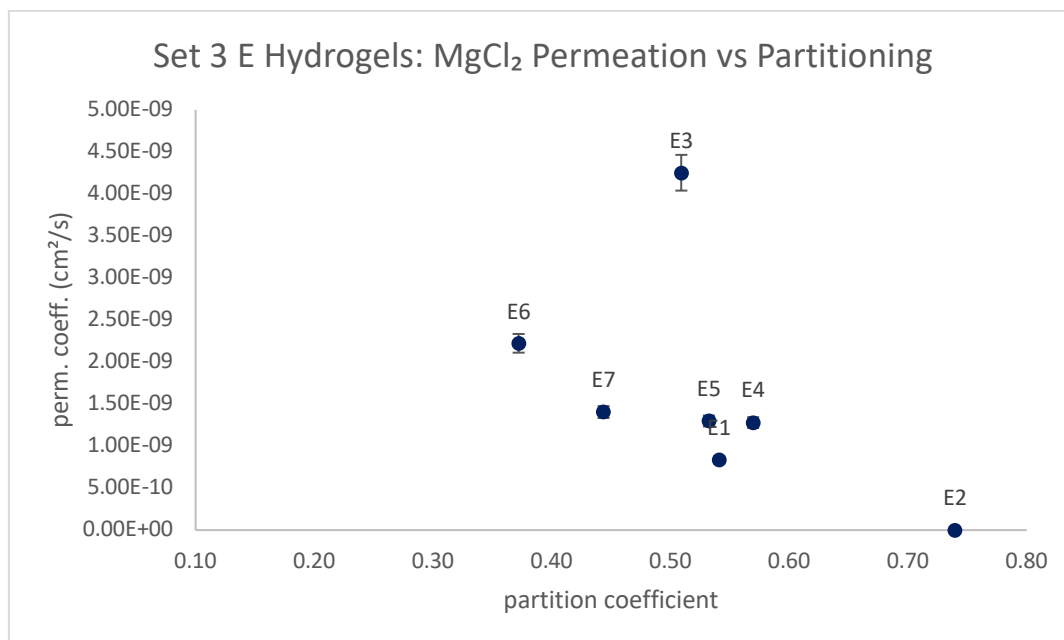


Figure 5.28 Set 3 E hydrogels – MgCl₂ Permeation vs Partitioning

Set 3 F Hydrogels: the order of increase for the partition coefficients remained the same against calcium and sodium chloride in this set, with hydrogel F1 having the smallest coefficient and hydrogel F3 having the largest. Against these salts, the permeation coefficients of the F hydrogels increased across the sets

in their consecutive order. However, with potassium and magnesium chloride, the order was lost and there also was not a connection between permeation and partitioning.

5.4.3.2 Diffusion vs Permeation

It is known that the process of solute transportation through a hydrogel polymer depends on 3 aspects:

- Solubility: the solute must be solubilised in order to enter the polymer matrix. In the case of this study, the solute was the varying metal ions of the chloride salt used which were dissolved in deionised water, acting as a solution.
- Diffusion: the solute has to move and spread through the matrix. The rate at which a solute does this is described using the diffusion coefficient. Partitioning can hinder this diffusion rate and this depends on interactions between the solute and the polymer chains.
- Permeation: the solute must be released from the hydrogel matrix to complete the process of transportation.

A solute with a higher diffusion rate through the hydrogel should have an increased permeation rate so it was expected to see the permeation coefficients of the hydrogels increasing as the diffusion coefficients also increased.

This was seen across all the E hydrogels of sets 1-3. Trendlines with the set 1 and 3 E hydrogels were more definitive and relatively linear than those with the set 2 hydrogels. However, all trends displayed expressed the originally expected notion that increased diffusion coefficients of the different salts will have a positive impact on their permeation behaviours.

With the F hydrogels of set 1 and 2, the connection was more apparent enabling certain salts to be compared to others. For the set 1 hydrogels, only the coefficients of calcium chloride demonstrated a consecutive and upward trend. In the case of the set 2 hydrogels, the coefficients of sodium and magnesium chloride also showed this consecutive trend whilst all of the salts with the set 3 F hydrogels followed an upward trend. Overall, the expected relationship was seen across majority of the E & F hydrogels.

5.5 Conclusion

Overall, the permeation coefficients of the set 3 hydrogels were the largest when compared to those of set 1 and 2. Those of the set 1 hydrogels were the lowest. Potassium chloride was the most permeated salt whilst magnesium chloride was the least. The most common permeation pattern from all the chloride salts was *potassium chloride* → *calcium chloride* → *sodium chloride* → *magnesium chloride*. It was thought that the monovalent salts – the smaller ions – would be permeated the most before the dichloride salts but this was not the case. However, some hydrogels followed this expected permeation pattern, but they were considered to be exceptions.

Hydrogel F3 remained among the most permeable of the hydrogels from set 1 to 3 whilst hydrogel F1 maintained its impermeability towards all the salts across the sets too. Hydrogel E2 demonstrated a decline in permeability from one set to the next, its set 3 version reaching a level that mirrored that of hydrogel F1. This occurrence suggests the particular combination of monomers in the hydrogel E2 formulation as well as the reaction conditions of set 3 could be used to replicate the impermeability that high levels of the TRIS monomer were capable of producing in all versions of hydrogel F1.

Whilst determining the relationship between the formulation of the hydrogels and their permeation coefficients, a range of trends were seen. The TRIS monomer did not appear to influence the permeation behaviours of the hydrogels. With the set 1 E hydrogels, there was a decline in the permeation coefficients against the monovalent salts as the hydrophilic monomer content of NVP increased across the set (hydrogel E7-E1). With the set 2 versions, a clear relationship between the hydrophilic monomer, DMA and the permeation coefficients was not established but with the set 3 E hydrogels, there was a clear decline in the permeation coefficients as NVP content increased.

Equilibrium water content trends also differed between the sets. With the set 2 and 3 E hydrogels, their permeation coefficients declined as EWC increased across the set whilst the F hydrogels of set 1 and 2 showcased increases as their EWC increased across the set. With the other water types, relationships differed largely between the sets. Noticeably, the water types that have been associated with reduced mobility (NFWC & PAWC) were associated with upward trends of the permeation coefficients of the set 2 E & F hydrogels.

Relationships between partitioning and permeation differed across the different sets of hydrogels. The set 1 E hydrogels demonstrated an increase in their permeation coefficients as the partition coefficients also increased. With the set 2 and 3 hydrogels, no relationship was established between these two parameters with the exception of the magnesium chloride coefficients which demonstrated a decline as the partitioning of this salt increased across the set.

The results showcased clear differences in permeation behaviour between the E and F hydrogels from set 1-3. This highlighted the effects and importance of reaction conditions on determining the characteristics of the hydrogels. The instances in which the hydrogels did not follow the rules of conventional permeation patterns or relationships with water content, formulation and partitioning further highlighted the complexities of self-assembled silicone-based hydrogels.

6 Multiple-salt Permeation

6.1 Introduction

Rationale: following on from the previous chapter, this results chapter explores the effects of formulation on the permeation abilities of the hydrogels on a single-salt basis. Although the work discussed in this chapter does not focus solely on the relationship between formulation and multiple-salt permeation but there was an opportunity to see which formulations would bring about certain permeation patterns.

In the previous chapter, the single-salt permeation behaviour of the hydrogels was discussed as well as its relationships with other characterising parameters such as partitioning, diffusion, water content and formulation.

However, during the course of the project, it was of interest to determine how the hydrogels would handle permeating a mixture containing all the chloride salts at once. In a real-life biomedical application, the hydrogels would have to permeate multiple components, of different sizes, charges and molecular weights, at the same time. Utilising all the different chloride salts in a permeation experiment to determine how the hydrogels would transport the solutes based on their different sizes would provide insight to how the hydrogels could possibly behave in such an application.

Multiple-ion permeation studies in the literature pertaining to silicone-based hydrogels were not found. This study was novel and did not rely on existing methodologies to plan or execute experiments. The principal basis for analysis was the use of inductively coupled plasma optical emission spectroscopy (ICP-OES). This technique allows for the identification of individual elements present within a mixture based on an element's unique wavelength that is emitted from its photons (Fassel & Kniseley, 1974). The methodology for this elemental analysis has been described in the methodology chapter (2.8).

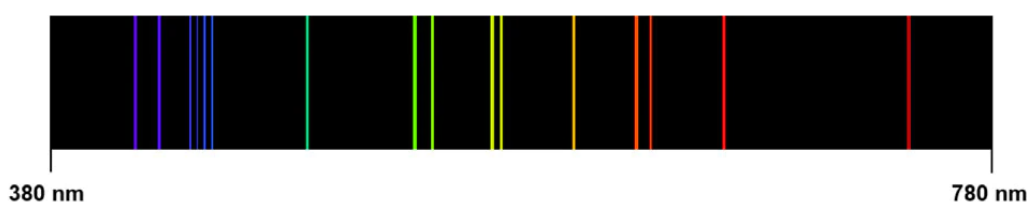


Image 6.1 Visible emission spectrum of calcium (image source: [Thermo-Scientific](#) (N.D))

The analytical procedure of ICP-OES depends on samples being introduced to the plasma, within which they are de-solvated, ionised and excited. During this excitation, characterising photons are emitted. The elements within a sample can be identified by the emission lines caused by the photons and quantified by the intensity of the same lines (Khan et al, 2021). Image 6.1 shows the emission spectrum of calcium. There are multiple wavelengths emitted by its photons that are unique to the element. ICP-OES takes advantage of this and is capable of identifying elements within a mixture based on this principle.

The equipment used to analyse the samples from the multi-salt permeation experiments was able to measure the intensity of a selected element. For each of the metal ions (calcium, potassium, sodium and magnesium), two intensities were measured to expand the scope of the analysis. Spectral interferences between elements were avoided as none of their intensities overlapped. The intensities used have been listed below:

- Calcium: 393.366 & 396.847 nm
- Potassium: 404.414 & 766.490 nm
- Sodium: 588.995 & 589.592 nm
- Magnesium: 279.553 & 280.270 nm

When developing the calibration curves for each of the elements, it was noted that the lower intensity of potassium was unreliable: regardless of changes in concentration, the equipment detected the same concentration. For this reason, this particular intensity (404.414) will be excluded from analysis and discussion.

The hydrogels selected for these particular permeation experiments were on the basis of range – on a single-salt permeation basis, hydrogels E6 and F3 represent the more permeable hydrogels of the different series whereas hydrogel E2 and F1 were the least permeable. Hydrogels E1 and E4 were chosen for their formulation – E1 to compare against hydrogel F1 as they contain the same amount of the hydrophilic monomer whilst hydrogel E4 contains both hydrophilic monomers – DMA & NVP – in equal quantities in addition to the TRIS monomer.

The methodology for these experiments has been described in the materials & methodology chapter (2.3.2). In the single-salt permeation experiments, each experimental run made use of a 250mM solution of an individual salt. During the multiple salt experiments, a 250mM of each chloride salt was combined to make a multi-salt solution at 250mM and this mixture was used per hydrogel.

6.2 Results

A selection of E & F hydrogels from sets 1-3 were chosen for these experiments:

Hydrogel E1: set 2 + set 3

Hydrogel E6: set 2

Hydrogel E2: set 2 + set 3

Hydrogel F1: set 1

Hydrogel E4: set 3

Hydrogel F3: set 1-3

Concentrations with negative values can be assumed to be zero.

Table 6.1 Permeated Concentrations (ppm) of hydrogel E1 of set 2

Hour	Ca ²⁺ (396.847)	K ⁺ (766.490)	Na ⁺ (589.592)	Mg ²⁺ (279.553)
1	-0.2	0.2	1.7	-0.7
2	-0.5	1.3	-0.5	-0.7
3	-0.4	1.4	-0.6	-0.6
4	-0.2	1.4	-0.6	-0.6
5	0	2.9	0.1	-0.4
6	0.4	4.2	0.7	-0.2
7	0.4	3.9	0.5	-0.2

Table 6.2 Permeated Concentrations (ppm) of hydrogel E1 of set 3

Hour	Ca ²⁺ (393.366)	K ⁺ (766.490)	Na ⁺ (589.592)	Mg ²⁺ (279.553)
1	-0.8	-0.6	-0.3	-0.7
2	-0.6	-0.1	-0.1	-0.6
3	-0.1	1.4	0.5	-0.3
4	0.9	4.4	1.7	0.2
5	0.3	2.8	1	-0.1
6	0.4	3.1	1.1	0
7	1	4.8	1.9	0.3

Table 6.3 Permeated Concentrations (ppm) of hydrogel E2 of set 2

Hour	Ca ²⁺ (396.847)	K ⁺ (766.490)	Na ⁺ (589.592)	Mg ²⁺ (280.270)
1	-0.6	0	0.1	-0.8
2	-0.5	0.4	2.7	-0.8
3	-0.6	1.8	3.6	-0.8
4	-0.4	3.3	2.9	-0.7
5	-0.3	3.9	4	-0.6
6	-0.7	0.4	0.7	-0.8
7	-0.4	1.9	1.6	-0.6

Table 6.4 Permeated Concentrations (ppm) of hydrogel E2 of set 3

Hour	Ca ²⁺ (393.366)	K ⁺ (766.490)	Na ⁺ (589.592)	Mg ²⁺ (280.270)
1	-0.3	-1	2.5	-0.9
2	-0.5	-0.8	2.5	-0.9
3	-0.7	-1.3	2	-0.9
4	-0.6	-0.9	2	-0.9
5	-0.6	-1.1	2.1	-0.9
6	-0.5	-1.1	3	-0.8
7	-0.6	-0.8	1.9	-0.9

Table 6.5 Permeated Concentrations (ppm) of hydrogel E4 of set 3

Hour	Ca ²⁺ (396.847)	K ⁺ (766.490)	Na ⁺ (589.592)	Mg ²⁺ (279.553)
1	-0.8	-0.7	-0.3	-0.7
2	-0.3	1.3	0.3	-0.4
3	0.1	2.8	0.6	-0.1
4	0.4	3.5	0.6	0.1
5	0.6	4.1	0.9	0.3
6	1.1	5.8	1.3	0.7
7	1.8	8.2	1.9	1.2

Table 6.6 Permeated Concentrations (ppm) of hydrogel E6 of set 2

Hour	Ca ²⁺ (393.366)	K ⁺ (766.490)	Na ⁺ (589.592)	Mg ²⁺ (279.553)
1	-0.8	0	-0.1	-0.7
2	-0.8	-0.1	-0.3	-0.7
3	-0.5	1.2	0.4	-0.5
4	-0.3	2.1	0.7	-0.3
5	-0.4	1.8	0.7	-0.4
6	0.1	4.1	1.4	-0.1
7	0.1	4	1.4	-0.1

Table 6.7 Permeated Concentrations (ppm) of hydrogel F1 of set 1

Hour	Ca ²⁺ (396.847)	K ⁺ (766.490)	Na ⁺ (589.592)	Mg ²⁺ (280.270)
1	-0.7	-1.8	1.9	-0.9
2	-0.8	-1.7	2.4	-0.9
3	-0.8	-2.2	2.1	-0.9
4	-0.8	-1.8	2	-1
5	-0.8	-1.9	1.9	-1
6	-0.8	-1.8	1.9	-1
7	-0.8	-1.8	2.1	-1

Table 6.8 Permeated Concentrations (ppm) of hydrogel F3 of set 1

Hour	Ca ²⁺ (396.847)	K ⁺ (766.490)	Na ⁺ (589.592)	Mg ²⁺ (280.270)
1	-0.6	-1.4	-0.4	-0.8
2	-0.5	-0.6	0	-0.7
3	0.3	2.7	1.4	-0.2
4	1.9	7.5	3.7	0.8
5	2.5	9.6	4.6	1.1
6	4	14.4	6.5	2
7	4.5	15.8	7.5	2.3

Table 6.9 Permeated Concentrations (ppm) of hydrogel F3 of set 2

Hour	Ca ²⁺ (393.366)	K ⁺ (766.490)	Na ⁺ (589.592)	Mg ²⁺ (279.553)
1	-0.5	-0.3	0.1	-0.6
2	-0.1	1.2	0.7	-0.3
3	0.9	4	2.1	0.2
4	1.8	7.3	3.7	0.8
5	2.5	9.4	4.7	1.1
6	3.5	12.5	6.3	1.7
7	4.8	16.8	8	2.5

Table 6.10 Permeated Concentrations (ppm) of hydrogel F3 of set 3

Hour	Ca ²⁺ (393.366)	K ⁺ (766.490)	Na ⁺ (589.592)	Mg ²⁺ (279.553)
1	-0.6	-1	-0.1	-0.6
2	-0.5	-0.7	0.2	-0.6
3	0.2	1.5	1.3	-0.2
4	1.1	4.6	2.6	0.2
5	2.2	7.8	4.2	0.8
6	3	10.3	5.4	1.2
7	3.8	12.7	6.5	1.7

6.2 Discussion

6.2.1 Permeation profiles

The ethos behind conducting these experiments was to understand how well the hydrogels would perform at permeating the varying metal ions, of different sizes and charges, simultaneously. It was of interest to understand whether permeation would be governed by the size and charge of the ions or whether the hydrogels would be able to discern between the different ions in the same mixture at all.

In multiple cases, the results of the multiple-ion permeation experiments showed the potassium ion was permeated the most whilst the magnesium ion was permeated the least. The permeation profile of hydrogel E4 of set 3 is shown in Figure 6.1. The pattern of permeation seen somewhat reflects the results seen in the previous chapter in which, on an individual basis, the majority of the hydrogels permeated the potassium ion the most and the magnesium ion the least, suggesting the hydrogels are capable of distinguishing between the different ions when faced with a mixture containing all of them.

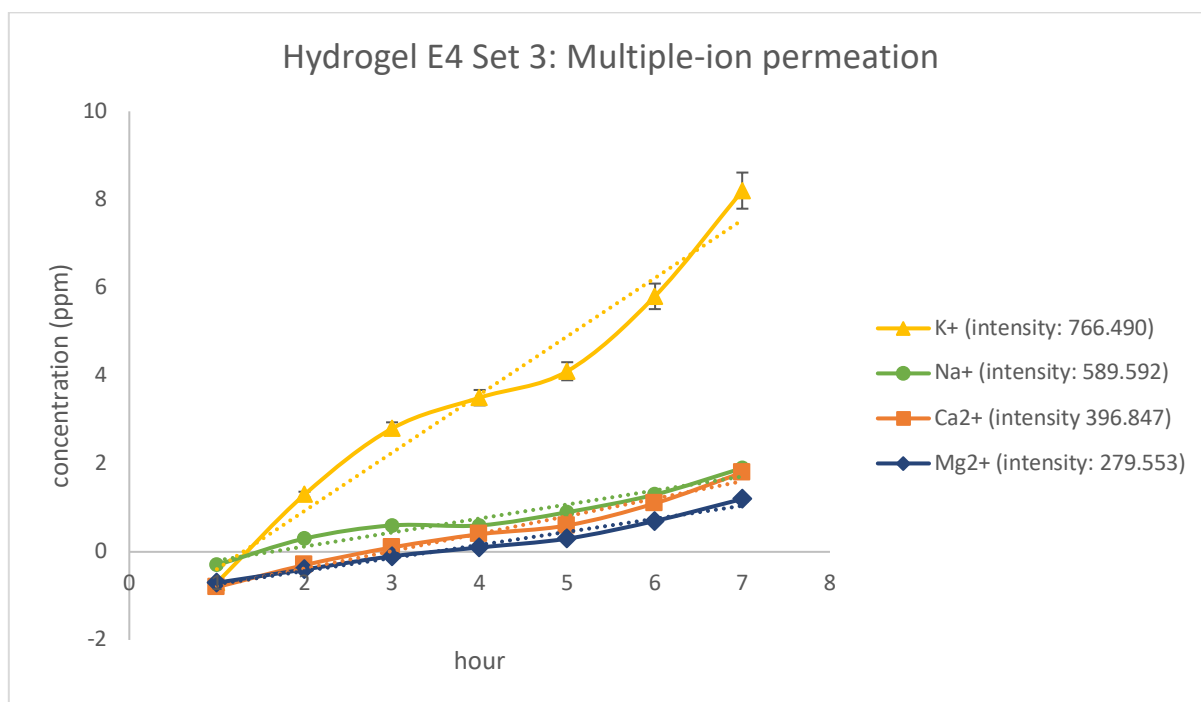


Figure 6.1 Hydrogel E4 Set 3: Multiple-ion permeation profile

Hydrogel E4 of set 3 permeated potassium at a much higher rate than the other ions. The sodium ion was the second most permeated ion, followed by calcium then magnesium. On a single-salt basis, this same hydrogel followed the permeation order of *potassium* → *calcium* → *sodium* → *magnesium*. It should also be said that this hydrogel displayed very similar permeation rates between sodium and magnesium on a single-salt basis. However, this hydrogel demonstrated that on a multi-salt basis, it is able to permeate the smaller, single-charged ions before the larger ions, suggesting size and charge is the governing basis for permeation when the hydrogel is faced with a mixture of the ions.

With hydrogel F3, it was possible to test the multiple-salt permeation ability of all the versions of this hydrogel from sets 1-3, and to establish whether differences in the reaction conditions between each set would influence the permeation ability of the hydrogel towards multiple chloride salts at once. The permeation profile of hydrogel F3 of set 3 is shown in Figure 6.2.

The pattern displayed by this hydrogel shows the potassium ion being permeated at a higher rate than the other metal ions, followed by sodium then the larger ions of calcium and magnesium. The rate and permeation order demonstrated by the set 3 version of hydrogel F3 was mirrored in both the sets 1 and 2 versions of itself. However, this hydrogel demonstrated that there are clear differences between the transportation rate of the sodium, calcium and magnesium ions as opposed to the closeness of the rates seen with hydrogel E4 (Figure 6.1). On a single-salt basis, all versions of hydrogel F3 followed a permeation order of *potassium* → *calcium* → *sodium* → *magnesium*, each salt being permeated at different rates across the membrane which is seen in the multiple-salt assays.

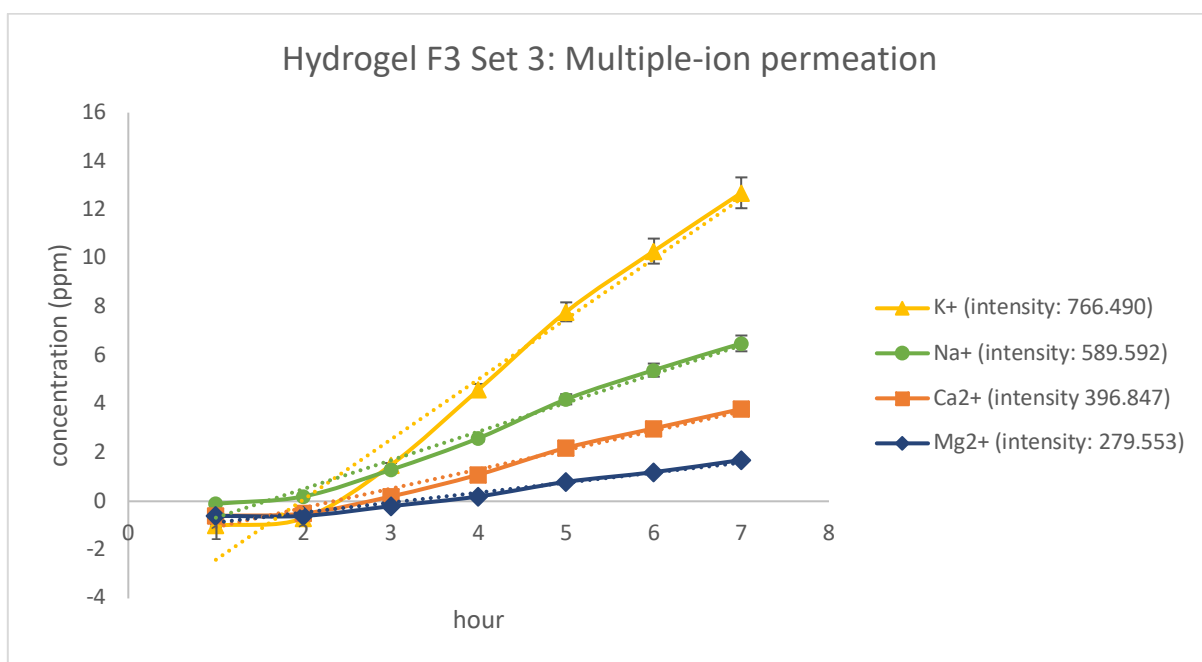


Figure 6.2 Hydrogel F3 Set 3: Multiple-ion permeation profile

Hydrogel E6 of set 2 demonstrated permeation towards the smaller monovalent ions of potassium and sodium but not towards those of the divalent ions of calcium and magnesium. The permeation profile of this hydrogel is shown in Figure 6.3.

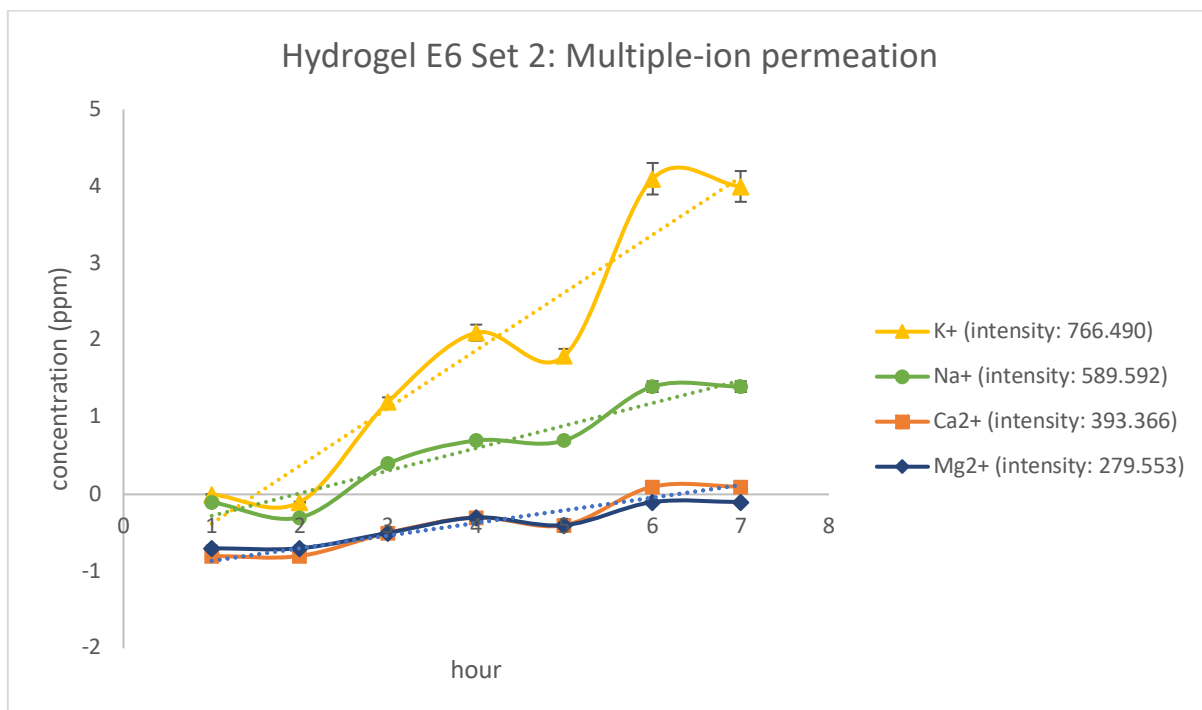


Figure 6.3 Hydrogel E6 Set 2: Multiple-ion permeation profile

This hydrogel demonstrated that when faced with a mixture of the ions, it would not permeate the larger ions at a rate at which it did the smaller ones. On a single-salt basis, this hydrogel followed the permeation order that majority of the hydrogels followed as mentioned above: *potassium* → *calcium* → *sodium* → *magnesium*. It should be noted that magnesium was permeated considerably lower than the other salts during the single-salt experiments, reaching an end concentration of 83ppm, compared to that of potassium which reached a concentration of 245ppm.

Referring to Figure 6.3, the hitches that occur in the trendlines of potassium and sodium permeation at hour 5 could be a result of experimental error during the dilution of the samples derived from the permeation rig prior to ICP-OES analysis, and less so an indication of a decline in permeation at that particular time. This is supported by the conductivity meter readings taken during the experiment, which show a steady increase over the 7-hour period of the experiment, shown in Figure 6.4. For context, Figure 6.4 shows the linear change in conductivity (μS) over time for this particular hydrogel.

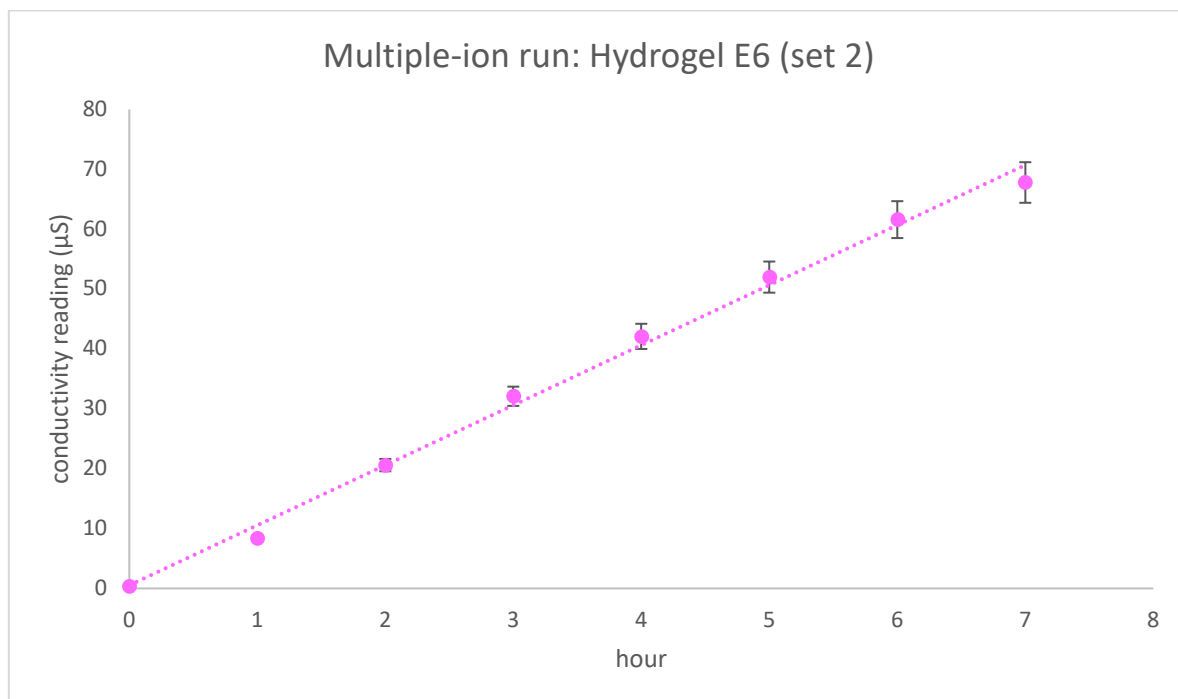


Figure 6.4 Hydrogel E6 Set 2: Conductivity (μS) vs. time

As mentioned in the single-salt permeation chapter (5.3), hydrogel F1 was consistently the least permeable hydrogel of both the E & F series. Hydrogel E2 of set 3 also showed similarly low permeation rates that were comparable to those of hydrogel F1, also discussed in that chapter. These two hydrogels were tested in the multiple-ion permeation experiments to determine whether their impermeability would be replicated when faced with permeating multiple ions at once.

In the case of both hydrogels F1 (set 1) and E2 (set 3), the concentration of all the metal ions except sodium was in the negative (Tables 6.3 & 6.7). At first, it was thought the hydrogels were displaying selective permeability towards the sodium ion, only allowing this ion to pass through the hydrogel membrane. The permeation profile of hydrogel F1 of set 1 is shown in Figure 6.5.

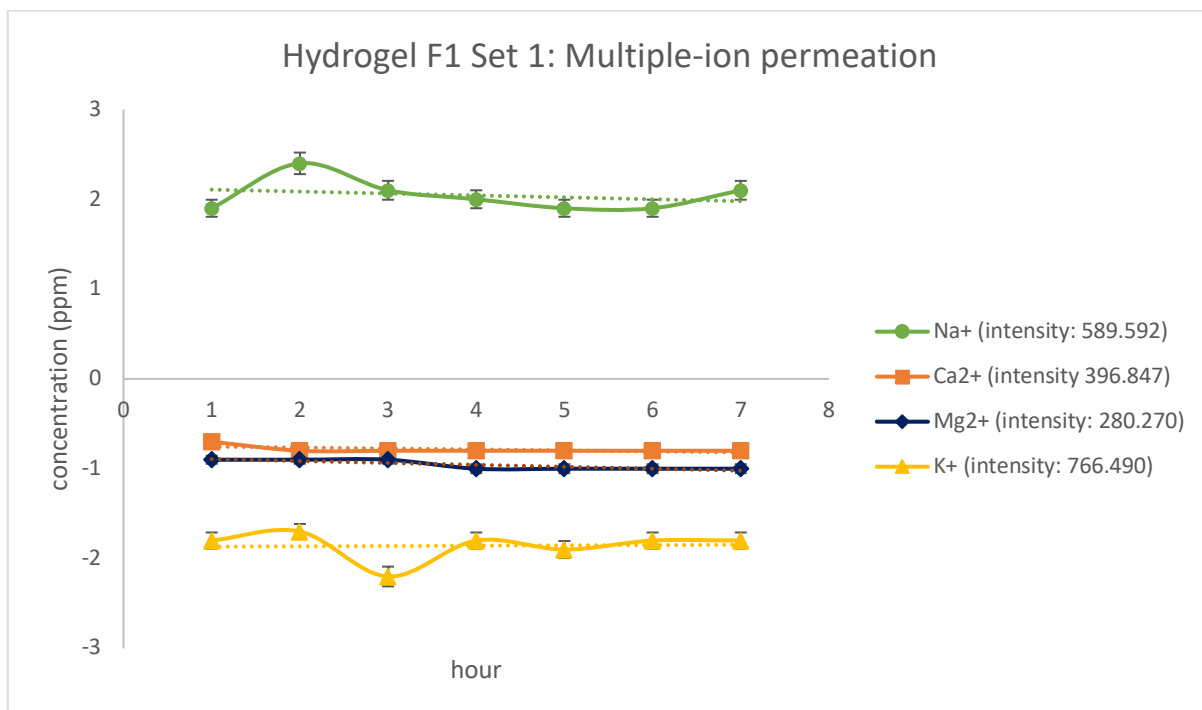


Figure 6.5 Hydrogel F1 Set 1: Multiple-ion permeation profile

However, such an occurrence would be associated with an increase in the concentration of sodium over time. The fact that the concentration of this ion remained relatively constant suggested permeation was not the reason for its positive concentration but more so highlighted the ubiquitous nature of sodium in water, even when this water is deionised.

During the nanofiltration of water, ions such as calcium and magnesium are more readily removed due to the tightness of the water bonds to the ion in their respective hydration shells, making them easier to remove during the filtration process whereas sodium and potassium ions have smaller hydration radii. Bonds between the surrounding water molecules and these ions are not as tightly bound, increasing the likelihood of detaching during the filtration process, thus increasing the premise of residual sodium presence in filtered water (Tansel et al, 2006).

6.2.2 Factors influencing multiple-ion permeation

As was the case with single-salt permeation, it is important to consider the influences of other characterising parameters of the hydrogels on their multiple-ion permeation behaviours.

A number of factors need to be considered when analysing the results of permeation experiments, especially the make-up of the hydrogels in terms of their water content and their morphology as indicated by the degree of opacity (which will be further expanded upon in the next chapter) and formulation.

The hydrogels that demonstrated increased levels of permeation included hydrogels E4 (set 3), E6 (set 2) and hydrogel F3 (set 1-3). Although the results from analysis via ICP-OES were conducted on samples that were diluted (see methodology chapter 2.8), hydrogel F3 permeated all the ions the most

in direct comparison to the aforementioned hydrogels, in terms of concentration. Meanwhile, hydrogels F1 (set 1) and E2 (set 3) demonstrated impermeability towards the different ions.

Water Content: despite the equilibrium water contents (EWC) of the different versions of hydrogel F3 decreasing from sets 1-3, they remained amongst the highest of all the hydrogels (88%, 71% and 66% respectively).

The EWC of hydrogel E4 (set 3) and E6 (set 2) were very similar: 57% & 56% respectively but hydrogel E4 demonstrated an increased permeation ability compared to hydrogel E6. Alongside this, hydrogel E4 showcased an ability to permeate all the ions, although it could be argued that there was a preference for the potassium ion. Hydrogel E6 demonstrated a clear preference for the potassium and sodium ions over magnesium and calcium (refer to Figure 6.3).

The non-freezing water contents (NFWC) of both these hydrogels were also very similar – 16% & 15% respectively – but hydrogel E6 (set 2) had less freezing water than hydrogel E4 (set 3), at 31% & 40% respectively, and it can be said that this was reflected in its lower permeation rate than that of hydrogel E4.

With the different versions of hydrogel F3, the NFWC of the hydrogels were larger than that of hydrogels E4 and E6, at 31%, 24% & 29% respectively from sets 1-3. However, despite a decrease in FWC between sets 1-3, the permeation of hydrogel F3 did not necessarily decline between the sets. It is often thought that increased levels of freezing water would be associated with an increase in permeation due to the relatively unhindered mobility of this water type within the hydrogels (Hetcher et al, 1960). However, as discussed in the previous chapter (5.3.3.2) in addition to the behaviour of hydrogel F3, changes in freezing water may not always be accompanied by changes in permeation.

With an EWC of 26%, and a FWC/NFWC of 13%, hydrogel F1 (set 1) has the lowest water content of any of the hydrogels from the E & F series. In this case, it became clear that the low water content of this hydrogel contributes to its impermeability towards the different ions when faced with a mixture of them. The only other hydrogel to replicate this behaviour was hydrogel E2 (set 3) whose water content was much larger than that of hydrogel F1, with an EWC of 60%, FWC of 29% and NFWC of 31%. There is no commonality between these two hydrogels in terms of water content. The difference in behaviour between the E & F hydrogels demonstrates the complexity of permeation in self-assembled silicone-based hydrogels.

Formulation: a pattern was noticed across the hydrogels that displayed increased levels of permeation towards the varying ions. Hydrogels E4, E6 and F3 all contain the DMA monomer in their formulation, hydrogels E6 and F3 having more of this monomer when compared to the other hydrogels utilised in the multiple-ion experiments. Hydrogel E4 contains 30% DMA, hydrogel E6 contains 50% DMA and hydrogel F3 is made up of 70% DMA. Of all the hydrogels utilised, these 3 showcased increased levels of permeation whereas hydrogels E1, E2 and F1 did not show sustained levels of permeation and these hydrogels either do not contain the DMA monomer or have low levels of the monomer included in their formulation.

As mentioned in previous chapters, hydrogel F1 has the most hydrophobic formulation of all the hydrogels with 65% TRIS and 30% NVP. Hydrogel E2 contains 50% NVP in its formulation. Although the NVP monomer is hydrophilic in nature, the impermeability of hydrogel E2 of set 3 can be attributed to the combination of its particular formulation in addition to the reaction conditions of the series: a post-cure in addition to using a diluent.

As mentioned earlier in the chapter, the size and charge of the ions are important to know when considering the permeation patterns exhibited by the hydrogels. Although the potassium ion is larger than the sodium ion when bare (0.133 nm vs. 0.095 nm), sodium has a larger hydration number than potassium (Israelachvili, 2011). The atomic weight of sodium is also smaller than potassium and so it is able to surround itself with more water molecules, making its hydrated ion larger: the smaller an ion, the greater its attraction to water. Meanwhile, a larger charge on an ion also results in an increase in its hydration number (Clark, 2010).

From the permeation rates displayed by the different hydrogels, there is an indication of selectivity within the channels that facilitate ion transport within them. Such behaviour is an indication of the competing interactions between the dissolved ions and water, also influenced by the microscopic structure of water and the specific nature of the ion hydration shell of individual ions (Mancinelli et al, 2007). At this point, the concept of ions acting as either 'structure-makers' or 'structure-breakers' in relation to the structure of water becomes important when trying to understand the permeation behaviours seen. Such properties have the ability to influence the solubility of substances within water.

When a salt, such as the chloride salts utilised, is dissolved in water, the ions dissociate and become hydrated. These ions bear a large electric field around themselves which cause the water in their hydration shells to rearrange to a different orientation to the water molecules surrounding the ions (Marcus, 2012). A structure-making ion has the ability to break the hydrogen bonding between water molecules and force surrounding water to rearrange into an ordered hydration structure whilst a structure-breaking ion interacts weakly with surrounding water molecules and causes a disorderly rearrangement of this water. The potassium ion (K^+) is considered to be a structure-breaker whilst the sodium and calcium ions (Na^+ & Ca^{2+}) are thought to be structure-makers (Collins, 2004).

The sodium ion has been found to reduce the average diffusion of water by suppressing the formation of transitional state water. In the case of the potassium ion, it binds to this transitional state and stabilises it, thus increasing the diffusion of water (Shimizu & Matubayasi, 2018). It could be argued that the association of potassium with increasing the diffusion of water could also increase the diffusion of potassium when being carried by water during transportation. It has also been established that structure-breaking ions such as potassium also increase the average diffusion of water at certain concentrations, ranging between 0.25-2M (Ishai et al, 2013). Seeing as the concentration of the salt solutions utilised during single and multiple-salt experiments were kept at 0.25M (0.25M of each different chloride salt), this could provide an explanation for its increased permeation rate through water/channels within the hydrogel when compared to the other metal ions.

It has also been determined that the sodium ion has stronger interactions between its first hydration shell than that of potassium, making the hydrated potassium ion a more flexible structure (Carrillo-Tripp et al, 2003). All these characteristics of the potassium ion provide insight into its permeation behaviour and also provides context for its continuously high permeation rate seen in the majority of the hydrogels.

The effects of the chloride ion on water structure have been determined to be negligible: during solvation, the chloride ion (Cl⁻) does not drastically cause distortions to the orientation of surrounding water molecules (Mancinelli et al, 2007) and so, it is safe to ignore the chloride ion during permeation analysis.

When looking at how the different hydrogels permeated each metal ion over the seven-hour period of their permeation experiments, all versions of hydrogel F3 consistently performed the highest, with the set 1 and set 2 version of the hydrogel often interchanging the top spot between them. Referring to the previous chapter (5.2.2), potassium chloride was responsible for the largest diffusion coefficients of all the hydrogels from sets 1-3 whilst the magnesium ion was responsible for the lowest diffusion coefficients and it is reflected in the multiple-ion experiments too.

To further illustrate the effects that size and charge of the eluting ion have on permeation, refer to the permeation profiles of the potassium ion and the magnesium ion in Figures 6.6 & 6.7, respectively. Figure 6.6 displays the transport rates of the different hydrogels against the potassium ion (intensity: 766.490). There is a clear difference in this rate seen between all the versions of hydrogel F3 compared to the remaining hydrogels (negative concentration rates excluded from profile).

Hydrogel F3, on both a single and multiple-salt basis, demonstrated an increased permeation ability and the pattern shown in Figure 6.6 is repeatedly seen with the other metal ions as well. This suggests the hydrogel is highly permeable and could be utilised in applications that depend on this ability whereas hydrogels such as F1 (set 1) and E2 (set 3) are the opposite, thus less suitable for applications that rely on such processes.

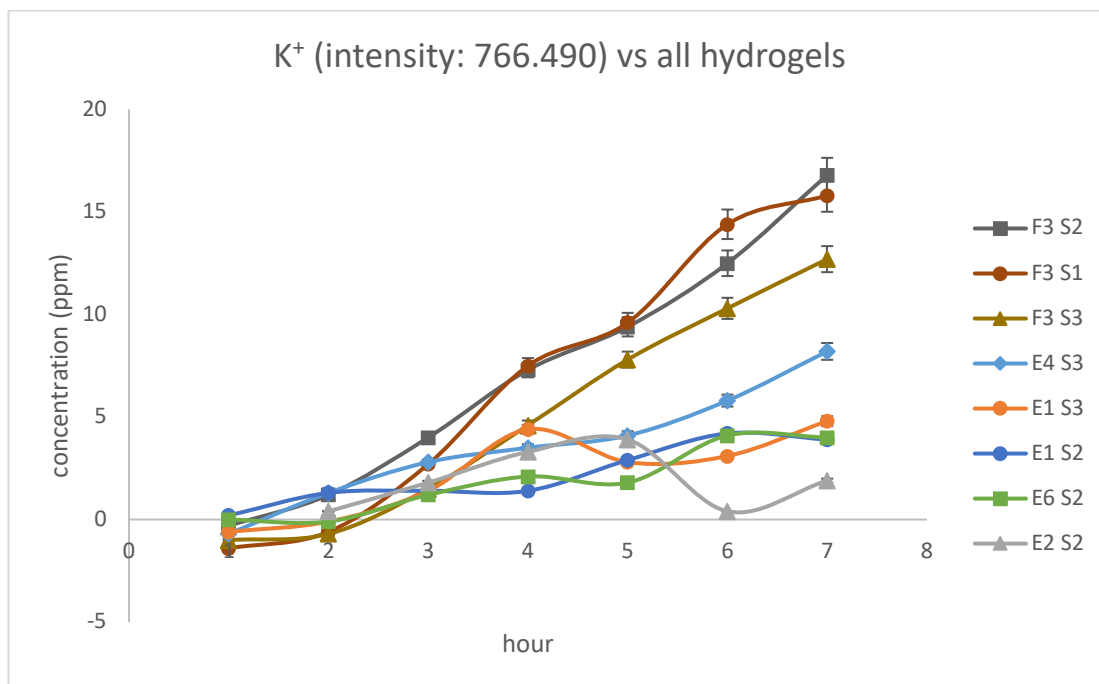


Figure 6.6 K⁺ (intensity: 760.490) permeation profile

Also, more hydrogels demonstrated an ability to permeate the potassium ion and the general concentrations upon elution were higher. Referring to the permeation profile of the magnesium ion (intensity: 279.553), hydrogel F3 (sets 1-3) was also the top transporter of this ion. Noticeably, less hydrogels were capable of permeating the larger ion of magnesium in comparison to potassium.

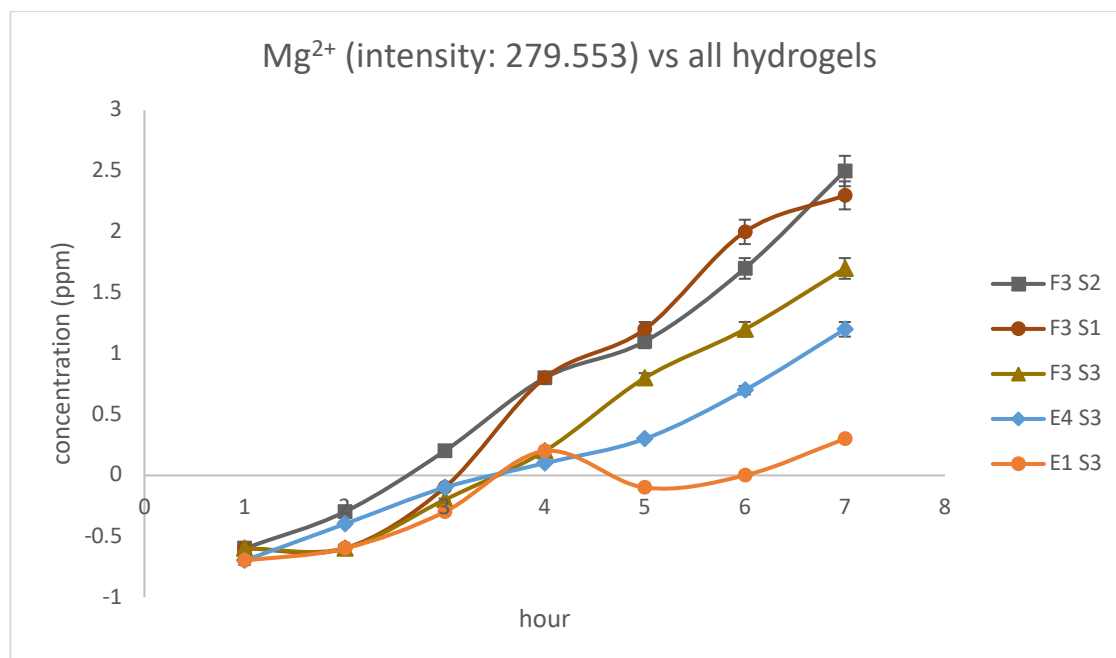


Figure 6.7 Mg²⁺ (intensity: 279.553) permeation profile

The same could be said about the profiles of calcium and sodium, which can be found in appendix 4.2. Hydrated, the magnesium ion has a radius of 0.43 nm compared to that of potassium at 0.33 nm (Israelachvili, 2011).

6.3 Conclusion

The hydrogels included in the multiple-ion permeation experiments demonstrated a range of activity. In the hydrogels that demonstrated permeability, the potassium ion was often permeated the most and the magnesium ion the least. The hydrogels showcased the ability to permeate the ions in order of their size, with the smaller ions like potassium and sodium being permeated first before the larger ions of calcium and magnesium. In comparison to results from the single-salt permeation experiments, which saw a majority of the hydrogels following a permeation order of *potassium* → *calcium* → *sodium* → *magnesium*, the hydrogels when faced with a mixture of the ions permeated the ions in the order of *potassium* → *sodium* → *calcium* → *magnesium*.

Hydrogel F3 (sets 1-3) was consistently the highest performing hydrogel whilst hydrogel E6 (set 2) which demonstrated increased permeation levels on a single-salt basis showed a reduced permeation rate towards calcium and magnesium. Hydrogels F1 (set 1) and E2 (set 3) maintained their impermeability when faced with a mixture of all the ions.

It was found that water content, especially freezing water, did not have a clear effect on the permeation rate of the hydrogels towards the different ions. A pattern emerged between the hydrogels that demonstrated a permeation ability and those that did not, or their ability was reduced: the NVP monomer was the majority hydrophilic monomer in the formulation of the reduced ability hydrogels whilst the DMA monomer had increased amounts in the formulation of higher performing hydrogels.

Certain characteristics of the potassium ion have been considered to provide context for its increased transport rate in the hydrogels in comparison to the other ions.

Overall, it has been shown that certain formulations and reaction conditions of the synthesised silicone-based hydrogels have the ability of differentiating and permeating ions of different sizes and charges, further demonstrating their potential suitability in processes that depend on this ability.

7 Membrane Characteristics

7.1 Introduction

Rationale: it is important to understand the phase structure and morphology of the synthesised silicone-based hydrogels as it plays a role in determining certain characteristics such as permeation capabilities and water content. There is not a definitive answer in terms of what the morphology of silicone-based hydrogels are typically like as it is not entirely known but the work discussed in this chapter contributes to this knowledge. Also, it is important to determine the distribution of elements at the surface of a hydrogel, as it is hypothesised that there is a relationship between the surface composition and surface hydrophilicity of silicone hydrogels (Zhao et al, 2015), an important parameter to understanding a hydrogel's permeability behaviour as increased hydrophilicity will promote ion transport. The goal for this chapter is to paint a picture of the internal hydrogel structure, which in addition to the previously discussed experimental parameters, could further aid the understanding of the trends and behaviours seen.

It is a commonly accepted notion that distinct phases develop in these types of hydrogels due to the incompatibility of the hydrophobic silicone monomer and hydrophilic monomers such as NVP and DMA. Typically, silicone is added to the formulation of conventional hydrogels to increase oxygen permeability due to the suitability of silicon-oxygen bonds for gas transmission (Zhao et al, 2014). This silicone tends to form clusters whilst the hydrophilic monomers form clusters of their own, resulting in discrete regions of hydrophobicity and hydrophilicity along the polymer chain (Liu, 2016).

In biomedical applications that depend on separation and release processes, clearance rates can be affected by the charge and pore size of the membrane and the interaction of the eluting solute with the membrane. Parameters such as the size and charge of eluting solutes and their impact on permeation were determined during permeation studies, as discussed in chapters 5 & 6. Although characteristics such as pore size can be suggested via permeation, it would be ideal to have images of these porous structures, and this can be achieved using microscopic techniques.

Many different analytical methods have been used to understand the morphology of silicone hydrogels such as atomic force microscopy (AFM), solid-state nuclear magnetic resonance (NMR), X-ray scattering and environmental scanning electron microscopy (ESEM).

The prefix of 'environmental' in ESEM refers to the need to introduce a specific gas such as water vapour or use of a specific temperature while taking measurements (Stokes, 2012). This analytical technique can also make use of a high vacuum and it is this vacuum that allows for the imaging of wet samples due to the presence of water vapour pressure in the imaging chamber. This is especially advantageous in its use with hydrogel samples as they can be examined in their natural format without needing to be dehydrated or frozen, allowing for accurate image capture (Bhagyaraj et al, 2018) as it has been reported that dehydrated samples rearrange themselves upon rehydration, making the original snapshot relatively unreliable (Seitz et al, 2017).

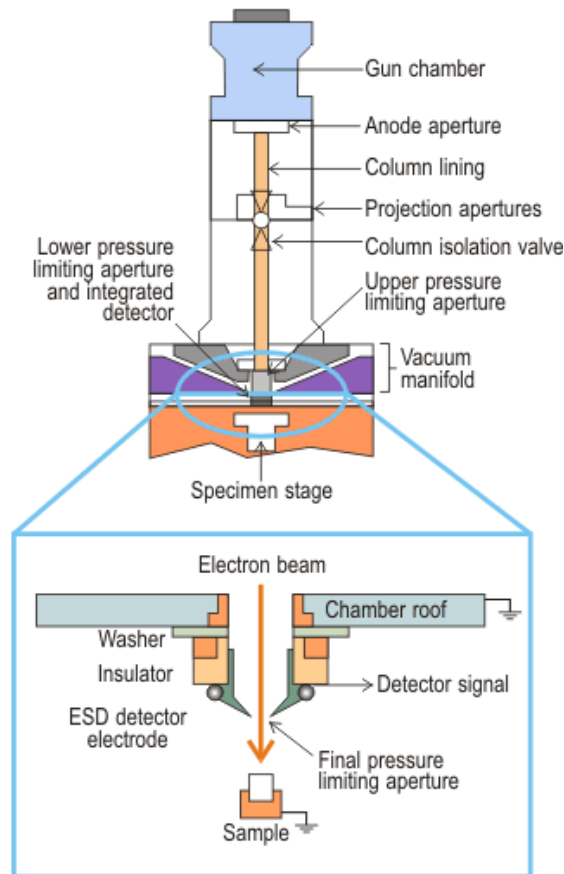


Image 7.1 schematic representation of environmental scanning electron microscope (Image source: Zimmermann et al, 2007)

The principle of ESEM is based on the use of electrons. An electron gun produces electrons that are aimed and beamed at the sample through a series of lenses and apertures (Goldstein et al, 2017). As the sample is bombarded by these electrons, they knock out electrons from the sample including secondary electrons and backscattered electrons. These ejected electrons hit a detector that feeds an electronic signal to the equipment's corresponding computer to compose an image of the sample. Secondary electrons are used to determine a sample's morphology and topography (SERC, 2017).

In addition to ESEM imaging, energy-dispersive X-ray spectroscopy (EDX) was utilised on the hydrogel samples to determine the elemental composition of their surfaces. During ESEM imaging, the bombardment of the sample with the electron beam causes excitation of the sample's electrons. As these excited electrons return to lower energy states, they produce X-rays that are of a fixed wavelength. These x-rays correspond to a particular element and this describes how EDX is able to provide information on the elemental composition of a sample (SERC, 2017). The principle of EDX depends on Moseley's Law which states that the square root of the frequency of the emitted x-ray is approximately proportional to the atomic number of an element (Gaston & Protter, 2020).

X-ray photoelectron spectroscopy (XPS) is a different analytical technique used to determine the elemental composition of the surface of a sample and it was utilised in this project as well. It can also be used to determine the empirical formula and chemical & electronic state of the elements within a material. The technique makes use of X-rays beamed at a sample whilst a detector measures the kinetic/binding energy of ejected electrons.

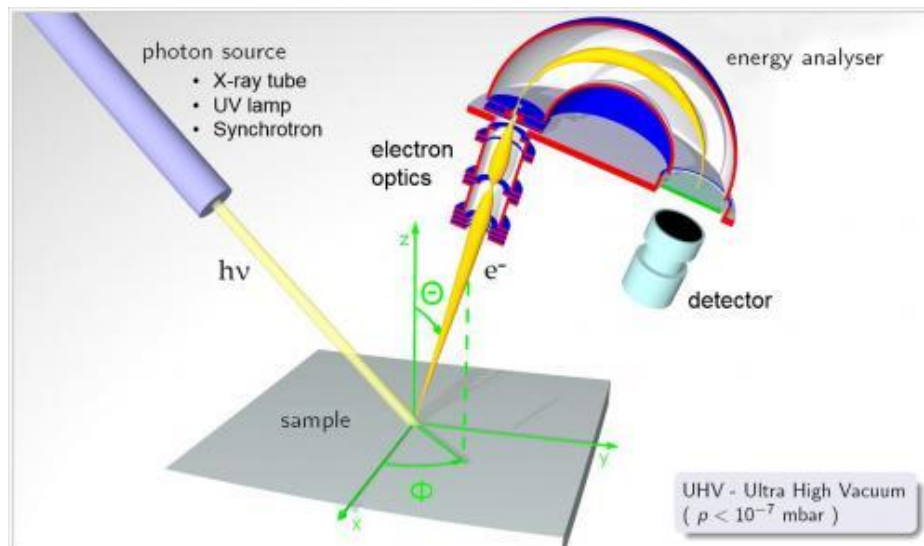


Image 7.2 schematic representation of X-ray photoelectron spectroscopy (image source: [Yale University](#) (N.D))

The principle upon which XPS is based on works similarly to EDX, in that the kinetic energies of the detected electrons correspond to a particular element. Unlike EDX, XPS is only capable of penetrating the top 1-10nm of the sample and so this technique is used to characterise the surface of samples as opposed to the bulk (Thermo Scientific).

7.2 Results

7.2.1 EDX

For EDX analysis, both the surface and cross-section of the hydrogel samples were analysed. By doing so, the cross-section is meant to represent the bulk of the hydrogel and provide insight to the bulk composition. These results were derived using the EDX analysis method as described in methodology sub-chapter 2.6.1 and were analysed using Pathfinder (v 1.3), the analytical equipment's accompanying data analysis software. The hydrogel samples were analysed in a hydrated state.

Tables 7.1 & 7.2 below detail the elemental compositions of hydrogels E1 and F1 of sets 1 & 2 as well as hydrogels E4 and E6 of set 3. A poly-HEMA contact lens was used as a control sample, the results have been included in the tables as well.

The spectra for each hydrogel's analysis can be found in appendix 5.1. Trace elements including calcium, copper, fluorine, chromium, iron and bromine were excluded from the Tables of each hydrogel/spectra if they were detected during analysis.

Table 7.1 EDX data for hydrogels tested (surface)

<i>Hydrogel + Set</i>	<i>Element (%)</i>			
	Carbon	Nitrogen	Oxygen	Silicon
E1 Set 1	24.16	2.26	55.79	17.78
F1 Set 1	22.95	4.79	57.22	15.04
E1 Set 2	29.49	1.57	53.95	14.98
F1 Set 2	42.67	0.00	38.53	18.8
E4 Set 3	33.59	2.53	43.27	10.8
E6 Set 3	29.66	6.87	47.22	16.25
Poly-HEMA contact lens	26.45	0.00	72.76	0.79

Table 7.2 EDX data for hydrogels tested (cross-section)

<i>Hydrogel + Set</i>	<i>Element (%)</i>			
	Carbon	Nitrogen	Oxygen	Silicon
E1 Set 1	41.72	0.00	46.22	12.07
F1 Set 1	42.27	0.00	37.54	20.19
E1 Set 2	30.57	0.30	57.45	11.68
F1 Set 2	41.22	0.00	40.85	17.93
E4 Set 3	22.56	3.25	64.41	9.78
E6 Set 3	13.48	3.47	74.18	8.87
Poly-HEMA contact lens	36.83	0.00	62.17	1.00

7.2.2 XPS

For XPS analysis, only the surface of the hydrogel samples was analysed as that is the sole purpose of this technique – the analysis is able to provide information regarding the top 1-10nm of a sample's surface. These results were derived using the method described in methodology sub-chapter 2.6.2. The hydrogel samples were analysed while in a dehydrated state.

Tables 7.3 – 7.6 below detail the surface elemental compositions of hydrogels E1, E4, E7 and F1 from sets 1-3. The spectra for each hydrogel's analysis can be found in appendix 5.2. Trace elements including chlorine, calcium and sodium were excluded from the Tables of each hydrogel/spectra if they were detected during analysis.

Table 7.3 XPS data for hydrogel E1 of set 1-3

Elemental composition (%)				
Hydrogel	Carbon	Oxygen	Silicon	Nitrogen
E1 S1	65.7	20.8	8.5	5.0
E1 S2	70.7	16.4	7.4	5.5
E1 S3	72.6	15.1	7.4	4.9

Table 7.4 XPS data for hydrogel E4 of set 1-3

Elemental composition (%)				
Hydrogel	Carbon	Oxygen	Silicon	Nitrogen
E4 S1	66.5	19.6	6.8	6.5
E4 S2	70.1	16.1	7.1	6.8
E4 S3	68.3	17.3	7.9	6.5

Table 7.5 XPS data for hydrogel E7 of set 1-3

Elemental composition (%)				
Hydrogel	Carbon	Oxygen	Silicon	Nitrogen
E7 S1	65.3	18.5	8.2	6.1
E7 S2	71.9	16.1	6.9	4.3
E7 S3	69.8	16.8	4.7	8.7

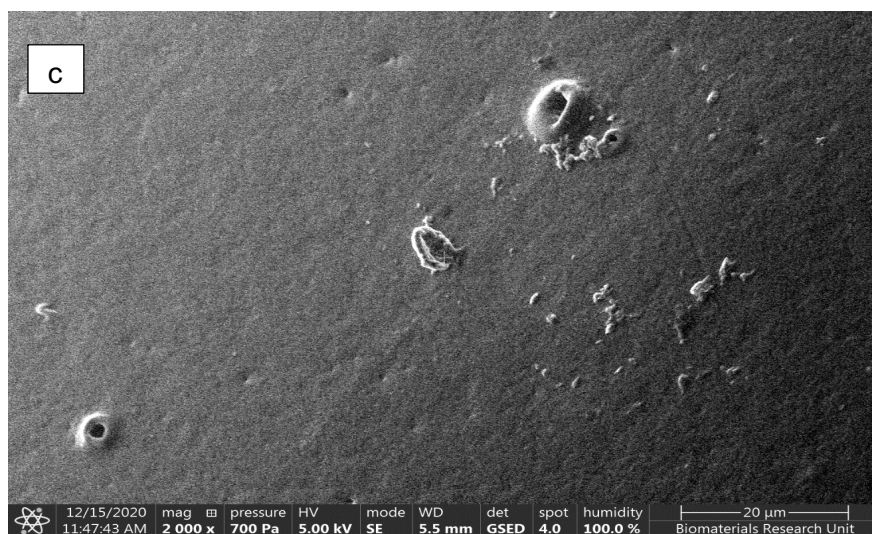
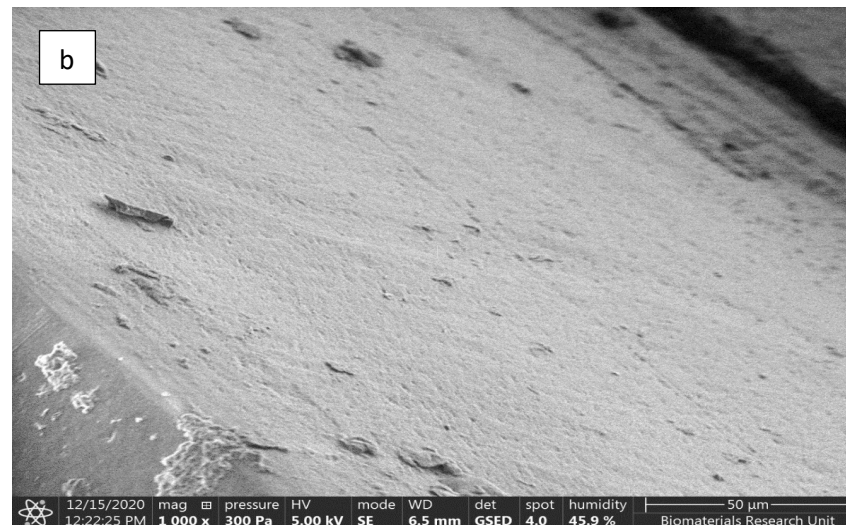
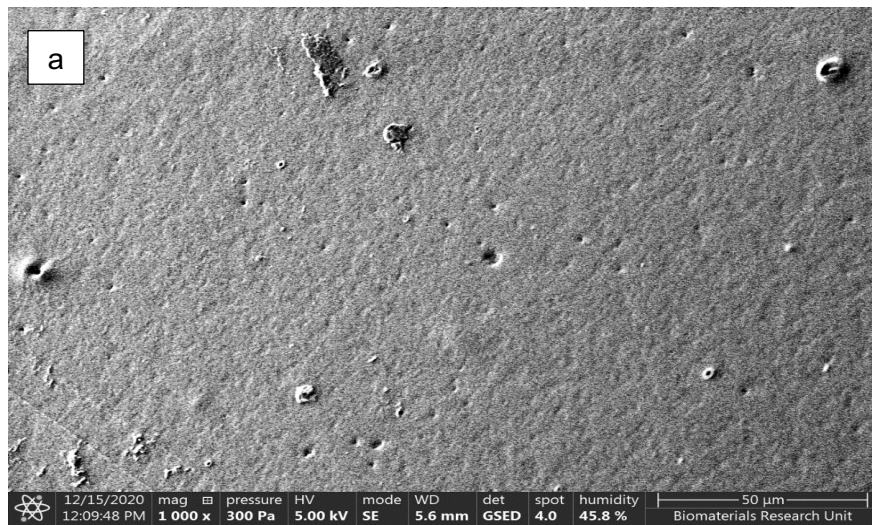
Table 7.6 XPS data for hydrogel F1 of set 1-3

Elemental composition (%)				
Hydrogel	Carbon	Oxygen	Silicon	Nitrogen
F1 S1	65.4	19.9	11.0	3.6
F1 S2	66.1	18.8	11.9	3.3
F1 S3	67.2	18.2	10.2	3.3

7.2.3 ESEM Imaging

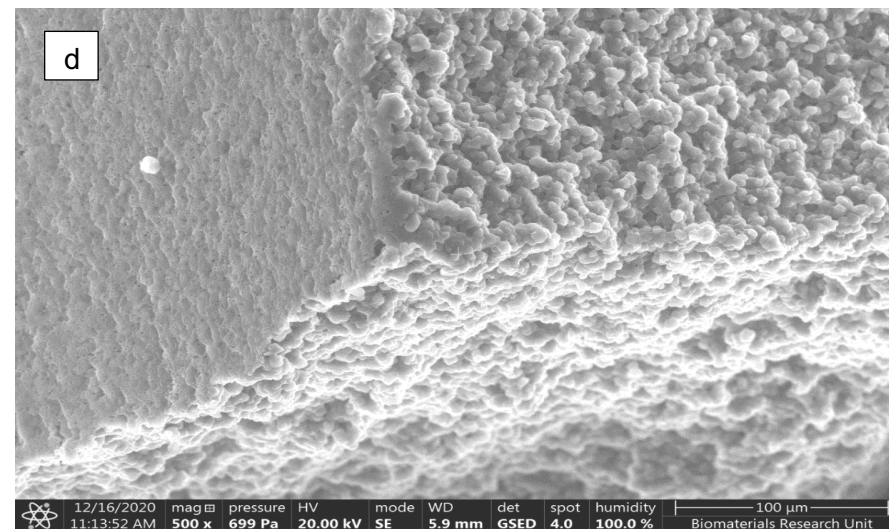
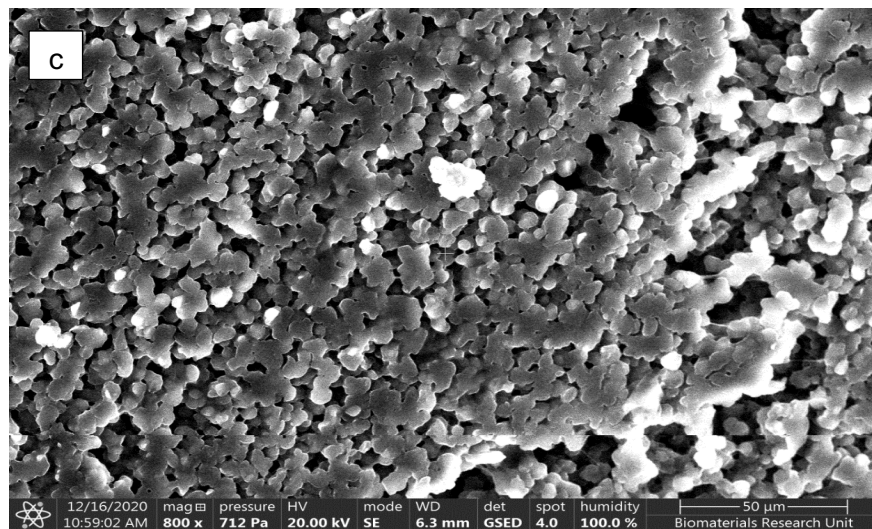
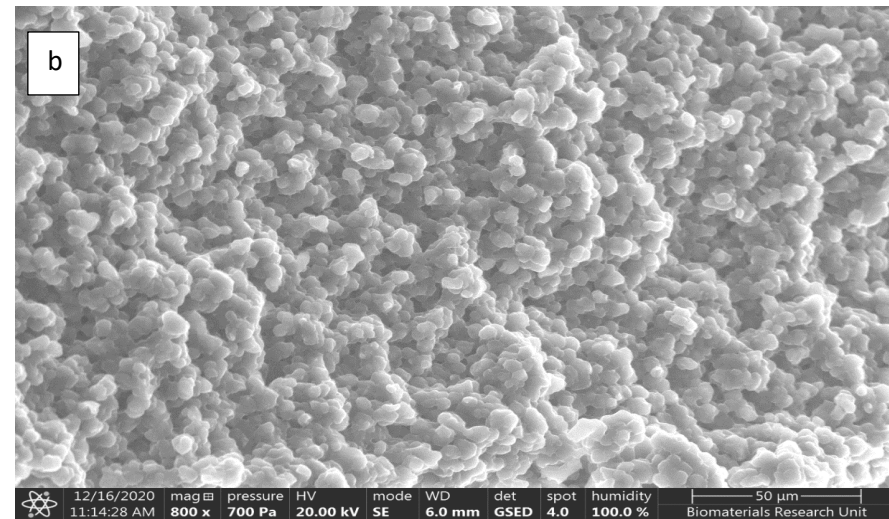
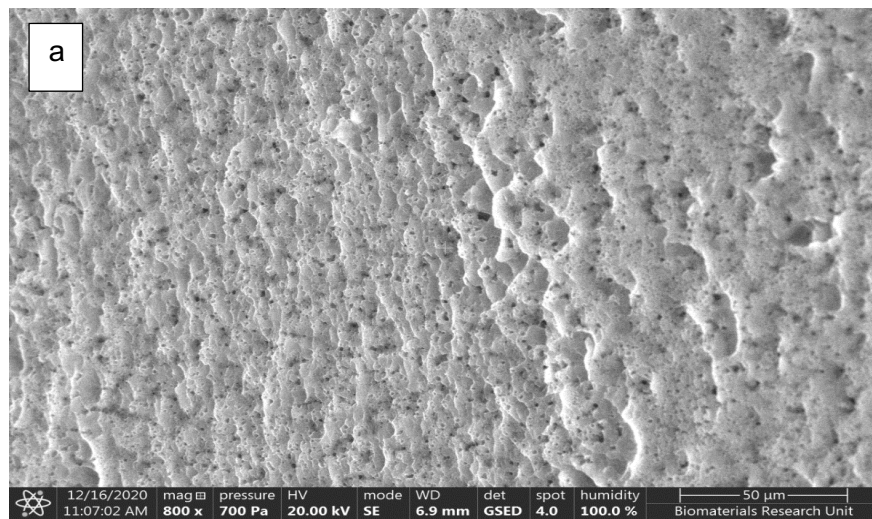
ESEM analysis produced magnified images for hydrogels E1 and F1 from sets 1 & 2 and hydrogels E4 and E6 from set 3. The method used to acquire the images is described under the methodology sub-chapter 2.6.1. Images of the hydrogel's cross-section and surface were captured while they were in a hydrated state. A poly-HEMA contact lens was used as a reference material against the hydrogels, these images can be found in the appendix as well as the remainder of the images acquired. Images were taken of the hydrogel's surface and cross-section. The images of the control p-HEMA sample can be found in appendix section 5.3.

Table 7.7 Hydrogel E1 Set 1



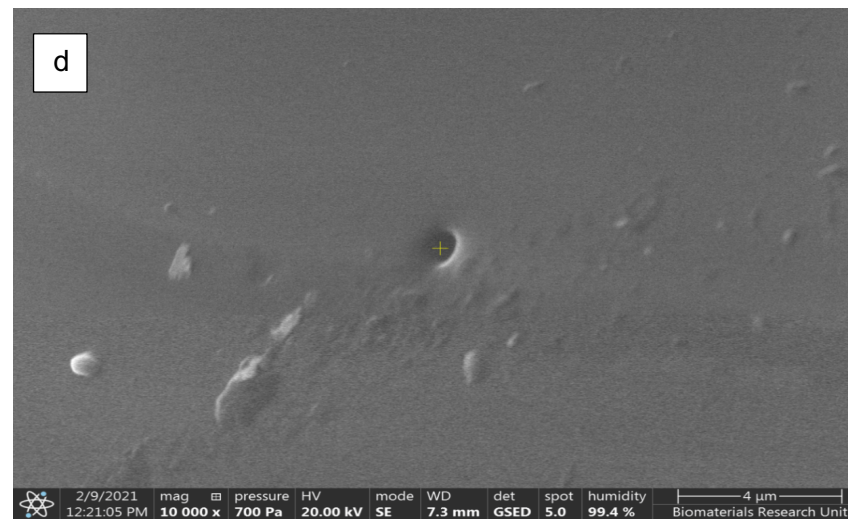
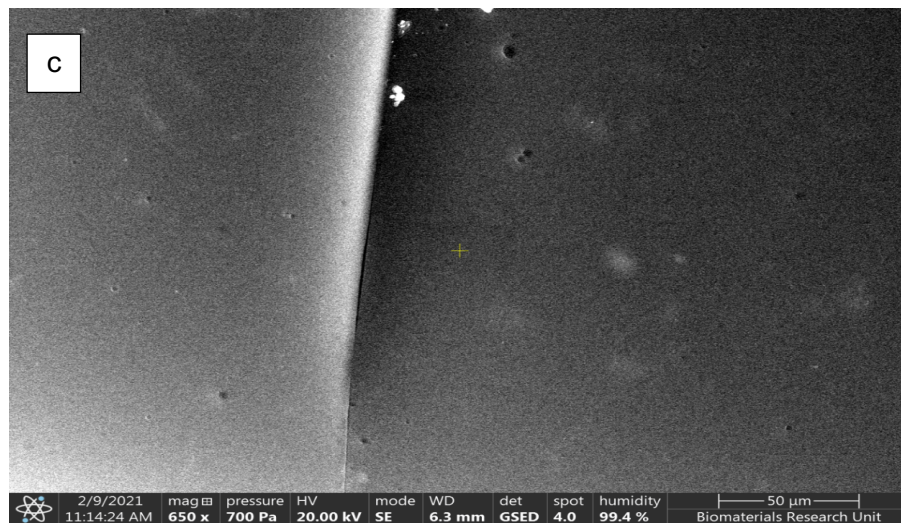
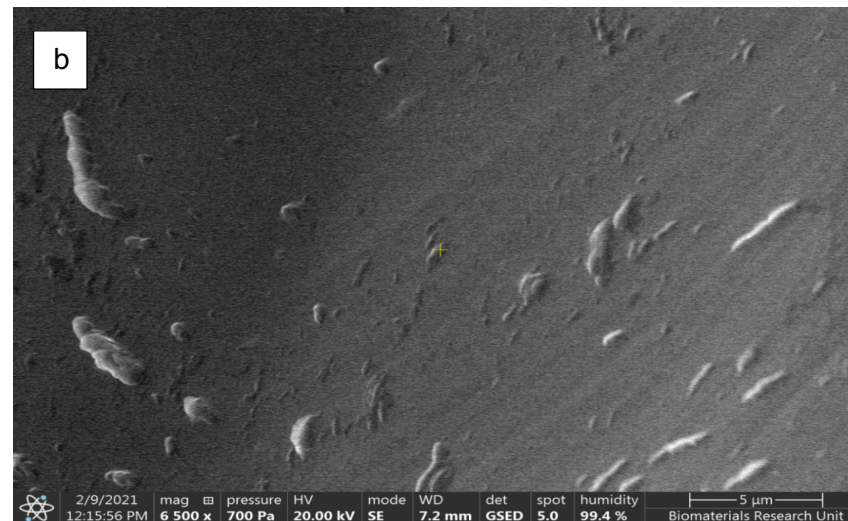
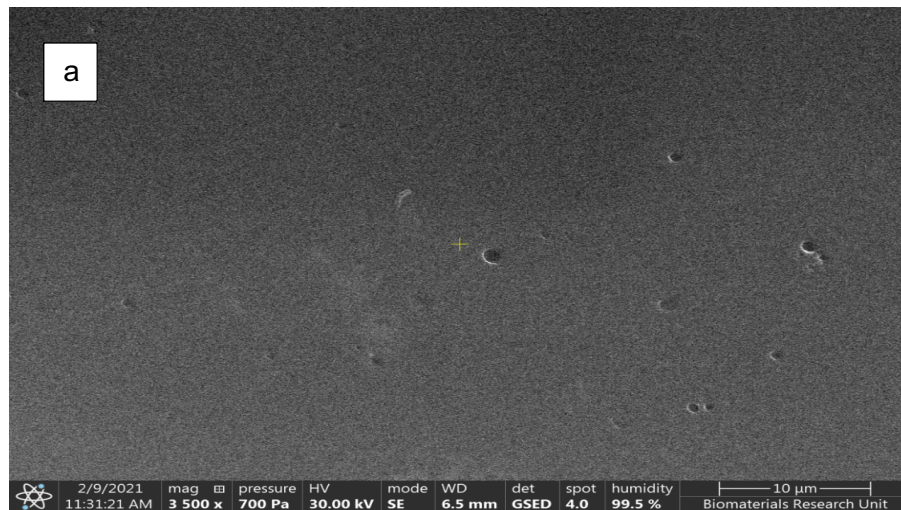
Images a) and c) are of the surface of the hydrogel, images b) and d) are of the cross section, image b) shows the corner of the hydrogel.

Table 7.8 Hydrogel E1 from Set 2



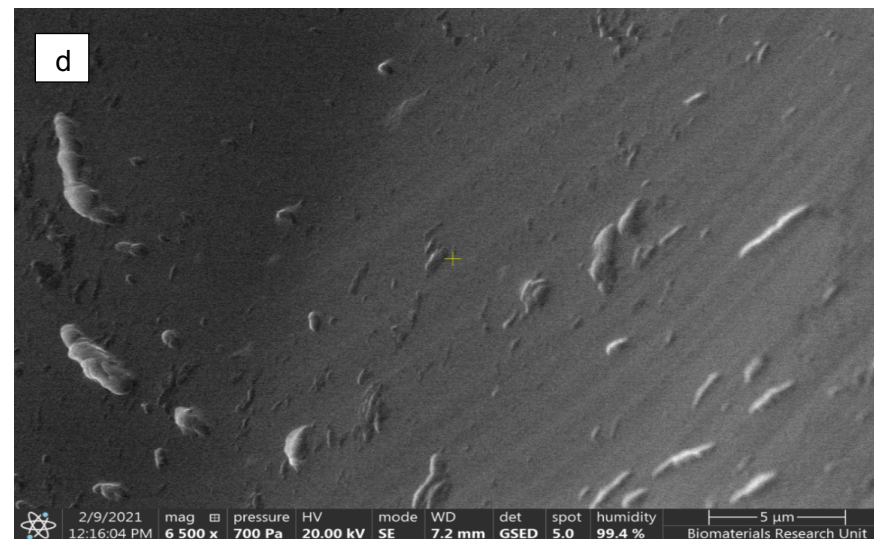
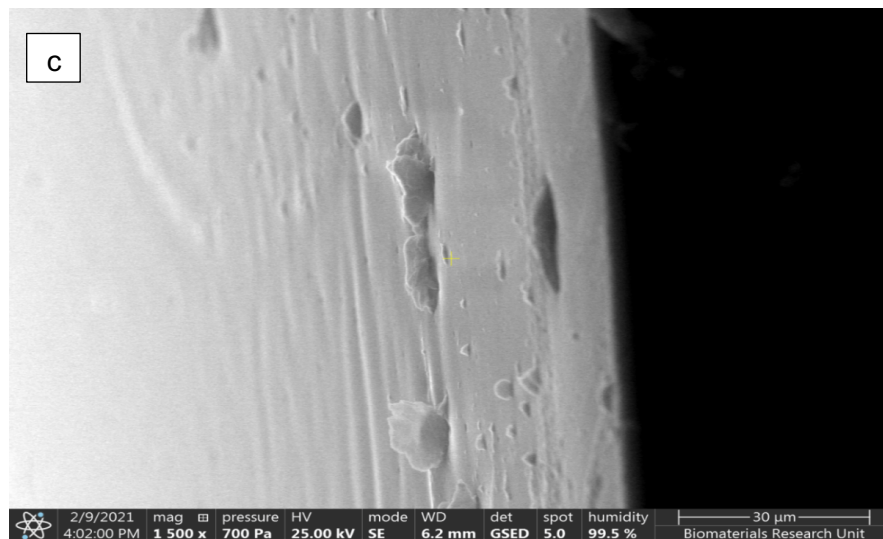
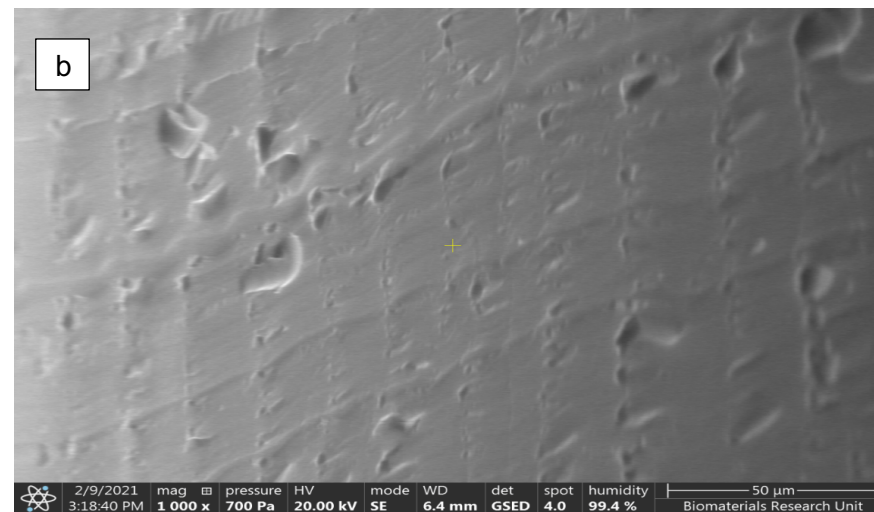
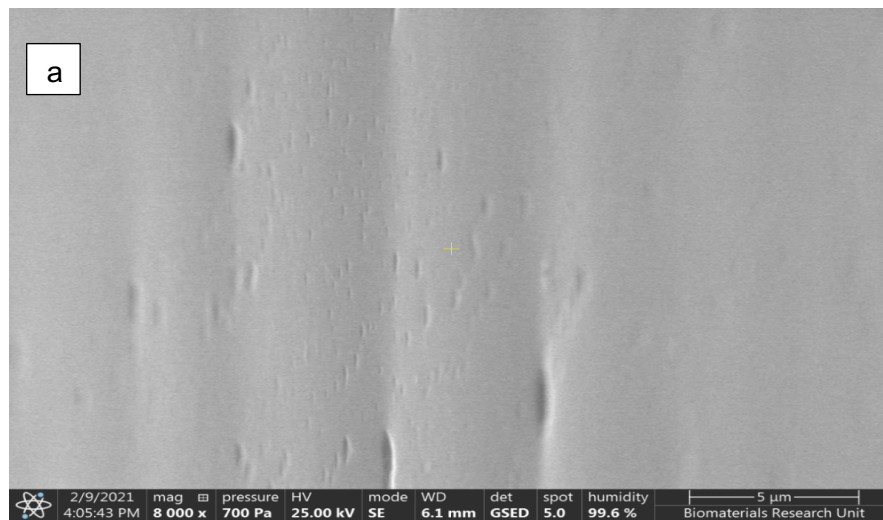
Images a) and c) are of the surface of the hydrogel, images b) and d) are of the cross section, image d) shows the corner of the hydrogel.

Table 7.9 Hydrogel E4 from Set 3



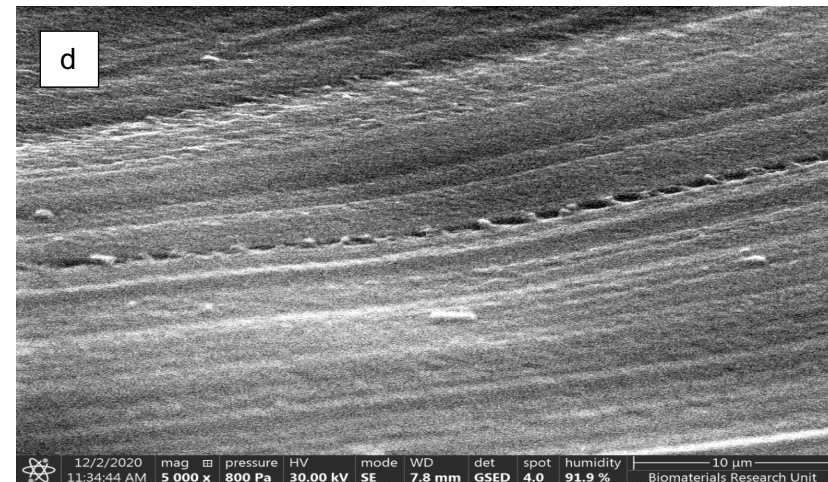
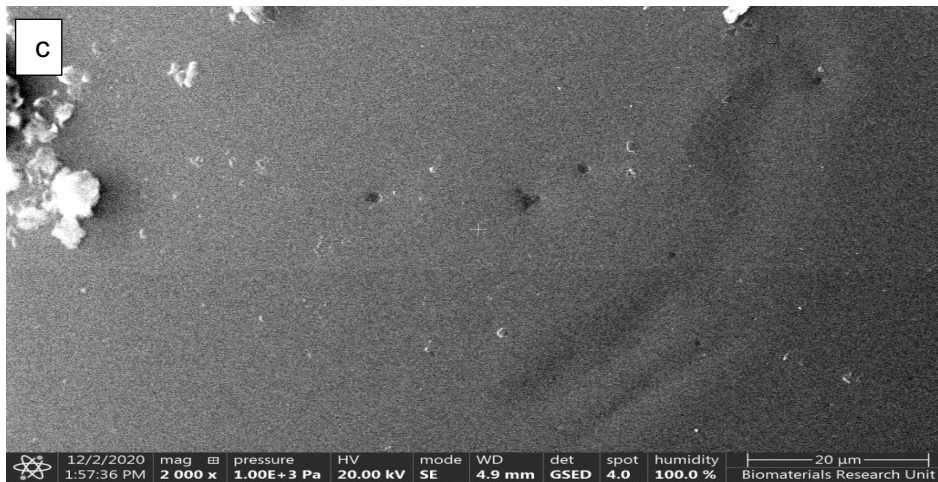
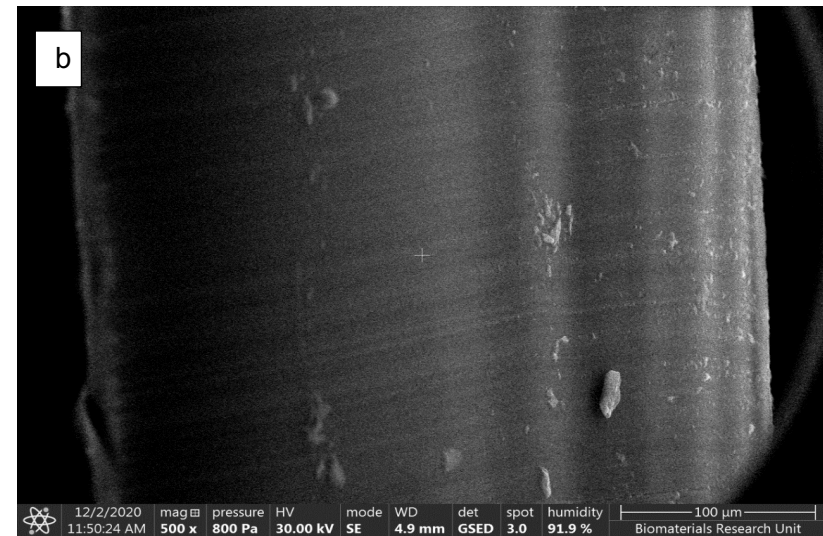
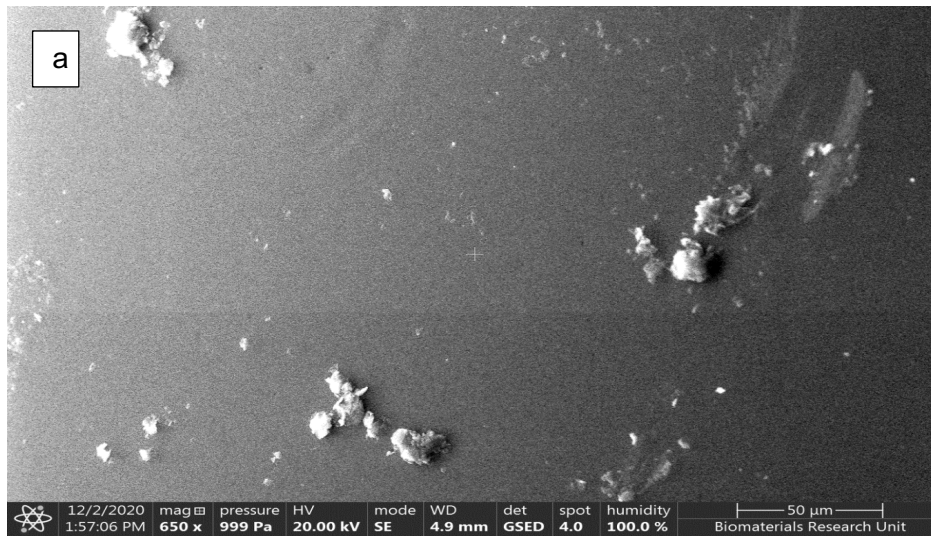
Images a) and c) are of the surface of the hydrogel, images b) and d) are of the cross section, image c) shows a dent in the surface of the hydrogel.

Table 7.10 Hydrogel E6 from Set 3



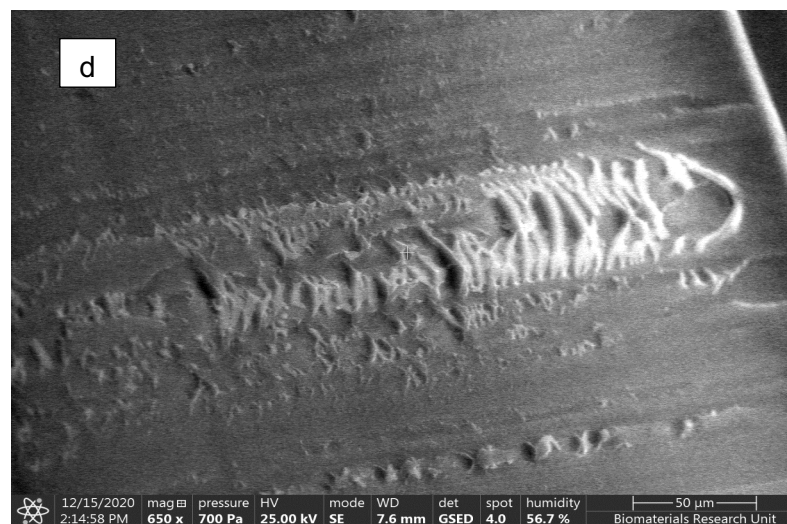
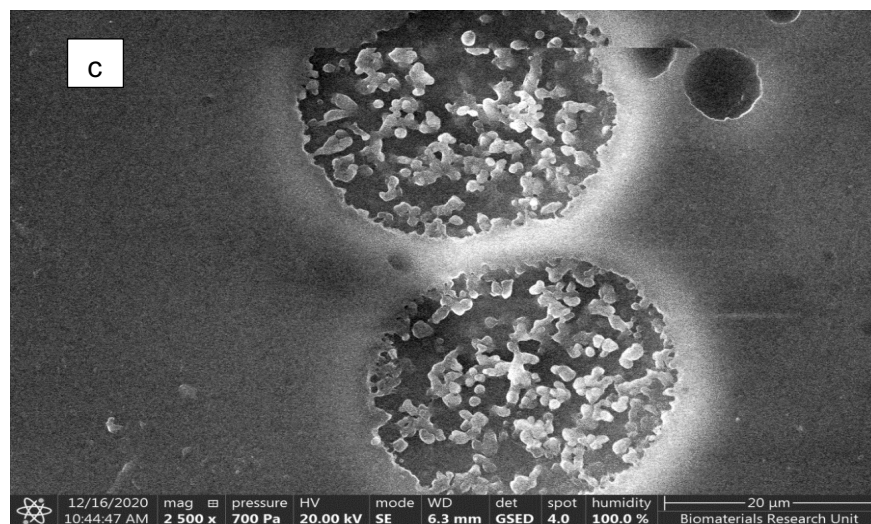
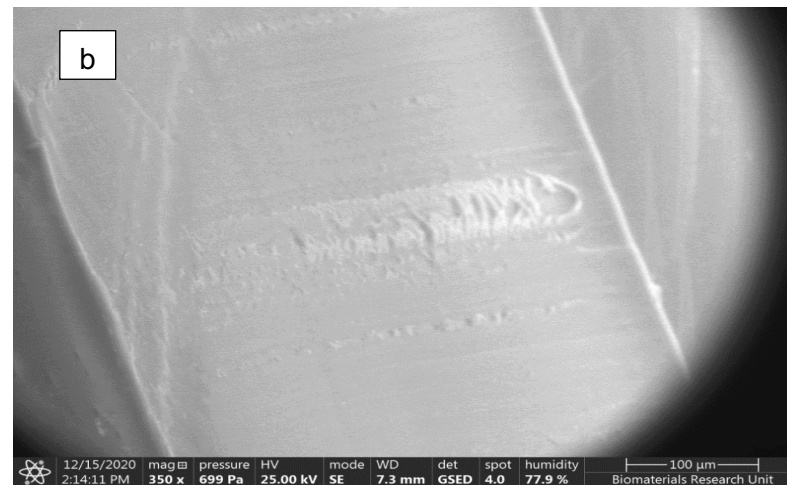
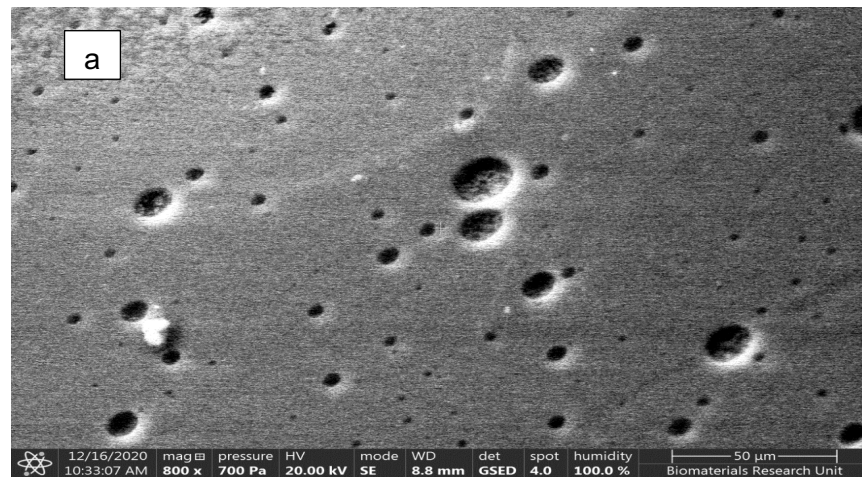
Images a) and c) are of the surface of the hydrogel, images b) and d) are of the cross section, image c) shows the corner of the hydrogel.

Table 7.11 Hydrogel F1 from Set 1



Images a) and c) are of the surface of the hydrogel, images b) and d) are of the cross section.

Table 7.12 Hydrogel F1 from Set 2



Images a) and c) are of the surface of the hydrogel, images b) and d) are of the cross section. Images a) and c) show craters in the surface of the hydrogel

7.3 Discussion

7.3.1 ESEM Image Interpretation & Phase Separation

In silicone-based hydrogels, it is a generally accepted notion that there will be formation of two separate phases: the hydrophilic phase and the silicone phase (hydrophobic phase) due to the immiscibility of the monomers based on their water-attracting properties. Silicone is typically included in hydrogel formulations to increase the oxygen permeability of the gel. However, this addition comes at the expense of water content due to the hydrophobic nature of the silicone-based monomer. To boost the water absorption ability of the hydrogel, hydrophilic monomers including DMA and NVP are added to the formulation to increase the water-attracting nature of the hydrogel, which in turn should increase its water content.

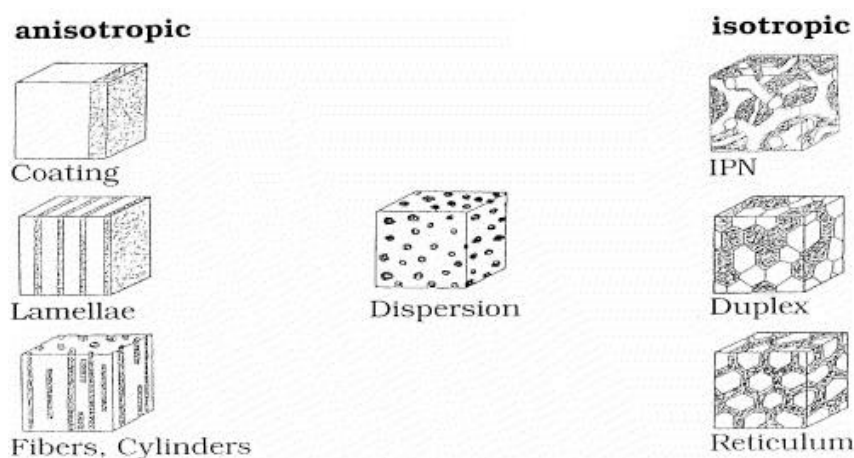


Figure 7.3 various morphologies a phased hydrogel could express (source: Nicolson & Vogt, 2001)

Polymeric membranes can be categorised into two classes: isotropic and anisotropic membranes. Isotropic membranes have a uniform composition throughout and a decrease in membrane thickness is correlated with an increase in permeation rate. Anisotropic membranes have a number of layers with different structures and permeability capabilities. Such a membrane often consists of a permselective layer and support-providing substructure.

There are three different types of isotropic membranes:

- Microporous: separation of molecules via this membrane occurs based on pore size and the molecular size of eluting substances.
- Non-porous (dense): permeation with these membrane types occurs by diffusion driven by pressure, concentration and electrical potential gradient. Separation occurs based on the diffusivity and solubility of the membrane material.
- Electrically-charged: this membrane can also be referred to as an ion-exchange membrane in which separation occurs based on the charge of the eluting substance.

Based on the permeation behaviour exhibited by the hydrogels as well as their physical appearance as shown via ESEM imagery, it is thought that the hydrogels synthesised in this project fall under microporous and non-porous isotropic membrane classification.

Hydrogels E1 and F1 from set 1 as well as hydrogels E4 and E6 from set 3 appear to have a single-phase morphology due to the smooth appearance of their surfaces and cross-sections in the images derived from ESEM (see tables 7.7, 7.11, 7.9 to 7.10). A study conducted by Sharma et al (2019) came to a similar conclusion regarding their hydrogels. They attributed the occurrence of phase separation to the appearance of dark spots on images, which can also be said for hydrogels E1 and F1 from set 2 (see tables 7.8 & 7.12).

In literature, it is highly uncommon for papers that discuss the connection between morphology and permeability in silicone hydrogels to be referring to the permeability of electrolytes. Rather, the focus looks at the effects of morphology on the permeability of oxygen through the hydrogel. With that in mind, a number of the references included in this sub-chapter refer to the permeability of oxygen.

It is important to understand how the structure of the hydrogel directly influences the parameters of the hydrogel, including permeability and whether these structural changes indicate the permselectivity of the hydrogels and to what degree they possess this quality.

Phase separation occurs when the cohesive interactions between chemically identical molecules overpowers the adhesive interactions between chemically different molecules (Nicolson & Vogt, 2001). Seeing as silicone-based hydrogels are commonly utilised as contact lenses, optical clarity is a requirement. To achieve this, these hydrogels have to be homogenous at scales of 100 nm and above. Phase separation may occur at a small scale but overall, homogeneity is required and the morphology greatly affects permeability (Wu et al, 2021).

The homo- and heterogeneity of the hydrogels was revealed via ESEM imaging. Many stipulations can be drawn from the images but it is important to understand the complexities of such imaging, how these images can be affected by external factors separate from the chemical composition of the hydrogels such as the distortion of captured images taken at the edge of the lens, the sample history (introduction of impurities) and how this can create or exaggerate visual effects that may or may not be representative of the hydrogel sample being visualised.

Hydrogel E4 of set 3: the smoothness of the hydrogel as seen in image 7.4 indicates the hydrogel may possess a degree of homogeneity. This homogeneity is seen at both the surface and cross-section of most of the hydrogels analysed using ESEM. At the 100µm viewing range, the surface of hydrogel E4 of set 3 appears to be smooth with no obvious signs of phase separation. In image 7.4, the edge of the sample can be seen (see arrow).

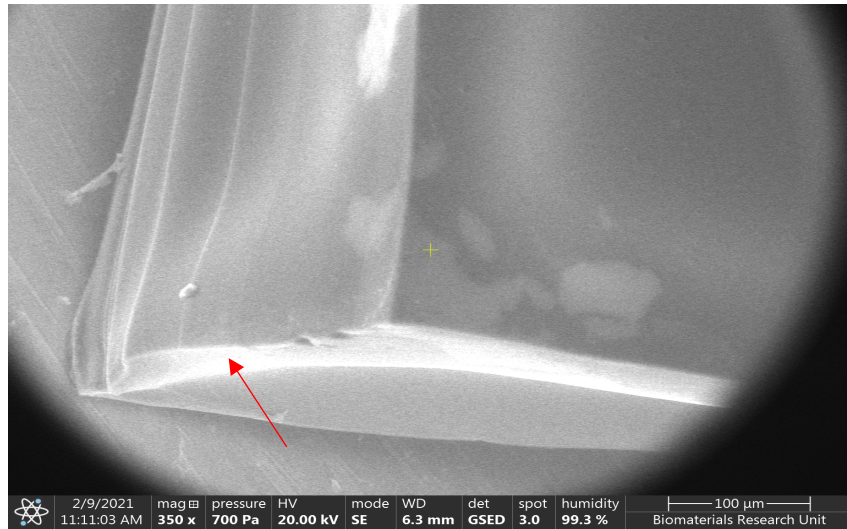


Image 7.4 hydrogel E4 of set 3, surface corner (image source: author's own)

A closer view of the hydrogel at 50µm also reveals a relatively smooth and homogenous hydrogel surface as well as the appearance of indentations (see arrow) on the surface as seen in image 7.5.

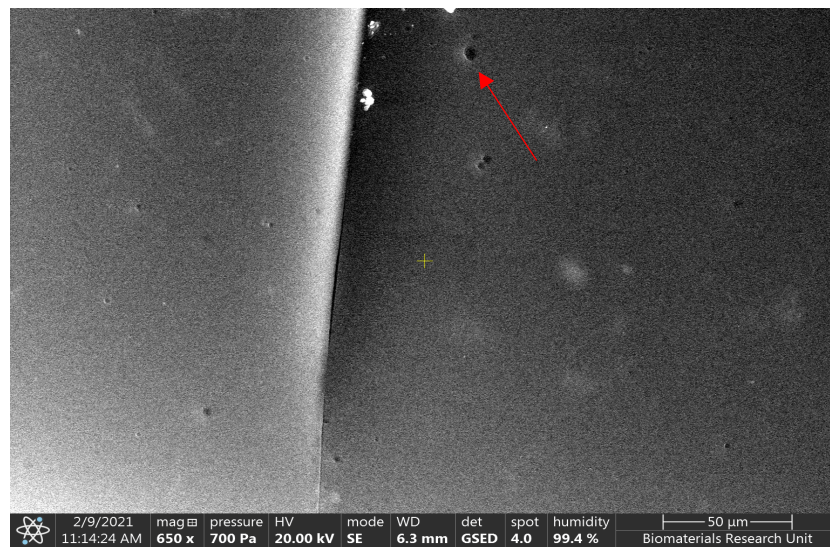


Image 7.5 hydrogel E4 of set 3, surface view at 50µm (image source: author's own)

At 10µm, these indentations (see arrows) become more evident. Surrounding areas on the hydrogel also appear smooth, the homogeneity of the hydrogel remaining evident.

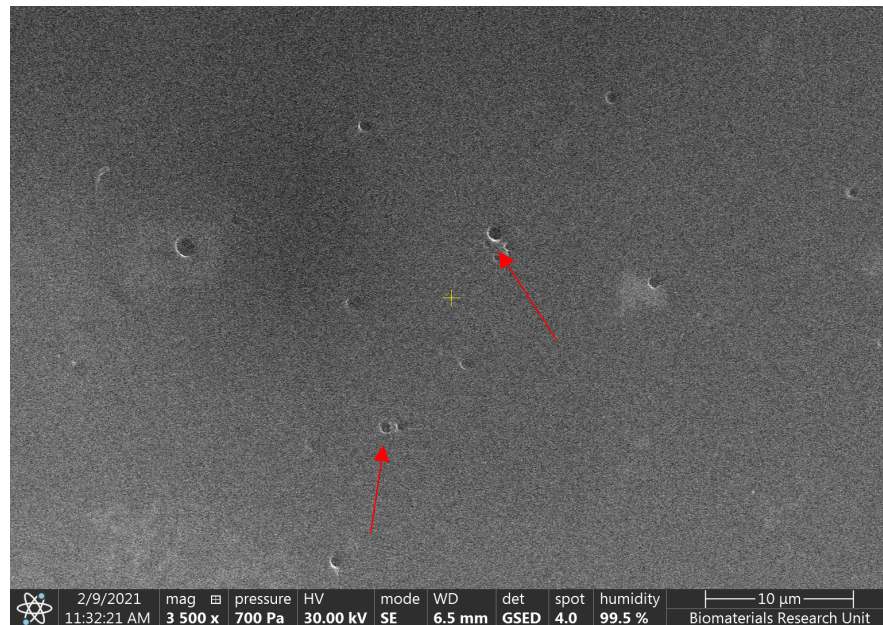
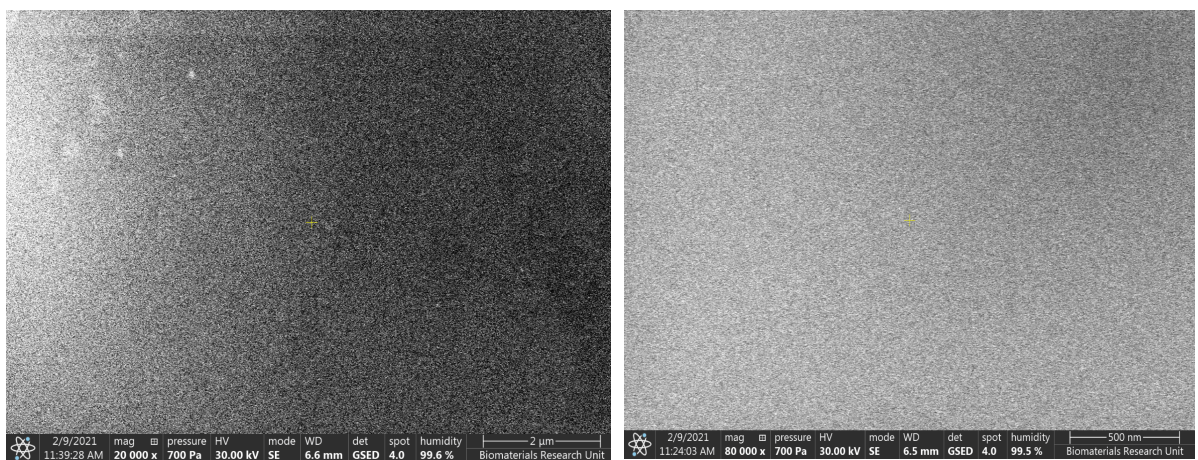


Image 7.6 hydrogel E4 of set 3, surface view at 10µm (image source: author's own)

However, at 1µm and 500nm, it may appear to be homogenous but the highly speckled nature of the images raises questions about the occurrence of the phase separation that seems to be inevitable in the case of silicone-based hydrogels, no matter how small it may be. The degree of this separation appears to be smaller in comparison with other hydrogels, mentioned further on in the discussion.



Images 7.7 & 7.8 (L-R): hydrogel E4 of set 3, surface view at 2µm & 500nm (image source: author's own)

A similar occurrence is seen in the surface images of hydrogel E6 also of set 3. The appearance or lack thereof of phase separation between the hydrophilic and hydrophobic regions, as indicated by the smoothness of the surface, seems minimal and the hydrogel is also optically clear, the same can be said about hydrogel E4. This backs the notion brought forward by Wu et al (2021) that homogeneity of the hydrogel is required at the larger scale to appear clear as well as being an indication of minimal phase separation on the smaller scale.

Hydrogel E1 of set 2: in the case of hydrogel E1 of set 2, the surface reveals the appearance of tiny spheres clustered together to form the body of the hydrogel. This may be a key indication of phase

separation occurring in this particular hydrogel. This pattern repeats itself throughout the entirety of the hydrogel seen at all levels of visibility afforded by the microscopic abilities of the ESEM analytical technique.

At 100 μm , there are clear and distinct spherical clusters that make up the surface. The edge of the hydrogel sample can be seen in the image below (see arrow).

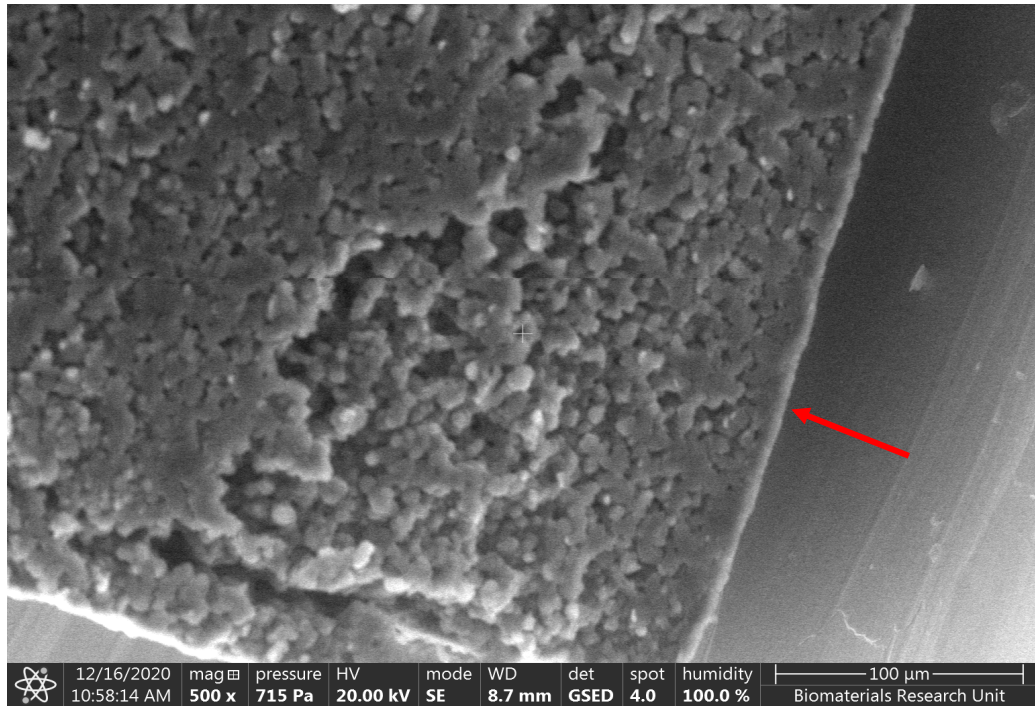


Image 7.9 hydrogel E1 of set 2, surface corner at 100 μm (image source: author's own)

This spherical effect continues to reveal itself as magnification increases, as shown in the image below, looking at the surface of the hydrogel at 50 μm .

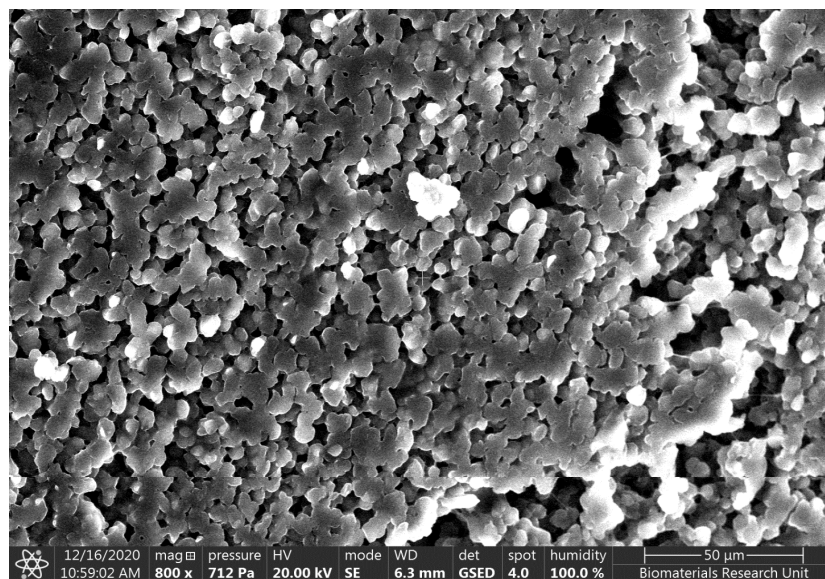
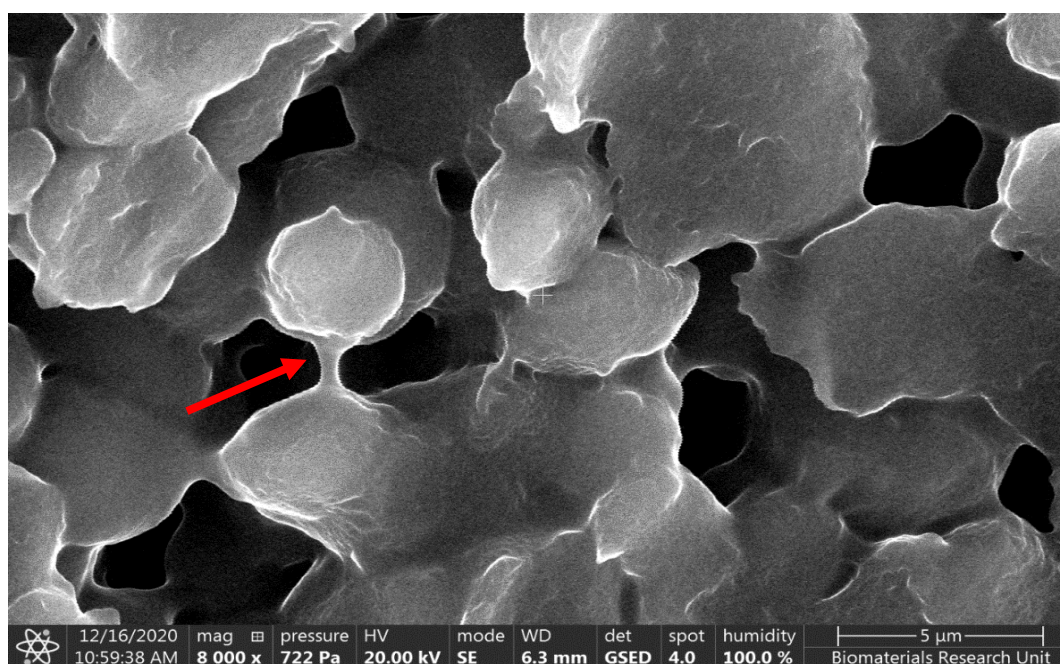
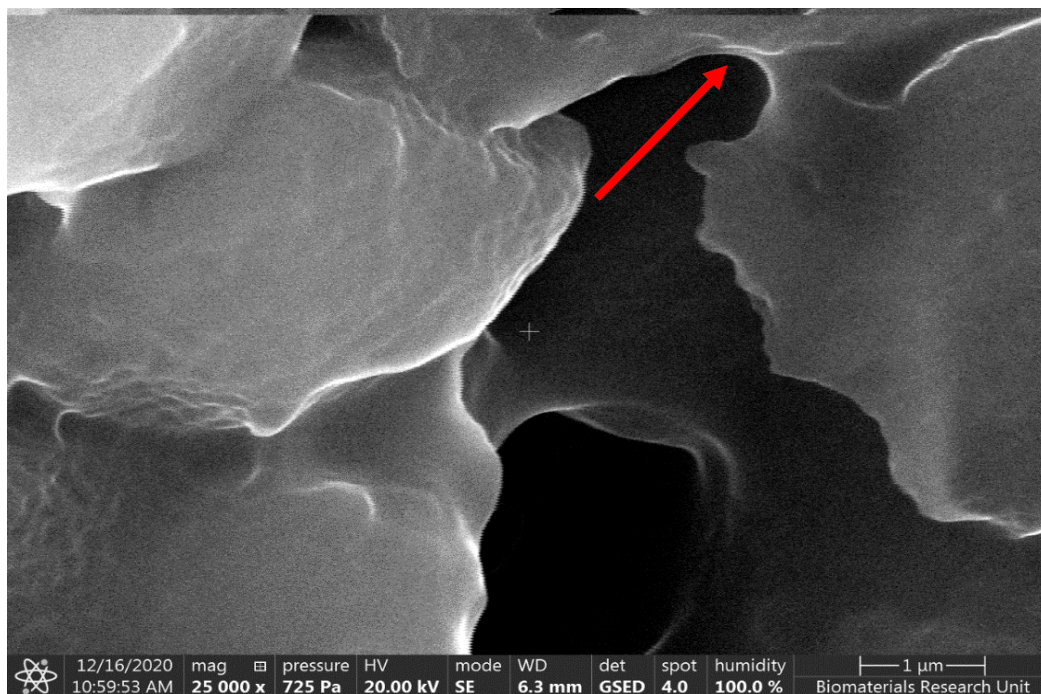


Image 7.10 hydrogel E1 of set 2, surface view at 50 μm (image source: author's own)

These spheres may be an indication of the heterogeneity of the hydrogel when compared against images derived from other hydrogels as previously shown. The spherical nature of the pattern is confirmed as the viewing range of the images increases to 5 and 1 μ m as shown below. The spheres also seem to be connected (see arrow).



Images 7.11 & 7.12 (L-R): hydrogel E1 of set 2, surface view at 5 μ m & 1 μ m (image source: author's own)

The lack of apparent homogeneity on all scales of this hydrogel resulted in an optically-opaque hydrogel and this was the case for all the E1 formulations from sets 1 to 3, providing insight to the micro-arrangement of the monomers NVP and TRIS when used in a formulation together in the absence of DMA.

Hydrogel F1 of set 2: ESEM images of this hydrogel revealed patterns that had been seen previously in hydrogel E4 of set 3 and hydrogel E1 of set 2.

At 100 μm , the surface of the hydrogel appeared relatively smooth with the addition of indentions. These indentions varied in size but remained in a circular shape however, some of these indentions appeared “empty” (see red arrow) whilst the larger ones appeared as if they contained material (see yellow arrow).

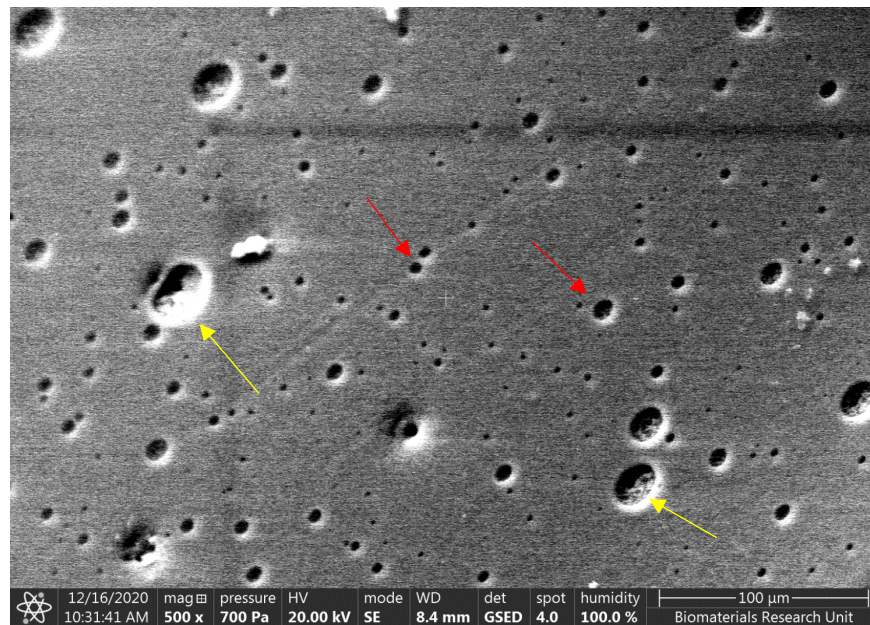


Image 7.13 hydrogel F1 of set 2, surface view at 100 μm (image source: author's own)

Taking a closer look at these indentions – at 50 μm – revealed the presence of the same spherical cluster pattern (see yellow arrow) that was seen throughout the entirety of hydrogel E1 of the same set.

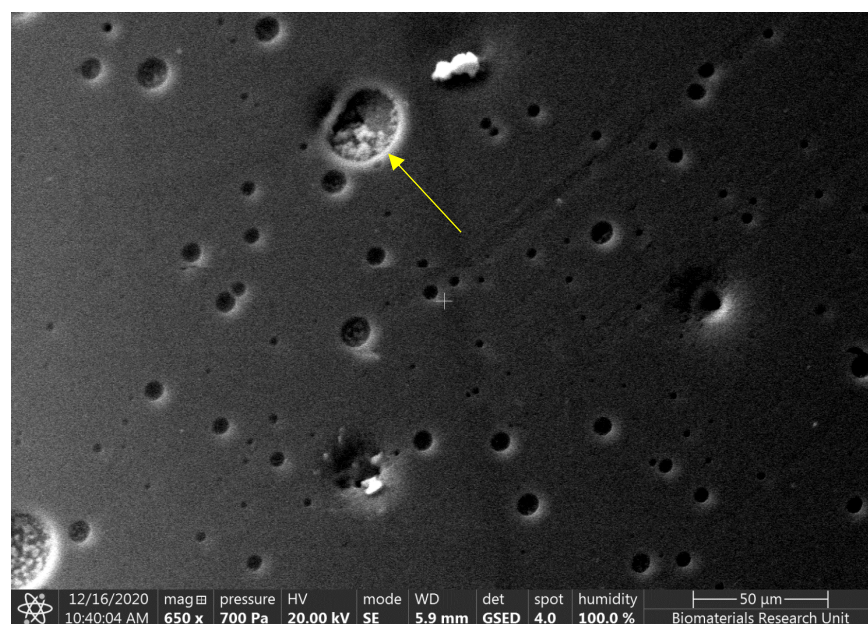
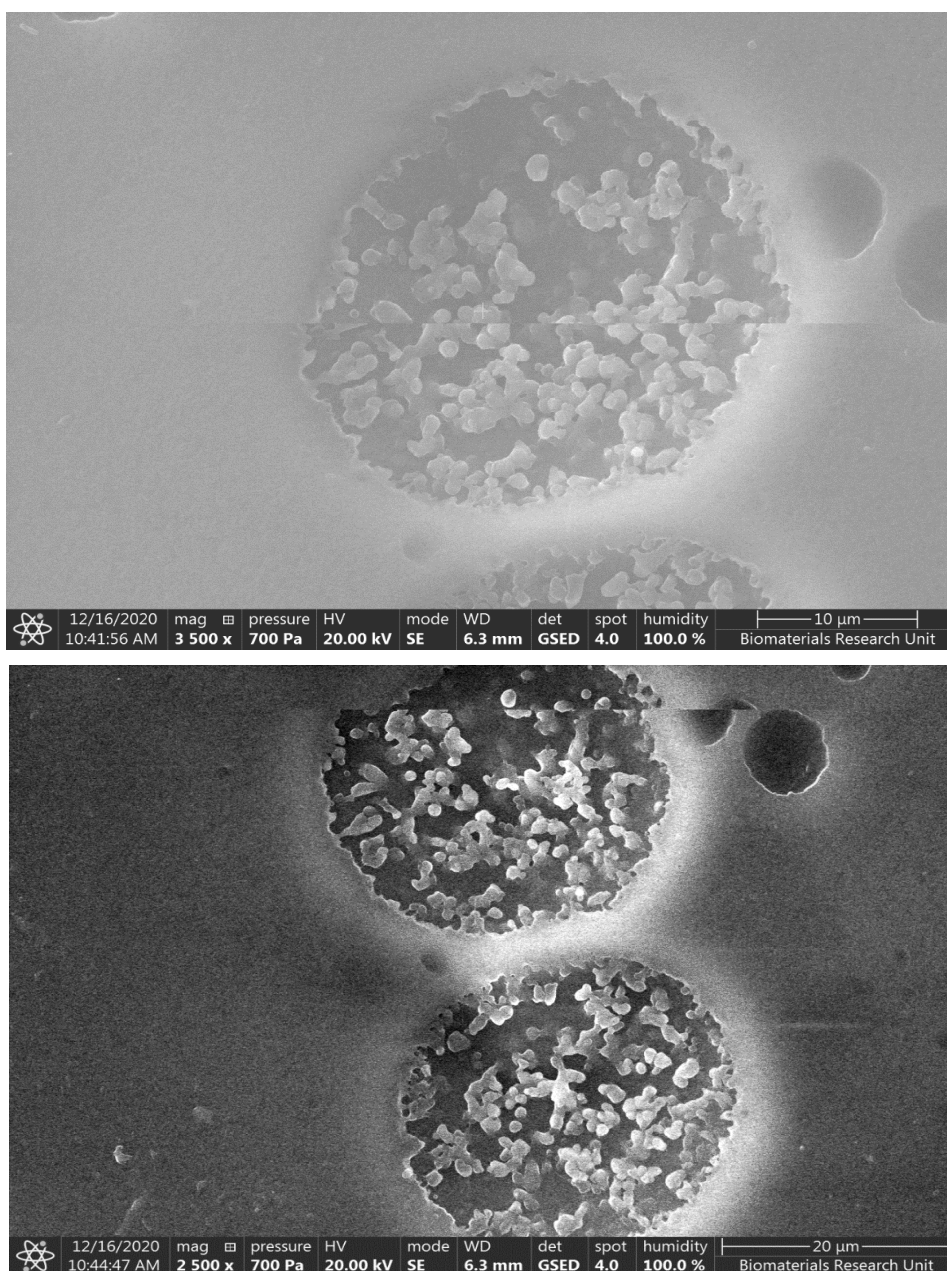


Image 7.14 hydrogel F1 of set 2, surface view at 50 μm (image source: author's own)

Looking within these indentations further reveals the spherical cluster again at a closer view which may be an indication of separation happening between the hydrophilic monomer and the siloxane monomer but just below the surface of the hydrogel.



Images 7.15 & 7.16 (L-R) surface view of hydrogel F1 set 2 + magnified view of same surface at 20 & 10µm respectively (image source: author's own)

Optically, hydrogel F1 is just on the brink of appearing hazy but can still be seen through. The presence of the spherical pattern in addition to the apparent homogeneity of the surface could be the underlying reason for this.

It is safe to assume these clusters seen in hydrogels E1 and F1 of set 2 are caused by the silicone-based monomer as Seitz et al (2017) found randomly distributed granular silicone domains in the >10nm size range when analysing silicone hydrogels using small-angle X-ray scattering (SAXS), another

analytical technique used to understand the morphology of silicone hydrogels based on their nanoscale density differences.

Both hydrogels E1 and F1 have the same amount of NVP in their formulation, however F1 has a considerably higher amount of TRIS. The re-occurrence of this pattern in both the hydrogels may speak to the polymerisation reaction between NVP and TRIS under the reaction conditions of set 2 (a post-cure but no inclusion of a diluent) and how this results in distinct phase separation but to different degrees. This may be caused by the low incorporation of NVP into the polymer chain due to its low reactivity ratio. Post-cures are often used to improve the polymerisation of monomers like NVP to increase its presence in the final polymer structure. As listed in Table 7.13, hydrogel F1 appears to be on the precipice of haziness whilst E1 appears entirely opaque, also an indication of the different levels of phase separation within the hydrogels.

7.3.2 The relationship between optical clarity & morphology

In addition to the degree of homogeneity, the optical clarity of the hydrogels can also indicate the degree of hydration of the hydrogel structure when encountering water for the first time. An opaque hydrogel such as E1 indicates that its polymerisation reaction could have been homogenous but the hydration of its polymer network was not, resulting in phase separation between the polymer and primary attached water. A clear gel, like the majority of the hydrogels synthesised, suggest both the polymerisation and hydration were homogenous which reduces the formation of phases.

On an individual basis, the siloxane monomer – TRIS – and hydrophilic monomers – DMA and NVP – are clear/clear in appearance with a low refractive index, meaning light entering the substance will not change direction as much when compared to a substance with a higher refractive index (Saez-Martinez et al, 2020). For context, water has a refractive index of 1.33 whilst TRIS has an index of 1.41, NVP has an index of 1.51 and DMA has an index of 1.47. However, it is known that co-polymerisations between these monomers can cause phase separation between the hydrophobic silicone regions and hydrophilic regions. When such a co-polymerised hydrogel is brought into contact with water, the physical appearance of the hydrogel becomes an indicator of this phase separation. Depending on the size of the phasing, the hydrogels can appear hazy or opaque. The wavelength of visible light is 450 nm and when hydrogels appear opaque, it indicates that the hydrogel cannot absorb wavelengths around or above this hence, it reflects it. An opaque hydrogel also indicates that there are refractive index differences between the different phases within the gel and visible light that disallow for the passage of this visible light through the hydrogel.

Table 7.13 descriptions of the physical appearance of each hydrogel

Hydrogel	Set 1	Set 2	Set 3
E1	opaque	opaque	opaque
E2	hazy	clear	onset of haziness
E3	clear	clear	clear
E4	clear	clear	clear
E5	clear	clear	clear
E6	clear	clear	clear
E7	clear	clear	clear
F1	onset of haziness	onset of haziness	hazy
F2	opaque	opaque	opaque
F3	clear	clear	clear

Sharma et al (2019) found that hydrogels synthesised from 2-hydroxyethyl methacrylate (HEMA) were unable to form optically clear hydrogels when polymerised with TRIS alone. The study found that the DMA monomer had to be included in the formulation of the hydrogel in equal proportion to the HEMA monomer in order to produce a clear gel that also showed no evidence of micro-phase separation. A similar scenario was seen in hydrogels E4 and E6 of set 3. Focusing on hydrogel E4, whose formulation included the hydrophilic monomers NVP and DMA in equal proportions of 30% each in conjunction with TRIS at 35%: although optically clear gels were achieved using differing NVP-DMA-TRIS ratios in formulation, the lack of phase separation showcased by hydrogel E4 (see images 7.5-7.8) speaks to the polymerisation reaction between DMA and TRIS that minimises the formation of these phases.

In the same study, Sharma et al (2019) found that utilising a different polymerisation technique such as solution polymerisation of the monomers HEMA, TRIS and DMA with ethylene glycol dimethacrylate (EGDMA) as a cross-linker resulted in a hydrogel with no evidence of phase separation whereas the same combination of monomers and cross-linker in a bulk polymerisation reaction resulted in phase separation. However, this project has demonstrated that it may be possible to produce a hydrogel without evident phase separation using bulk free-radical polymerisation.

Diffusion through a polymer is influenced mainly by the free volume of the hydrogel and its morphology (Tao et al, 2017). Free volume is one of the three theoretical frameworks upon which the diffusion of solutes in hydrogels are modelled. The remaining two include the hydrodynamic theory which proposes diffusion depends on the friction between the diffusing solute and the hydrogel matrix; and obstruction theory which assumes the polymer matrix acts as a barrier for the diffusion of the solute within a liquid (Axpe et al, 2019). The free volume theory assumes that the solute is transported via dynamic empty spaces between molecules and this would be directly influenced by the feed composition of the hydrogels during polymerisation. Even though the same hydrophilic and silicone components were utilised for the hydrogels, the specific amounts in their feed compositions differed, suggesting both free volume and morphology are at play when determining the gels' varying diffusion coefficients/abilities.

7.3.3 Elemental compositions: EDX

In order to understand how the feed formulation used during polymerisation translates to the actual composition of the final hydrogel, it is important to calculate the theoretical composition of the hydrogels. The monomers used were composed of carbon, oxygen, hydrogen, nitrogen and silicon. Hydrogen is not included in the elemental data tables 7.3-7.6 as EDX as an analytical technique is used to detect elements with an electron shell above K. The K-shell in relation to hydrogen contains one electron which is involved with covalent bonding (Nordholm & Bacskay, 2020).

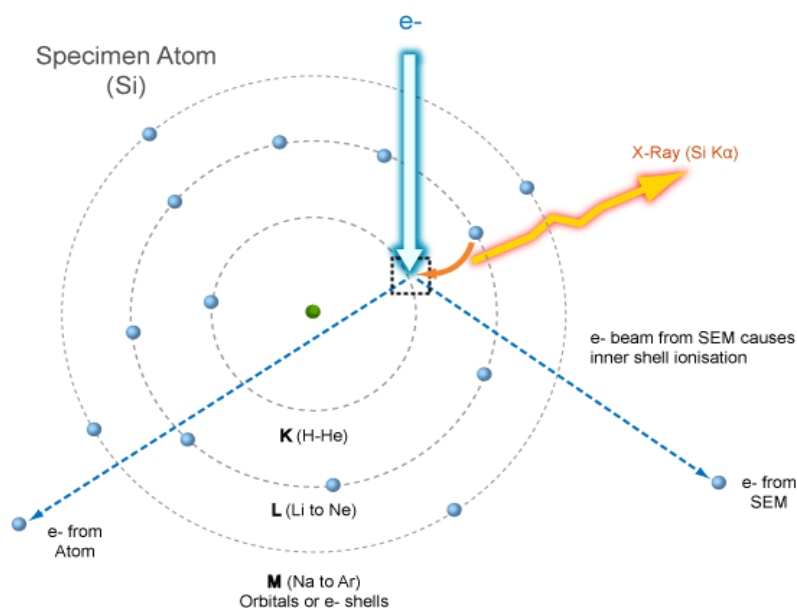


Image 7.17 schematic detailing the valence shells for different elements and the energy transfer that occurs during ionisation (image source: Microscopy Australia, 2014)

These theoretical compositions can be used to cross-check values derived from analytical techniques such as EDX and XPS. However, these compositions assume a number of parameters including that the hydrogels are homogenous and the entirety of the feed composition during hydrogel synthesis has been incorporated into the final polymer. This is unlikely, although the use of a post-cure increases the chances of monomer incorporation, specifically that of NVP and DMA. Lastly, theoretical compositions are only representative of the bulk of the hydrogel and less so of the surface.

The theoretical compositions were calculated based on the monomers used in each hydrogel's composition. Hydrogels E4 and E6 made use of all monomers: DMA, NVP and TRIS whilst hydrogels E1, E7 and F1 made use of either DMA or NVP in addition to TRIS. With that in mind, Table 7.14 details the theoretical compositions of the aforementioned hydrogels.

Table 7.14 theoretical compositions of hydrogels E1, E4, E6, E7 & F1 in a dehydrated state

Element	Hydrogels E4 & E6 (%)	Hydrogels E1, E7 & F1 (%)
Carbon	46.2	56.5
Nitrogen	3.6	3.1
Oxygen	28.7	21.5
Silicon	21.6	18.9

Beginning with silicon, it was expected that the amount of this element would be considerably greater at the surface of the hydrogel than that of the cross-section mainly because of the hydrophobicity of the element. Polymer chains are flexible and rotate to reach a configuration that not only expends the least energy but also ensures the hydrophilic and hydrophobic groups along the chain are in conducive environments. With that in mind, EDX analysis revealing silicon was present in greater quantities at the surface than that of the cross-section fits the narrative, as shown in tables 7.1 and 7.2. This was the case for hydrogels E1 of sets 1 and 2 who presented a surface silicon composition of 17.8% and 14.9% respectively whilst their bulk silicon composition was 12.1% and 11.7%. Hydrogel E4 of set 3 showed a silicon composition of 10.8% at the surface and hydrogel E6 of the same set showed a surface composition of 16.3% whilst the bulk composition of the element for each hydrogel was 9.7% and 8.8% respectively.

In the case of hydrogel F1, the surface silicon composition of the set 1 hydrogel came to 15% and that of set 2 came to 18.8%. However, in set 1, the bulk amount of the element was higher than that of the surface at 20.2%. This could be caused by a number of reasons: during analysis, the hydrogel sample had to be cut for images of the cross-section to be taken. By cutting the hydrogel, this creates a new “surface” for silicone to reach, resulting in a higher amount of the hydrophobic element at this new surface than the original; another reason points to the feed composition of the F1 hydrogel itself - at 65% TRIS, it has the most of this silicon-rich monomer compared to the rest of the hydrogels of both the E and F series whose feed compositions consisted of 35% and 25% TRIS respectively. At almost double the TRIS content, it makes sense for the overall silicon composition of the F1 hydrogel, at both the surface and cross-section, to be higher than the majority of the hydrogels.

It was expected for nitrogen levels to be considerably lower than the rest of the elements due to the effect of dilution (nitrogen is soluble in water). This was relatively the case, especially in relation to the cross-section values for the element in each hydrogel. Zero nitrogen was detected at the cross-section of hydrogels E1 of set 1 and F1 of sets 1 & 2. Again, this fits the narrative: the water within the bulk of the hydrogel will undoubtedly be greater than that at the surface and so a greater degree of dilution is expected, seeing as the cross-section provides a snapshot view of the bulk of the hydrogel.

At the surface of hydrogel E1 of set 1, nitrogen made up 2.3% of its composition and with hydrogel F1 of the same set, it was considerably higher at 4.8%. In hydrogel E1 of set 2, 0.3% was detected at the cross-section and 1.57% at the surface. However, with the set 3 hydrogels E4 and E6, nitrogen was

detected, albeit below 10%, at both the surface and the cross-section. Nitrogen was detected at 6.9% at the surface of hydrogel E6 and 3.5% at its cross-section whilst 2.5% was detected at the surface of hydrogel E4 and 3.25% at the cross-section.

It is known, based on LogP values, that NVP has a lower incorporation rate into the polymer chain during polymerisation compared to DMA. LogP refers to the affinity a compound has for lipophilic substances. A negative LogP value indicates the monomer has an increased affinity for hydrophilic compounds whilst a positive LogP value indicates increased affinity for hydrophobic compounds. DMA, NVP and TRIS have LogP values of -0.77, 0.37 and 8.18 respectively (Leo & Hoekman, 1995). This results in hydrogels with considerably lower amounts of nitrogen when compared against their feed compositions. However, a post-cure is meant to increase this incorporation via providing the kinetic energy to boost said incorporation. Set 3 hydrogels were exposed to a post-cure in the presence of a diluent and its effects are seen in hydrogels E4 and E6 with their increased amounts of detected nitrogen at both the surface and cross-section.

7.3.3 Elemental compositions: XPS

XPS analysis was carried out on hydrogels E1, E4, E7 and F1 from sets 1-3 and so a side by side comparison from one set to the next is achievable.

As mentioned above, it was expected for silicon expression at the surface of the hydrogel to be considerably higher due to its hydrophobicity. The hydrogel with the highest amount of silicon overall was hydrogel F1 expectedly, due to its increased TRIS quantity in its feed composition. Set 2 produced the hydrogel with the highest amount of silicon at 11.9% whilst set 3 produced the least at 10.2%.

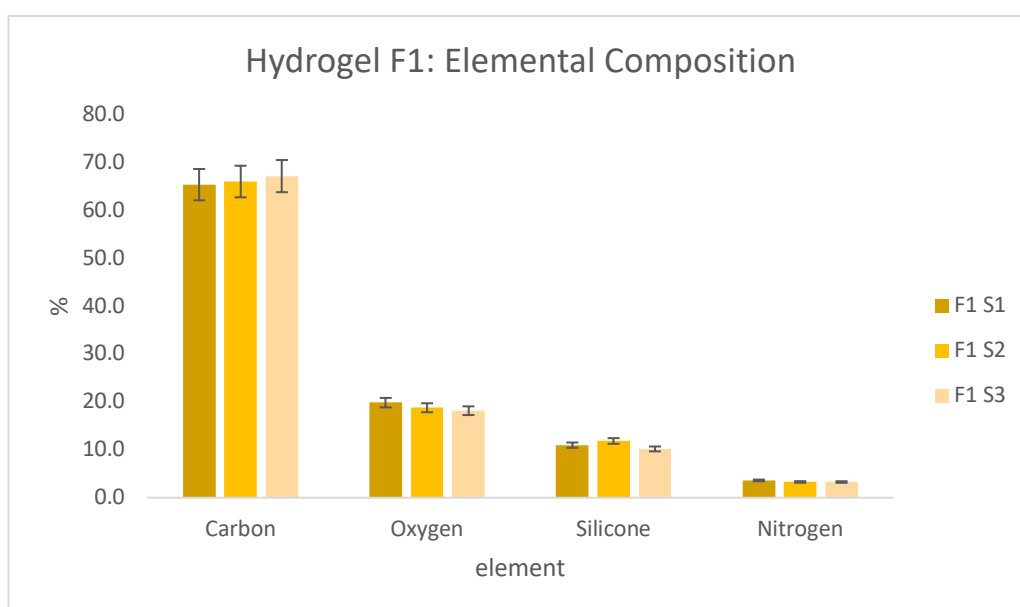


Figure 7.1 Hydrogel F1 (sets 1-3) surface elemental composition via XPS analysis

Noticeably, nitrogen content was the lowest in this hydrogel across all sets as seen in Figure 7.1, remaining constant at 3.3% in set 2 and 3 and peaking at 3.6% in set 1. This could also be attributed to

the low polymerisation rate of the NVP monomer which was the sole hydrophilic monomer in hydrogel F1's formulation. Carbon expression increased from sets 1 to 3 whilst oxygen expression decreased.

As previously mentioned, hydrogel F1 had the lowest nitrogen at its surface according to the XPS results and this was followed by hydrogel E1. The hydrogel also had the highest occurrence of nitrogen at its surface in set 2 at 5.5%. There was very little difference in the amount of nitrogen between sets 1 and 3, coming in at 5% and 4.9% respectively. This may be attributed to the same reason as F1: NVP being the sole hydrophilic monomer in its formulation thus the only source of nitrogen for the hydrogel.

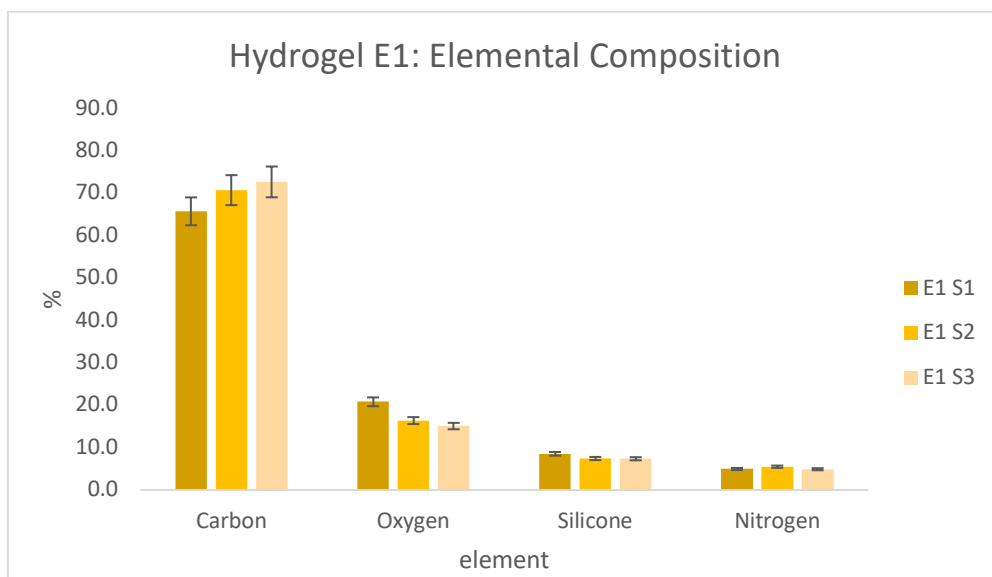


Figure 7.2 Hydrogel E1 (sets 1-3) surface elemental composition via XPS analysis

The expression of silicon in hydrogel E1 was the highest in set 1 at 8.5% and remained constant in sets 2 and 3 at 7.4%, as seen in Figure 7.2. Oxygen was at its highest in set 1 at 20.8% and dropping to 16.4% in set 2 then slightly lower to 15.1% in set 3. Carbon at the surface of hydrogel E1 saw an increase from sets 1 to 3. There was a 5% increase between sets 1 and 2, going from 65.7% to 70.7%. The increase between sets 2 and 3 was half of that, going from 70.7% to 72.6%.

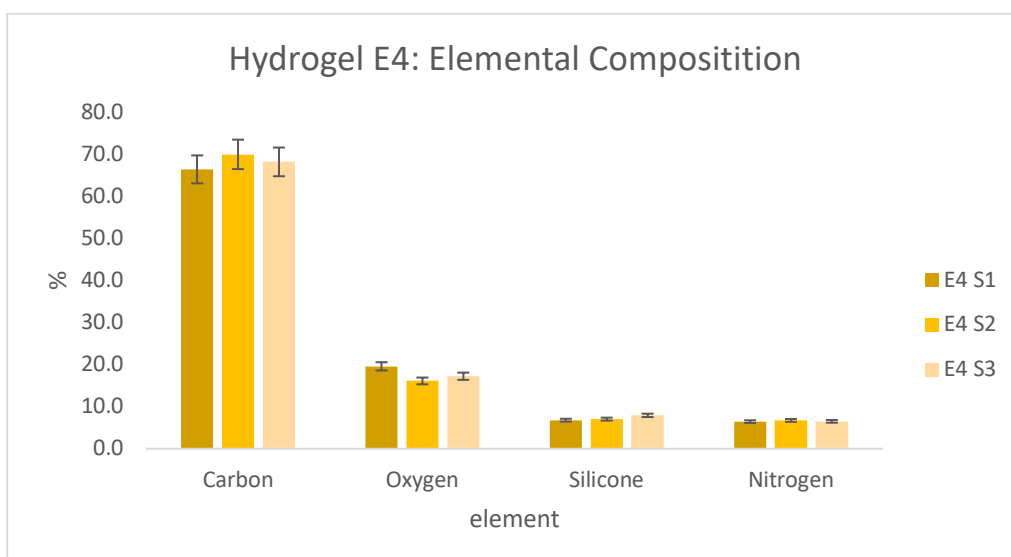


Figure 7.3 Hydrogel E4 (set 1-3) surface elemental composition via XPS analysis

Referring to Figure 7.3, the overall description of hydrogel E4's elemental composition was very similar to that of hydrogel E1 in that an increase in carbon from sets 1 to 3 occurred as a decrease in oxygen from sets 1 to 3. Nitrogen remained constant from set 1 to 2 at 6.5% and it was at its highest in set 3 at 6.8%. Silicone was at its highest in set 3 at 7.9% and at its lowest in set 1 at 6.8%.

Hydrogel E7 shows a deviation from the trend, in figure 7.4, of carbon increasing as oxygen decreases and no trend was noticed in terms of a correlation between other elements. Nitrogen was at its highest in set 3 at 8.7% which suggests DMA incorporation is considerably greater than NVP and is enhanced by a post-cure in the presence of a diluent. Set 2 which lacked a diluent but had a post-cure had the lowest nitrogen at 4.3%. With silicon, the amount almost doubled from sets 3 to 1 from 4.7% to 8.2%. Oxygen was at its highest in set 1 at 18.5% whilst carbon was at its highest in set 2 at 71.9%.

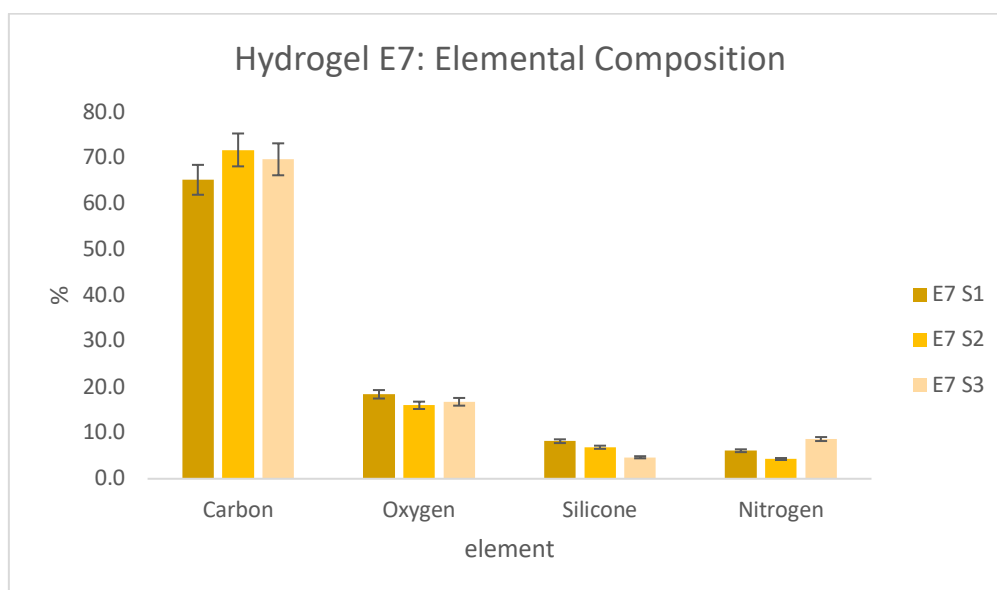


Figure 7.4 Hydrogel E7 (set 1-3) surface elemental composition via XPS analysis

7.3.4 The influence of reactivity ratios on monomer incorporation

The reactivity ratio of a monomer is a measure of the tendency for a monomer to show preference for insertion into a growing chain in which the last inserted unit on the polymer chain was the same, rather than the other monomer being used in the reaction (Tait & Barry, 1989).

These ratios are often represented as:

$$r_1 \cdot r_2 \tag{7.1}$$

When the sum of the reactivity ratios is equal to 1, the last monomer unit added onto the polymer chain does not influence the next unit to be added on, resulting in a random polymerisation. When the sum of the ratios is equal to 0, influence from the last monomer unit or second to last unit will be present but not as influential resulting in an alternating polymerisation. Lastly, when the sum of the ratios is more than 1, the last unit added to the chain will have overriding control on what unit is to be added next,

resulting in a block polymerisation. Examples of the random, alternating and block co-polymers are illustrated in Figure 7.5 with N representing the monomer NVP and D representing the monomer DMA.

$r_1 \cdot r_2 = 1$	random	DDNDNDNDNN
$r_1 \cdot r_2 < 1$ or $= 0$	alternating	DNDNDNDNDND
$r_1 \cdot r_2 > 1$	block	DDDDNDNDND

Figure 7.5 schematic representing different types of co-polymers influenced by reactivity ratios

During a free radical polymerisation reaction, when one monomer has a greater reactivity ratio than the other, the radical would prefer to add the more reactive monomer to the polymer chain. If the difference in reactivity ratios is large enough, long sequences of this more reactive monomer will make up the majority of the polymer chain (Rudin & Choi, 2012).

In the case of this project, the monomers in question would relate to NVP and DMA. Touchal et al (2004) investigated the reactivity ratios of DMA and NVP when used in tandem during a polymerisation reaction using a numerical integration model. They found that $r_{DMA} = 5.67$ whilst $r_{NVP} = 0.37$. This suggests the majority of the polymer chain in hydrophilic phases will be made up of DMA. Again, this is reflected in the low nitrogen levels seen across all the hydrogels at both the surface and cross-section. As mentioned above, a post-cure is meant to combat this low incorporation by providing the kinetic energy required to increase NVP attachment to the polymer chain which is reflected in the increased nitrogen levels of hydrogels E4 and E6 of set 3. Although DMA and NVP are both nitrogen-containing monomers, it is clear that only one source of nitrogen is majority at play in the hydrogels with significantly reduced nitrogen levels and that may be the otherwise dominant monomer of DMA.

It is thought that utilising siloxane groups – like those present in a monomer such as TRIS – in the bulk of a polymer, will result in a surface with a high expression of silicon, making the surfaces more hydrophobic than a conventional hydrogel (Teichroeb et al, 2008).

The formulation of hydrogel F1 contains considerably more TRIS than the rest of the hydrogels (65% compared to 35%) and the effects of this are documented in the XPS results. Hydrogel F1 has the highest silicon levels of all the hydrogels analysed using this analytical technique. Set 1 showed a silicon level of 11%, rising to 11.9% in set 2 then dropping in set 3 to 10.2%.

The effects of NVP/DMA incorporation on nitrogen and how this is affected by a post-cure were documented nicely in the case of hydrogel E7. Set 1 hydrogels made use of a diluent but were not subjected to a post-cure, set 2 gels did not contain a diluent but made use of a post-cure whilst set 3 made use of both. XPS showed that nitrogen made up 6.1% of hydrogel E7 of set 1. This dropped to 4.3% in set 2 then doubled in set 3 to 8.7%. Here, the effects of a post-cure and how it improves NVP incorporation to the polymer chain were seen. The reverse was seen in hydrogel E1 from sets 1 to 3 which saw an increase in nitrogen from sets 1 to 2 then a decrease in set 3. This could be attributed to the phase separation that is most likely occurring in this hydrogel, indicated by its opaque appearance.

7.4 Conclusion

Analytical techniques including EDX and XPS were used to determine the elemental composition of the hydrogels. Generally, EDX revealed that nitrogen levels at the cross-section was considerably lower or non-existent in set 2 hydrogels in comparison to the sets 1 and 3 hydrogels. Silicon content was generally higher at the surface than at the cross-section and this has been attributed to the hydrophobic nature of the monomer resulting in the polymer chains rotating to minimise silicon's interaction with bulk water.

XPS revealed less of a trend in regards to majority of the elements but in comparison with EDX showed a much lower oxygen and silicon percentage overall. However, disparities between the techniques were expected. Increased oxygen levels documented by either analytical technique may be due to increased cross-linking of the hydrogels by the cross-linking agent TEGDMA.

The generally low levels of nitrogen in the hydrogels can be attributed to the low polymerisation rate of the NVP monomer in comparison to DMA and TRIS which has been explained in terms of its reactivity ratios.

ESEM images showcased the phase separation occurring in hydrogel E1 of set 2 on a macro scale resulting in the opaque appearance of the gel. The distinct pattern seen in the magnified images of this hydrogel were also seen in hydrogel F1 of the same set. This corroborated the notion that phase separation is most likely to occur when the quantity of the DMA monomer in a formulation is less than that of NVP or when DMA is absent from a formulation altogether. It also confirmed that the optical clarity of a hydrogel is a direct indication of phase separation occurring at a micro-level within the polymer structure.

8 Summary & Future Works

8.1 Summary

The purpose of this project was to synthesise different varieties of silicone-based hydrogels with formulations inspired by those commonly utilised in contact lens manufacturing and determine certain parameters of these hydrogels including their water content, partition coefficient, permeability towards different salt ions and their morphology.

Two distinct series of hydrogels were synthesised: the E and F series. The E series hydrogels contained the hydrophilic monomers *N*-vinyl-2-pyrrolidone (NVP) and *N,N*-dimethylacrylamide (DMA) in alternating quantities as well as the hydrophobic silicon-containing monomer tris(trimethylsiloxy)-3-methylacryloxypropyl silane (TRIS) at a constant quantity. The F series hydrogels contained either the NVP or DMA monomer in addition to the TRIS monomer but the ratio of the monomers did not follow a strict regime like the E series. Both series made use of 2,2'-azobis(2-methylpropionitrile) (AIBN) and tetraethylene glycol dimethacrylate (TEGDMA) as initiator and cross-linker respectively. The hydrogels were also exposed to different reaction conditions, as denoted by the term 'sets', as described in Table 8.1. For each set, the post-cure and use of diluent were varied to establish whether these conditions would trigger different behaviours in the hydrogels.

Table 8.1 Synthesis conditions for each hydrogel set

Condition	Set 1	Set 2	Set 3
72-hour synthesis @ 60°C	Yes	Yes	Yes
3-hour post-cure @ 90°C	No	Yes	Yes
Use of 3-octanol as diluent	E series – yes F series – no	No	Yes

The choice of monomers was advantageous in that the formulation had already been used in the contact lens industry, meaning the synthesis of the hydrogels was likely to be successful but also, if the hydrogels were to be used in biomedical applications later, their safety and toxicology had already been established.

A series of characterisation experiments were conducted in order to understand the general behaviour of the hydrogels. The most important characteristic to determine was the water content of the hydrogels, as described in the third chapter of the thesis. The ability for hydrogels to meet human tissue without triggering immunological responses is also attributed to the water-retaining capability of the materials. It is also stated often that the permeability of a hydrogel is dictated by the amount of freezing water it contains. Freezing water is a type of water within hydrogels that freezes at 0 °C and has increased mobility within the polymer matrix. This water type as well as non-freezing and equilibrium water content were determined experimentally and their relationships with the permeation, partitioning and monomer content of the hydrogels investigated. It was determined that the TRIS-NVP-DMA formulation was G.Durowoju, PhD Thesis, Aston University 2022.

capable of producing a silicone-based hydrogel with an EWC within the range of 50-60%, regardless of the use of a diluent or not. The ratio of the hydrophilic monomers – DMA and NVP – proved to be important in relation to the equilibrium water content of the E series of hydrogels but less so with the freezing and non-freezing water contents. Patterns with the F series of hydrogels were less straightforward but notably, hydrogel F1 demonstrated an increase in its EWC from set 1 to 3 despite having the most hydrophobic formulation. Generally, the results highlighted that the hydrophilicity of the monomers may not be the sole source of influence in determining the water-absorbing abilities of a hydrogel.

Chapter four focused on the partition coefficient of the hydrogels, which describes the internal environment of a hydrogel by showcasing the ratio of salt ions that remain within it to that of its surroundings. Seeing as permeation can be described as an uptake and release process, understanding the partition coefficient of the hydrogels provided further insight to this behaviour. Overall, the set 2 hydrogels had the highest partition coefficients and this was displayed against all the salt ions (calcium, potassium, sodium and magnesium). The larger ions, calcium and magnesium, were partitioned the least in the E and F series hydrogels from the different reaction condition sets. The coefficient's relationship with water content and monomer content was established: the set 1 hydrogels showed that the partitioning of the larger salt ions decreased as EWC increased across the set. That was the most definitive trend between EWC and the partitioning behaviour of the hydrogels whilst trends with FWC/NFWC varied widely. Similarly to the relationship between monomer content and partitioning, trends varied between sets but it can be said that there were clear differences in partitioning behaviour between the E and F series hydrogels from sets 1-3. The hydrogels displayed ranges of behaviour between the salt ions, highlighting the varying potential applications for them.

There were two sets of permeation studies: single-salt and multiple-salt, described in chapters five and six of the thesis. The purpose of carrying out two sets of experiments was to compare the behaviour of the hydrogels when they were faced with permeating an individual salt versus a mixture at the same time, the latter being more representative of the real-life workloads the hydrogels could encounter if included in biomedical applications as a membrane. The permeation abilities of the different hydrogels were compared against each other and relationships between formally established parameters such as water content, partitioning and formulation were determined. There were slight variations with the order in which the hydrogels permeated the salt ions but the most common pattern on a single-salt basis was *potassium chloride* → *calcium chloride* → *sodium chloride* → *magnesium chloride* whilst on a multiple-salt basis, the hydrogels followed the order of *potassium chloride* → *sodium chloride* → *calcium chloride* → *magnesium chloride*, demonstrating the ability of the hydrogels to differentiate between the different ions and elute them according to their size and/or charge. Although the hydrogels with the larger water contents were not always the most permeable on either a single or multiple-salt basis, the hydrogel with the lowest water content (hydrogel F1) maintained its impermeability towards all the salts. Permeation relies on the diffusion of ions through the polymer matrix of the hydrogels and as the diffusion coefficients of the hydrogels increased, so did their single-salt permeation coefficients. Overall, the results showed that different formulations and different reaction conditions have the ability to produce hydrogels with varied permeation behaviours, suggesting their suitability for varied release and uptake processes.

Lastly, certain aspects of the physical morphology of the hydrogels were determined in chapter seven, the final results chapter of the thesis. With ESEM, the hope was to capture clear images that showed the occurrence of porous structures in the hydrogel macrostructure or the lack thereof. Images derived from ESEM imaging showed the variety of morphologies a hydrogel can possess when the formulation ratio differs as well as the reaction conditions. Some hydrogels showed indications of phase separation whereas the smoothness of images seen in others could be taken as homogeneity. EDX and XPS provided information relating to the elemental composition of the hydrogels which provided a better understanding of monomer incorporation during the polymerisation of the hydrogels. Expression of the silicon element tended to be increased at the surface compared to the bulk, highlighting its hydrophobic nature whilst overall low levels of nitrogen expression across the hydrogels suggested low incorporation of the NVP monomer.

8.2 Future Works

During the course of this project, there were three apparent opportunities to expand the scope. It would be beneficial to establish a different version of the set 1 F series hydrogels that maintained their formulation but included a diluent as well as a post-cure. As it stands, these particular hydrogels did not make use of a diluent, as described in Table 8.1. It would be of interest to know whether those changes in reaction conditions could trigger changes in their behaviour in regards to their water content and the other parameters that were established. Diluents have been found to increase the pore volume of cross-linked hydrogels and produce pores with a relatively large diameter (Okay, 2000). These pores form part of the internal matrix of a hydrogel as well as being the structures that fill with water during the hydration stage of hydrogel synthesis. It could also be helpful to determine whether varying the amount of diluent included in the formulation would influence any of its parameters.

The size of the hydrated salt ions used in this study ranged between 0.33 – 0.43 nm (Israelachvili, 2011). It would be beneficial to know whether the hydrogels were capable of permeating larger ions that were also salts, a method that has demonstrated reliability. Zinc chloride could be a suitable salt for these studies – it is soluble in water and has a hydrated ion size of approximately 0.6 nm (Shannon, 1976), significantly larger than that of magnesium chloride. The use of a larger ion could bring about changes in permeation rates by way of size exclusion as well as different partitioning behaviours compared to the salts previously used. Another avenue to drive permeation studies further would be to include peptides in assays. Although the intended application was different from that suggested in this thesis, Siemiradzka et al (2021) tested the efficacy of semi-solid hydrogels as a carrier to deliver the peptide corticotropin through the skin. Peptides would be included in the components that liver dialysis would handle in the case of treating a patient with an ineffective liver (Zvereva et al, 2016) and so its clearance by a hydrogel membrane is important to establish.

It would be of interest to investigate the partition coefficients of the hydrogels on a multiple-salt basis, using the mixture described during the multi-salt experiments to see whether partitioning behaviour also changes on this basis.

To further the determination of what biomedical applications the hydrogels could be included in, understanding their mechanical properties is of high importance. The synthesised hydrogels displayed ranged in texture, feel and structure, with some hydrogels being very rigid and others more malleable but fragile. It would be beneficial to carry out tests that would quantify these differences by identifying the physical properties that are responsible for them such as mechanical stiffness, tensile strength (Li et al, 2018) as well as identifying its Young's modulus. Also known as the elastic modulus, this property can be identified by establishing how much force must be applied to the hydrogel in order to deform its structure by way of the compression or tensile method (Lee et al, 2018). A rheometer can also be used to perform these tests which converts the shear modulus of the hydrogel to calculate the Young's modulus, taking Poisson's ratio into account (Katoh et al, 2013).

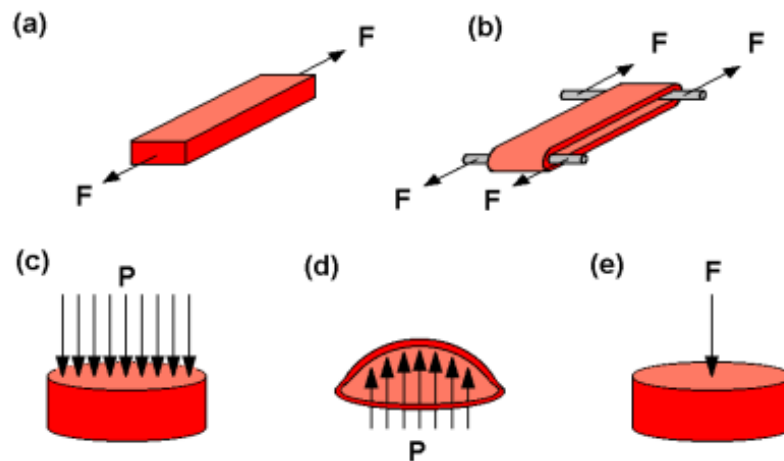


Figure 8.1 Conventional techniques to mechanically characterize hydrogels: (a) strip extensometry; (b) ring extensometry; (c) compression test; (d) bulge test; (e) indentation (F = force, P = pressure) (Image source: Ahearne et al, 2008)

These tests are often used when characterising hydrogels for the potential use in tissue engineering. Their biocompatibility makes them suitable for use in that industry, but their poor mechanical skills limit their utilisation (Orwin et al, 2003).

References

- Ahearne, M., Yang, Y., & Liu, K. (2008). Mechanical characterisation of hydrogels for tissue engineering applications. *Topics in tissue Engineering*, 4(12), 1-16.
- Ahmed, E. M. (2015). Hydrogel: Preparation, characterization, and applications: A review. *Journal of advanced research*, 6(2), 105-121.
- Allen, A. M., Kim, W. R., Moriarty, J. P., Shah, N. D., Larson, J. J., & Kamath, P. S. (2016). Time trends in the health care burden and mortality of acute on chronic liver failure in the United States. *Hepatology*, 64(6), 2165-2172.
- American Liver Foundation (2022). How Liver Diseases Progress. Available at: <https://liverfoundation.org/about-your-liver/how-liver-diseases-progress/> [Last Accessed 12 December 2022].
- American Liver Foundation (2022). The Healthy Liver. Available at: <https://liverfoundation.org/about-your-liver/how-liver-diseases-progress/the-healthy-liver/> [Last Accessed 12 December 2022].
- Amsden, B. (1998). Solute diffusion within hydrogels. Mechanisms and models. *Macromolecules*, 31(23), 8382-8395.
- Archives of American Academy of Optometry*, 48(7), 545-555.
- Arunan, E., Desiraju, G. R., Klein, R. A., Sadlej, J., Scheiner, S., Alkorta, I., . . . Hobza, P. (2011). Definition of the hydrogen bond (IUPAC Recommendations 2011). *Pure*
- Aswathy, S., Narendrakumar, U., & Manjubala, I. (2020). Commercial hydrogels for biomedical applications. *Heliyon*, 6(4), e03719.
- Austin, D., & Kumar, R. (2005). Ionic conductivity in hydrogels for contact lens applications. *Ionics*, 11(3), 262-268.
- Axpe, E., Chan, D., Offeddu, G. S., Chang, Y., Merida, D., Hernandez, H. L., & Appel, E. A. (2019). A multiscale model for solute diffusion in hydrogels. *Macromolecules*, 52(18), 6889-6897.
- Bag, M. A., & Valenzuela, L. M. (2017). Impact of the hydration states of polymers on their hemocompatibility for medical applications: A review. *International journal of molecular sciences*, 18(8), 1422.
- Bahram, M., Mohseni, N., & Moghtader, M. (2016). An introduction to hydrogels and some recent applications. In *Emerging concepts in analysis and applications of hydrogels*: IntechOpen.
- Bandyopadhyay, A., & Bose, S. (2013). *Characterization of biomaterials*: Newnes.
- Bartos, C., Szabó-Révész, P., Horváth, T., Varga, P., & Ambrus, R. (2021). Comparison of Modern In Vitro Permeability Methods with the Aim of Investigation Nasal Dosage Forms. *Pharmaceutics*, 13(6), 846.
- Ben Ishai, P., Mamontov, E., Nickels, J. D., & Sokolov, A. P. (2013). Influence of Ions on Water Diffusion: A Neutron Scattering Study. *The Journal of Physical Chemistry B*, 117(25), 7724-7728.
- Bhagyaraj, S. M., Oluwafemi, O. S., Kalarikkal, N., & Thomas, S. (2018). Applications of nanomaterials: advances and key technologies.
- Bhutta, B. S., Alghoula, F., & Berim, I. (2022). Hypoxia. In *StatPearls* [Internet]: StatPearls Publishing.
- Bouttell, J., Lewsey, J., Geue, C., Antony, G., Briggs, A., McCartney, G., ... & Heydtmann, M. (2016). The Scottish alcoholic liver disease evaluation: a population-level matched cohort study of hospital-based costs, 1991-2011. *Plos one*, 11(10), e0162980.

- Brini, E., Fennell, C. J., Fernandez-Serra, M., Hribar-Lee, B., Luksic, M., & Dill, K. A. (2017). How water's properties are encoded in its molecular structure and energies. *Chemical reviews*, 117(19), 12385-12414.
- British Liver Trust. (2019). The alarming impact of liver disease in the UK: facts and statistics.
- Buwalda, S. J., Boere, K. W., Dijkstra, P. J., Feijen, J., Vermonden, T., & Hennink, W. E. (2014). Hydrogels in a historical perspective: From simple networks to smart materials. *Journal of controlled release*, 190, 254-273.
- Campo, E. A. (2008). Polymeric materials and properties. *Selection of Polymeric Materials*, 1-39.
- Carrillo-Tripp, M., Saint-Martin, H., & Ortega-Blake, I. (2003). A comparative study of the hydration of Na⁺ and K⁺ with refined polarizable model potentials. *The Journal of Chemical Physics*, 118(15), 7062-7073.
- Cengel, Y. A., Boles, M. A., & Kanoğlu, M. (2011). *Thermodynamics: an engineering approach* (Vol. 5, p. 445). New York: McGraw-Hill.
- Chai, Q., Jiao, Y., & Yu, X. (2017). Hydrogels for biomedical applications: their characteristics and the mechanisms behind them. *Gels*, 3(1), 6.
- Chen, L.-Q. (2019). Chemical potential and Gibbs free energy. *MRS Bulletin*, 44(7), 520-523.
- Chien, S. C., Chen, C. Y., Lin, C. F., & Yeh, H. I. (2017). Critical appraisal of the role of serum albumin in cardiovascular disease. *Biomarker research*, 5(1), 1-9.
- Chirani, N., Yahia, L., Gritsch, L., Motta, F. L., Chirani, S., & Farè, S. (2015). History and applications of hydrogels. *Journal of biomedical sciences*.
- Chou, B. (2008). The evolution of silicone hydrogel lenses—The chemistry and material characteristics of current disposable silicone hydrogels in the United States. *Contact Lens Spectrum*.
- Chung, H. J., Lee, Y., & Park, T. G. (2008). Thermo-sensitive and biodegradable hydrogels based on stereocomplexed Pluronic multi-block copolymers for controlled protein delivery. *Journal of controlled release*, 127(1), 22-30.
- Chung, H. J., & Park, T. G. (2009). Self-assembled and nanostructured hydrogels for drug delivery and tissue engineering. *Nano Today*, 4(5), 429-437.
- Clarson, S. J., & Semlyen, J. A. (1993). *Siloxane polymers*: Prentice Hall.
- Costa, A. M., Halfwerk, F., Wiegmann, B., Neidlin, M., & Arens, J. (2022). Trends, Advantages and Disadvantages in Combined Extracorporeal Lung and Kidney Support From a Technical Point of View. *Frontiers in Medical Technology*, 4.
- Cruz, D., Bellomo, R., Kellum, J. A., De Cal, M., & Ronco, C. (2008). The future of extracorporeal support. *Critical care medicine*, 36(4), S243-S252.
- Cui, Z., & Muralidhara, H. (2010). *Membrane technology: a practical guide to membrane technology and applications in food and bioprocessing*: Elsevier.
- Dong, L., Hoffman, A., & Yan, Q. (1994). Macromolecular penetration through hydrogels. *Biomater. Sci. Polym*, 5, 473-484.
- Dursch, T. J., Taylor, N. O., Liu, D. E., Wu, R. Y., Prausnitz, J. M., & Radke, C. J. (2014). Water-soluble drug partitioning and adsorption in HEMA/MAA hydrogels. *Biomaterials*, 35(2), 620-629.
- Dušek, K., & Patterson, D. (1968). Transition in swollen polymer networks induced by intramolecular condensation. *Journal of Polymer Science Part A-2: Polymer Physics*, 6(7), 1209-1216.
- Energy in Agriculture*, 21(2), 91-96.
- engineering chemistry research*, 44(22), 8213-8217.

Engineering: C, 114, 111023.

environmental bioengineering-from analysis

Fatt, I., & St Helen, R. (1971). Oxygen tension under an oxygen-permeable contact lens. *American Journal of Optometry*

Forni, L., & Hilton, P. (1997). Continuous hemofiltration in the treatment of acute renal failure. *New England Journal of Medicine*, 336(18), 1303-1309.

Fujiyabu, T., Li, X., Shibayama, M., Chung, U.-i., & Sakai, T. (2017). Permeation of water through hydrogels with controlled network structure. *Macromolecules*, 50(23), 9411-9416.

Fujiyabu, T., Yoshikawa, Y., Chung, U.-i., & Sakai, T. (2019). Structure-property relationship of a model network containing solvent. *Science*

Gavara, R., & Compañ, V. (2017). Oxygen, water, and sodium chloride transport in soft contact lenses materials. *Journal of Biomedical Materials Research Part B: Applied Biomaterials*, 105(8), 2218-2231.

Gehrke, S. H., Fisher, J. P., Palasis, M., & Lund, M. E. (1997). Factors determining hydrogel permeability. *Annals of the New York Academy of Sciences*, 831, 179-207.

general crystallography, 32(5), 751-767.

Germani, G., Burroughs, A. K., & Dhillon, A. P. (2010). The relationship between liver disease stage and liver fibrosis: a tangled web. *Histopathology*, 57(6), 773-784.

Goldstein, J. I., Newbury, D. E., Michael, J. R., Ritchie, N. W., Scott, J. H. J., & Joy, D. C. (2017). *Scanning electron microscopy and X-ray microanalysis*: Springer.

Grabowski, B. (2016). "P < 0.05" might not mean what you think: American Statistical Association clarifies P values. *JNCI: Journal of the National Cancer Institute*, 108(8).

Guan, L., Jiménez, M. G., Walowski, C., Boushehri, A., Prausnitz, J., & Radke, C. (2011). Permeability and partition coefficient of aqueous sodium chloride in soft contact lenses. *Journal of Applied Polymer Science*, 122(3), 1457-1471.

Gulrez, S. K., Al-Assaf, S., & Phillips, G. O. (2011). Hydrogels: methods of preparation, characterisation and applications. *Progress in molecular*

Gun'ko, V. M., Savina, I. N., & Mikhalovsky, S. V. (2017). Properties of water bound in hydrogels. Gels, 3(4), 37.

Hall, N. A., & Fox, A. J. (2006). Renal replacement therapies in critical care. *Continuing Education in Anaesthesia, Critical Care*

Hamidi, M., Azadi, A., & Rafiei, P. (2008). Hydrogel nanoparticles in drug delivery. *Advanced drug delivery reviews*, 60(15), 1638-1649.

Hamilton, C. J., Murphy, S. M., Atherton, N. D., & Tighe, B. J. (1988). Synthetic hydrogels: 4. The permeability of poly (2-hydroxyethyl methacrylate) to cations—An overview of solute—Water interactions and transport processes. *Polymers*, 29(10), 1879-1886.

Harris, R., Harman, D. J., Card, T. R., Aithal, G. P., & Guha, I. N. (2017). Prevalence of clinically significant liver disease within the general population, as defined by non-invasive markers of liver fibrosis: a systematic review. *The lancet Gastroenterology & hepatology*, 2(4), 288-297.

Hoffman, A. S. (2012). Hydrogels for biomedical applications. *Advanced drug delivery reviews*, 64, 18-23.

Honda, N. (N.D) Water Molecules Still Shrouded in Mystery - Unlocking the secrets of the mysterious structure and patterns of motion of water molecules. Available at:

http://www.spring8.or.jp/en/news_publications/research_highlights/no_54/ [Last Accessed 21 December 2022]

- Holly, F. J., & Refojo, M. F. (1975). Wettability of hydrogels I. Poly (2-hydroxyethyl methacrylate). *Journal of Biomedical Materials Research Part B: Applied Biomaterials*, 9(3), 315-326.
- Hribar, B., Southall, N. T., Vlachy, V., & Dill, K. A. (2002). How ions affect the structure of water. *Journal of the American Chemical Society*, 124(41), 12302-12311.
- Humphrey, J. D., Dufresne, E. R., & Schwartz, M. A. (2014). Mechanotransduction and extracellular matrix homeostasis. *Nature reviews Molecular cell biology*, 15(12), 802-812.
- Institute of Industrial Science, The University of Tokyo. (2019). Colloidal gel properties under the microscope. *ScienceDaily*. Available at: [sciencedaily.com/releases/2019](https://www.sciencedaily.com/releases/2019/09/) [Last Accessed 10 September 2022]
- Iskeleli, G., Karakoc, Y., Ozkok, A., Arici, C., Ozcan, O., & Ipcioglu, O. (2013). Comparison of the effects of first and second generation silicone hydrogel contact lens wear on tear film osmolarity. *International Journal of Ophthalmology*, 6(5), 666.
- Israelachvili, J. (2011). Interactions involving polar molecules. *Intermolecular Derivatives*, 16, 147-156.
- Jenkins, K. (2015). Post Curing Silicone - What is it & How Does it Impact Silicone? *Silicone Engineering*. Available at: [silicone.co.uk/news/what-is-post-curing](https://www.silicone.co.uk/news/what-is-post-curing) [Last Accessed 10 September 2022]
- Jhon, M. S., & Andrade, J. D. (1973). Water and hydrogels. *Journal of Biomedical Materials Research Part B: Applied Biomaterials*, 7(6), 509-522.
- Kalhapure, A., Kumar, R., Singh, V. P., & Pandey, D. (2016). Hydrogels: a boon for increasing agricultural productivity in water-stressed environment. *Current science*, 1773-1779.
- Kanduč, M., Kim, W. K., Roa, R., & Dzubiella, J. J. A. n. (2020). How the shape and chemistry of molecular penetrants control responsive hydrogel permeability. *ACS Nano*, 15(1), 614-624.
- Katoh, Y., Vasudevamurthy, G., Nozawa, T., & Snead, L. L. (2013). Properties of zirconium carbide for nuclear fuel applications. *Journal of Nuclear Materials*, 441(1-3), 718-742.
- Khan, S. R., Sharma, B., Chawla, P. A., & Bhatia, R. (2022). Inductively coupled plasma optical emission spectrometry (ICP-OES): a powerful analytical technique for elemental analysis. *Food Analytical Methods*, 15(3), 666-688.
- Khosrow-Pour, D. (2005). *Encyclopedia of information science and technology*: IGI Global.
- Kim, J., Kim, H. S., Lee, N., Kim, T., Kim, H., Yu, T., . . . Hyeon, T. (2008). Multifunctional uniform nanoparticles composed of a magnetite nanocrystal core and a mesoporous silica shell for magnetic resonance and fluorescence imaging and for drug delivery. *Angewandte Chemie*, 120(44), 8566-8569.
- Kim, I. S., Jeong, Y. I., & Kim, S. H. (2000). Self-assembled hydrogel nanoparticles composed of dextran and poly (ethylene glycol) macromer. *International journal of pharmaceuticals*, 205(1-2), 109-116.
- KJ Chemicals Corp. (2017). N,N-Dimethyl acrylamide. Available at: [kjchemicals.co.jp/en/product](https://www.kjchemicals.co.jp/en/product) [Last Accessed 10 September 2022]
- Kołodziejńska, D., Skiba, A., Górecka, B., & Hubicki, Z. (2016). Hydrogels from fundamentals to application. *Emerging concepts in analysis*
- Kopeček, J. (2007). Hydrogel biomaterials: a smart future? *Biomaterials*, 28(34), 5185-5192.
- Kopeček, J. (2009). Hydrogels: From soft contact lenses and implants to self-assembled nanomaterials. *Journal of Polymer Science Part A: Polymer Chemistry*, 47(22), 5929-5946.

- Kopeček, J., & Yang, J. (2012). Smart self-assembled hybrid hydrogel biomaterials. *Angewandte Chemie International Edition*, 51(30), 7396-7417.
- Kopeček, J., Vacik, J., & Lim, D. (1971). Permeability of membranes containing ionogenic groups. *Journal of Polymer Science Part A-1: Polymer Chemistry*, 9(10), 2801-2815.
- Kotsmar, C., Sells, T., Taylor, N., Liu, D. E., Prausnitz, J., & Radke, C. (2012). Aqueous solute partitioning and mesh size in HEMA/MAA hydrogels. *Macromolecules*, 45(22), 9177-9187.
- Kuhn, W., Hargitay, B., Katchalsky, A., & Eisenberg, H. (1950). Reversible dilation and contraction by changing the state of ionization of high-polymer acid networks. *Nature*, 165(4196), 514-516.
- Lai, Y. C. (1997). A novel crosslinker for UV co of *N*-vinyl pyrrolidone and methacrylates to give hydrogels. *Journal of Polymer Science Part A: Polymer Chemistry*, 35(6), 1039-1046.
- Ledebo, I., & Blankestijn, P. J. (2010). Haemodiafiltration—optimal efficiency and safety. In (Vol. 3, pp. 8-16): Oxford University Press.
- Lee, D., Zhang, H., & Ryu, S. (2018). Elastic modulus measurement of hydrogels. Springer International Publishing, 1-21.
- Lee, S. W., Joo, W. C., Kwon, S. H., Lee, J. W., Song, J. H., & Kim, M. J. (2010). The use of single-pass albumin dialysis to correct severe hyperbilirubinemia in acute hepatitis A: a case report. *Korean Journal of Nephrology*, 29(2), 260-264.
- Leo, A., & Hoekman, D. (1995). Exploring QSAR: American Chemical Society.
- Li, X., Sun, Q., Li, Q., Kawazoe, N., & Chen, G. (2018). Functional hydrogels with tunable structures and properties for tissue engineering applications. *Frontiers in chemistry*, 6, 499.
- Lin, C. H., Cho, H. L., Yeh, Y. H., & Yang, M. C. (2015). Improvement of the surface wettability of silicone hydrogel contact lenses via layer-by-layer self-assembly technique. *Colloids and Surfaces B: Biointerfaces*, 136, 735-743.
- Liu, D., Dursch, T., Oh, Y., Bregante, D., Chan, S., & Radke, C. (2015). Equilibrium water and solute uptake in silicone hydrogels. *Acta biomaterialia*, 18, 112-117.
- Lutovska, M., Mitrevski, V., Pavkov, I., Babić, M., Mijakovski, V., Geramitcioski, T., & Stamenković, Z. (2017). Different methods of equilibrium moisture content determination. *Journal on Processing*.
- Macpherson I., Abeysekera K.W.M., Harris R., Specialist Interest Group in the Early Detection of Liver Disease, et al (2022). Identification of liver disease: why and how. *Frontline Gastroenterology*, 13, 367-373.
- Mahon, H., & Lipps, B. (1971). Encyclopedia of Polymer Science and Technology, 15. In: Interscience publishers, New York. USA.
- Mancinelli, R., Botti, A., Bruni, F., Ricci, M., & Soper, A. (2007). Hydration of sodium, potassium, and chloride ions in solution and the concept of structure maker/breaker. *The Journal of Physical Chemistry B*, 111(48), 13570-13577.
- Mandell, R. B., Polse, K. A., & Fatt, I. (1970). Corneal swelling caused by contact lens wear. *Archives of Ophthalmology*, 83(1), 3-9.
- Mann, A., Sáez-Martinez, V., Lydon, F., & Tighe, B. (2019). Investigating the permeation properties of contact lenses and its influence on tear electrolyte composition. *Journal of Biomedical Materials Research Part B: Applied Biomaterials*, 107(6), 1997-2005.
- Marcus, Y. (2012). Ions in water and biophysical implications: from chaos to cosmos: Springer Science & Business Media.

- McKeen, L. (2015). 1—Introduction to Creep, Polymers, Plastics and Elastomers. Factors on Plastics and Elastomers, 1-41.
- McKenzie, T. J., Lillegard, J. B., & Nyberg, S. L. (2008). Artificial and bioartificial liver support. In *Seminars in liver disease* (Vol. 28, No. 02, pp. 210-217). © Thieme Medical Publishers.
- Merck. (2022) 3-[Tris(trimethylsiloxy)silyl]propyl methacrylate. Available at: sigmaaldrich.com/GB/en/product [Last Accessed 10 September 2022]
- Miller, A., & Jedrzejczak, W. W. (2001). Albumin—biological functions and clinical significance. *Postepy Higieny i Medycyny Doswiadczalnej*, 55(1), 17-36.
- Min, L., Edgar, T., Zicheng, Z., & Yee, Y. (2015). Biomaterials for bioprinting. *3D Bioprinting modeling to technology applications*, 117150.
- Moller, J. C., Berry, R. J., & Foster, H. A. (2020). On the nature of epoxy resin post-curing. *Polymers*, 12(2), 466.
- Moosavi, S. M., & Ghassabian, S. (2018). Linearity of calibration curves for analytical methods: A review of criteria for assessment of method reliability. In (Vol. 109): IntechOpen Limited London, UK.
- Ng, S.-F., Rouse, J. J., Sanderson, F. D., Meidan, V., & Eccleston, G. M. (2010). Validation of a static Franz diffusion cell system for in vitro permeation studies. *Aaps Pharmscitech*, 11(3), 1432-1441.
- Nguyen, E. P., Silva, C. d. C. C., & Merkoçi, A. (2020). Recent advancement in biomedical applications on the surface of two-dimensional materials: From biosensing to tissue engineering. *Nanoscale*, 12(37), 19043-19067.
- Nicolson, P. C., & Vogt, J. (2001). Soft contact lens polymers: an evolution. *Biomaterials*, 22(24), 3273-3283.
- Nie, F.-Q., Xu, Z.-K., Huang, X.-J., Ye, P., & Wu, J. (2003). Acrylonitrile-based copolymer membranes containing reactive groups: surface modification by the immobilization of poly (ethylene glycol) for improving antifouling property and biocompatibility. *Langmuir*, 19(23), 9889-9895.
- Nordholm, S., & Bacskey, G. B. (2020). The basics of covalent bonding in terms of energy and dynamics. *Molecules*, 25(11), 2667.
- Nuttelman, C. R., Rice, M. A., Rydholm, A. E., Salinas, C. N., Shah, D. N., & Anseth, K. S. (2008). Macromolecular monomers for the synthesis of hydrogel niches and their application in cell encapsulation and tissue engineering. *Progress in polymer science*, 33(2), 167-179.
- Offeddu, G., Axpe, E., Harley, B., & Oyen, M. (2018). Relationship between permeability and diffusivity in polyethylene glycol hydrogels. *AIP advances*, 8(10), 105006.
- Okay, O. (2000). Macroporous copolymer networks. *Progress in polymer science*, 25(6), 711-779.
- Orwin, E. J., Borene, M. L., & Hubel, A. (2003). Biomechanical and optical characteristics of a corneal stromal equivalent. *Biomech. Eng.*, 125(4), 439-444.
- Ostrowska-Czubenko, J., Pieróg, M., & Gierszewska-Drużyńska, M. J. P. o. C. (2011). State of water in noncrosslinked and crosslinked hydrogel chitosan membranes—DSC studies. *Progress on Chemistry*, 6(5), 197-202.
- Pasqui, D., De Cagna, M., & Barbucci, R. (2012). Polysaccharide-based hydrogels: the key role of water in affecting mechanical properties. *Polymers*, 4(3), 1517-1534.
- Pedley, D. G., Skelly, P. J., & Tighe, B. J. (1980). Hydrogels in biomedical applications. *British Polymer Journal*, 12(3), 99-110.

- Peng, C.-C., & Chauhan, A. (2012). Ion transport in silicone hydrogel contact lenses. *Journal of membrane science*, 399, 95-105.
- Penzel, E., Ballard, N., & Asua, J. M. (2018). *Journal: Ullmann's Encyclopedia of Industrial Chemistry*, 2018, p. 1-20. *Ullmann's Encyclopedia of Industrial Chemistry*, 1-20.
- Pimenta, A., Ascenso, J., Fernandes, J., Colaço, R., Serro, A., & Saramago, B. (2016). Controlled drug release from hydrogels for contact lenses: Drug partitioning and diffusion. *International Journal of Pharmaceutics*, 515(1-2), 467-475.
- Pissis, P., & Kyritsis, A. (2013). Hydration studies in polymer hydrogels. *Journal of Polymer Science Part B: Polymer Physics*, 51(3), 159-175.
- Pless, G. (2007). Artificial and bioartificial liver support. *Organogenesis*, 3(1), 20-24.
- Plieva, F., Huiting, X., Galaev, I. Y., Bergenståhl, B., & Mattiasson, B. (2006). Macroporous elastic polyacrylamide gels prepared at subzero temperatures: control of porous structure. *Journal of Materials Chemistry*, 16(41), 4065-4073.
- Polmanteer, K. E. (1981). Current perspectives on silicone rubber technology. *Rubber Chemistry and Technology*, 54(5), 1051-1080.
- Polymer Database. (2015). Properties of Silicones. Available at: polymerdatabase.com/polymerclasses/silicone [Last Accessed 10 September 2022]
- Polymer Science*, 295(1), 205-213.
- Pozuelo, J., Compañ, V., González-Méijome, J. M., González, M., & Mollá, S. (2014). Oxygen and ionic transport in hydrogel and silicone-hydrogel contact lens materials: An experimental and theoretical study. *Journal of membrane science*, 452, 62-72.
- Qiu, B., Stefanos, S., Ma, J., Lalloo, A., Perry, B. A., Leibowitz, M. J., ... & Stein, S. (2003). A hydrogel prepared by in situ cross-linking of a thiol-containing poly (ethylene glycol)-based copolymer: a new biomaterial for protein drug delivery. *Biomaterials*, 24(1), 11-18.
- Raj Singh, T. R., Woolfson, A. D., & Donnelly, R. F. (2010). Investigation of solute permeation across hydrogels composed of poly (methyl vinyl ether-co-maleic acid) and poly (ethylene glycol). *Journal of Pharmacy*
- Rajbhandary, A., & Nilsson, B. L. (2016). Self-assembling hydrogels. In *GELS HANDBOOK: Fundamentals, Properties and Applications Volume 1: Fundamentals of Hydrogels*. 219-250.
- Rudin, A., & Choi, P. (2012). *The elements of polymer science and engineering*: Academic press.
- Russell, S. M., & Carta, G. (2005). Mesh size of charged polyacrylamide hydrogels from partitioning measurements. *Industrial*
- Saez-Martinez, V., Mann, A., Lydon, F., Molock, F., Layton, S. A., Toolan, D. T., . . . Tighe, B. J. (2021). The influence of structure and morphology on ion permeation in commercial silicone hydrogel contact lenses. *Journal of Biomedical Materials Research Part B: Applied Biomaterials*, 109(1), 137-148.
- Sastri, V. R. (2014). High-temperature engineering thermoplastics: polysulfones, polyimides, polysulfides, polyketones, liquid crystalline polymers, and fluoropolymers. *Plast Med Devices*, 173-213.
- Savina, I. N., Gun'ko, V. M., Turov, V. V., Dainiak, M., Phillips, G. J., Galaev, I. Y., & Mikhalovsky, S. V. (2011). Porous structure and water state in cross-linked polymer and protein cryo-hydrogels. *Soft Matter*, 7(9), 4276-4283.

- Seitz, M. E., Wiseman, M. E., Hilker, I., Loos, J., Tian, M., Li, J., . . . Bulters, M. (2017). Influence of silicone distribution and mobility on the oxygen permeability of model silicone hydrogels. *Polymer*, 118, 150-162.
- Sekine, Y., Kobayashi, R., Chi, S., Fernandez-Baca, J. A., Suzuya, K., Fujisaki, F., . . . Yamauchi, H. (2015). Neutron Diffraction of Ice and Water in Hydrogels. Paper presented at the Proceedings of the 2nd International Symposium on Science at J-PARC—Unlocking the Mysteries of Life, Matter and the Universe—.
- Sery, T. W., & Hehre, E. J. (1956). Degradation of dextrans by enzymes of intestinal bacteria. *Journal of bacteriology*, 71(3), 373-380.
- Serero, Y., Aznar, R., Porte, G., Berret, J.-F., Calvet, D., Collet, A., & Viguier, M. (1998). Associating polymers: from “flowers” to transient networks. *Physical Review Letters*, 81(25), 5584.
- Shahid, S. A., Qidwai, A. A., Anwar, F., Ullah, I., & Rashid, U. (2012). Improvement in the water retention characteristics of sandy loam soil using a newly synthesized poly (acrylamide-co-acrylic acid)/AlZnFe₂O₄ superabsorbent hydrogel nanocomposite material. *Molecules*, 17(8), 9397-9412.
- Shannon, R. D. (1976). Revised effective ionic radii and systematic studies of interatomic distances in halides and chalcogenides. *Acta crystallographica section A: crystal physics, diffraction, theoretical*
- Sharma, A., Bhat, S., Dasgupta, D., Samantara, L., Kalyanachakravarthi, K., Manchanda, B., . . . Mondal, T. (2020). Structure–property correlation of silicone hydrogels based on 3-[tris (trimethylsilyloxy) silyl] propyl methacrylate monomer. *Journal of Applied Polymer Science*, 137(27), 49198.
- Shekar, K., Fraser, J. F., Taccone, F. S., Welch, S., Wallis, S. C., Mullany, D. V., . . . Roberts, J. A. (2014). The combined effects of extracorporeal membrane oxygenation and renal replacement therapy on meropenem pharmacokinetics: a matched cohort study. *Critical care medicine*, 18(6), 1-9.
- Shimizu, S., & Matubayasi, N. J. P. C. C. P. (2018). Ion hydration: Linking self-diffusion and reorientational motion to water structure. *Physical Chemistry Chemical Physics*, 20(8), 5909-5917.
- Siemiradzka, W., Dolińska, B., & Ryszka, F. (2021). Modelling and control of corticotropin permeation from hydrogels across a natural membrane in the presence of albumin. *Processes*, 9(9), 1674.
- Singh, M. R., Patel, S., & Singh, D. (2016). Natural polymer-based hydrogels as scaffolds for tissue engineering. In *Nanobiomaterials in soft tissue engineering* (pp. 231-260): Elsevier.
- Stange, J. (2011). Extracorporeal liver support. *Organogenesis*, 7(1), 64-73.
- Stange, J., & Mitzner, S. (1996). A carrier-mediated transport of toxins in a hybrid membrane. Safety barrier between a patients blood and a bioartificial liver. *The International journal of artificial Organs*, 19(11), 677-691.
- Stange, J., Mitzner, S. R., Rislér, T., Erley, C. M., Lauchart, W., Goehl, H., ... & Schmidt, R. (1999). Molecular adsorbent recycling system (MARS): clinical results of a new membrane-based blood purification system for bioartificial liver support. *Artificial organs*, 23(4), 319-330.
- Stokes, D. (2012). Environmental scanning electron microscopy for biology and polymer science. *Microscopy*

- Su, A., Smith, B. E., & Herr, A. E. (2019). In situ measurement of thermodynamic partitioning in open hydrogels. *Analytical chemistry*, 92(1), 875-883.
- Surface Forces, 3, 71-90.
- Suzuki, A., & Tanaka, T. (1990). Phase transition in polymer gels induced by visible light. *Nature*, 346(6282), 345-347.
- Tait, P. J., & Berry, I. G. (1989). Monoalkene : Co. *Comprehensive Polymer Science.*, 4, 575-584.
- Tamás, H., Ambrus, R., & Szabóné, R. P. (2015). Investigation of permeability of intranasal formulations using Side-Bi-Side horizontal diffusion cell. *Acta Pharmaceutica Hungarica*, 85(1), 19-28.
- Tanaka, T. (1978). Collapse of gels and the critical endpoint. *Physical Review Letters*, 40(12), 820.
- Tansel, B., Sager, J., Rector, T., Garland, J., Strayer, R. F., Levine, L., . . . Bauer, J. (2006). Significance of hydrated radius and hydration shells on ionic permeability during nanofiltration in dead end and cross flow modes. *Separation*
- Tao, H., Zhang, X., Sun, Y., Yang, H., & Lin, B. (2017). The influence of molecular weight of siloxane macromere on phase separation morphology, oxygen permeability, and mechanical properties in multicomponent silicone hydrogels. *Colloid technology of advanced materials*, 20(1), 608-621.
- Tapper, E. B., & Parikh, N. D. (2018). Mortality due to cirrhosis and liver cancer in the United States, 1999-2016: observational study. *BMJ*, 362.
- Teichroeb, J. H., Forrest, J. A., Ngai, V., Martin, J. W., Jones, L., & Medley, J. (2008). Imaging protein deposits on contact lens materials. *Optometry*
- Tighe, B. (2004). Silicone hydrogels: structure, properties and behaviour. *Silicone Hydrogels: continuous-wear contact lenses*.
- Tong, J., & Anderson, J. L. (1996). Partitioning and diffusion of proteins and linear polymers in polyacrylamide gels. *Biophysical journal*, 70(3), 1505-1513.
- Touchal, S., Jonquieres, A., Clément, R., & Lochon, P. (2004). Co of 1-vinylpyrrolidone with N-substituted methacrylamides: monomer reactivity ratios and copolymer sequence distribution. *Polymer*, 45(25), 8311-8322.
- Tran, N.-P.-D., & Yang, M.-C. (2019). Synthesis and characterization of silicone contact lenses based on TRIS-DMA-NVP-HEMA hydrogels. *Polymers*, 11(6), 944.
- Tsai, W.-T. (2007). The prediction of environmental fate for trifluoromethyl sulfur pentafluoride (SF₅CF₃), a potent greenhouse gas. *Journal of hazardous materials*, 149(3), 747-751.
- UCLA Chemistry & Biochemistry. Illustrated Glossary of Organic Chemistry. Available at: chem.ucla.edu/vinyl-group [Last Accessed 10 September 2022]
- Van Amerongen, G. J. (1951). Influence of Structure of Elastomers on their Permeability to Gases. *Rubber Chemistry and Technology*, 24(1), 109-131.
- Vedadghavami, A., Minooei, F., Mohammadi, M. H., Khetani, S., Kolahchi, A. R., Mashayekhan, S., & Sanati-Nezhad, A. (2017). Manufacturing of hydrogel biomaterials with controlled mechanical properties for tissue engineering applications. *Acta biomaterialia*, 62, 42-63.
- Veerman, J., & Vermaas, D. (2016). Reverse electrodialysis: fundamentals. *Sustainable energy from salinity gradients*, 77-133.
- Vision Science, 85(12), 1151-1164.
- Voxco. Anova vs T-test: Definition & Working (2021). Available at: voxco.com/blog/anova-vs-t-test-with-a-comparison-chart [Last Accessed 10 September 2023]

- Wan, L. S., Xu, Z. K., Huang, X. J., Wang, Z. G., & Ye, P. (2005). Hemocompatibility of poly (acrylonitrile-co-N-vinyl-2-pyrrolidone) s: swelling behavior and water states. *Macromolecular bioscience*, 5(3), 229-236.
- Warrick, E. L., Pierce, O. R., Polmanteer, K. E., & Saam, J. C. (1979). Silicone elastomer developments 1967–1977. *Rubber chemistry and Technology*, 52(3), 437-525.
- Wichterle, O., & Lim, D. (1960). Hydrophilic gels for biological use. *Nature*, 185(4706), 117-118.
- Williams, D. F. (2009). On the nature of biomaterials. *Biomaterials*, 30(30), 5897-5909.
- Williams, R., Aspinall, R., Bellis, M., Camps-Walsh, G., Cramp, M., Dhawan, A., ... & Smith, T. (2014). Addressing liver disease in the UK: a blueprint for attaining excellence in health care and reducing premature mortality from lifestyle issues of excess consumption of alcohol, obesity, and viral hepatitis. *The Lancet*, 384(9958), 1953-1997.
- Yale University, West Campus Materials Characterization Core (N.D). X-ray Photoelectron Spectroscopy (XPS). Available at: <https://ywcmatsci.yale.edu/xps> [Last Accessed 21 December 2022]
- Yasuda, H., Lamaze, C., & Ikenberry, L. (1968). Permeability of solutes through hydrated polymer membranes. Part I. Diffusion of sodium chloride. *Die Makromolekulare Chemie: Macromolecular Chemistry*
- Yazdi, M. K., Vatanpour, V., Taghizadeh, A., Taghizadeh, M., Ganjali, M. R., Munir, M. T., . . . Ghaedi, M. (2020). Hydrogel membranes: A review. *Materials Science*
- Yoder, C. H., Pasteris, J. D., Worcester, K. N., & Schermerhorn, D. V. (2012). Structural water in carbonated hydroxylapatite and fluorapatite: Confirmation by solid state 2H NMR. *Calcified Tissue International*, 90(1), 60-67.
- Zhang, H., & Cloud, A. (2006). The permeability characteristics of silicone rubber. *Global Advances in Materials and Process Engineering*, 72-75.
- Zhao, Z.-B., An, S.-S., Xie, H.-J., Han, X.-L., Wang, F.-H., & Jiang, Y. (2015). The relationship between the hydrophilicity and surface chemical composition microphase separation structure of multicomponent silicone hydrogels. *The Journal of Physical Chemistry B*, 119(30), 9780-9786.
- Zhu, J., & Marchant, R. E. (2011). Design properties of hydrogel tissue-engineering scaffolds. *Expert review of medical devices*, 8(5), 607-626.
- Zimmermann, F., Ebert, M., Worringer, A., Schütz, L., & Weinbruch, S. (2007). Environmental scanning electron microscopy (ESEM) as a new technique to determine the ice nucleation capability of individual atmospheric aerosol particles. *Atmospheric Environment*, 41(37), 8219-8227.
- Zustiak, S. P., Boukari, H., & Leach, J. B. (2010). Solute diffusion and interactions in cross-linked poly (ethylene glycol) hydrogels studied by fluorescence correlation spectroscopy. *Soft Matter*, 6(15), 3609-3618.
- Zvereva, I., Semenistaya, E., Krotov, G., & Rodchenkov, G. (2016). Comparison of various in vitro model systems of the metabolism of synthetic doping peptides: Proteolytic enzymes, human blood serum, liver and kidney microsomes and liver S9 fraction. *Journal of proteomics*, 149, 85-97.